# Plasticity of Mammary Cell Boundaries Governed by EGF and Actin Remodelling

by Wai Ying Yvonne Tang

Thesis submitted in accordance with the requirements of the University of Liverpool for the degree of Doctor of Philosophy

October 2014

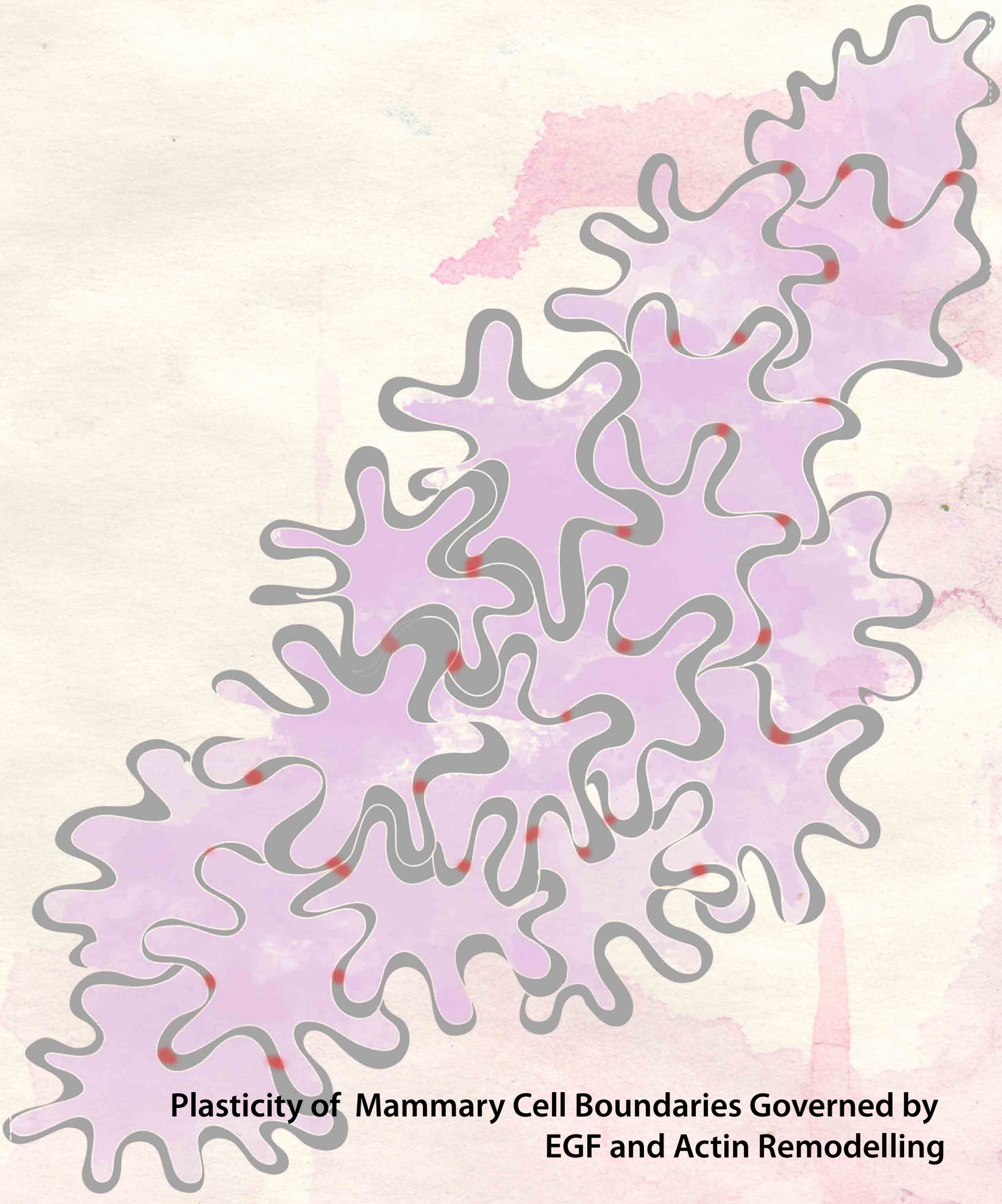

# Plasticity of Mammary Cell Boundaries Governed by EGF and Actin Remodelling

# DVD pocket

Inside cover: Artistic rendering of interdigitations formed between confluent MCF10A cells described in this thesis and by Tang et al. (2014). Interdigitations are established over 12-24 hours following EGF withdrawal and can be rapidly dissolved (1-3 hours) following reapplication of EGF. Actin cables project from the tips of these interdigitations and actin polymerisation/myosin II activity is required for their dissolution. Interdigitated cells are restricted in their ability to undergo lateral movement within a confluent monolayer. Red spots represent the desmosomes that are enriched within interdigitations. Original image: Septavera Sharvia.

## Abbreviations

| | |
|---|---|
| 2D | two-dimensional |
| 3D | three-dimensional |
| 4EBP1 | eukaryotic initiation factor 4E binding protein |
| Abi1 | Abl interactor 1 |
| AJ | Adherens junction |
| AKT/ PKB | Protein kinase B |
| AP2 | Adaptor protein 2 |
| AREG | Amphiregulin |
| Arp2/3 complex | actin-related protein 2/3 complex |
| ArpC2 p34 | Actin-related protein 2/3 complex, subunit 2, 34kDa |
| Bleb | Blebbistatin |
| BSA | bovine serum albumin |
| BTC | Betacellulin |
| cAMP | cyclic adenosine monophosphate |
| CDC42 | Cell division control protein 42 homolog |
| CDKN2A | Cyclin dependent kinase inhibitor 2A |
| CGH | Comparative genome hybridisation |
| CHX | Cycloheximide |
| CSA | cross surface area |
| DAPI | 4'6-diamidino-2-phenylindole |
| DP | Desmoplakin |
| DKD | Double (pooled siRNA) knockdown |
| DMSO | Dimethyl sulfoxide (used as drug vehicle control) |
| DNA | Deoxyribonucleic acid |
| DNA | Deoxyribonucleic acid |
| ECACC | European Collection of Cell Cultures |
| ECM | Extracellular matrix |
| EEA1 | Early Endocytic Antigen 1 |
| EGFR | Epidermal growth factor receptor |
| EGR1 | Early Growth Response 1 |
| ELK | ETS domain containing protein Elk 1 |
| EMT | Epithelial-to-mesenchymal |
| EPGN | Epigen |
| EREG | Epiregulin |

| | |
|---|---|
| ERK 1/2 | Extracellular signal-regulated kinases 1/2 |
| ERM | Ezrin, Radixin and Moesin |
| FBS | fetal bovine serum |
| FOXO | Forkhead family of transcription factors |
| Gab1/2 | Grb2-associated-binding protein 1/2 |
| GAP | GTPase activating proteins |
| GEF | Guanine nucleotide exchange factor |
| GBM | glomerular basement membrane |
| GDI | Guanine nucleotide dissociation inhibitors |
| gDNA | genomic DNA |
| GEF | guanine nucleotide exchange factor |
| GINS complex | Sld5, Psf1, Psf2 and Psf3 complex |
| GPCR | G coupled protein receptors |
| Grb2 | Growth factor receptor-bound protein 2 |
| GS | goat serum |
| GST | Glutathione sepharose beads |
| HB-EGF | Heparin-binding EGF-like growth factor |
| HGF | Hepatocyte growth factor |
| HNSCC | Head and neck squamous cell carcinoma |
| HUVEC | Human umbilical vein endothelial cells |
| IF | Immunofluorescence |
| IR | Insulin receptor |
| LB broth | Luria Bertani broth |
| MAPK | Mitogen activated protein kinase |
| MEK 1/2 | Mitogen-activated protein kinase kinase 1/2 |
| Met-R | Hepatocyte growth factor receptor |
| NGF | Nerve growth factor |
| NRG1 | Neuregulin 1 |
| NSCLC | non small cell lung cancer |
| NSCLC | Non small cell lung cancer |
| P70S6 | Ribosomal protein S6 kinase, 70kDa polypeptide |
| PAK | Human p21 activated kinase 1 |
| PAK-PBD | PAK- Rac1/CDC42 (p21) binding domain |
| pAKT | phospho- protein kinase B |
| Par | Parental cells |
| PCR | Polymerase Chain Reaction |

| | |
|---|---|
| PDK1 | Phosphoinositide dependent kinase 1 |
| pEGFR | phospho- EGFR |
| pERK | phospho- extracellular signal-regulated kinases |
| PG | Plakoglobin |
| PI3K | Phosphatidyl-inositol 3 kinase |
| $PIP_3$ | Phosphatidyl-inositol 3,4,5-triphosphate |
| PLCγ | Phospholipase C gamma |
| PTEN | Phosphatase and tensin homolog |
| PTPN6 | Protein tyrosine phosphatase non-receptor type 6 |
| Rac | Ras-related C3 botulinum toxin substrate |
| Raf | MAP kinase kinase kinase |
| Rho GTPases | Ras homologous family small GTPases |
| RIPA | Radioimmunoprecipitation assay |
| RT | Room temperature |
| RTK | receptor tyrosine kinase |
| SDS | sodium dodecyl sulphate |
| siRNA | small interfering ribonucleic acids |
| SLD5 | DNA replication complex GINS protein SLD5 |
| SNP | Single-nucleotide polymorphism |
| ssDNA | single stranded DNA |
| STAT5b | Signal transducer and activator of transcription 5b |
| TEM | transmission electron microscope |
| TGFα | Transforming growth factor-α |
| THAP1 | THAP domain containing apoptosis associated protein 1 |
| TMEPAI | Transforming growth factor-β induced transmembrane protein |
| WASP | Wiskott-Aldrich syndrome protein |
| WB | Western Blot |
| WT | wild type |

## List of Tables

## List of Movies and movie legends

| Movie | Movie legend |
|---|---|
| Movie 3.1 | (related to Figure 3.2, Figure 3.3.)<br>**Withdrawal of EGF leads to loss of cellular lateral mobility.**<br><br>MCF10A monolayers grown in complete growth medium, +EGF (left panel) or –EGF (right panel). Left panel. MCF10A cells were cultured in complete growth medium (+EGF) for 46 hours before exchange for fresh medium (+EGF), from which point images were collected by time-lapse phase contrast microscopy. Frames were taken every 15 mins for 24 hours saved for playback at 100ms intervals.<br><br>Right panel. MCF10A cells were cultured in growth medium lacking EGF for 67 hours. Images were captured using an inverted microscope (Eclipse Ti-E, Nikon) at 20x magnification. Frames were collected every 15 mins for the final 24 hours saved for playback at 100ms interval. |
| Movie 4.1 | (related to Figure 4.2)<br>**Induction of interdigitation in MCF10A cells upon removal of EGF (+EGF→ –EGF).**<br><br>MCF10A cells were cultured in complete growth medium (+EGF) for 46 hours before exchange of medium to (-EGF) (20ng/ml). Images were captured by time-lapse phase contrast microscopy using an inverted microscope (Eclipse Ti-E, Nikon) at 20x magnification. Frames were collected every 15 mins for 24 hours and saved for playback at 100ms intervals. |

| | |
|---|---|
| Movie 4.2 | (related to Figure 4.7)<br>**Dissolution of interdigitation in MCF10A cells upon addition of EGF (-EGF → +EGF).**<br><br>MCF10A cells were cultured in growth medium lacking EGF for 68.8 hours before addition of EGF (20 ng/ml). Interdigitations started to resolve at time 1:30 hours (addition of EGF). Images were analysed by time-lapse phase contrast microscopy using an inverted microscope (Eclipse Ti-E, Nikon) at 20x magnification. Frames were collected every 2 mins for 13 hours and saved for playback at 100ms interval. Imaging started 1.5 hours before addition of EGF and lasted for 13 hours. |
| Movie 5.1 | (related to Figure 5.2)<br>**Interdigitations are independent of actomyosin contractility.**<br><br>MCF10A cells were cultured in complete growth medium for 50 hours before medium exchange to ±20ng/ml EGF. Blebbistatin (25μM- top row) or DMSO vehicle control (bottom row) was added 16 hours after medium exchange before digits were induced. Images were analysed by time-lapse microscopy using an inverted microscope (Eclipse Ti-E, Nikon) at 20x magnification. Cells were imaged every 10 minutes for 8 hours after addition of drugs and saved for playback at 100ms interval. |
| Movie 5.2 | (related to Figure 5.20)<br>**Induction of interdigitations requires protein synthesis.**<br><br>MCF10A cells were cultured in complete growth for 50 hours before medium exchange to include ±20ng/ml EGF with CHX or vehicle control, DMSO for 16 hours overnight. Images were analysed by time-lapse microscopy using an inverted microscope (Eclipse Ti-E, Nikon) at 20x magnification. Cells were imaged every 10 minutes for 8 hours the following day and saved for playback at 100ms interval. |

| | |
|---|---|
| Movie 5.3 | (related to Figure 4.12, 5.24)<br>**Wound closure of MCF10A cells is specific to addition of EGF.**<br><br>MCF10A cells were cultured in growth medium lacking EGF for 69 hours before addition of growth factor; EGF (20ng/ml), HGF (20ng/ml) or NRG1 (6ng/ml). Wound closure is most efficient upon addition of EGF (bottom left). Images were analysed by time-lapse phase contrast microscopy using an inverted microscope (Eclipse Ti-E, Nikon). Imaging started 3 hours before addition of growth factors and frames were collected every 15 minutes for 19 hours, saved for playback at 100ms interval. |
| Movie 5.4A | (related to Figure 5.27A)<br>**Interdigitated cells are able to withstand hypo-osmotic stress.**<br><br>MC10A cells were cultured in growth medium ±EGF for 48 hours before medium exchange to hypotonic buffers at [77mM NaCl], left panel or [35mM NaCl], right panel. Images were analysed by time-lapse microscopy using an inverted microscope (Eclipse Ti-E, Nikon) at 20x magnification. Cells were imaged every 5 minutes for 8+ hours after exchange to hypotonic and saved for playback at 100ms interval. |
| Movie 5.4B | (related to Figure 5.27B)<br>**Interdigitated cells are able to withstand hypo-osmotic stress.**<br><br>MCF10A cells were cultured as 5.4A before exchange to isotonic buffer at [35mmM NaCl]. Images were captured and analysed as above. |

# Dedication

I would like to dedicate this thesis in loving memory of my Grandfather, *Kwong Chuen Tang*, and father, *Chew Foong Tang*.

To my mother, *Lee Yoong Choong* for her endless supply of enthusiasm and love, without which this journey would not have been possible.

**Acknowledgement**

"Keep calm and carry on"

That is the mantra that I have kept in mind throughout the four exciting years of this PhD led by my supervisors (in alphabetical order), Prof. Michael Clague and Prof. Sylvie Urbé. I am grateful for their invaluable time, patience and insightful discussions that led to the completion of this thesis. May this fascinating journey in cell biology based research continue beyond the scope of this thesis…

Thanks to Alison Beckett and Ian Prior for their TEM expertise. To the current and previous members of MC/ SU/ JC/ IP groups, I am grateful for the lab meetings and the conducive research environment. Special thanks to past and present members of the lab especially Jia Lih, Amos, Han, Mo, Vero, Viktor, Craig, Dean, Fi, Claire, Alice and Rosanna for the scientific discussions, kind advise and help in times of need.

I would like to thank Cancer Research UK and University of Liverpool for funding this PhD and Horizon Discovery Ltd. for providing the panel of isogenic MCF10A cells. Also, I am thankful to Prof. Laura Machesky and Prof. David Garrod for their provision of GTP-LifeAct construct, desmosomal antibodies and the opportunities for discussions. Thanks to Dr. Tobias Zech and Prof. Val Brunton for accepting our invitation to become the viva examiners.

Personally, I cannot express enough gratitude to Chang Ming for the unending support and encouragement, Septavera Sharvia for putting up with me through good times and bad, for the nuggets of wisdom and also for her fabulous illustration of digits that grace the inner cover of this thesis. To Carmen, Veron, Zara and Kuche (Lai Yee), thanks for all the love and for constantly cheering me up with updates from home.

## Abstract

Molecular mechanisms governing the plasticity of cellular boundaries in confluent epithelial monolayers are poorly characterised. In this thesis, we report a drastic reorganisation of cellular boundaries, provoked by the prolonged withdrawal of EGF from non-malignant mammary epithelial cells, MCF10A and HMT-3522 cells. EGF withdrawal induces actin-rich interdigitations that protrude into neighbouring cells and are enriched in desmosomes. These protrusions allow the cellular sheets to resist mechanical and osmotic perturbation. Mobility of the cells within monolayers is also restricted. Overexpression of constitutively active Rac opposes interdigitations and induces membrane ruffling. EGF application reverses the interdigitations rapidly in a process that requires actin polymerisation and actomyosin contraction. We report here a simple *in vitro* system that can be utilised as a visual readout to dissect novel signaling pathways specific to EGFR activation and mammary morphogenesis. This thesis focuses on the initial efforts to characterise this dramatic remodeling of cellular boundaries and will discuss the potential investigations that can be pursued further hereon.

## Executive summary

This thesis consists of six chapters. Chapters 1 and 6 present the introduction and final discussion of the results obtained throughout the 4 years of my PhD. The remaining Chapters 2, 3, and 4 record the results that have been attained. Each result chapter is presented with a separate introduction, discussion and accompanied by results figures and movies (listed after Table of Contents). The copies of time-lapse imaging recorded are saved on the appended DVD. Results presented in this thesis have also been recently published in *Cell Reports* referenced below and the hard copy of this manuscript is attached in the Appendices.

Tang, W.Y.Y., Beckett, A.J., Prior, I.A., Coulson, J.M., Urbé, S. and Clague, M.J. (2014) Plasticity of mammary cell boundaries governed by EGF and actin remodeling, *Cell Reports,* vol. 8, September 25, 1-9.

Chapter 1 of this thesis forms the introduction that sets the scene for subsequent results. This chapter explores the beginnings and evolution of research on EGF signalling and is followed by an introduction to the culture of non-tumorigenic mammary epithelial cells used to generate the results reported here, MCF10A with their isogenic counterparts (licensed from Horizon Discovery Ltd.; Methods: Table 2.4) and HMT-3522 cells. In accordance to the title of this thesis, the subsequent sections introduce the effect of EGF signalling on the structural regulation of cell shape involving cell-cell junctions and the actin cytoskeleton. Physiological relevance of interdigitations reported in the literature are explored followed by a brief summary and graphical abstract summarising the results of this thesis. Chapter 2 catalogues the materials and methods that have been used to undertake experiments described throughout this book.

Chapters 3 and 4 present the morphological and preliminary mechanistic characterisation of the MCF10A and the isogenic counterparts (listed in Methods: Table 2.4) in two-dimensional (2D) and three-dimensional (3D) assays using immunofluorescence microscopy. EGF associated signalling profiles of these cells are also examined using Western Blotting procedures. The formation and reversal of interdigitations are explored as separate processes utilising different experimental configurations. Similarities and differences of the cell phenotype between the MCF10A isogenic cells are analysed in the discussion sections of both chapters.

Chapter 5 focuses on the ultrastructure, junction and cytoskeleton-related aspects of this drastic reversible remodelling of cell membranes. Here, I have included Transmission Electron Microscope (TEM) images obtained from a fruitful collaboration with the TEM unit at the University of Liverpool (Alison Beckett and Ian Prior). Subsequent discoveries following on from this ultrastructural analysis are reported in the context of EGF signalling and the regulation of cell-cell junctions and actin cytoskeleton. In addition, preliminary results linking microtubule and Golgi apparatus organisation to this phenomenon are explored. The functional consequences of the formation of interdigitations are revealed. This chapter discusses tantalising links between EGF and GTPase signalling that regulate the reorganisation of the cytoskeleton and the number of cell-cell junctions. Chapter 6 discusses the results and implications of previous chapters, limitations and proposes future perspectives.

# Chapter 1
# Introduction

# Introduction

## 1.1 Epidermal Growth Factor Receptor (EGFR) signalling pathway

### *1.1.1 Discovery of EGF and the elucidation of its receptor*

For decades, Epidermal Growth Factor Receptor (EGFR) signalling has been studied in key cellular processes including cell survival, proliferation and cytoskeletal arrangements (Yarden and Sliwkowski, 2001). This has stemmed from early growth factor research back in 1952 when Rita Levi-Montalcini discovered that mouse tumour cells secreted a factor that promoted neurite outgrowth in chicken embryos (Levi-Montalcini et al., 1952). Her subsequent work with Stanley Cohen led to the discovery of nerve growth factor (NGF) purified from snake venom and mouse salivary-gland extracts and a novel growth factor, which when injected, induced precocious eyelid opening and tooth eruption in newborn mice (Cohen, 1962; Cohen et al., 1957; Levi-Montalicini et al., 1960) This novel growth factor was termed epidermal growth factor (EGF) and they were awarded the Nobel Prize in Physiology or Medicine in 1986 for their discoveries.

Their discovery of EGF subsequently led to studies that identified the EGF receptors using $^{125}$I-labelled EGF and fibroblasts from different species. The receptor was further characterised as a 170kDa membrane component that was phosphorylated in response to EGF treatment in A-431 epidermoid carcinoma cells (Carpenter et al., 1975; 1978). The EGFR is the founding member of the ErbB family of receptor tyrosine kinases that together coordinate complex signalling systems that underpin organogenesis and differentiation of several cell lineages (Citri and Yarden, 2006). The ErbB family also comprise of 3 other members: HER2/Neu/ErbB2, HER3/ ErbB3 and HER4/ErbB4. It includes an extracellular-binding domain, a transmembrane domain and an intracellular domain containing active tyrosine kinase (Yarden and Sliwkowski, 2001). The EGFR can be activated by different ligands containing the EGF motif that is ~40 amino acids in length with 6 cysteines arranged as amino acid disulphide bridges (Schneider and Wolf, 2009). These bridges are between C1 and C3, C2 and C4, C5 and C6 to form the ABC loops (Figure 1.1). Ligands include EGF, transforming growth factor-α (TGFα), heparin-binding EGF-like growth factor (HB-EGF), betacellulin (BTC), amphiregulin (AREG), epiregulin (EREG), epigen (EPGN) and neuregulins (NRG) (Scneider and Wolf, 2009). The ligands are differentially expressed depending on tissue type (Yarden and Sliwkowski, 2001).

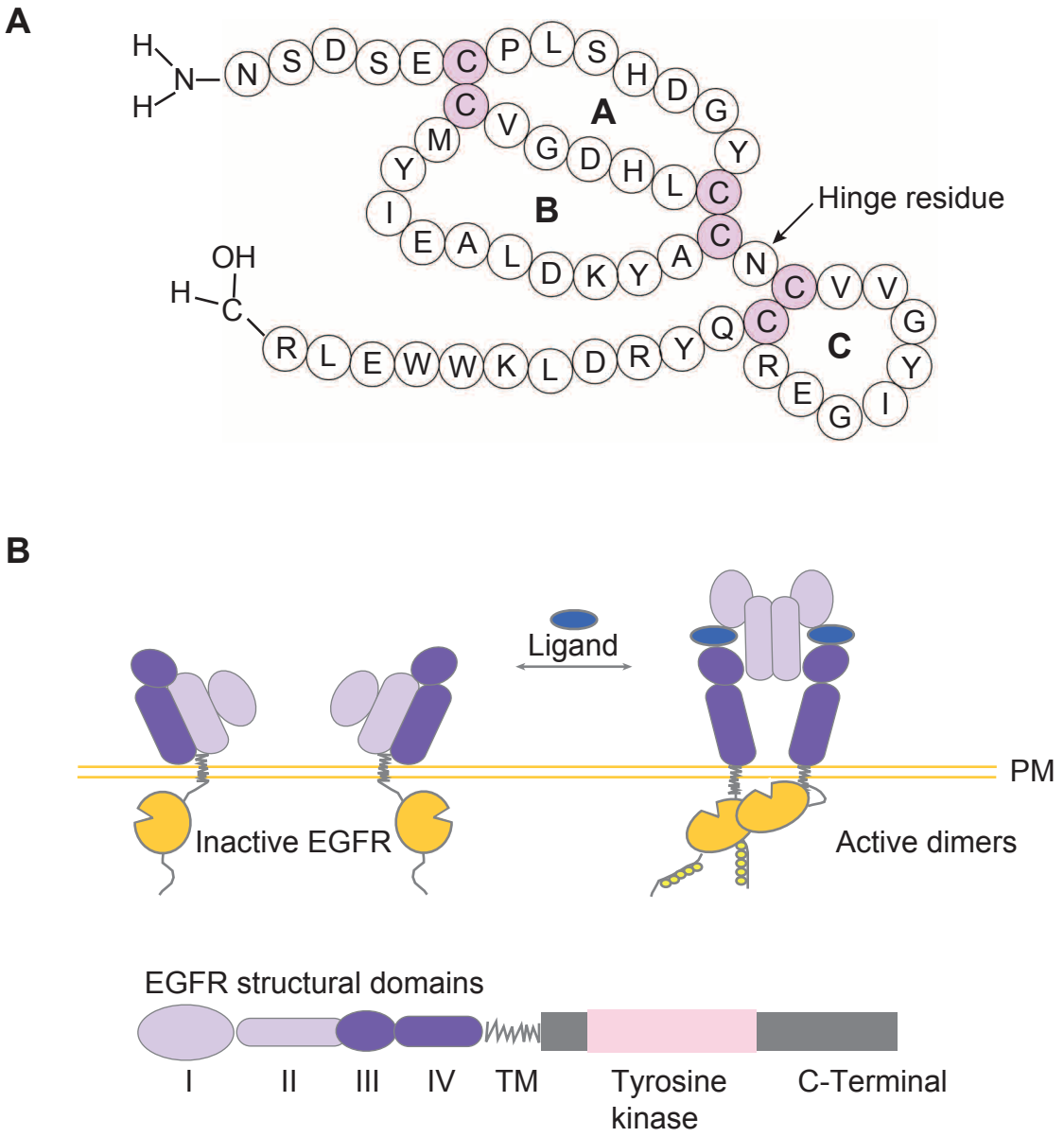


**Figure 1.1. The structures of the EGF and its receptor.** The schematic representation of the secondary structure of the EGF motif (~40 amino acids) show interaction between the six conserved cysteines and the resulting loops (A, B and C). The single amino acid between B and C loops is known as the 'hinge residue' proposed to function as a hinge where both segments of the protein can move. (Adapted from Schneider and Wolf, 2009).(B) Ligand binding to domain I and III of EGFR allows conformation change that exposes dimerisation site on domain II to dimerise EGFR and allow downstream phosphorylation on the cytoplasmic tails of receptors. PM, plasma membrane; TM, transmembrane, roman numerals, domain numbers. (Adapted from Lemmon and Schlessinger, 2010; Kumar et al., 2008).

The first effort to partially clone the gene of EGFR obtained from A431 cells disclosed high amino acid sequence homology to the oncogenic kinase of avian erythroblastosis virus (v-ErbB) that transformed chicken fibroblasts (Downward et al., 1984). Subsequent revelation of the full cDNA sequence of human EGFR isolated from normal placental cells and A431 tumour cells showed that the virus had maintained only the kinase portion of the chicken EGFR omitting the extracellular domain (Ullrich et al., 1984). The cDNA of EGFR was overexpressed in oncogenic A431 cells when compared to placental cells. That was further supported by the findings that revealed elevated EGFR levels in head and neck squamous carcinoma (HNSCC) tissue specimens (Hendler et al., 1984). This subversion of the EGFR kinase activity by the avian virus was proposed to promote tumorigenesis.

A few years previously, Hunter and Sefton discovered that protein can be modified by tyrosine phosphorylation in sarcoma tumour virus, v-Src (Hunter and Sefton, 1980). This was the first indication that deregulated protein tyrosine phosphorylation may drive tumorigenesis. Building on this discovery, Ullrich and colleagues discovered that the ligand of the insulin receptor (IR), insulin, activated a chimeric receptor comprising of extracellular region of IR combined with transmembrane and intracellular domains of the EGFR (Riedel et al., 1986). This and other studies subsequently established that receptor tyrosine kinases (RTKs) dimerise and are autophosphorylated at key tyrosine residues of their catalytic domains in response to ligand activation (Gschwind et al., 2004; Schlessinger, 1988).

### *1.1.2 Mechanism of EGFR activation*

EGFR consist of 4 extracellular subdomains (I-IV), a transmembrane domain, intracellular juxtamembrane domain followed by the kinase domain and the C-terminal tail that has phosphorylation sites to provide docking sites for downstream effector signalling molecules (Citri and Yarden, 2006). Bivalent ligand binding to the extracellular domains I and III of the EGFR leads to a conformational change that exposes domain II (dimerisation arm). This allows dimerisation of EGFRs (Figure 1.1; Lemmon and Schlessinger, 2010). DOMAINS II in inactive receptors interact with extracellular domain IV in a ‘tethered’ conformation to inhibit ligand binding and receptor dimerisation. Formation of homo- or heterodimers of EGFR and members of the ErbB family is succeeded by the formation of asymmetric kinase domain dimer in the juxtamembrane region. This head-to- tail configuration catalyses the trans and autophosphorylation of tyrosine sites on the C-terminal tail of the receptors (Kumar et al., 2008). Phosphorylation of tyrosine residues in the C-

terminal tail provides docking sites for multiple downstream effectors (Schulze et al., 2005; Figure 1.2).

The identity of ligand and dimerisation partners of EGFR dictate the autophosphorylation sites on the dimerised EGFR which in turn allows the binding and activation of specific cytoplasmic target proteins, although degeneracy of effectors binding to the EGFR has been reported (Yarden and Sliwkowski, 2001; Citri and Yarden, 2006). For example, Grb2 (growth factor receptor bound protein 2) is able to associate directly to the EGFR but also through Shc (Src homology 2 domain containing transforming protein 1). Although the Grb2 binding to the EGFR may be redundant, the different modes of binding of Grb2 to the EGFR may recruit different effector proteins and the duration of binding may alter the biological outputs.

### *1.1.3 Canonical downstream signalling pathways regulated by EGFR*

EGF stimulation initiates multiple signalling cascades including the phosphatidyl-inositol 3 kinase, PI3K and several mitogen activated protein kinase, MAPK pathways (Figure 1.3) of which the ERK pathway is best understood (Katz et al., 2007).

The PI3K signalling pathway can be activated by different ligands that bind to the receptors in the ErbB family. For example, Neuregulin 1 (NRG1) preferentially binds to Erb3 which heterodimerises with ErbB2 to activate PI3K (Roskoski, 2014). PI3K phosphorylates phosphatidylinositol 4,5-biphosphate ($PIP_2$) to form phosphatidylinositol 3,4,5-triphosphate ($PIP_3$) that binds and activate Akt (Figure 1.3). The PI3K-Akt pathway relays pro-survival signals throughout the cytoplasm and in the nucleus. For example, PI3K-AKT signals inhibit translocation of transcription factor FOXO (Forkhead family of transcription factor) into the nucleus, thus inhibiting transcription of pro-apoptotic FOXO target genes such as Bcl2 family members (Fu and Tindall, 2008; Nyati et al., 2006).

Stimulation of EGFR by EGF activates the RAS-MAPK cascade either directly via the Grb2 adaptor protein or indirectly via Shc1 adaptor proteins (Nyati et al., 2006; Yarden and Sliwkowski, 2001). Ras in turn is activated by its guanine nucleotide exchange factor (GEF), son of sevenless (SOS) (Figure 1.3). Activated Ras then binds to Raf (MAP kinase kinase kinase) to trigger phosphorylation of MEK1/2 (mitogen-activated protein kinase kinase 1/2) and ERK1/2 (extracellular signal-

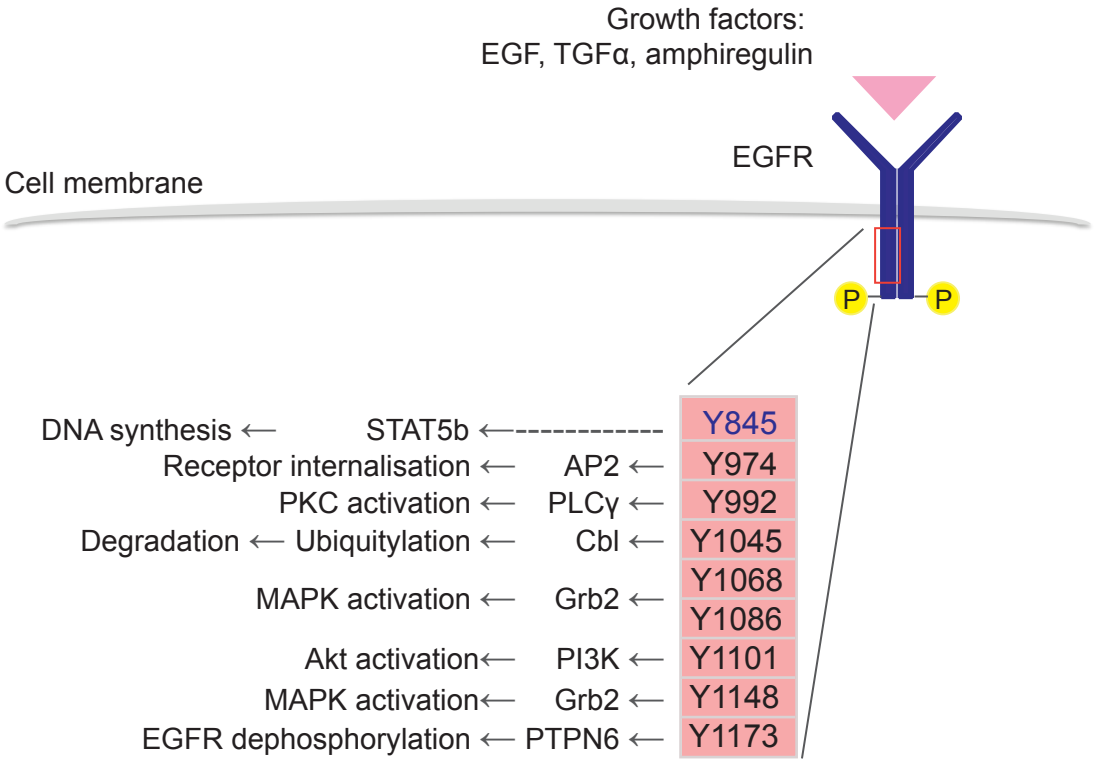


**Figure 1.2. A simplified schematic view of EGFR showing key phosphorylation residues and main downstream cascades.** Ligand binding activates receptor to form homo or heterodimers that activate auto or trans-phosphorylation sites within the C-terminus as annotated above (Schulze et al., 2005). Y845 phosphorylation (Src kinase phosphorylation site in purple) maintains receptor in an activated state by stabilising the activation loop to regulate signal transducer and activator of transcription 5b (STAT5b) activity. Y974 acts as docking site for adaptor protein 2 (AP-2) binding motif to allow receptor internalisation upon ligand stimulation. Phosphorylated Y992 site allows binding of phospholipase Cγ (PLCγ) to activate the Protein kinase C (PKC) signalling pathway. Phosphorylation at Y1045 forms a docking site for Cbl to facilitate receptor ubiquitylation and degradation. Phosphorylated sites at Y1068 and Y1086 allows binding of growth factor receptor-bound protein 2 (Grb2) via its Src homology 2 (SH2) domain to activate downstream MAPK signalling. Binding of Protein tyrosine phosphatase, non receptor type 6 (PTPN6) dephosphorylates EGFR. Receptors are not drawn to scale and this is not a comprehensive list of phospho-tyrosine binding sites (Adapted from Nyati et al., 2006; Olayioye et al., 2000).

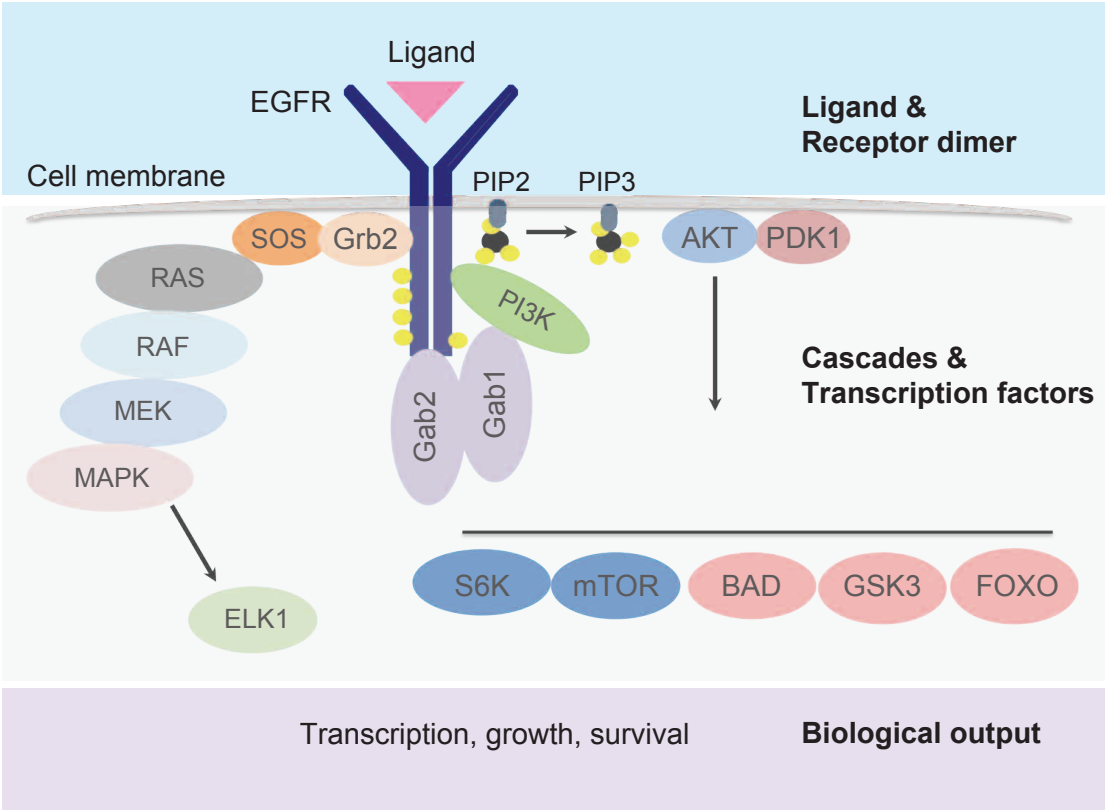


**Figure 1.3. Main effector pathways activated by EGFR.** Binding of ligand to EGFR can activate both the Ras/ MAPK and the PI3K/Akt signalling pathways. Recruitment of Grb2 via the SH2 domain activates SOS which binds and activate Ras. Activated Ras binds RAF to stimulate the MEK and MAPK leading to the translocation of ERK1/2 (component of MAPK) into the nucleus to activate various transcription factors such as ELK1. Ligand activation can also recruit adaptors Gab1 and Gab2 that binds to PI3K, allowing the phosphorylation of PIP2 to PIP3. PIP3 binds AKT at its pleckstrin homology (PH) domain and activated Akt recruits PDK1 to the membrane, activating downstream cascades of signals. The ligand and receptor dimer represent signal input, cascades and transcription factor reflect the relay of signals in cytoplasm and the nucleus which leads to biological outputs. The signalling cascades illustrated do not include all the known components in the given pathway and cross talk is not shown to simplify schema. Target proteins (coloured ovals) are not drawn to scale. Abbreviated protein names are listed in Abbreviations (Adapted from Nyati et al., 2006; Yarden and Sliwkowski, 2001).

regulated kinases 1/2). Phosphorylated ERK is imported into the nucleus to activate various transcription activators such as ELK (ETS domain containing protein Elk-1) that allow target gene transcription (Katz et al., 2007). From a cell biological perspective, the key EGF-mediated responses defined are mitogenic and motogenic.

### *1.1.4 Multi-layered network of EGFR signalling and its therapeutic potential*

Detailed characterisation of ErbB family structures and specificity of ligands led to the proposal that the parallel linear signalling cascades feed into multi-layered signalling networks to integrate extracellular stimuli to affect downstream transcription and biological outputs (Yarden and Sliwkowski, 2001). This ultimately provides many possible therapeutic targets for diseases that stem from aberrant ErbB family signalling events (Gschwind et al., 2004; Yarden and Sliwkowski, 2001; Yarden and Pines, 2012). Mutation and overexpression constitutively activate the network in a variety of carcinomas, rendering the ErbB family receptors as rational drug targets for therapeutic intervention (Gschwind et al., 2004).

Her2/ErbB2 receptor is found to be overexpressed in 20% to 25% of breast cancers and has been effectively targeted for therapy (Masuda et al., 2012). EGFR overexpression on the other hand is observed in all subtypes of breast cancer but is more commonly overexpressed in triple negative breast cancer (negative for oestrogen, progesterone and Her2) and inflammatory breast cancer (Masuda et al., 2012). Approximately 20% of human breast cancer immunohistochemical samples have been characterised with EGFR overexpression, which negatively correlates with clinical prognosis and therapeutic response (Abd El-Rehim et al., 2004). Paradoxically, the ability of cells to redirect signals via parallel cascades allows tumour cells to develop resistance to targeted treatments.

Mendelsohn and colleagues pioneered the development of mouse monoclonal antibodies that targeted extracellular epitopes of EGFR to limit EGF signalling in cultured tumour cell lines and rodent models (Gill et al., 1984; Kawamoto et al., 1983; Sato et al., 1983). Almost in tandem, Umezawa et al. (1986) detected an inhibitor compound of EGFR autophosphorylation, Erbstatin isolated from the medium of Gram-positive bacteria. Subsequently, the design of EGFR inhibitors based on the structure of Erbstatin inhibited the proliferation of EGFR overexpressing A431 cells (Yaish et al., 1988). Nearly two decades later, Gefitinib was approved as a small molecule tyrosine kinase inhibitor to treat non-small cell

lung cancer (NSCLC) in Japan and America followed the year after (Cohen et al., 2003; Fukuoka et al., 2003). However, the targeted action of small molecule inhibitors have been increasingly associated with cancer recurrence due to the ability of tumour genome to evolve and overcome drug therapies after prolonged treatment. It remains a caveat to develop effective cancer therapies that prevent or override drug resistance.

### *1.1.5 Physiological relevance of EGF signalling*

The EGF was first discovered for its ability to induce early eyelid opening and tooth eruption in newborn mice (Cohen et al., 1962). Since then, endless studies have evaluated the relevance of EGF signalling in animal and cell models to mimic developmental and oncogenic processes. For example, mice lacking EGFR show defects in hair follicle, eyelid closing, heart valve and lung maturity. These effects were also recapitulated in mice that were deficient in EGFR ligands (Schneider and Wolf, 2009).

EGF has not been reported to be important during involution of adult mouse mammary gland. Instead, addition reduced the number of ducts per mammary gland in the highly proliferative glands of pubertal mice (Coleman and Daniel, 1990; Watson and Khaled, 2008). EGF was reported to induce mammary epithelial cell branching in collagen organotypic culture and rescued mammary development of ovariectomised pubertal mice (Coleman et al., 1988; Nelson et al., 2006). The EGFR has also been found in either the stromal cells during mouse pubertal development or in luminal ductal epithelial cells during lactation suggesting specific roles in autocrine and paracrine signalling (DiAugustine et al., 1997; Wiesen et al., 1999). Downstream of the EGFR, branching of the mammary duct depends on sustained MAPK signalling while proliferation of epithelial cells follows transient MAPK signalling (Gjorevski and Nelson 2011; Fata et al., 2007). This suggests that the EGFR in different cell types within the mammary gland plays different roles according to the available spatial-temporal cues at different phases of mammary morphogenesis. Also, EGF is known to stimulate mouse mammary cell differentiation and circulating levels *in vivo* increase during gestation (Okamoto and Oka, 1984).

### 1.2 Implication of EGFR signalling on cell-cell junctions

Cell-cell adhesion is essential to maintain tissue integrity, allowing differentiation and communication within multicellular organisms and between cells and its environment (Wong, 2010; Franke 2009). Modulation of cell-cell adhesion occurs in epithelial-to-mesenchymal (EMT) transition that is important in development, wound healing and cancer cell metastasis (Kalluri and Weinberg, 2009; Lorch et al., 2004; Nekrasova and Green, 2013). The signalling cascades that relate alteration of intercellular adhesion to tumour invasion and metastasis are not well understood. EGFR activation has been shown to reduce intercellular adhesive strength in murine keratinocytes and also promote cancer cell metastasis (Kalluri and Weinberg, 2009; Yin et al., 2005).

In vertebrates, cellular adhesion sites include tight junctions that act as epithelial barriers, gap junctions which binds neighbouring cells electrically and chemically, and cadherin-based anchoring junctions: Adherens junctions (AJ) and desmosomes that link transmembrane cadherin proteins to actin and intermediate filaments respectively (Figure 1.4). These junctions synergise to confer adhesive strength between cells (Huen et al., 2002). Both types of adhesive junctions are connected to the cytoskeleton via adaptor proteins. One such, Plakoglobin (PG) is a constitutent of both AJ and desmosomes. Another, Desmoplakin (DP), is specific to desmosomes and is required for strong cellular adhesion and integrity of epithelia *in vitro* and *in vivo* (Figure 1.5).

Desmosomes were first identified in vertebrates and are historically considered ‘spot weld’ sites of cell-cell adhesion that maintains the mechanical integrity of cells by tethering intermediate filaments to the plasma membrane (Garrod, 2010; Green et al., 2010; Nekrasova and Green, 2013). These are most abundant in stratified epithelia and appear as paired electron-dense plaques that between neighbouring cells and contain two members of the Cadherin family proteins, Desmogleins and Desmocollins (Dubash and Green, 2011; Franke, 2009). Mechanisms that govern the assembly of desmosomal components have not been substantively studied due to the biochemical insolubility of desmosomes (Nekrasova and Green, 2013).

It has been reported that desmosomal assembly and stability can be regulated by the status of EGFR activation. Prolonged EGF stimulation (18 hours) in murine keratinocytes led to the phosphorylation of PG that promoted the dissociation of DP away from the desmosomes, to reduce intercellular strength (Yin et al., 2005).

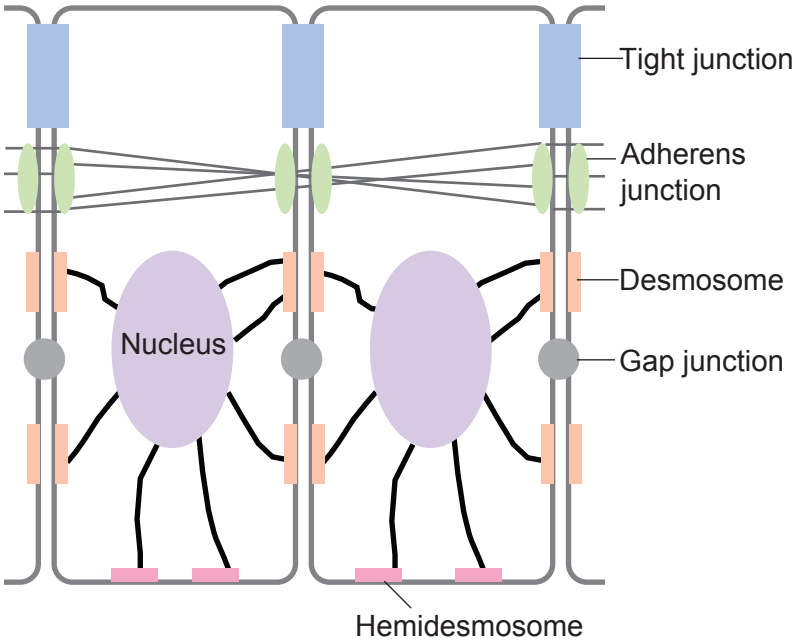


**Figure 1.4. Schematic representation of junctional complex in epithelial cells.** The junctional complex in epithelial cells consist of tight junctions, adherens junctions and desmosomes. Together with gap junctions these allow cells to function as polarised epithelial sheets. Hemidesmosomes are commonly found at the basal side where cells attach to subtratum. Geometrical shapes represent types of junctions as annotated. Light grey lines depict actin microfilaments connected to adherens junctions and black lines represent intermediate filaments tethered by desmosomes. (Adapted from Green and Gaudry, 2000).

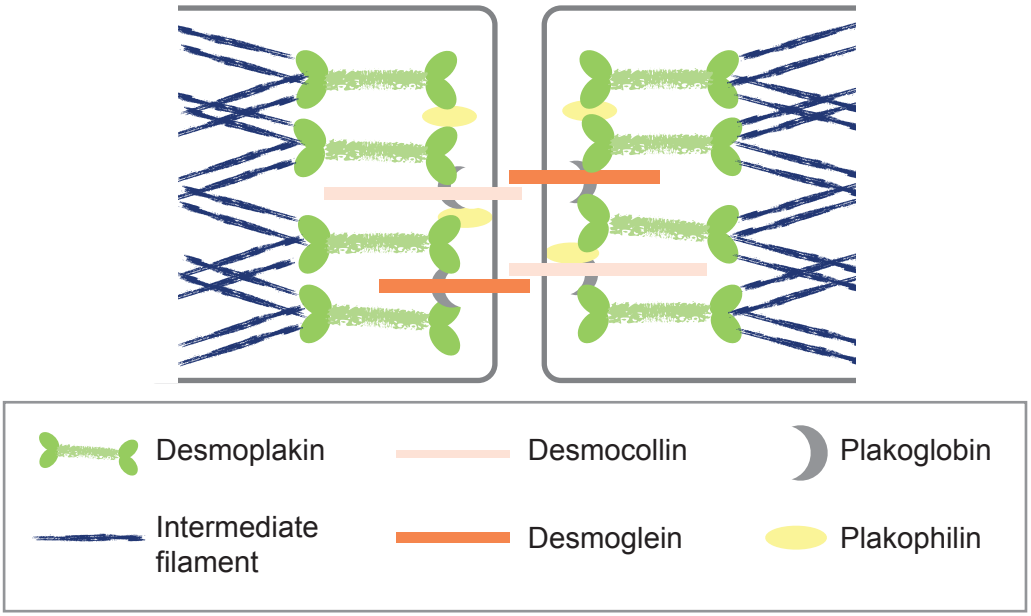


**Figure 1.5. A simplified model of desmosomal components.** Desmosomes confer adhesive strength between cells. Desmosomal plaques consist of Cadherin family proteins, Desmocollin and Desmoglein which interact on apposing cell membranes. These are connected to adaptor molecules, Plakoglobin and Plakophilin which allows tethering of plaques to Desmoplakin. Desmoplakin links the desmosomal plaques near cell membranes to intermediate filaments throughout cells. (Adapted from Fuchs and Raghavan, 2002).

However, short term EGF application (1 hour) failed to mimic this observation. In squamous carcinoma cells, EGFR inhibition reduces phosphorylation of Dsg2 and PG leading to an opposite phenotype, where desmosome assembly and intercellular adhesive strength is enhanced (Klessner et al., 2009; Lorch et al., 2004; Nekrasova and Green, 2013). This enhancement of adhesive strength is proposed to be mediated by the inhibition of proteolytic shedding of Dsg2 ectodomain, allowing recruitment of desmosomal cadherin and DP to cell-cell borders. However, in these studies, the authors did not report whether these assembly processes are reversible. Klessner et al., (2009) speculated that the desmosome-associated components might become relevant therapeutic targets in cancers to oppose the loss of cellular adhesion that is common prior to the migration of cancer cells.

Adherens junctions consist of cadherin/ catenin complex and nectin/ afadin complex which has been reviewed in detail elsewhere (Niessen and Gottardi, 2008). The discovery of the first component of AJ, E-cadherin (epithelia) was required to compact morula in the early stages of embryogenesis in chinese hamster lung cells, V79, in a calcium dependent manner (Takeichi 1977; Yoshida-Noro et al., 1984). In retrospect, cadherins have been reported to appear in single-celled organisms, ie. *Monosiga brevicollis* and is speculated to aid the binding of bacterial prey (King et al., 2008). Subsequent identification of other classical cadherins includes P-cadherin (placental), N-cadherin (neuronal) and VE-cadherin (vasoendothelial) (Pettitt, 2005). Assembly of AJ is reported to supersede the assembly of other intercellular junctions (Gumbiner et al., 1988; Green et al., 2010). Inactivation and ablation of the E-cadherin gene in mice caused perinatal death due to defective tight junction assembly, which led to leaky epidermal water barrier and disrupted the assembly of desmosomes (Tunggal et al., 2005; Lewis et al., 1997). Activation of EGFR has been reported to disrupt cell surface E-cadherin stability and induce motility (Duan et al., 2010). On the other hand, interaction of surface E-cadherin inhibits transphosphorylation of EGFR at Y845 and downstream activation of STAT5 (Signal Transducers and Activators of Transcription 5) that limits cell growth in confluent monolayers, termed cell-cell contact inhibition (Perrais et al., 2007).

### *1.2.1 Endocytosis maintains dynamic junctions*

Endocytosis is the process of trafficking membrane bound components, activated receptors and solute molecules into cells to undergo different fates (Maxfield and McGraw 2004). The different endocytic routes commit trans-membrane proteins such as E-cadherin to achieve three main fates: recycling back to the membrane,

temporary sequestration of E-cadherin by routing proteins to sorting and recycling endosomes or trafficking to the late endosomes for lysosomal degradation (Bryant and Stow, 2004).

Adherens junctions of cells can be regulated via endocytosis and the dysregulation in this process leads to pathogenicity (Green et al., 2010). Stimulation of cells with EGF favours the internalisation of E-cadherin leading to increased mobility (Duan et al., 2010) whilst inhibition of EGFR disrupts internalisation of E-cadherin and Desmoglein 2 to increase adhesion of tumour cells (Lorch et al., 2004; Klessner et al., 2009). Disruption of cadherins endocytosis has also been implicated in tumour progression (Mosesson et al., 2008). In non-malignant cells, E-cadherin is constantly internalised, recycled and turnover to maintain dynamicity of cell-cell adhesion especially in epithelial morphogenesis (Wirtz-Peitz and Zallen, 2009).

Both adherens and desmosomal junctions are maintained in a calcium dependent manner. However, desmosomal junctions can achieve a hyper-adhesive state that is calcium independent in confluent and prolonged culture (Kimura et al., 2007). However, internalisation of desmosomal cadherins have been linked to the autoimmune disease pemphigus vulgaris (Green et al., 2010). Stimulation of human squamous carcinoma cells with pemphigus vulgaris (PV) autoantibody induced clathrin and dynamin independent internalisation of soluble pool of Desmoglein 3 proposed to disrupt assembly of nascent desmosomes (Aoyama and Kitajima, 1999). Bo Van Deurs' group reported internalisation of mature desmosomes upon chelation of calcium independent of clathrin dependent endocytosis but requires actin polymerisation (Holm et al., 1993).

## 1.3 Regulation of cytoskeleton remodelling

### *1.3.1 The cytoskeleton*

The cytoskeleton serves three main roles in eukaryotic organisms: to physically separate contents within cells, to allow traffic of intra and intercellular cargoes, and to allow force generation needed for cell movement and morphogenesis (Fletcher and Mullins, 2010). The most studied groups of cytoskeleton polymers include actin filaments, microtubules and intermediate filaments that have largely been studied as separate entities. However, burgeoning evidence of dynamic crosstalk between these filamentous polymers is emerging to provide clues as to how the cytoskeletal network co-ordinate molecular signals, cell shape and mechanics.

The different cellular polymers differ in mechanical stiffness, assembly programmes, polarity and associated molecular motors (Fletcher and Mullins, 2010). Microtubules are most rigid with complex assembly and disassembly programmes. These are dynamically unstable as microtubules can dynamically grow and rapidly shrink. During mitosis, the dynamic microtubules form the mitotic spindle to align and separate chromosomes. The rapidity of microtubule growth and shrinkage allows these polymers to sense space quicker than other polymers that respond to either chemotactic gradients or activity of other regulatory proteins (Fletcher and Mullin, 2010).

Actin filaments are less rigid but are able to form stiff, organised networks that can be either bundled or branched (Fletcher and Mullins, 2010). Bundled actin filaments are commonly seen in filopodial protrusions that allow chemical sensing in the intercellular environment (Gupton and Gertler, 2007). Branched filaments are enriched especially at the leading edges of motile cells or cells forming initial contact with neighbouring cells (Ridley, 2011; Hoelzle and Svitkina, 2012). These branches of filaments generate forces that allow shape changes to accommodate cell movements. The presence and location of actin regulators: nucleation factors such as Arp2/3 complex and formins dictate the organisation of networks formed (Ridley, 2011; Section 1.3.3). Steady addition of nucleotide monomers to the growing end of actin filaments provide sustained mechanical forces to advance migrating cells (Fletcher and Mullins, 2010).

Many cell types form intermediate filaments to allow cells to resist mechanical stress such as those seen in keratinocytes and airway epithelial cells (Fletcher and Mullins, 2010). Actin and microtubules depend on nucleotide binding, hydrolysis and polarise to allow trafficking of molecular motors (Chang and Goldman, 2004). Intermediate filaments are not reported to have enzymatic activity and lack the ability to polarise compared to the actin and microtubule filaments (Fletcher and Mullins, 2010). Instead, these least stiff polymers resist tensile forces and can be cross-linked to each other, actin filaments and microtubules by plectins, which organises a subset of intermediate filaments in cells (Fletcher and Mullins, 2010). These networks extend in all directions, from the cell surface (to tether mature desmosomal plaques) to cage-like structures surrounding the nucleus that contains polymerised nuclear lamins (Chang and Goldman, 2004). When nuclear lamins are phosphorylated by cyclin-dependent kinase, this triggers the nuclear envelope initial breakdown in

mitosis, suggesting that they provide mechanical integrity to the eukaryotic nucleus (Fletcher and Mullins, 2010).

### *1.3.2 Cell migration*

Cell migration requires changes in cell shape mediated by the actin cytoskeleton in response to extracellular stimuli (Schmidt and Hall, 1998). Movement of cells has been studied extensively in animal development and cell cultures (Friedl and Gilmour, 2009; Ridley, 2011). To move across substrates, cells at the front, 'leading edge cells' have to extend their membranes (Ridley, 2011). Currently, four types of membrane protrusions coordinated by actin polymerisation have been identified. Leading edge protrusions include lamellipodia, filopodia, invadopodia and membrane blebs. Each type of structure aids cell migration depending on the biological circumstance. For example, lamellipodia protrusions propel cells through extracellular matrix (ECM) *in vivo* (Friedl and Gilmour, 2009). Filopodia act as sensors for chemo-attractants and are involved in relaying signals between cells (Gupton and Gertler, 2007). Invadopodia are protrusions that enable the degradation of the ECM to allow cell invasion (Mader et al., 2011). In development, membrane blebbing has been reported to direct cell migration (Charras and Paluch, 2008). These different types of protrusions can act separately or synergistically at the leading edge. For example, lamellipodia and filopodia coexist dynamically during the initial cell-cell junctions assembly in endothelial cells (Hoelzle and Svitkina, 2012).

### *1.3.3 Regulation of the actin cytoskeleton organisation*

Membrane associated complexes such as adherens junctions have been reported to act as nucleation sites of actin (Yamada and Geiger, 1997). Actin polymerisation is important to generate mechanical force for the cells to move forward. Numerous actin binding regulators mediate actin polymerisation, nucleation and cross linking to allow the dynamic assembly of actin monomers into polymers and eventually filamentous networks (Schmidt and Hall, 1998). One of the main drivers of new actin filament formation near membranes is the Arp2/3 complex (Actin related protein 2/3 complex) (Ridley, 2011). WASP (Wiskott-Aldrich syndrome protein) acts as a nucleation-promoting factor to stimulate the activity of the Arp 2/3 complex (Stevenson et al., 2012). The Arp2/3 complex binds the side branches of actin filaments to nucleate new branched actin filaments via actin polymerisation. Dysregulated expression of these proteins has been implicated in diseases. For

example, N-WASP (Neural WASP) has been found to be overexpressed in human invasive ductal carcinoma (Yu et al., 2012).

### *1.3.4 Regulation of the actin cytoskeleton orchestrated by GTPases signalling*

The network of actin cytoskeleton network also acts as a signalling hub in different cell structures (Schmidt and Hall, 1998; Yu et al., 2012). Ras homologous (Rho) family small GTPases are key signal regulators that integrate extracellular or intracellular stimuli with the assembly and organisation of actin cytoskeleton (Ridley, 2011; Schmidt and Hall, 1998). The most conserved Rho GTPases associated with actin-specific structures and migration include the Rac, CDC42 and RhoA that drive the formation of lamellipodia, filopodia and stress fibres initially discovered in fibroblasts (Abercrombie et al., 1970; Boureux et al., 2007; Ridley, 2011; Ridley and Hall, 1992; 2004). These Rho GTPases function as binary switches that cycle between active GTP-bound form and inactive GDP-bound forms (Figure 1.6). These molecular switches are regulated by guanine nucleotide exchange factors (GEF), GTPase activating proteins (GAP) or guanine nucleotide dissociation inhibitors (GDI) (Cook et al., 2014). RhoGEFs favour the formation of Rho-GTP to Rho-GDP by accelerating the intrinsic exchange activity (Ridley, 2011). RhoGAPs stimulate the intrinsic GTP hydrolysis activity of Rho GTPases to form the inactive GDP-bound state. RhoGDI binds Rho-GDP and sequesters the RhoGTPases from the cell membrane where RhoGTPases can be activated (Cook et al., 2014). The first RhoGEF discovered, Dbl from genomic DNA of the MCF7 human breast carcinoma cell line caused tumorigenic growth when transfected into NIH 3T3 fibroblasts (Fasano et al., 1984). Aberrant expression of GTPases and their regulators have since been implicated in cancer such as upregulation of Rac-GEF PRex1 in human breast cancer that leads to cancer metastasis (Sosa et al., 2010; Wertheimer et al., 2012). In non-tumorigenic mammary epithelial cells, Rac1 activation via RacGEF Vav2 on cell membranes was implicated in the disassembly of adherens junctions implying the possibility of cell migration (Duan et al., 2011).

### *1.3.5 EGF regulation of cell shape*

Upstream of the cytoskeletal signalling modulators, EGF has been shown separately to induce cell shape change and is implicated in cell motility. Often, this has been studied in oncogenic cell systems. For example, metastatic rat mammary adenoma cells, MTLn3 extend lamellipodia towards EGF upon stimulation (Bailly et al., 1998; Bailly et al., 2000). Invasive bladder cancer cells displayed higher levels of EGFR at the tumour regions than the sites further from the tumours (Rao et al.,

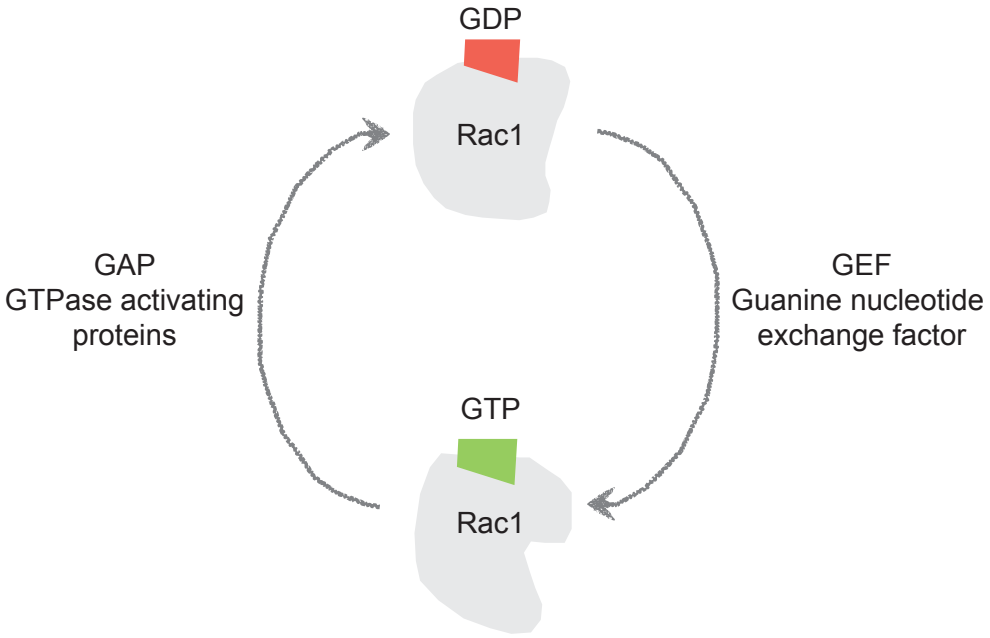


**Figure 1.6. Schematic representation of modulation of Rac activity by GEFs and GAPs.** Rac GTPase cycles between active GTP-bound state to inactive GDP-bound state to regulate actin cytokeleton organisation. This molecular switch is regulated by guanine nucleotide exchange factors (GEF) which accelerates the intrinsic exchange activity to favour the Rac-GTP bound form. In contrast, GTPase activating proteins (GAP) stimulate the intrinsic GTP hydrolysis activity of Rac to form Rac-GDP. (Adapted from Ridley, 2011; Wertheimer et al., 2012).

1993). EGF also disrupts adhesion of weakly metastatic A431 cells by rounding up and ruffling (Chinkers et al., 1981). Non-malignant human mammary epithelial cells acquire dose dependent motility upon EGF stimulation (Joslin et al., 2007). The similar motogenic effects of EGF in both oncogenic and non-tumorigenic systems highlight the subversion of a normal cell feature into an oncogenic property.

### 1.4 Physiological contexts of interdigitations in non-tumorigenic systems

Interdigitations are common features in other complex epithelial cells and have been reported in kidney podocytes, keratinocytes and endothelial cells (Baluk et al., 2007; Hoelzle and Svitkina, 2012; Mundel et al., 1995; Vasioukhin et al 2000). Ultrastructural studies have described well-developed cytoplasmic interdigitations of mammary epithelial cells isolated from human donor post weaning breast milk (Russo et al., 1975). During early embryonic development and puberty, the elongated tips of mammary buds form multi-layered epithelia, and cells within the interior layers show prominent interdigitation and high levels of desmosomes (Ewald et al., 2012).

Podocytes in kidney have been characterised to form interdigitating foot processes that attach to glomerular basement membrane (GBM) but remain connected via slit membranes (Mundel and Kriz, 1995). The gaps between digits allow ions and solutes to filter through the glomerulus. In keratinocytes and endothelial cell cultures, interdigitations form prior to the assembly of stable adherens junctions and cell-cell contact (Hoelzle and Svitkina, 2012; Vasioukhin et al., 2000). These structures require actin reorganisation and reflect basal phenomena in subconfluent cell cultures without ligand stimulation. Oak leaf-shaped lymphatic endothelial cells display striking interdigitations decorated by cadherins and tight junctions (Baluk et al., 2007; Yao and McDonald, 2014). These were reported to reside specifically at the initial rather than the distal lymphatics to facilitate flow of fluids especially in newborn mice (Pflicke et al., 2009; Yao and McDonald, 2014). In induced inflammation, digits regressed and fluid flow was disrupted. Despite burgeoning evidence of interdigitation in physiological systems, molecular pathways that control the decision between smooth and interdigitated cell boundaries have not been dissected in vitro.

## 1.5 Non-tumorigenic mammary epithelial cells

### *1.5.1 MCF10A cells*

MCF10A are non-tumorigenic mammary epithelial cell, which were originally derived from subcutaneous mastectomy tissue of a 36 year-old parous, premenopausal woman diagnosed with benign fibrocystic disease (Tait et al., 1990; Soule et al., 1990). These cells were spontaneously immortalised and were characterised as pseudodiploid luminal ductal cells (Tait et al., 1990). MCF10A cells are negative for oestrogen receptors, and have been classified as both basal and luminal of origin, depending on the method of classification. Histocytochemical staining of relevant keratins in MCF10A favours the luminal classification (Tait et al., 1990). On the other hand, technologies using DNA, CGH (Complete Genome Hybridisation) arrays and their phenotype in 3D culture tend to classify MCF10A as basal breast epithelial cells (Debnath et al., 2003; Neve et al., 2006; Charafe-Jauffret et al., 2006; Simpson et al., 2008).

Modern single-nucleotide polymorphism (SNP) arrays revealed that immortalisation of MCF10A cells was due to the amplification of Myc on chromosome 8q24 and deletion of CDKN2A (cyclin-dependent kinase inhibitor 2A) gene on chromosome 9q21.3 (Kadota et al., 2010). C-Myc is a proto-oncogene that acts as a multifunctional transcription factor regulating a myriad of cellular processes including cell cycle, growth, metabolism and genomic stability (Campaner and Amati, 2012). CDKN2A/ p16 induces cell cycle arrest in G1 and G2 phase, and the homozygous loss has been postulated to initiate the process of immortalisation of MCF10A cells (Cowell et al., 2005). Karyotypic analysis of late passage cells demonstrated the genetic stability of these cells in culture with relatively minimal rearrangements (Soule et al., 1990; Vitolo et al., 2009). Another group that used CGH arrays showed that MCF10A cells overexpress SLD5 (DNA replication complex GINS protein SLD5), THAP1 (THAP domain containing apoptosis associated protein 1) and TMEPAI (transforming growth factor-β (TGF-β)–induced transmembrane protein) (Neve et al., 2006). SLD5 in the GINS complex has been characterised as a novel factor to initiate and elongate DNA during DNA replication (MacNeill, 2010). THAP1 is a DNA binding transcription factor that regulates endothelial cell proliferation and G1/S cell-cycle progression (Cayrol et al., 2007). TMEPAI overexpression has been linked to growth of breast cancer cells (Singha et al., 2010). Despite identification of these genetic aberrations, none have been reported to confer malignancy or transform MCF10A cells without exposure to external carcinogen.

Experimentally, MCF10A cells are characterised as 'near normal mammary epithelial cells' as growth in culture requires hormones and growth factors. In 2D cell culture, they organise into 'cobblestone' monolayers (Soule et al., 1990). They also grow and form three-dimensional structures in collagen and Matrigel (Debnath et al., 2003; Soule et al., 1990). Crucially these cells lack anchorage-independent growth and tumorigenicity in nude mice (Soule et al., 1990).

### *1.5.2 MCF10A cells in three-dimensional (3D) culture*

The mammary gland is a unique organ named after an entire class of animal and demonstrates remarkable plasticity throughout a mammalian's lifetime from development to puberty and finally during pregnancy and lactation (Gjorevski and Nelson, 2011). It consists of a branching network of ducts lodged within an adipocyte rich environment (Campbell and Watson, 2009). The bilayer of luminal and myoepithelial cells maintains the ductal epithelium with the latter in contact with the basement membrane (Figure 1.7). Knowledge of the signals and mechanisms regulating gland remodelling *in vivo* remain fragmented due to the difficulty in mimicking the exact processes *in vitro* (Campbell and Watson, 2009).

MCF10A cells have been cultured in 3D environments using different substrates such as collagen and reconstituted basement membrane, Matrigel. Culture in collagen allows formation of duct-like structures whereas in Matrigel, growth suppressed cyst-like acini spheroids form from MCF10A cells (Debnath et al., 2003; Soule et al., 1990; Chapter 3: Figure 3.10).

The development of MCF10A cells into complex structures *in vitro* allows extensive research to interrogate the molecular mechanisms involved in mammary gland morphogenesis during normal processes and the subsequent dysregulation in cancers. Brugge and colleagues have dissected in detail the morphogenetic processes involved in the formation and polarisation of non-malignant MCF10A cells within acini (Debnath et al., 2003; Debnath et al., 2005). One of the important non-malignant characteristics preserved in MCF10A acini is the suppression of proliferation and lumen clearance observed in the final stages of acini development. This parameter allows researchers to elucidate the effects of introducing oncogenic mutations in this aspect of mammary alveolar morphogenesis (Debnath et al., 2003; Isakoff et al., 2005).

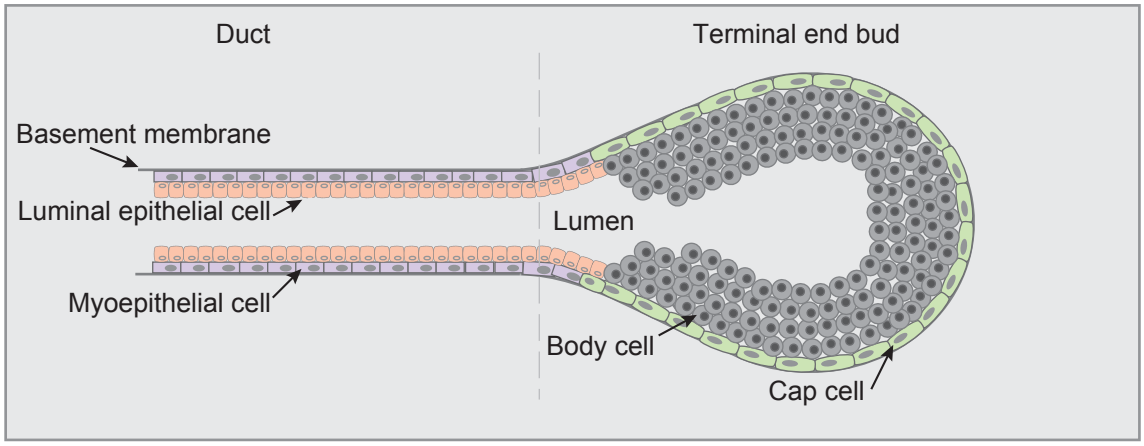


**Figure 1.7. Simplified schema of mammary duct and terminal end bud.** In mature mammary glands, branches of mammary ducts are embedded within mammary fat pad. Mammary ducts consist of myoepithelial cells that surround luminal epithelial cells and attach to basement membrane. These ducts mature into terminal end buds during puberty. Terminal end buds contain body cells that have reduced polarity and undergo dynamic rearrangements with a surrounding layer of cap cells at the leading edge. (Adapted from Gjorevski and Nelson, 2011).

### *1.5.3 HMT-3522 cells*

HMT-3522 cells are a non-tumorigenic human mammary epithelial cell line characterised by Briand et al (1987). The cells were isolated from an explant of mammary tissue from a 50-year old Caucasian woman with non-malignant fibrocystic breast tissue, similar to MCF10A cells. Since then, HMT-3522 cells have been characterised in 2D culture as 'normal human mammary epithelial cells that remain undifferentiated in subconfluent cultures and near diploid, non-tumorigenic in athymic mice. Although undifferentiated, they were originally classified as luminal due to their immunohistochemical expression of the luminal marker, cytokeratin 18 (Briand and Lykkesfeldt, 2001). In 2D culture, the polygonal cells form characteristic small, and uniform islands.

The HMT-3522 S1 cells that have been used in this thesis were obtained from ECACC (European Collection of Cell Cultures). These were derived from the original HMT-3522 cells (passage 34) cultured without collagen (Briand and Lykkesfeldt, 2001). The HMT-3522 cells have wild-type TP53. They show minor kartotypic abnormalities including the loss of chromosomes in group D (chromosomes 13-15) and the presence of extrachromosomal gene amplification in 10% of metaphases counted (Briand et al., 1987). At the ultrastructural level, the monolayer of the epithelial cells are polarised and show microvilli on the apical surface whilst foldings and irregular projections decorate the basolateral surface (Briand et al., 1987). The cells are maintained in a monolayer by well-developed desmosomes with associated bundles of intermediate filaments such as those characterised in MCF10A cells (Briand et al., 1987; Underwood et al., 2006). In 3D culture basement membrane assays, the HMT 3522 cells form acinar structures resembling normal MCF10A spheroids and breast tissue *in vivo* (Kenny et al., 2007; Underwood et al., 2006).

### *1.5.4 Growth medium of MCF10A cells*

Historically, the MCF10A cells have been cultured in complex medium to form epithelial monolayers (Soule et al., 1990). The growth medium consists of horse serum, EGF, insulin and cholera toxin as listed below:

| | Final concentration |
|---|---|
| DMEM/ F12 | 100% |
| Horse serum (HS) | 5% |
| EGF | 20ng/ ml |
| Insulin | 0.01mg/ml |
| Hydrocortisone | 500ng/ml |
| Cholera toxin | 100ng/ml |

**Table 1.1 Composition of MCF10A cell culture medium.** Brooks and collegues used this recipe during the establishment of MCF10A cells (Soule et al., 1990).

The additional supplements aid cell growth and proliferation via different signalling pathways. EGF and insulin are growth factors known to stimulate similar downstream signalling pathways such as the MAPK and PI3K pathways, which are implicated in cell survival, growth, proliferation, protein synthesis and cytoskeletal regulation (Engelman et al., 2009). EGF directly activates EGFR to propagate mitogenic pERK signals while insulin preferentially binds insulin receptor (IR) to relay pro-survival signals via the PI3K pathway (Boyer, 2008; Yarden and Sliwkowski, 2001; Siddle, 2011; Zielinski, 2009). In MCF10A cells, Boyer (2008) showed that EGF activated the MAPK (Mitogen activated protein kinase) and P70S6 (Ribosomal protein S6 kinase, 70kDa polypeptide). EGF also activated pAKT to a lesser extent when compared to insulin stimulation. Both ligands activated the 4EBP1 (eukaryotic initiation factor 4E binding protein) to a similar degree, indicating crosstalk downstream of the receptors. In HEK 293 and Swiss 3T3 cells, insulin and EGF synergise to enhance the mitogenic cue for proliferation (Borisov et al., 2009; Crouch et al., 2000). Together, this would explain the ability of MCF10A cells to proliferate without EGF, albeit at a slower growth rate (Soule et al., 1990).

Hydrocortisone (glucocorticoid) binds to glucocorticoid receptors in the cytoplasm, which translocate into the nucleus to regulate gene expression (Kadmiel and Cidlowski, 2013). It is also a lactogenic stimulus in cultured mammary tissue

explants (Okamoto and Oka, 1984). Hydrocortisone acts in synergy with fetal bovine serum (FBS) to promote human mammary epithelial cell cluster attachment and colony formation (Gaffney and Pigott, 1978). The combination of hydrocortisone, insulin and prolactin is required for functional differentiation of mammary epithelia in culture (Okamoto and Oka, 1984). Cholera toxin is a virulent factor released by the pathogen, *Vibrio cholerae* (Serezani et al., 2008). This heterodimeric AB toxin binds to cell membranes using the B subunit to allow translocation of the A subunit into the target cells. In the cytoplasm, the A subunit catalyses the ADP ribosylation of Gαs subunits bound to GPCR (G protein coupled receptors). The ribosylated Gα subunit then binds and stimulate adenylyl cyclase that generates cyclic AMP (adenosine monophosphate) to regulate gene expression in many processes including cell growth. In the context of MCF10A cells, cAMP has since been shown to support the polarisation of acini, by promoting the clearance of luminal space in 3D culture (Nedvetsky et al., 2012). Together, this cocktail of supplements support the growth and proliferation of MCF10A cells in laboratory culture.

### *1.5.5 Isogenic cells derived from the MCF10A cell line*

Due to their relative genomic stability, the MCF10A cells provide an excellent system to generate isogenic cell panels (Soule et al., 1990; Vitolo et al., 2009). They are extensively used to model dynamic morphogenesis during mammary development and also progression of breast cancers (Pauley et al., 1993). Hence, Horizon Discovery Ltd. has systematically introduced EGFR related oncogenic mutations into these cells with the aim of developing a platform to screen for adjuvant synthetic lethal inhibitors (Table 1.2).

| MCF10A cells | Mutation | Effect of mutation |
|---|---|---|
| Parental | None | --- |
| EGFR | Heterozygous ΔE746-A750 | EGFR activating mutation, in-frame deletion (exon 19), near ATP binding cleft, predicted to stabilise ATP or competitive ATP inhibitors binding to the EGFR (Imai and Takaoka, 2006). |
| PI3K | Heterozygous H1047R | catalytic p110α subunit of the Class 1 PI3K, activating mutation in the conserved kinase domain (exon 20). |
| | Heterozygous E545K | catalytic p110α subunit of the Class 1 PI3K, activating mutation in the conserved helical domain (exon 9). |
| KRAS WT | None | WT paired to KRAS G12V cells. |
| KRAS G12V | Heterozygous G12V | Ras activating mutation. |
| PTEN WT | None | WT paired to PTEN null mutated cells. |
| PTEN null | Homozygous | PTEN knock out, loss of function mutation. |

**Table 1.2 Oncogenic mutations engineered into MCF10A cells by Horizon Discovery Ltd.** Mutations downstream of the EGFR signalling pathway were introduced into MCF10A cells using the recombinant adeno-associated virus (rAAV) technology (Introduction: 1.2.5 below). WT (Wild-type) cells represent cells that have undergone similar gene editing processes to be used as control for the matched isogenic mutated cells. Information in this table was gathered from datasheets and discussions with Horizon Discovery Ltd and literatures as stated.

### *1.5.6 Recombinant adeno-associated virus (rAAV) based gene editing*

The isogenic MCF10A cells have the same genetic background as the parental cells except for the somatic mutations introduced via the recombinant adenovirus-associated technology (rAAV) as listed in Table 1.2 (Di Nicolantonio et al., 2008). Recombinant AAV knock-in constructs were generated to introduce the specific mutation into the homologous alleles in the genome of MCF10A cells (Figure 1.8). Single stranded DNA (ssDNA) containing the mutation and an endogenous ssDNA were cloned between two AAV inverted terminal repeats (ITR) to make up the

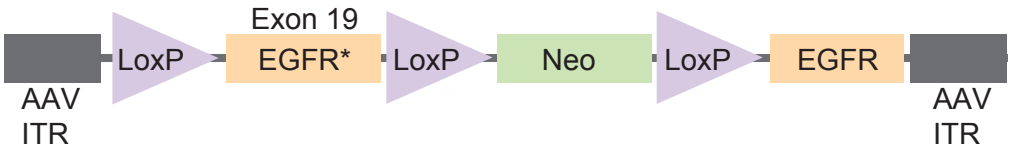


**Figure 1.8. Structure of AAV targeting construct.** The schematic representation show AAV vector carrying the EGFR ΔE746-A750 (EGFR*) oncogenic allele in the 5' arm, used to introduce the mutation into MCF10A parental cells by homologous recombination. ITR, inverted terminal repeat; Neo, geneticin-resistance gene; triangle, LoxP sites. AAV, adeno-associated virus. (Adapted from Di Nicolantonio et al., 2008).

recombination cassette. An antibiotic selection marker was placed in between the homology arms flanked by two LoxP sites, to enable Cre-recombinase mediated excision of the antibiotic cassette from the genome of the targeted cells after antibiotic selection. Only a small portion of the cassette with the relevant mutation remains in the genome of the cells, with minimal alteration in the length of genome. After targeted rAAV infection and antibiotic selection, resultant clones with the locus-specific integration of the targeted alleles were identified using a polymerase chain reaction (PCR) screen. Selected clones positive for the edited alleles were expanded and genomic DNA (gDNA) and RNA were extracted to confirm the presence and expression of the mutations introduced.

This technology allows the mutated gene to be expressed under the control of its endogenous promoter instead of heterologous expression of transfected genes using viral promoters. The mutated isogenic cells can be used with matched controls, either the MCF10A parental cells or MCF10A wild-type (WT). The MCF10A parental cells are the original cells of which the isogenic cells are based on. MCF10A WT cells are parental cells that have undergone the rAAV gene editing but did not retain the introduced somatic mutations. Paired with the mutated isogenic cells, it is possible to screen for inhibitors based on the concept of synthetic lethality (Figure 1.9). Two genes are synthetic lethal if mutation of either one maintains cell viability but simultaneous inhibition of both genes confers cell death (Kaelin, 2005).

NSCLC patients with the EGFR ΔE746-A750 have shown high sensitivity to the EGFR kinase inhibitor, Gefitinib (Fukuoka et al., 2003). However, drug resistance within a year of treatment has propelled the search for adjuvant therapies to delay or inhibit the occurrence of secondary mutations that cause the resistance (Yoshida et al., 2010). Comparing the viability of paired MCF10A parental and EGFR ΔE746-A750 cells using drug compound libraries in a high-thoroughput manner may provide new targets for the design of adjunct therapies (Kaelin, 2005). In this setting, drug compounds that antagonise or kill cells in a genotype-specific manner can be identified and further validated in different biological contexts.

Mutations in the PIK3CA (catalytic p110$\alpha$ subunit of the Class 1 PI3K) gene are commonly found in cancers. The PIK3CA mutation hotspots include E542K, E545K and H1047R (Karakas et al., 2006). Over-expression of cDNAs with these PIK3CA mutations promoted cellular transformation of chicken embryonic fibroblasts (Kang et al., 2005). The average mutational frequency of PIK3CA mutations from literature

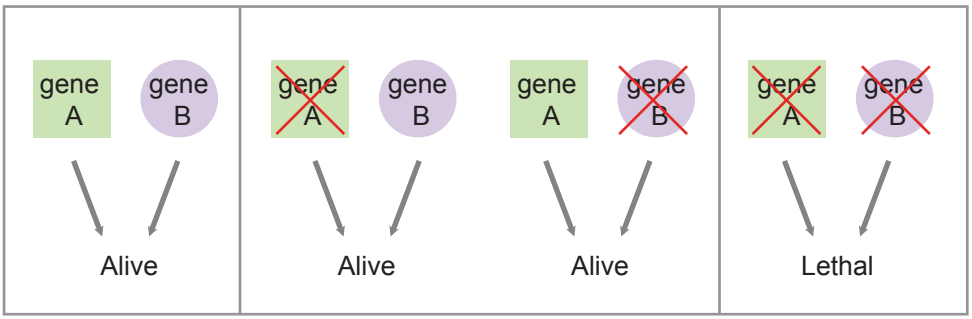


**Figure 1.9. A simplified scheme representing the concept of synthetic lethality.** In the example above, inactivation (red cross) of either gene involved in survival processes (gene A, gene B) does not affect the viability of organism. Concurrent inactivation of both gene confers lethality. (Adapted from Nijman, 2011).

mining is up to 25% in breast cancer, 26% in colon cancer and 36% in liver cancer (Karakas et al., 2006). However, variations exist within the same type of cancer, due to differences in geography, patient cohorts and methods of DNA testing and preservation.

Inversely, PTEN (Phosphatase and Tensin homologue) acts to suppress the PI3K-AKT signalling network that promotes cell growth and proliferation (Leslie and Brunton, 2013). Reduction or loss of PTEN, commonly found in human cancers, is mediated through the loss of heterozygosity and epigenetic silencing of the alleles (Leslie and Brunton, 2013; Vitolo et al., 2009). In 50-75% of breast cancer, loss of PTEN expression and acquisition of PIK3CA mutations relate to poor prognosis and resistance to chemotherapies, which highlight the importance of the PI3K pathway in breast cancer (Vitolo et al., 2009). In MCF10A cells, Bachman's group showed that the heterozygous loss of PTEN was sufficient to sustain the activation of the PI3K-AKT pathway (Vitolo et al., 2009). Moreover, homozygous absence of PTEN expression further increased the sustained activation. PTEN deletion also allowed growth factor independent proliferation of MCF10A cells which conferred resistance to PI3K inhibitor (LY 294002) and MEK 1/2 inhibitor (UO126). This was accompanied by resistance to apoptosis even when the MCF10A PTEN null cells were starved in minimal media (1% charcoal stripped dextran treated FBS, 100 units/ ml penicillin, streptomycin without growth factors) for up to 9 days. Therefore, the PTEN null isogenic MCF10A cells can be screened for using different drug compounds to find alternative inhibitors. The proteome of drug resistant PTEN null cells can also be compared to the isogenic PTEN WT cells to identify target proteins that confer resistance, allowing the rational design of combination therapy.

### 1.6 Project summary

In this thesis, I report that confluent monolayers of mammary epithelial cells are capable of drastic membrane reorganisation to form interdigitating structures prompted by EGF withdrawal (Figure 1.10). Downstream MAPK and PI3K signalling cascades synergistically aid the formation of digits. The formation of interdigitations is followed by elevated numbers of desmosomal junctions and related adaptor proteins. Ultrastructural analysis exhibited bundled actin cables emanating from the tips of these structures. Upon re-application of EGF, actin polymerisation and contraction is required to reverse such interdigitations. The functional outputs of interdigitations include immobility within confluent monolayers, impaired wound healing and enhanced mechanical stability.

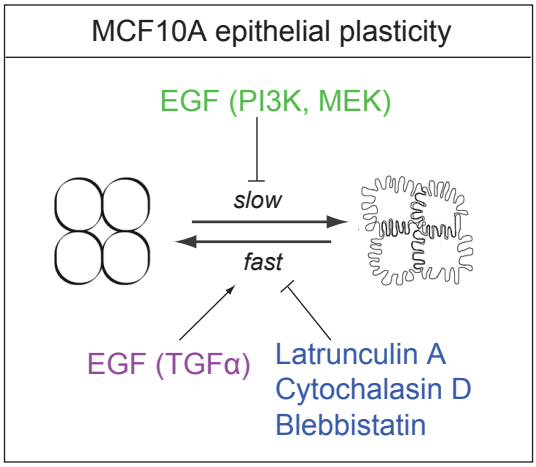


**Figure 1.10. Graphical abstract summarising the plasticity of mammary epithelial cells governed by EGF and actin cytoskeleton remodelling.** Non-malignant mammary epithelial cells require EGF in their culture medium. Removal of EGF induces interdigitations in confluent monolayers. EGF and canonical downstream signaling cascades mediate formation of interdigitations over a relatively long period (>12 hours). Formation of digits is accompanied by the restricted mobility of cells within confluent monolayers and enhanced resistance to mechanical and osmotic stress. Digits are reversed relatively rapidly (1 hour onwards) by EGFR specific ligands, (EGF & TGFα). Reversal of digits requires actin polymerisation and actomyosin contraction based on inhibition when treated with actin depolymerising drugs, Latrunculin A, Cytochalasin D and myosin inhibitor, Blebbistatin. Reversal of digits restores ability of cells to move within confluent monolayers and yet maintain enhanced cell-cell adhesion.

# Chapter 2
# Materials and Methods

## 2.1 Mammalian Cell Culture

### *2.1.1 Cell culture inhibitors, reagents and antibodies*

Gefitinib, AZD6244, Lapatinib, Erlotinib, GDC0941, CP724714 were purchased from Stratech (Suffolk, UK); Cytochalasin D, Latrunculin A, Blebbistatin and EHop-016 from Sigma (Dorset, UK); PI103, LY294002 from Calbiochem (Merck, Germany, UK), EHT1864 and NSC23766 from R&D Systems (Minneapolis, USA). $IC_{50}$ and inhibitors' concentration used are listed in Table 2.1. Culture media and supplements used were: Dulbecco's modified Eagles's medium (DMEM) F12 GlutaMax and fetal bovine serum (FBS) (Invitrogen, Paisley, UK), HS (First Link, Birmingham, UK), recombinant human EGF, TGFα, NRG1 (PeproTech, London, UK), HGF (Genentech, California, USA) hydrocortisone, insulin, cholera toxin (Sigma). Primary and secondary antibodies used in protein biochemistry and microscopy are listed in Table 2.2 and 2.3.

### *2.1.2 Two-dimensional (2D) culture*

#### *MCF10A cells*

MCF10A parental and isogenic cell lines (Table 2.4) (Horizon Discovery, Cambridge, UK) were cultured at 37$^{o}$C, in 5% $CO_2$ in (DMEM)/F12 GlutaMax supplemented with 5% horse serum (HS) EGF (20ng/ml, PeproTech), hydrocortisone (500ng/ml), insulin (0.01mg/ml) and cholera toxin (100ng/ml, Sigma) referred to as 'maintenance medium' hereafter (Soule et al 1990). For maintenance, confluent monolayers of cells (75-95%) were split every two days at 1:5-1:8 dilutions as follows: Confluent monolayers were washed 3x with PBS, then incubated with 0.5-1ml of 0.05% trypsin with EDTA (Gibco) for 10 minutes at 37$^{o}$C. Cells were resuspended in 6ml of maintenance medium in either 25cm$^2$or 75cm$^2$canted neck, vented cap flasks (Corning, New York, USA) in the recommended volumes. MCF10A cells were seeded in six-well plates at densities shown in (Table 2.5). Medium was exchanged for complete medium with 10% FBS ('growth medium') instead of the HS, with or without 20ng/ml EGF. Different experimental configurations are summarised in Table 2.6. Conditioned medium was obtained by harvesting medium from cells cultured in parallel to the cells used for the experiment. Inhibitors were added directly to wells or together with fresh or conditioned medium. In the reversal experiments, growth factors were added directly to cells cultured in medium without EGF.

| Inhibitor | Target inhibition | Source | Catalogue # | *In vitro* $IC_{50}$ | [Lab Stock] | [Final] |
|---|---|---|---|---|---|---|
| Gefitinib | EGFR ATPase binding pocket | Stratech (Selleckchem) | 1025 | 7nM, 37nM | 10mM | 300nM |
| Erlotinib hydrochloride | EGFR | Stratech (Selleckchem) | S1023 | 2nM | 5mM | 100nM |
| Lapatinib ditosylate | EGFR/ Her2 | Stratech (Selleckchem) | S1028 | EGFR: 10.2 nm Her2: 9.8nM | 10mM | 1μM |
| CP724714 | Her2 | Stratech (Selleckchem) | 1167 | EGFR: 6.4μM ErbB2 kinase domain: 32nM | 10mM | 250nM |
| AZD6244 | MEK | Stratech (Selleckchem) | S1008 | MEK1: 14nM ERK1/2: <40nM | 10mM | 300nM |
| PI103 | Pan PI3K | Calbiochem | 528100 | 8-150nM | 10mM | 100nM |
| LY294002 | Pan PI3K | Calbiochem | 440202 | PI3K: 1.4μM | 10mM | 20μM |
| GDC-0941 | PI3K I, II, III | Stratech (Selleckchem) | S1065 | PI3Kα/ δ:3nM | 10mM | 500nM |
| Cytochalasin D | Actin polymerisation | Sigma | C8273 | NIH3T3: 0.104μM | 10mM | 5μM |
| Latrunculin A | Actin polymerisation | Sigma | L5163 | MDA-MB-435: 94.88 nM | 10mM | 5μM |
| Blebbistatin | Myosin II | Sigma | B0560 | 2μM | 17.1mM or 23.2mM | 25μM (3hrs) |
| EHT1864 | Rac1 GTP displacement | R&D systems (Tocris) | 3872 | Rac1 40nM, Rac1b 50nM, Rac2 60 nM, Rac3 250nM | 75mM | 5μM |
| EHop-016 | Rac1/ Vav2 interaction | Sigma | SML0526 | 1μM | 5μM | 23.2mM |
| NSC 23766 | Rac1-GEF(Trio/ Tiam1) inhibitor | R&D systems (Tocris) | 2161 | 50μM | 100mM | 50μM |
| Cycloheximide | Protein translation | Sigma | C7698 | HeLa: 532.5nM | 35.5mM | 35.5μM(3hrs), 355nM (24hrs) |

**Table 2.1. Inhibitors and concentrations used.** Chemical structures of inhibitors accessed from manufacturers' websites are summarised in Appendices: Table2.1A.

| Antibody | Target | Epitope | Source | Output | Block | Incubation | Dilution |
|---|---|---|---|---|---|---|---|
| HECD1 | E-cadherin | N-term | CRUK | IF, WB | 5% goat serum | 5% Milk or 5% BSA | IF/WB 1:1000 |
| EP700Y | E-cadherin | N-term | Abcam (#ab40772) | IF | 5% goat serum | 5% Milk or 5% BSA | IF 1:1000 |
| Desmopl-akin 1&2 | Desmopla-kin | C-term | David Garrod (#11-5F) | IF, WB | 5% goat serum | 5% BSA | IF 1:200 WB 1:30 |
| Desmogl-ein 1 | Desmogle-in | Cytoplas-mic repeat units of DSG | David Garrod (#33-3D) | IF, WB | 5% goat serum | 5% BSA | IF 1:100 WB 1:100 |
| ZO1 | ZO1 | mid-region | Zymed (#40-2200) | IF, WB | 5% goat serum | 5% BSA | IF 1:100 WB 1:1000 |
| Claudin-1 | Claudin-1 | C-term | Invitrogen (#51-9000) | IF, WB | 5% goat serum | 5% BSA | IF 1:100 WB 1:125 |
| Occludin | Occludin | C-term 150aa (GST) | Invitrogen (#33-1500) | IF, WB | 5% goat serum | 5% BSA | IF 1:25 WB 1:125 |
| pEGFR Y845 | pEGFR Y845 | c-Src phos. site | Cell Signalling (#2231) | WB | N/A | 5% BSA | WB 1:1000 |
| pEGFR Y992 | pEGFR Y992 | PLCγ binding site | Cell Signalling (#2235) | WB | N/A | 5% BSA | WB 1:1000 |
| pEGFR Y1045 | pEGFR Y1045 | c-Cbl docking site | Cell Signalling (#2237) | WB | N/A | 5% BSA | WB 1:1000 |
| pEGFR Y1068 | pEGFR Y1068 | Grb2 binding site | Cell Signalling (#2234) | WB | N/A | 5% BSA | WB 1:1000 |
| EGFR R1 | Total EGFR | Extracellu-lar | CRUK (#sc-101) | IF | 5% goat serum | N/A | IF 1:2000 |
| EGFR D38B1 | Total EGFR | C-term | Cell Signalling (#4267) | WB | N/A | 5% BSA | WB 1:1000 |
| pAKT | pAKT | Ser 473 | Cell Signalling (#4060) | WB | N/A | 5% BSA | WB 1:2000 |
| AKT | Total AKT | C-term | Cell Signalling (#9272) | WB | N/A | 5% BSA | WB 1:1000 |
| pERK | pERK | Thr 202, Thr 204 | Cell Signalling (#4370) | WB | N/A | 5% BSA | WB 1:2000 |

| Antibody | Target | Epitope | Source | Output | Block | Incubation | Dilution |
|---|---|---|---|---|---|---|---|
| EEA-1 | EEA-1 | | Ian Mills (#243/3) | IF | 5% goat serum | N/A | IF 1:1000 |
| rab11a | rab11a | C-term hypervar-. reg. | Invitrogen (#71- 5300) | IF | 5% goat serum | N/A | IF 1:200 |
| tfr/ CD71 | Transferrin | aa461-760 | Santa Cruz (#sc9099) | IF | 5% goat serum | N/A | IF 1:400 |
| VPS35 | VPS35 | C-term aa 783-796 | Abcam (#ab10099) | IF | 5% BSA | N/A | IF 1:150 |
| Actin | Actin | DDDIAALVIDNGSGK | Abcam (#ab6276) | WB | N/A | 5% BSA | WB 1:10000 |
| pERM | pERM | aa around Thr567 of Ezrin | Cell Signalling (#3141) | WB | N/A | 5% BSA | IF 1:1000 |
| alpha-Tubulin DM1A | alpha-Tubulin | C-term aa 246-430 | Sigma (#T6199) | IF | 5% goat serum | N/A | IF 1:1000 |
| Rac1 | Rac1 | | Cytoskeleton (#Arc03) | WB | N/A | 5% BSA | WB 1:500 |
| Cdc42 | Cdc42 | aa around Lys135 | Cell Signalling (#2462) | WB | N/A | 5% BSA | WB 1:1000 |
| PREX1 | PREX1 | Internal region peptide sequence CERSNLPTDASTTA | Sigma (#SAB2501302) | WB | N/A | 5% BSA | WB 1:500 |
| Vav2 (C64H2) | Vav2 | Near C-term | Cell Signalling (#2848) | WB | N/A | 5% BSA | WB 1:1000 |
| Caveolin | Caveolin | aa1-97 | BD (#610059) | WB | N/A | 5% BSA | WB 1:20000 |

**Table 2.2. Primary antibodies used for immunofluorescence and Western blotting.** Abbreviations used include IF: immunofluorescence, WB: Western Blotting, C-term: C-terminus, hypervar. reg.: hypervariable region, phos: phospho-, aa: amino acid.

| Secondary antibodies | Source | Application | Dilution |
|---|---|---|---|
| Donkey anti-mouse IRDye 800CW | LICOR Biosciences (#926-32212) | WB | 1:15000 |
| Donkey anti-mouse IRDye 680CW | LICOR Biosciences (#926-32222) | WB | 1:15000 |
| Donkey anti-rabbit IRDye 800CW | LICOR Biosciences (#926-32213) | WB | 1:15000 |
| Donkey anti-rabbit IRDye 680CW | LICOR Biosciences (#926-32223) | WB | 1:15000 |
| Donkey anti-rabbit AF488 | Invitrogen (#A21206) | IF | 1:500 |
| Donkey anti-rabbit AF594 | Invitrogen (#A21207) | IF | 1:500 |
| Donkey anti-mouse AF488 | Invitrogen (#A21202) | IF | 1:500 |
| Donkey anti-rabbit AF594 | Invitrogen (#A21203) | IF | 1:500 |

**Table 2.3. Secondary antibodies for Western Blotting and Immunofluorescence.**

| Reference | MCF10A | Clones |
|---|---|---|
| HD PAR-003 | Parental | BenHoPark (BHP), 245 |
| HD 101-010 | EGFR ∆E746-A750 | 8A5B1B7 |
| HD PAR-004 | K-Ras WT | N/A:SNB: 00119 |
| HD 101-004 | K-Ras (+/G12V) | 2 |
| HD 101-011 | PI3Kα (H1047R) | 1, 22, 23<br>(clone 22 & 23 matched to parental clone 245). |
| HD 101-002 | PI3Kα (E545K) | 10<br>(matched to parental clone 245). |
| HD PAR-021 | PTEN WT | N/a:SNB: 00291 |
| HD 101-006 | PTEN null | 10A5pc10 |

**Table 2.4 MCF10A isogenic cell panel licensed from Horizon Discovery Ltd.** Isogenic cells with introduced mutations in the EGFR associated pathways are matched to MCF10A parental (BHP) or Wild Type (WT) unless indicated. WT cells have undergone gene editing processes as the mutants but did not retain mutations. BHP parental cells are the original MCF10A cells of which all the other cells have been based on.

| MCF10A cells | Per well 6-well | Per well 6-well |
|---|---|---|
| | +EGF | -EGF |
| Parental | $1.0 \times 10^5$ | $1.5 \times 10^5$ |
| EGFR ΔE746- A750 | $3.0 \times 10^5$ | $5.0 \times 10^5$ |
| PI3K H1047R | $1.3 \times 10^5$ | $1.8 \times 10^5$ |
| PI3K E545K | $1.3 \times 10^5$ | $1.8 \times 10^5$ |

**Table 2.5. Experimental seeding densities of MCF10A cells in 2D culture.** Seeding numbers apply to cells seeded on plastic or glass coverslips in each well of 6-well plate.

***HMT 3522 cells***

HMT 3522 S1 cells (ECACC, Salisbury, UK) were maintained at 37°C, in 5% $CO_2$ with serum free DMEM/F12 GlutaMax supplemented with insulin (250ng/ml), EGF (10ng/ml), transferrin (10µg/ml), Na-selenite (2.6ng/ml), 17β-Estradiol (27.2pg/ml), hydrocortisone (0.5µg/ml) and recombinant human prolactin (5µg/ml). Confluent monolayers (75-95%) were split every five days at 1:3-1:5 dilutions depending on the degree of confluence, with fresh medium exchange every 2 days. Cells were detached using 0.05% trypsin with EDTA (Gibco) for 10 minutes, resuspended in 0.0125 % defined soybean trypsin inhibitor (Invitrogen) at a concentration ratio of 1:1 to trypsin and up to 6 ml of HMT 3522 maintenance medium. HMT 3522 S1 cells were seeded in six-well plates at a density of $3.0 \times 10^5$cells/well (on glass coverslips). Complete growth medium was exchanged to medium lacking EGF 96 hours after seeding, once cells were in a confluent monolayer. Cells were then left for another 166 hours in medium lacking EGF. In reversal experiments, EGF (20ng/ml) was added directly to cells that had been cultured in medium without EGF.

### *2.1.3 Three-dimensional (3D) mammary morphogenesis assay*

MCF10A parental, PI3K H1047R, PTEN wildtype and PTEN null cells (Horizon Discovery, UK) were maintained as described in 2.1.2.The 3D morphogenesis assay was adapted from both Debnath et al (2003) and Lee et al (2007). Each well of a 8 well tissue culture treated glass slides (BD, Oxford, UK) was coated with 48µl of Matrigel [8.9mg/ml protein concentration] on ice, centrifuged for 10 minutes at

| | FORWARD | INDUCTION | REVERSE |
|---|---|---|---|
| Configuration | 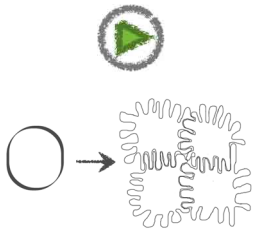 | 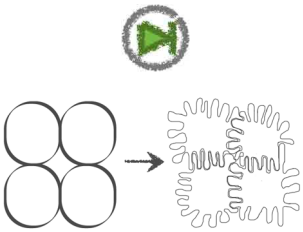 | 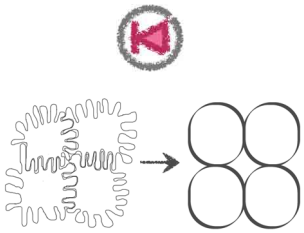 |
| Starting condition | -EGF | +EGF | -EGF |
| Timeline | 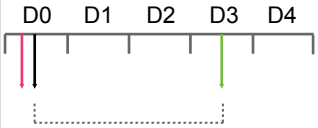  | 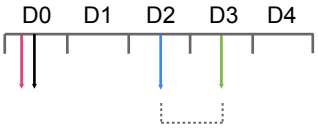  | 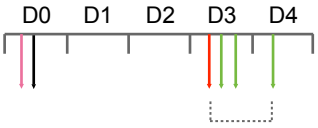  |
| Visibility of interdigitations | 60+ hours | 24hours | 1-24 hours reversal |

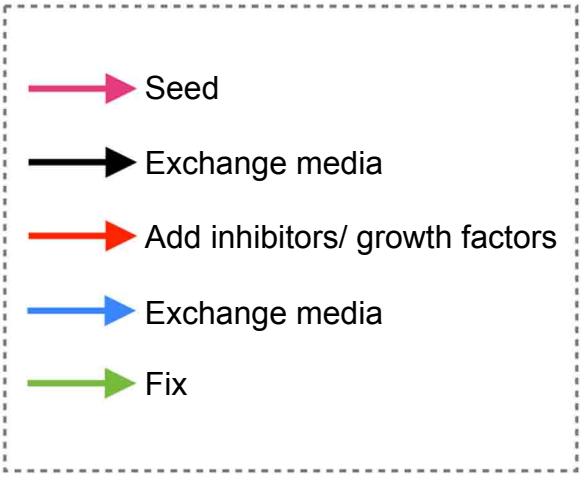


**Table 2.6. 2D Experimental configurations of MCF10A cells.** In the 'forward' experiments, cells were cultured from subconfluence whereas in the 'induction' experiments, interdigitations were induced in monolayers of MCF10A cells. This was done by exchange of growth medium to remove EGF. Interdigitated sheets in the 'reversal' experiment were pre-cultured as the forward experiment. EGF was then added to reverse the interdigitations.

300g (RT) and left to solidify for 30 minutes at 37°C. For 3D culture maintenance and experiments, media were prepared according to the recipe in Table 2.7.

| Component | Resuspension medium | Assay medium [-EGF] | Assay medium [+EGF] | Refeeding medium [-EGF] | Refeeding medium [+EGF] |
|---|---|---|---|---|---|
| | DMEM/ F12 Glutamax | DMEM/ F12 Glutamax | DMEM/ F12 Glutamax | DMEM/ F12 Glutamax | DMEM/ F12 Glutamax |
| HS | 20% | 2% | 2% | 2% | 2% |
| EGF | --- | --- | **10ng/ml** | --- | **5ng/ml** |
| Hydrocortisone | --- | 0.5µg/ml | 0.5µg/ml | 0.5µg/ml | 0.5µg/ml |
| Chlolera toxin | --- | 100ng/ml | 100ng/ml | 100ng/ml | 100ng/ml |
| Insulin | --- | 10µg/ml | 10µg/ml | 10µg/ml | 10µg/ml |
| Penicillin/ Streptomycin | --- | 100units/ml | 100units/ml | 100units/ml | 100units/ml |
| Matrigel | --- | --- | --- | 2.7% | 2.7% |

**Table 2.7. 3D culture media recipes.** Recipes were adapted from Debnath et al., (2003) and Lee et al. (2007).

Cells were trypsinised as previously described, and seeded in Assay medium [+EGF]. Every 4 days, medium was exchanged to Refeeding medium [+EGF] or [-EGF], with Matrigel added fresh. Gefitinib (300nM) was added daily from day 4 onwards or as indicated. MCF10A spheroids were fixed on days 14 and 22.

### *2.1.4 Small interfering RNA (siRNA) interference*

Cells were seeded at seeding densities show in Table 2.5. Just after seeding, cells were treated with RNAimax transfection reagent with 40nM ON-TARGET plus non-targeting oligonucleotide (NT1) or SMARTpool human oligonucleotides targeting Vav2 (siVav2) or Rac1 (siRac1) (Thermo Fisher Scientific, Waltham, MA) at a volume ratio of 1:1. The pooled sequence of oligonucleotides are listed below.

| Oligonucleotides (item #) | RNA targeting sequences |
|---|---|
| siRac1 #L-003560-00-0005 | GUGAUUUCAUAGCGAGUUU, GUAGUUCUCAGAUGCGUAA, AUGAAAGUGUCACGGGUAA, GAACUGCUAUUUCCUCUAA |
| siVav2 #L-005199-00-0005 | CUGAAAGUCUGCCACGAUA, UGGCAGCUGUCUUCAUUAA, GUGGGAGGGUCGUCUGGUA, GCCGCUGGCUCAUCGAUUG |

**Table 2.8. RNA targeting sequences of siRNA oligonucleotides used.** Oligonucleotides were made by Dharmacon and distributed by Thermo Fisher Scientific.

Medium was exchanged to FBS growth medium 5-6 hours later after the cells have attached on the same day. For the Rac1 pulldown experiments, cells were transfected again 48 hours later before GST-PBD beads pull-down of endogenous activated Rac-GTPase at 72 hours.

## 2.2 Molecular Biology

### *2.2.1 Plasmid transfection of MCF10A cells*

Medium was exchanged 5-8 hours post seeding, and cells were transfected 36-48 hours later once they had reached a minimum of 50% confluence. MCF10A parental cells were transfected with pEGFP-C1 (Clontech), GFP-LifeAct, GFP-RacG12V or GFP-RacT17N (gifts of Laura Machesky, Beatson Institute, Glasgow), using the Lipofectamine LTX transfection reagent (Invitrogen) according to manufacturer's instructions. Typical transfection efficiency obtained was approximately 20-30%. Transfection medium was replaced by complete medium with or without 20ng/ml EGF 5-6 hours after transfection. Transfected cells were visualised by time-lapse imaging or fixed with 4% PFA for immunofluorescence microscopy after 18-24 hours.

### *2.2.2 Bacterial transformation*

Plasmids were transformed as follows. 50µl of DH5α subcloning efficiency cells (Invitrogen) were thawed on ice and transferred to a polypropylene tube. Less than 100ng of DNA were added to the cell suspension and cells were incubated on ice for 20 minutes. The cell suspension was then heat-shocked at 42$^{o}$C in a water bath for 45 seconds and placed immediately on ice for 2 minutes. 200µl of SOC (Super Optimal Broth with Catabolite Repression, Invitrogen) medium was added to the cell suspension and the bacteria were incubated in a shaker at 250 rpm for 1 hour at 37$^{o}$C. Bacterial cells were then spread on selective Luria Bertani (LB, Lab M, Bury, UK) agar plates and incubated overnight at 37$^{o}$C.

### *2.2.3 Glycerol stock*

Glycerol stock was prepared from an overnight culture of transformed bacteria in LB broth. For this purpose, 5ml LB supplemented with either Kanamycin (25µg/ml) or Ampicillin (250µg/ml) were incubated in a rotating shaker at 37$^{o}$C and 245 rpm overnight. The next morning, the bacteria were centrifuged at 4000 rpm for 15 minutes. The supernatant was then discarded and the bacterial pellet resuspended in 40% glycerol in LB. The glycerol stock was catalogued and stored at -80$^{o}$C.

### *2.2.4 Plasmid DNA Purification*

A single bacterial colony from the transformed bacteria grown on LB agar plates were cultured in 5ml LB broth selection media supplemented with Kanamycin (25µg/ml) or Ampicillin (250µg/ml) overnight, at 37$^{o}$C and 245 rpm. For small scale preparations of DNA, Miniprep kits (Qiagen, Crawley, UK) were used and the procedures followed were according to manufacturers' instructions. Bacteria were centrifuged, resuspended (Buffer P1, 50mM Tris-Cl, pH 8.0, 10mM EDTA, 100ug/mL RNase A) and lysed in alkaline lysis buffer (Buffer P2, 200mM NaOH, 1% SDS). The lysates were neutralised (Buffer P3, 3.0M potassium acetate, pH 5.5) and spun at 14 000 rpm at RT (room temperature) for 10 minutes. The DNA containing aqueous phase supernatant was spun onto a filter and eluted in Buffer PB (10mM Tris-Cl, pH 8.5). For large-scale preparation, HiSpeed Maxiprep kits (Qiagen) were used. Transformed DH5α cells were inoculated into 150ml LB broth in selection antibiotics and cultured overnight at 37$^{o}$C and 245 rpm (as miniprep). Cells were harvested by centrifugation at 4500 rpm for 15 minutes and DNA isolated according to the manufacturers' instructions. The concentration of the DNA was determined using the Nanodrop ND1000 Spectrophotometer. DNA plasmids were catalogued and aliquots were stored at -20$^{o}$C.

### *2.2.5 Agarose gel electrophoresis*

Agarose gel electrophoresis was used to separate DNA according to size and to verify the concentration of plasmid of interest before DNA sequencing. Agarose was diluted to the appropriate concentration in 1x TAE buffer (0.8%, 40mM Tris-acetate, 1mM EDTA) and heated for 5 minutes in a microwave to dissolve the agarose. To stain the DNA, ethidium bromide (0.5%) was added to the dissolved agarose. Horizontal electrophoresis was performed in 1xTAE buffer. DNA bands were visualised using UV light with a UVIdoc transilluminator (UVItec).

### *2.2.6 DNA plasmid sequencing*

DNA plasmids: pEGFP-Rac G12V and pEGFP-Rac T17N were sent to The DNA Sequencing Services, University of Dundee for sequencing. The Rac1 accession number used for sequence alignment was *Homo sapiens* NM_006908. The pEGFP-C1 (Clontech) primer was used to sequence these plasmids.

## 2.3 Microscopy

### *2.3.1 Microscopy of 2D cell culture*

Cells on coverslips were rinsed twice with PBS (37°C, supplemented with 1mM

$CaCl_2$, 1mM $MgCl_2$), fixed in 4% paraformaldehyde (PFA) in PBS, permeabilised with 0.2% Triton-X-100 in PBS, blocked in 10% goat serum and incubated with primary and secondary antibodies in 5% goat serum in PBS (20 minutes each), all at RT. Alexa Fluor 488 or 594 conjugated secondary antibodies were incubated for 20 minutes. Cells were washed 3x in PBS after each antibody incubation and finally dipped into sterile deionised water ($dH_2O$) and mounted onto slides using Mowiol to which 0.5µg/ml of 4',6-diamidino-2-phenylindole (DAPI) had been added. Phase contrast and immunofluorescence images were taken using a Nikon Eclipse Ti-E microscope (CFI Super Plan Fluor 20x/0.45 NA or CFI Plan Apochromat 40x/ 0.45NA objective lens) and a digital camera (CoolSNAP EZ Turbo 1394; Photometrics). Confocal images were taken using a Leica SP2 microscope (HCX PL Apo 63x/ 1.40NA oil objective lens at 1.50 zoom). The images were then processed using NIS-Elements Software (Nikon, Surrey, UK), Leica Confocal Software (Leica Microsystem, London, UK), Photoshop CS5 Version 12.0 x64 and annotated in Illustrator CS5 version 15.0.0 (Adobe).

### *2.3.2 Microscopy of 3D spheroids*

The protocol for the fixation and staining of 3D cultures with the specified antibodies was adapted from Debnath et al 2003. Fixation and permeabilisation reagents were made in PBS buffer. 3D spheroids cultured in 8-well tissue culture treated slides were fixed immediately in 2% PFA for 20 minutes at 37$^{o}$C. Spheroids were then permeabilised with 0.5% Triton-X100 for 20 minutes at RT. All further steps were conducted at RT. Chambers were rinsed with 'Glycine rinse' (130mM NaCl, 7mM $Na_2HPO_4$, 3.5mM $NAH_2PO_4$, 100mM glycine), 3x 10 minutes each. Each chamber was then incubated in blocking buffer (10% goat serum (GS), TBS-T {20mM Tris, 137mM NaCl, pH7.6, 0.1% Tween 20}, 1% BSA) for 1 hour to block non-specific proteins binding sites. Spheroids were incubated with antibodies made in blocking buffer overnight. The next day, spheroids were rinsed with wash buffer (TBS-T, 1% BSA) for 3x 10 minutes. Spheroids were incubated in secondary antibodies and blocking buffer for 40 minutes. Spheroids were rinsed for 3x 10 minutes and mounted onto 24 x 60mm coverslips (thickness #1.5, Thermoscientific) with Mowiol and DAPI. Spheroids on coverslips were imaged using a Nikon Eclipse Ti-E microscope (CFI Plan Fluor DLL10x/0.3 NA), Leica SP2 microscope (HCX PL Apo 63x/ 1.40NA oil immersion objective, at 1.50 zoom) and Marianas spinning disk confocal microscope (3i, Intelligent Imaging Innovations, Germany) (63 x 1.4NA oil immersion objective). For quantitation of the spheroids, individual outlines of the spheroids were traced using the Wacom Bamboo pen tablet and pixels threshold

(500 pixels and above) was set using Image J software. Values obtained were then plotted onto bar charts using the Microsoft Excel 2007 package. Images were processed as described for 2D experiments.

***2.3.3 Electron Microscopy*** (with Alison Beckett, Biomedical Electron Microscopy Unit, University of Liverpool)

Confluent dishes of MCF10A cultured in ±EGF media were passed to Alison Beckett for further processing as described. Confluent monolayers were washed with 0.1M sodium cacodylate buffer pH7.4 before fixing with 2.5% (w/v) glutaraldehyde, 1mg/ml Ruthenium Red in sodium cacodylate buffer at RT for 1 hour. Following rinses with 0.1M sodium cacodylate buffer, cells were post-fixed with 1% osmium tetroxide, 1mg/ml Ruthenium Red in 0.1M cacodylate buffer at RT for 2 hours. After rinsing with $dH_2O$, cells were stained with 1% aqueous uranyl acetate (Agar) at RT for 1 hour and then dehydrated in a graded series of ethanol on ice. Cells were flat embedded using gelatine capsules in Epon and polymerised at 60°C for 2 days. Ultrathin serial sections (70-85nm) were cut longitudinally through the whole cell and stained with uranyl acetate and lead citrate before viewing at 100KV in a FEI Tecnai G2 Spirit transmission electron microscope (TEM). To quantify the number of junctions, a total of 33 micrographs were taken using AnalySIS (SIS, GmbH) with a final magnification of 16,500x for both ±EGF cells incorporating two biological repeats. 7 different grids from 6 separate resin capsules were used for -EGF and 4 grids from 2 different resin capsules for +EGF conditions. Areas imaged were chosen at random where cells were observed to be adjacent and membranes close enough for cell-to-cell adhesion. Apposing membranes were measured using AnalySIS and junctions counted and expressed as the number of junctions per µm.

## 2.4 Protein Biochemistry

### *2.4.1 Cell lysis*

Monolayers of adherent cells on 6 well plates were placed on a pre-cooled metal plate, washed 3x with ice-cold PBS and lysed with RIPA lysis buffer (10mM Tris pH7.5, 150mM NaCl, 1% sodium deoxycholate, 50mM NaF, 1% Triton X-100, 0.1% SDS) supplemented with 1x PhosStop phosphatase inhibitor (Roche) and 1x mammalian protease inhibitor cocktails (Sigma) for 10 minutes. Cells were clarified of insoluble material by centrifugation at 20,000g and 4°C for 10 min.

The protein concentration of the cell lysates was quantified using the BCA protein assay kit (Pierce, UK) according to the manufacturer's instructions. Absorbance was

measured at 562nm using the Thermo Labsystems Multiskan Spectrum spectrophotometer. Lysates were diluted in 5x sample buffer (15% w/v SDS, 312.5mM Tris HCl pH6.8, 50% glycerol, 16% Beta-mercaptoethanol) and adjusted to a final concentration of 0.5µg/µl in 1x sampler buffer.

### *2.4.2 Western Blotting*

Protein samples were resolved on NuPAGE 4-12% pre-cast Bis-Tris polyacrylamide gels (Life Technologies), run at a constant voltage of 200V for 1 hour. Resolved proteins were transferred onto Protran nitrocellulose membrane (0.45µm, Geneflow) at 25V for an hour using a Genie Blotter (Idea Scientific, Minneapolis, USA) in either MOPS buffer (4-Morpholinepropanesulfonic acid) for standard proteins, and MES buffers (4-morpholineethanesulfonic acid) for proteins less than 30kDa.The transferred proteins were visualised by Ponceau-S stain (Sigma) and the stain was removed by washing with TBS-T. Membranes were blocked with 5% Marvel milk powder in TBS-T. Primary antibodies were incubated in either 5% bovine serum albumin (BSA) or 5% milk as indicated (Table 2.1). Membranes were washed for 3x 4 minutes each using TBS-T, followed by incubation with fluorophore-conjugated secondary antibodies at RT for an hour (Table 2.2). Membranes were then washed once in TBS-T and 2x 4 minutes in TBS before acquisition of images on the LI-COR Odyssey Infrared Imaging system.

### *2.4.3 Glutathione- Sepharose (GST) beads pull-down of activated Rac1*

GTP-bound forms of Rac1 were pulled down using bacterially expressed, purified GST-PBD (p21-binding domain of PAK, Cytoskeleton Inc, Denver, USA). This protocol was adapted from Pellegrin and Mellor 2008. Confluent monolayers of cells in 10cm dishes seeded at 9 x $10^5$ cells (-EGF) were harvested on day 3. Cells were washed 3x with ice-cold PBS and lysed in RIPA lysis buffer (50mM Tris pH 7.2, 500mM Nacl, 1% Triton X-100, 0.1% SDS w/v, 10mM $MgCl_2$, 1x mammalian protease inhibitor (Sigma), 1x phosphatase inhibitor cocktails (Roche). The dishes were incubated on ice for 10 minutes. The lysates were transferred to 1.5ml eppendorf tubes and centrifuged at 20,000g, at 4°C for 10 minutes. Equal volumes of lysates (650µl) were incubated with 30 µg of purified GST-PBD beads (Cytoskeleton) at 4°C for 1 hour. 30µl of the remaining lysates were diluted in 7.5µl of 5x sample buffer, heated at 95$^o$C for 10 minutes and stored in -20$^o$C until later. The beads were centrifuged for 10 minutes, at 4$^o$C and 8000g. The supernatant was removed and beads were washed 3x with Tris wash buffer (50 mM Tris- HCl pH 7.5, 1%,Triton X-100, 150 mM NaCl, 10 mM $MgCl_2$ and 1x mammalian protease inhibitor

cocktail (Sigma), for 30 seconds and then centrifuged at 8000g at 4$^{o}$C. Proteins were eluted from the beads by adding 35µl of 2x sample buffer and centrifuged for 1 minute at 20000g. Protein samples were heated for 10 minutes at 95$^{o}$C. Samples were resolved on NuPAGE 4-12% pre-cast Bis-Tris polyacrylcamide gels with MES buffer (Life Technologies) and run at a constant voltage of 200V for 1 hour

## 2.5 Functional Assays

### *2.5.1 Wound healing assay*

MCF10A cells were grown to confluency in 6 well plates, in growth media with FBS ±EGF for 71 hours. A scratch wound was made with a pipette tip (multichannel tip 250µl; Anachem, Bedfordshire, UK). To remove dead cells the medium was exchanged for conditioned media taken from a prepared plate in parallel. Cells were then imaged as described below.

### *2.5.2 Time-lapse microscopy*

Cells in 6 well plates were incubated in 5% $CO_2$, at 37$^{o}$C throughout the duration of time-lapse microscopy. Cells were imaged within 30-40 minutes of scratching for 3 hours to record the basal condition of monolayers. Each well was imaged at 4 different positions. Growth factors (20ng/ml EGF and HGF, 6ng/ml NRG1) or medium was exchanged to buffers of different osmolarities: hypotonic [35mM NaCl], [77mM NaCl] and isotonic [35mM NaCl] (Table 2.9). Buffers were made without HEPES as the microscope has $CO_2$ flow and were adapted from Hyzinski-Garcia et al. (2011). Time-lapse microscopy movies captured images every 15 minutes for up to 24 hours, using a fully motorised Nikon Ti-E eclipse microscope (CFI Super Plan Fluor 20x/0.45 NA). Movies were processed using NIS-Elements software (Nikon), FijiIsJust ImageJ 1.48 (NIH) and MPEG Streamclip v1.9.2 (Squared5).

| Buffer | Recipe | [Final] |
|---|---|---|
| Basal isotonic buffer [135mM NaCl]<br>Proposed by Hyzinski-Garcia et al. (2011) | KCl | 3.8mM |
| | $MgSO_4$ | 1.2mM |
| | $CaCl_2$ | 1.3mM |
| | $KH_2PO_4$ | 1.2mM |
| | D-glucose | 10mM |
| | HEPES | 10mM |
| | **NaCl** | **135mM** |
| **Hypotonic buffer [77mM NaCl]**<br>Contents of basal buffer above except for the [NaCl] | **NaCl** | **77mM** |
| **Hypotonic buffer [35mM NaCl]**<br>Contents of basal buffer above except for the [NaCl] | **NaCl** | **35mM** |
| **Isotonic buffer [35mM NaCl]**<br>Contents of basal buffer above except for the [NaCl] and the addition of D-mannitol | **NaCl** | **35mM** |
| | D-mannitol | 200mM |

**Table 2.9. Recipes for buffers of different osmolarity.** Recipes were adapted from Hyzinksi-Garcia et al. (2011). [brackets] denote concentration. Highlighted in grey are the different concentrations of NaCl used to determine buffer osmolarity.

### *2.5.3 Dispase dissociation assay*

MCF10A cells were seeded in 60mm diameter dishes (+EGF: 1.75 x $10^5$ cells/dish and -EGF: 3.3 x $10^5$ cells/dish). 93 hours after seeding, dishes were washed 3x in PBS and incubated in 2ml Dispase in PBS (2.4U/ml; Roche, West Sussex, UK) for 30-40 minutes at 37$^o$C. 5ml of PBS were added into each dish and dislodged cell sheets were centrifuged for 4 minutes at 200g. The supernatants were removed and cell sheets were resuspended up and down in 1ml PBS, using a 1ml Gilson Pipette for the indicated number of strokes, Monolayer fragments (clusters of more than 1 cell) were counted using a haemocytometer.

# Chapter 3 Morphological characterisation of MCF10A cells

### 3.1 Introduction

Initially I aimed to characterise the growth and morphology of the MCF10A panel of isogenic cell lines licensed from Horizon Discovery Ltd (Methods: Table 2.4). These would provide a platform of isogenic cells for synthetic lethal inhibitor screens as had been discussed in the original project plan. At that time, these cells had not been extensively used in our laboratory. The different clones of isogenic cells were also matched to different MCF10A parental and Wild type (WT) cells (Methods: Table 2.4). MCF10A parental cells provided the genetic background into which other mutations were homologously recombined (Introduction: 1.2.5, 1.2.6). These isogenic cell lines were generated by Horizon Discovery Ltd. at different stages of expansion. In the later phases, they generated mutated isogenic MCF10A cells with a common matched WT control. WT cells have undergone the same rAAV homologous recombination processes but with empty vectors and these provide a more accurate 'control' to the mutated cells.

The original MCF10A cells have been routinely cultured in a complex medium (Methods: 2.1.2). The isogenic cells were separately cultured in different laboratories. Because they encoded mutations that are important for growth and survival, the culture medium recommended for the cells varied. Therefore, my initial aim was to establish the growth requirements of the cells by systematically varying the components of the growth medium. Subsequently, I worked towards standardising and optimising experimental protocols involving the MCF10A isogenic cell panel in 2D and 3D cultures (Table 3.1). The growth and morphology of the cells were visualised using bright field and immunofluorescence microscopy. Cells were stained with antibodies against E-cadherin and actin to visualise cell boundaries and the actin cytoskeleton respectively.

Surprisingly, confluent monolayers of MCF10A cells grown in complete growth medium without EGF (in the presence of other supplements and FBS in the medium) showed an unusual phenotype. Neighbouring cells rearranged cell boundaries to form interdigitations. Previous studies have focused on the effect of EGF on MCF10A cell growth and proliferation using biochemical approaches (Park et al., 2004, Soule et al., 1990). MCF10A cells are also famously used in 3D Matrigel basement membrane cultures, especially to model mammary gland development and tumour progression. Here, I have briefly characterised the growth and morphology of the MCF10A isogenic cells in 3D culture. The optimisation of the

protocol includes the testing of Matrigel batches, growth conditions and antibody staining of the 3D spheroids.

| MCF10A cells | Clone | Exp. assay | Chapter 3 Sections |
|---|---|---|---|
| Parental | BHP | 2D & 3D | 2D: 3.2.1,3.2.2, 3.2.3<br>3D: 3.3.1, 3.3.2, 3.3.3, 3.3.4 |
| Parental | 245 | 2D | 3.2.2 |
| EGFR ΔE746-A750 | 8A5B1B7 | 2D | 3.2.1, 3.2.3 |
| PI3Kα (H1047R) | 22, 23 | 2D | 3.2.2, 3.2.4 |
| PI3Kα (H1047R) | 1 | 2D & 3D | 2D: 3.2.2<br>3D: 3.3.1, 3.3.2, 3.3.3 |
| PI3Kα (E545K) | 10 | 2D | 3.2.2, 3.2.4 |
| PTEN WT | N/A | 3D | 3.3.1, 3.3.2, 3.3.3 |
| PTEN null | 10A5pc10 | 3D | 3.3.1, 3.3.2, 3.3.3 |

**Table 3.1. MCF10A isogenic cell panels tested in this thesis.** The different clone names represent isogenic cells that were cultured and generated in different laboratories. Exp, experimental; BHP, cells from Ben Ho Park's laboratory; 2D, two-dimensional assay; 3D, three-dimensional assay.

The initial characterisation of interdigitations is presented in this chapter. Based on this discovery, I realigned research effort towards elucidating mechanisms and the consequences of this membrane remodelling event as detailed in subsequent chapters. Although I preliminarily optimised the 3D experimental system, this assay was not pursued further as cells in the simpler 2D in vitro system provided a rational and simple assay to dissect the molecular mechanisms in detail.

## Results

### 3.2 Two-dimensional characterisation of MCF10A cells

#### *3.2.1 Morphological characterisation of MCF10A cells*

The traditional culture medium for MCF10A cells includes a cocktail of hormones and growth factors including EGF, insulin, hydrocortisone and cholera enterotoxin (Soule et al., 1990). To determine the necessity of the supplements in cell culture, each was removed from the culture medium. Cells were observed using brightfield and immunofluorescence microscopy at 62-70 hours after medium exchange.

A qualitative evaluation of cell growth was undertaken of MCF10A parental cells seeded at 20,000 cells/ well of a 3.8cm$^2$ well. MCF10A cells adopt a cobblestone-like morphology when grown as confluent monolayers (Soule et al., 1990). Cells achieved near-confluence in complete growth medium after 72 hours (Figure 3.1). Growth was severely impaired, reaching only ~10-15% confluence when cultured without any supplements. Removal of EGF alone allowed growth of small cell 'islands' that reached ~30% confluence. Removal of either insulin or cholera toxin did not adversely affect growth as cells still formed monolayers similarly to controls in complete growth medium. However, without hydrocortisone cells looked sick and did not form the characteristic cobblestone-like morphology (Figure 3.1). In comparison, isogenic MCF10A cells in which one allele of the endogenous EGFR gene has been engineered to express a constitutively active EGFR (ΔE746-A750), cells showed similar subconfluent flattened morphology under all conditions except following the removal of cholera toxin. Here, cell confluence was qualitatively increased and cells exhibited a mesenchyme-like phenotype (Figure 3.1).

Following these preliminary experiments, I adopted another protocol in which cells were seeded at a higher density in the presence of hydrocortisone (Methods: Table 2.5). E-cadherin antibody stains the plasma membrane and illustrates the smooth boundaries between control cells in complete growth medium. When EGF was removed, MCF10A cells continued to grow but developed 'finger-like' interdigitations (Figures 3.2, 3.3, Movie 3.1). Interdigitations as described henceforth refer to these structures when seen in confluent monolayers under –EGF condition. Although EGF and insulin activate similar downstream signalling pathways, the removal of insulin did not phenocopy the removal of EGF (Borisov et al., 2009). Monolayers of EGFR E746-A750 isogenic cells did not interdigitate upon EGF withdrawal (Figure 3.2A). Together, this suggests that active EGFR suppresses interdigitations. Simultaneous

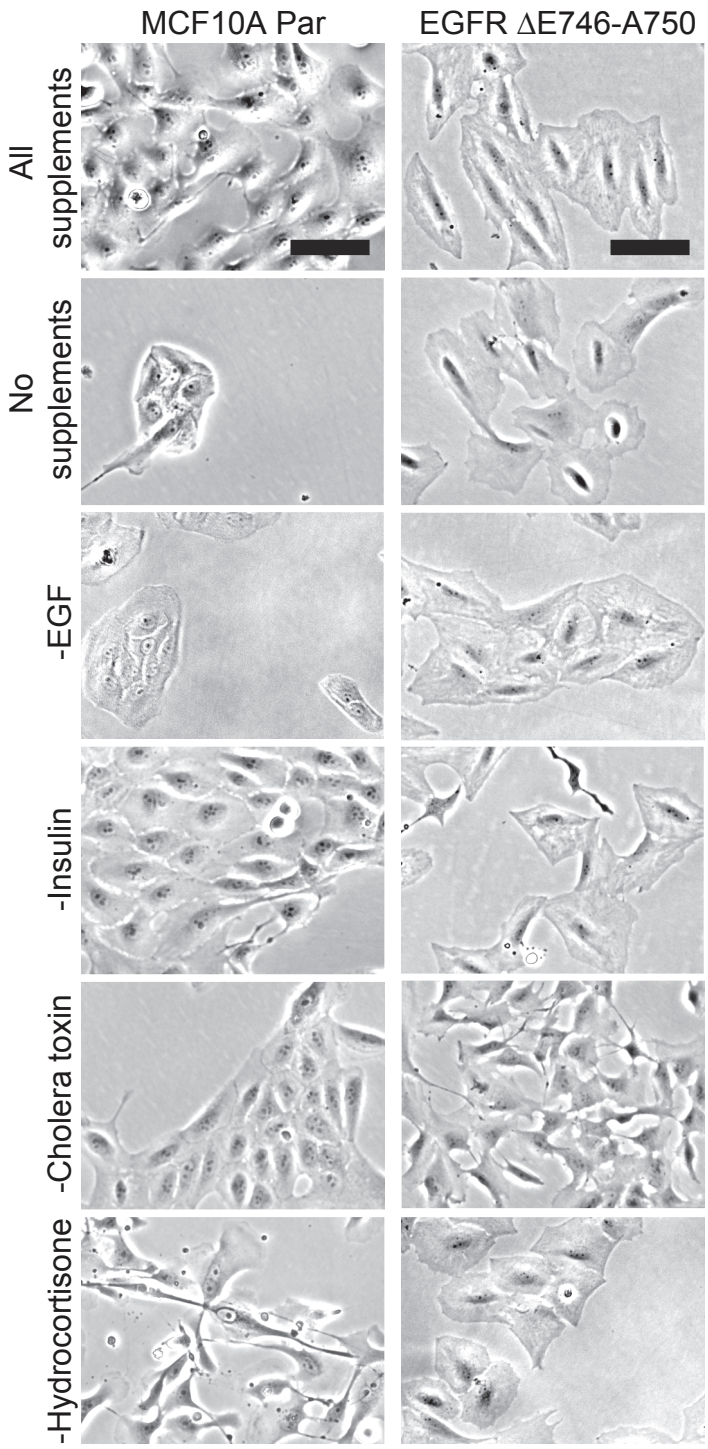


**Figure 3.1. Growth requirements of subconfluent MCF10A cells.** MCF10A parental and EGFRΔE746-A750 cells were cultured in complete growth medium and without supplements as annotated. Cells were seeded at 20,000 cells/well of 12 well plates. Complete growth medium was exchanged for medium ±supplements (as annotated) 3.5 hours post seeding. After 72 hours, representative images of cells at 50% confluence or less were visualised using bright field microscopy at 20x magnification. Scale; 40μm.

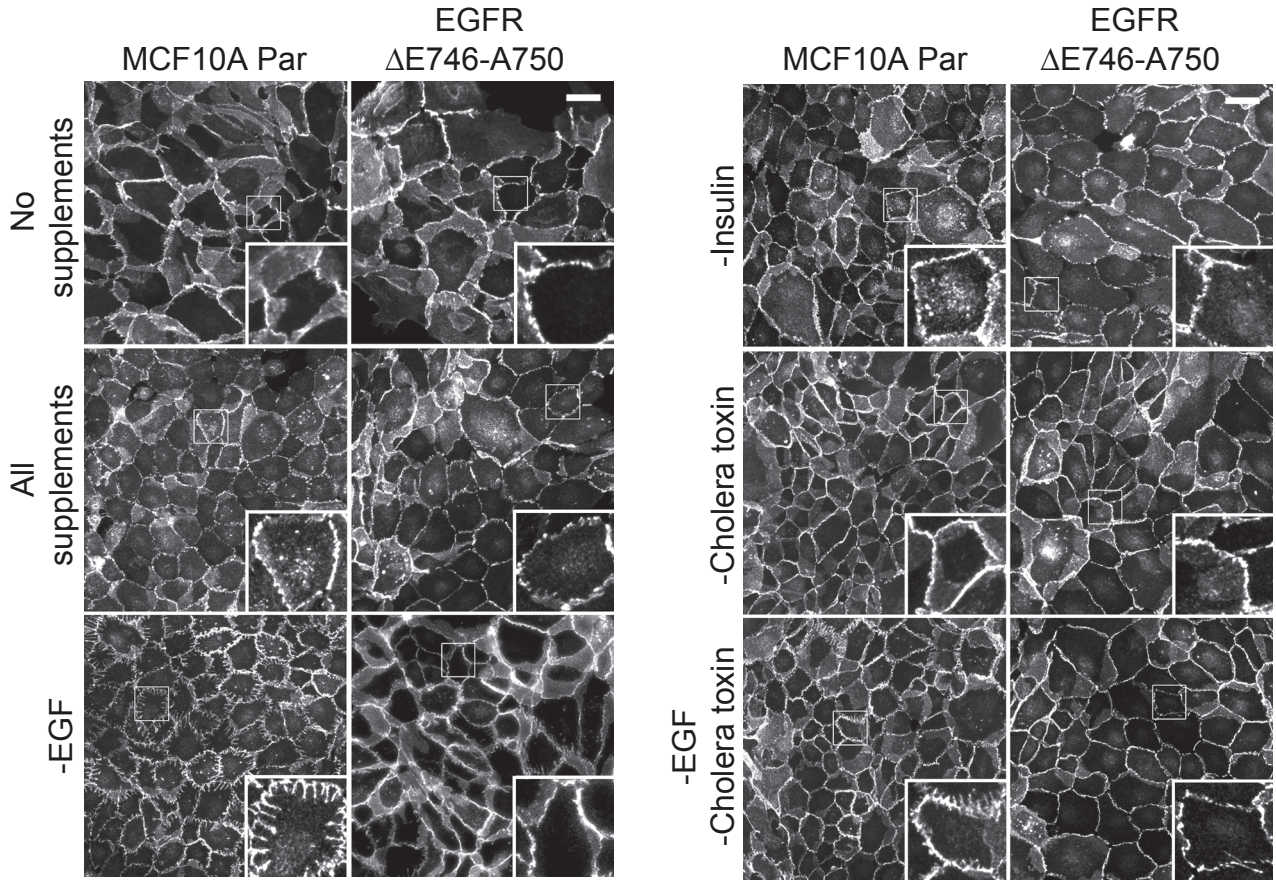


**Figure 3.2. (A) EGF withdrawal induces interdigitations in MCF10A cells.**
Effect of removal of different supplements from growth media of MCF10A parental or isogenic cells expressing EGFRΔE746-A750. Control MCF10A cells organised into "cobblestone" monolayers. Interdigitations seen following EGF removal were not apparent in EGFR mutant cells. Complete growth medium was exchanged six hours post seeding for medium without supplements as annotated. After 72 hours, cover-slips were fixed with 4% PFA and stained with E-cadherin. Cells were visualised using immunofluorescence microscopy at 20x magnification. Scale; 40μm.

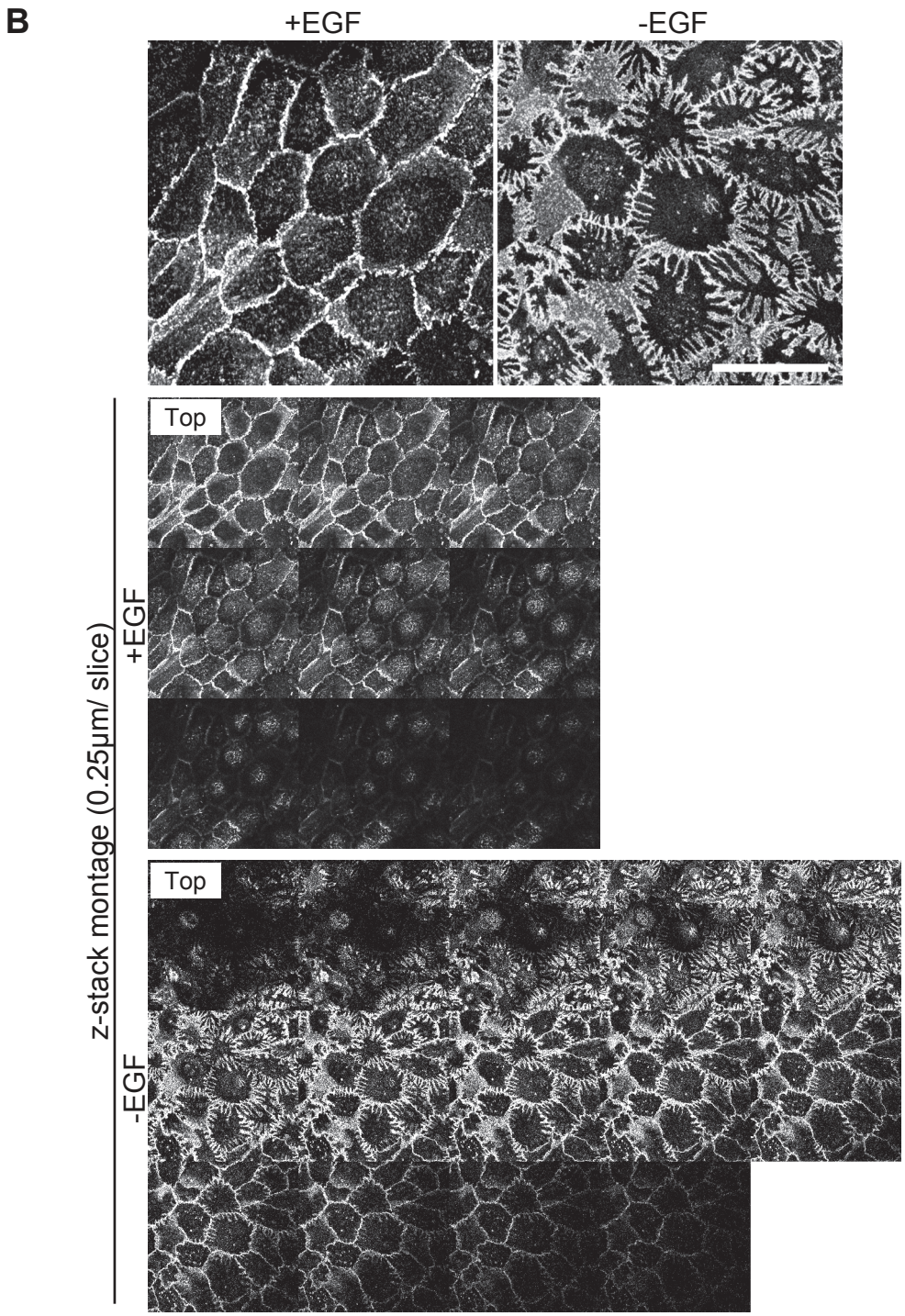


**Figure 3.2. (B) Montage of z-stack showing the relative position of interdigitations in MCF10A cells.** The montage shows MCF10A cells on coverslips at 2.25- 3.5µm thickness with interdigitations visible near the top of the cells. Subsequent z-stack images of cells were taken from the top to the bottom of the cells (left to right, continuously down each row of montage). Each z-stack image was taken at 0.25µm steps. MCF10A cells were cultured in ±EGF for 72 hours and immunostained with E-cadherin. Cells were fixed with 4% PFA and images were taken using confocal microscopy at 63x magnification (zoom 2). Scale; 40µm.

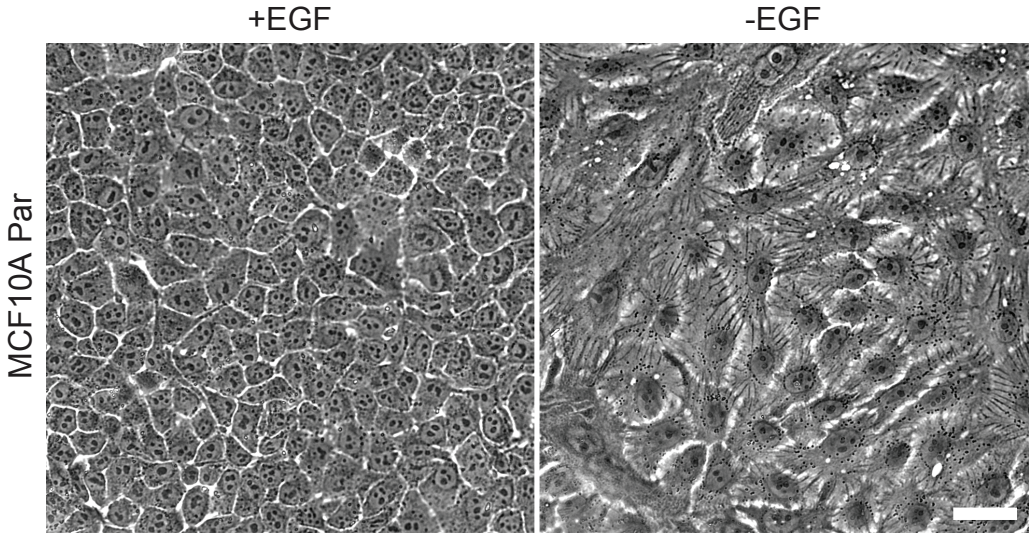


**Figure 3.3. EGFR signalling suppresses interdigitation of MCF10A cells.** Confluent monolayers of live cells on plastic dishes were imaged in growth medium with or without 20ng/ml EGF. More cells were seeded at 100,000-150,000 cells/well of 6 well plate compared to Figure 3.1. Complete growth medium was exchanged for medium ±20ng/ml EGF six hours post seeding. After 72 hours, confluent monolayers were visualised using bright field microscopy at 20x magnification. Scale; 40μm.

removal of cholera toxin together with EGF resulted in much fewer and shorter interdigitations. Using confocal microscopy, z-stack images of interdigitations were taken and assembled into a montage (Figure 3.2B). These images show that interdigitations are located near the top of cells at less than 3μm depth. Orthogonal sections of these images were not included as the cells were flat (up to 3μm in depth). Another independent clone of MCF10A parental cells (Clone 245) also showed interdigitations when cultured in medium lacking EGF (Figure 3.4).

### *3.2.2 Morphological characterisation of MCF10A PIK3CA mutant cell clones*

When PIK3CA mutated clones were subjected to the same experimental procedures, the appearance of interdigitations in the -EGF condition was dependent on the clones (Figures 3.5, 3.6). Only the PI3K E545K (clone 10) showed interdigitations whereas PI3K H1047R (clone 23) exhibited mild interdigitations (Figure 3.5). H1047R clone 1 and clone 22 cells failed to interdigitate in the absence of EGF (Figures 3.5, 3.6). I observed two distinct populations of the H1047R (clone 1) cells: cobblestone-like (E-cadherin stained) and mesenchyme-like (non E-cadherin stained) (Figure 3.6).

### *3.2.3 Optimisation of MCF10A cell lysis*

To obtain lysates of MCF10A cells for the initial biochemical analysis of EGFR status, I compared lysis buffers commonly used in this laboratory either with Triton X-100 or NP40 as detergent (Table 3.2). This was performed as initially I failed to harvest lysates that reproduced satisfactory signal strength when probed for EGFR. Cell lysates were probed for total EGFR and components of two downstream signalling signatures: pAKT and pERK. Actin was probed as loading control (Figure 3.7). MCF10A parental cells were cultured in complete growth medium for 48 hours. Medium was then exchanged to complete growth medium or medium lacking FBS to serum starve the cells for 16 hours (Zhan et al., 2006). Growth medium ±EGF was exchanged to acutely stimulate cells for 10 minutes. The levels of proteins were compared to HeLa cell lysates obtained from a colleague, which had been serum starved overnight and acutely stimulated with 1ng/ml EGF for 5 minutes before lysis. Total EGFR levels were highest in MCF10A cells not acutely stimulated with EGF. The blots show a remarkably rapid reduction of EGFR within 10 minutes of stimulation although EGFR downregulation has been shown to take between 30 minutes- 2 hours in other cells (Eden et al., 2009; Sorkin and Zastrow, 2002). The total EGFR reduction was similar to that observed in cells cultured either with or without serum starvation for 65 hours (Figure 3.7 A, B). Duan et al. (2011)

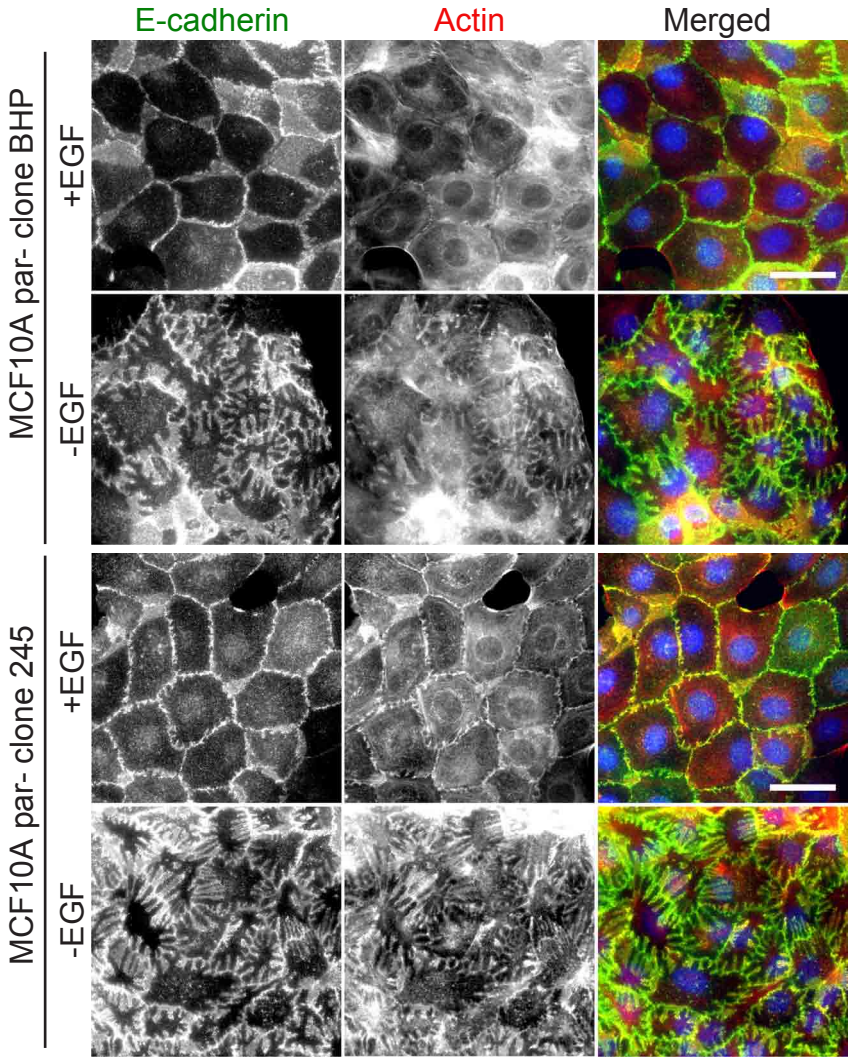


**Figure 3.4. Interdigitations observed in different clones of MCF10A parental cells.** Cells were cultured in growth medium ±20ng/ml EGF for 68 hrs. Coverslips were fixed with 4% PFA and stained with E-cadherin, F-actin and DAPI. Images of confluent areas were taken using immunofluorescence microscope at 40x magnification. Scale; 40μm.

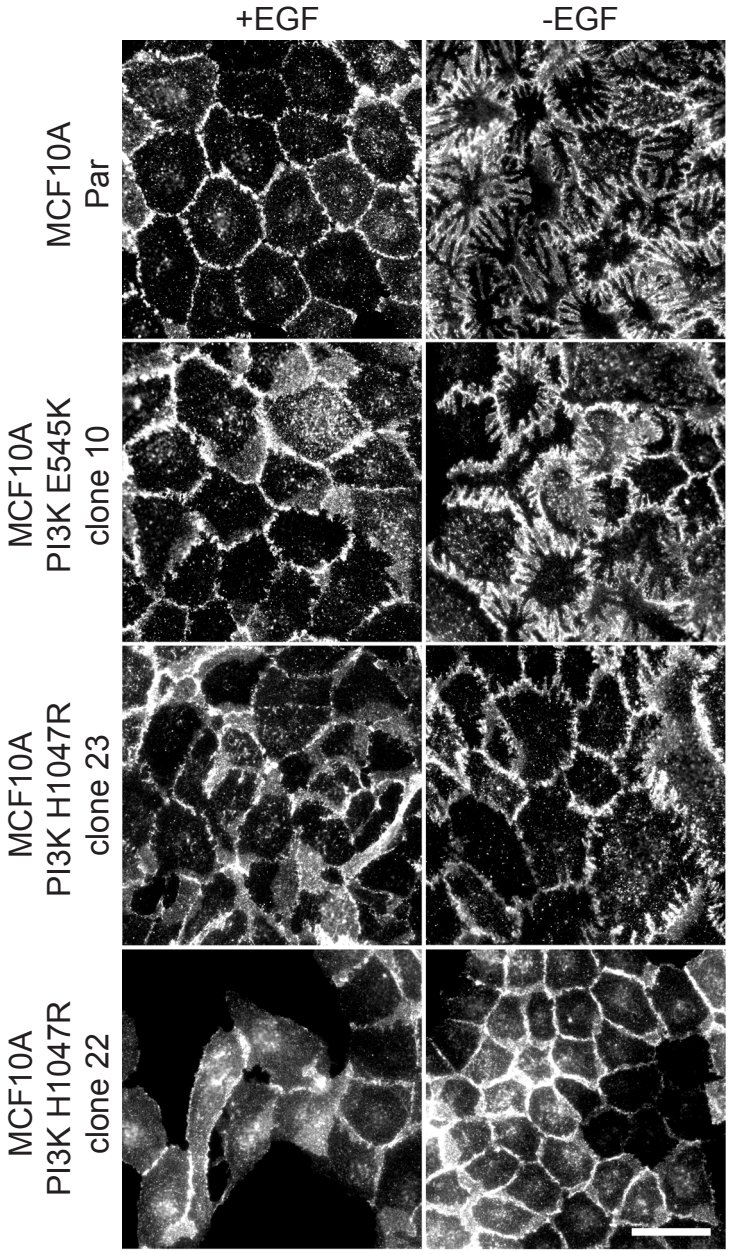


**Figure 3.5. Variable E-cadherin staining and ability to form interdigitated structures in PIK3CA mutated MCF10A cells.** MCF10A PI3K H1047R (clone 23) and PI3K E545K (clone 10) showed characteristic cobblestones monolayers in complete growth medium. Not all H1047R (clone 22) cells were E-cadherin stained. In medium lacking EGF, only E545K (clone 10) cells interdigitated. Cells were cultured in medium ±EGF for 47-68 hours. Coverslips were fixed with 4% PFA and stained with E-cadherin. H1047R (clone 22) were grown in DMSO as control for another experiment. Areas of monolayers were visualised using immunofluorescence microscopy at 40x magnification. Scale; 40µm.

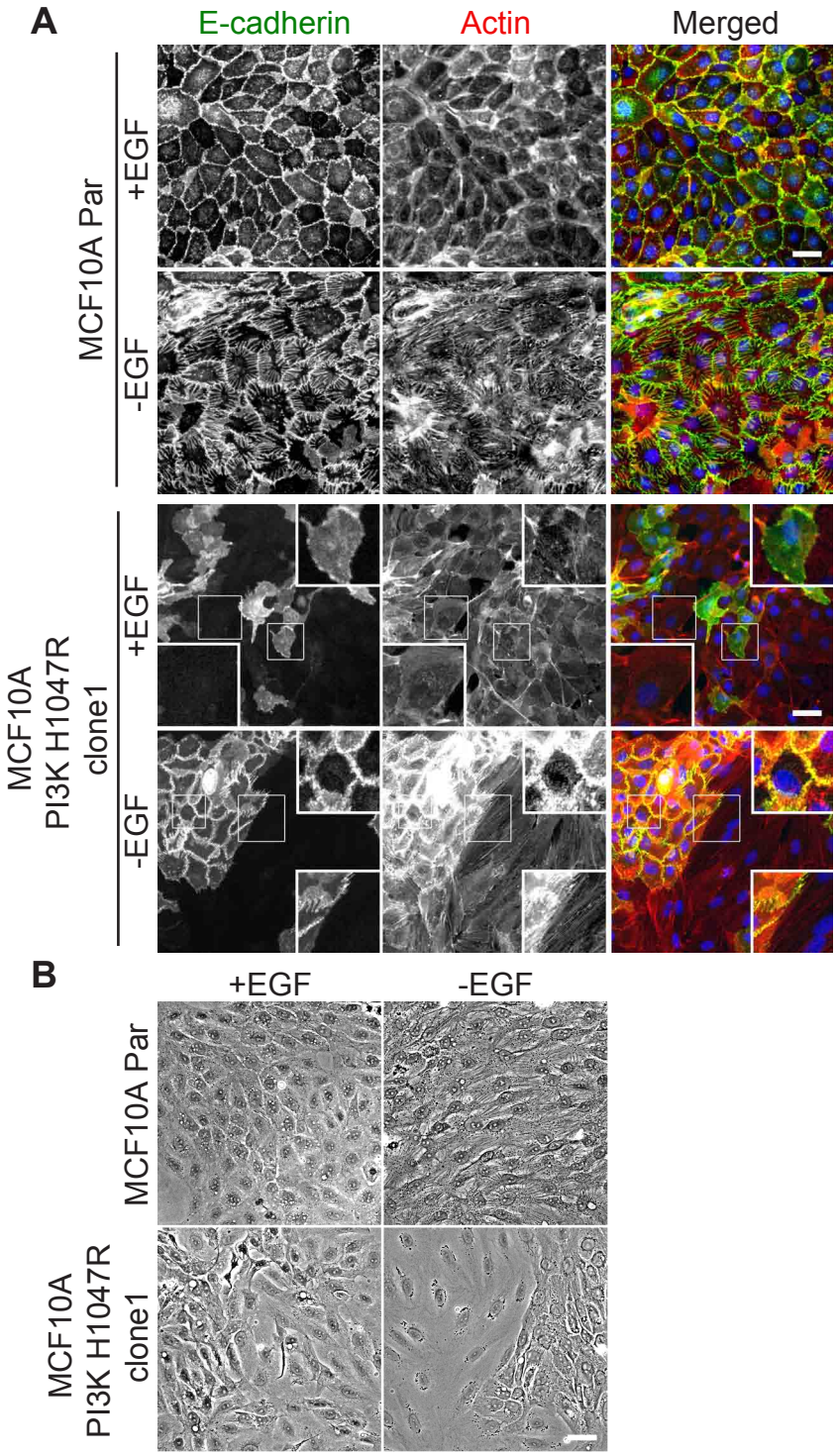


**Figure 3.6. MCF10A PI3K H1047R (clone 1) cells of two distinct phenotypes.** MCF10A PI3K H1047R (clone 1) showed two populations of cells; fibroblast-like and cobblestones when cultured in growth medium ±EGF. Cells were cultured in medium ±EGF for 69 hours. Coverslips were fixed with 4% PFA and stained with E-cadherin (green) and F-actin (red). Cells were visualised using (A) immunofluorescence or (B) bright field microscopy at 20x magnification. Scale; 40µm.

previously reported downregulation of EGFR with 100ng/ml EGF stimulation after 60 minutes but they did not show levels of EGFR at 10 minutes. EGFR reduction may be due to effective downregulation via the endocytic pathway or a post-translational modification induced by EGF stimulation that masked the antibody recognition epitope.

Most intense signals for EGFR, pERK and pAKT were obtained using NP40 lysis buffer 2 and TritonX lysis buffer 3 (Figure 3.7, Table 3.1). Levels of pAKT were slightly reduced after serum starvation but the band showed a slight upshift, characteristic of phosphorylation with the EGF stimulation seen using TritonX lysis buffer 1 and 3. In MCF10A cells, EGF stimulated the pERK pathway but its effect on pAKT was less clear as the different lysis buffers gave different results. Furthermore, the constant presence of insulin in the medium may explain the relatively high basal levels of pAKT observed. Henceforth, membranes show non-serum starved MCF10A cells lysed with the TritonX lysis buffer 3 which provided intense signals for pERK and pAKT similar to EGF stimulated HeLa cells.

I have also tested antibodies to probe for different phosphorylation sites on the EGFR comparing lysates of MCF10A parental and the constitutively activated EGFR$\Delta$E746-A750 cells (Figure 3.7). MCF10A cells cultured in medium with or without EGF for 65 hours were lysed without prior serum starvation. EGFR ubiquitylation acts as one of the internalisation signals upon EGF stimulation. This RTK is ubiquitylated by E3 ligase, Cbl after direct phosphorylation at Y1045 or indirectly via Grb2 adaptor proteins at phosphorylated Y1068 and Y1086 sites (Levkowitz et al., 1999; Motley et al., 2003; Roepstorff et al., 2008; Waterman et al., 2002). Without EGF, the EGFR phosphorylation was reduced at pY1068 and pY1045 in MCF10A parental cells (Figure 3.7). Accordingly, these were accompanied by high expression of EGFR indicative of reduced degradation. In contrast, the signal for pY992 in the same milieu increased although this signal was very weak, evident from the high intensity scanned blot. This may reflect the higher levels of EGFR that remained under -EGF condition.

Phosphorylation of EGFR at Y1045 of EGFR mutants was similar in ±EGF, although total EGFR reduced under +EGF condition. This indicates that EGFR activation is independent of EGFR expression levels. Direct binding of Cbl to the phosphorylated Y1045 site has been shown to be unnecessary for EGFR endocytosis while binding at Y1068 via Grb2 was needed for EGFR degradation (Grovdal et al., 2004;

| **Lysis Buffer 1 (0.1% TritonX lysis buffer)** | [Final] |
|---|---|
| Tris pH 7.2 | 10mM |
| NaCl | 158mM |
| EDTA | 1mM |
| Triton X-100 | 0.1% |
| MPI Sigma | 1:250 |
| Phosphatase Cocktail inhibitor II | 1:100 |
| **Lysis Buffer 2 (NP40 lysis buffer)** | |
| Tris pH 7.5 | 25 mM |
| NaCl | 100mM |
| NaF | 50mM |
| NP40 | 0.5% |
| MPI Sigma | 1:250 |
| Phosphatase Cocktail inhibitor II | 1:100 |
| **Lysis Buffer 3 (1% TritonX lysis buffer)** | |
| Tris-HCL pH 7.5 | 10mM |
| NaCl | 150mM |
| TritonX-100 | 1% |
| w/v SDS | 0.1% |
| Sodium deoxycholate | 1% |
| NaF | 50mM |
| MPI Sigma | 1:250 |
| Phosphatase Cocktail inhibitor II | 1:100 |

**Table 3.2. Recipes of lysis buffers.**

Roepstorff et al., 2008). The slight increase of EGFR pY1068 in the absence of EGF suggest that the constant activation of EGFR in these cells may be conferred dominantly at this phospho-site that also mediates the EGF stimulated degradation. The negative control HeLa cells were not serum starved but acutely stimulated with 1ng/ml EGF (7 minutes). Total levels of EGFR remained high in these cells and pEGFR was only modestly increased compared to the MCF10A parental and EGFR mutant cells. Henceforth, pEGFR Y1068 and total EGFR (clone D38B1) antibodies have been used to probe subsequent membranes presented in this thesis.

### *3.2.4 EGFR associated signatures of MCF10A isogenic cells*

Next, I characterised the status of pEGFR and the associated effectors in the MCF10A parental and the isogenic cell panel: EGFRΔE746-A750, PI3K H1047R clone 1, clone 22, clone 23 and PI3K E545K cells. Initially, only 8µg of samples

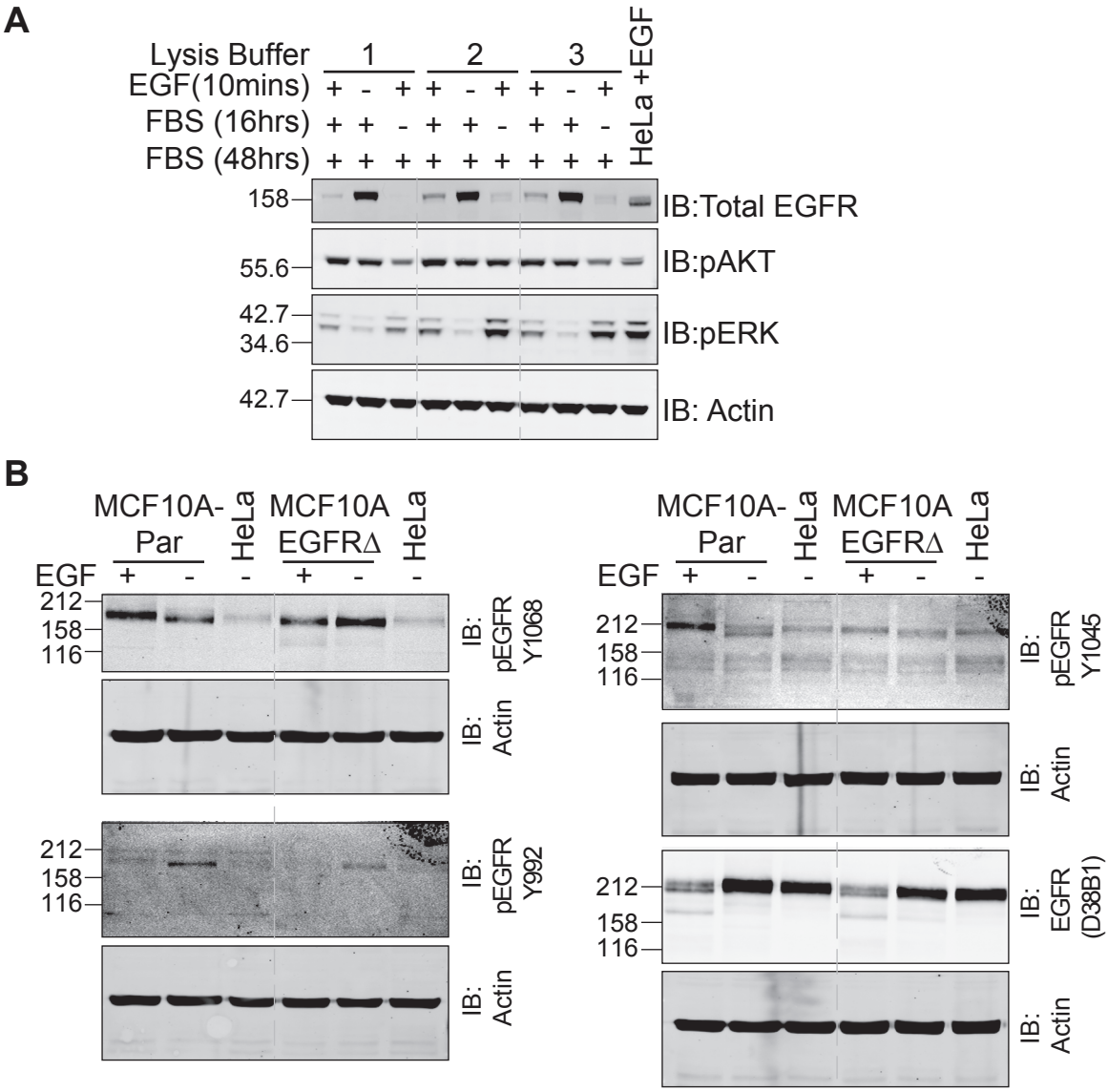


**Figure 3.7. Optimisation of lysis buffers and EGFR antibodies for MCF10A cell lysates.** (A) MCF10A cells were cultured in complete growth medium with EGF (48 hours) and medium was exchanged to medium ±FBS (16 hours). Second medium exchange to medium +EGF with FBS was to stimulate cells with EGF (10 minutes). Lysates were lysed separately with 3 different lysis buffers as detailed in Table 3.1. Positive control, HeLa cell lysates were acutely stimulated with 1ng/ml EGF (5 minutes) after overnight FBS starvation. (B) Phospho and total EGFR antibodies were tested on MCF10A cells cultured in complete growth medium for 65 hours without prior serum starve. HeLa cells were stimulated with 1ng/ml EGF (5 minutes) before lysis and did not undergo overnight serum starvation. 12.5µg of MCF10A cell lysates were loaded onto each lane.

were loaded into each lane. Levels of pEGFR Y1068 in -EGF condition were similar to +EGF control in MCF10A parental cells. This could be accounted for by the increased EGFR expression that may have masked the slight decrease of pY1068 (Figure 3.8). The isogenic PI3K H1047R (clone 1) cells show reduced pY1068 and increased total EGFR in -EGF condition as previously seen with MCF10A parental cells (Figure 3.7, 3.8). The levels of EGFR remained similar across the MCF10A cell panel. Lysates for the EGFR mutant cells were re-loaded as a technical repeat, confirming previous results (Figure 3.7, 3.8).

A biological repeat compared the EGFR profiles of different clones of MCF10A parental and PIK3CA mutants; H1047R and E545K cells at a higher concentration of lysates, 12.5µg (Figure 3.9). In +EGF culture, pEGFRY1068, pERK and pAKT signals were increased in comparison to –EGF (Figure 3.9). The accompanying total EGFR expression levels were reduced reflecting phospho-mediated degradation of EGFR. Total levels of ERK and AKT remained constant regardless of EGF stimulation, indicative of their protein half-lives that have been reported to be over 27 hours (Schwanhaeusser et al., 2011). In general, the EGFR associated signatures showed similar trends across the MCF10A isogenic cells. The PIK3CA mutants with constitutively active PI3K; H1047R and E545K cells, showed increased activation of pAKT both in ±EGF conditions when compared to the parental cells.

As seen in the graphs (Figure 3.8, 3.9) the phospho-EGFR in MCF10A isogenic cells show similar activity in basal ±EGF conditions. An exception is the EGFR ∆E746-A750 mutant cells that have a higher basal pEGFR Y1068 signal due to the presence of constitutively active EGFR. Although pEGFR signal in these cells was reduced in –EGF, this remained higher than that seen in parental and H1047R cells (Figure 3.8). Incidentally, the EGFR mutant cells did not form digits when cultured in the absence of EGF (Figure 3.2). The PIK3CA mutants H1047R and E545K revealed differential abilities to form digits when cultured in –EGF despite showing similar phospho-EGFR fluctuations in ±EGF culture conditions (Figure 3.5, 3.9). This suggests that the different oncogenic potency of the PIK3CA mutations may contribute to the ability of cells to form digits. With E545K cells reported as less potent in inducing tumour in mouse xenograft models, these cells are likened to less malignant cells and thus may have retained the ability to form digits compared to their H1047R counterparts (Isakoff et al., 2005). Concordance of EGFR and Rac-GTPase expression levels was good across the isogenic platform despite slight differences in overall protein concentrations due to inter-experimental variations.

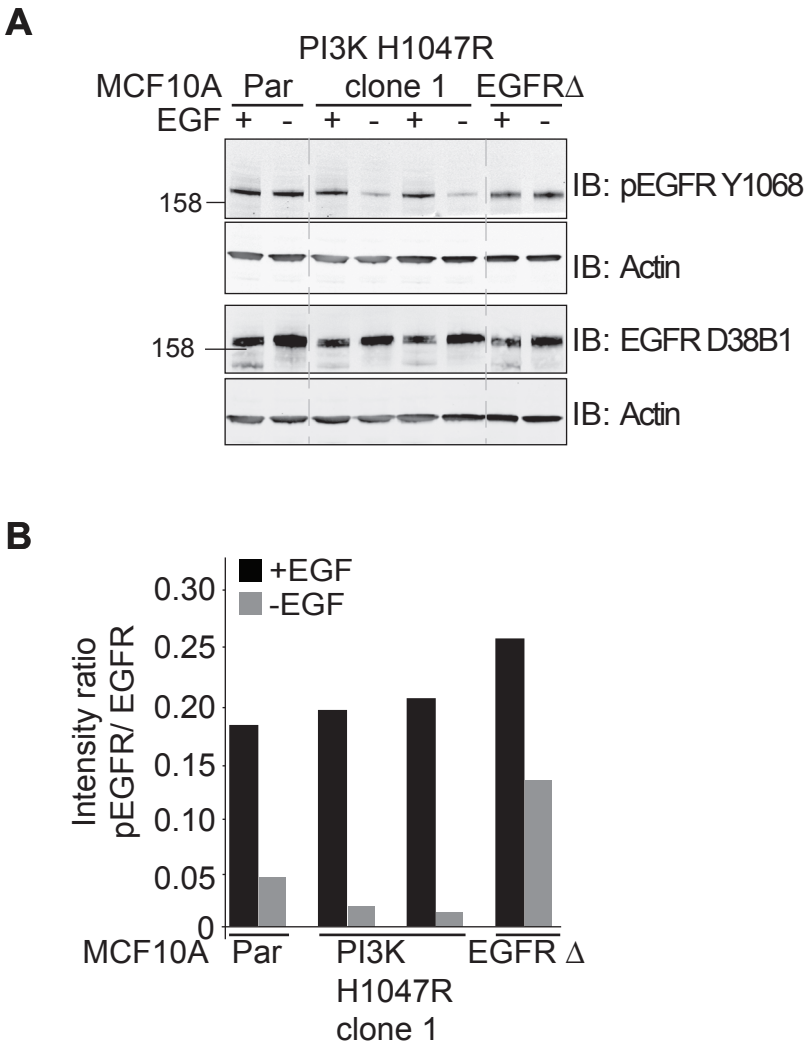


**Figure 3.8. EGFR profile of MCF10A parental, PI3K H1047R and EGFR ΔE746-750 mutants.** (A) MCF10A cells were cultured in complete growth medium ±EGF for 65-68.5 hrs. PI3K H1047R lysates duplicate lanes were technical repeats from the same experiment. EGFRΔE746-A750 lysates loaded were technical repeats of Figure 3.7B. 8µg of MCF10A cell lysates were loaded onto each lane. (B) The intensity of the bands quantified with the Odyssey software for pEGFR Y1068 were normalised to the total EGFR levels of each lane.

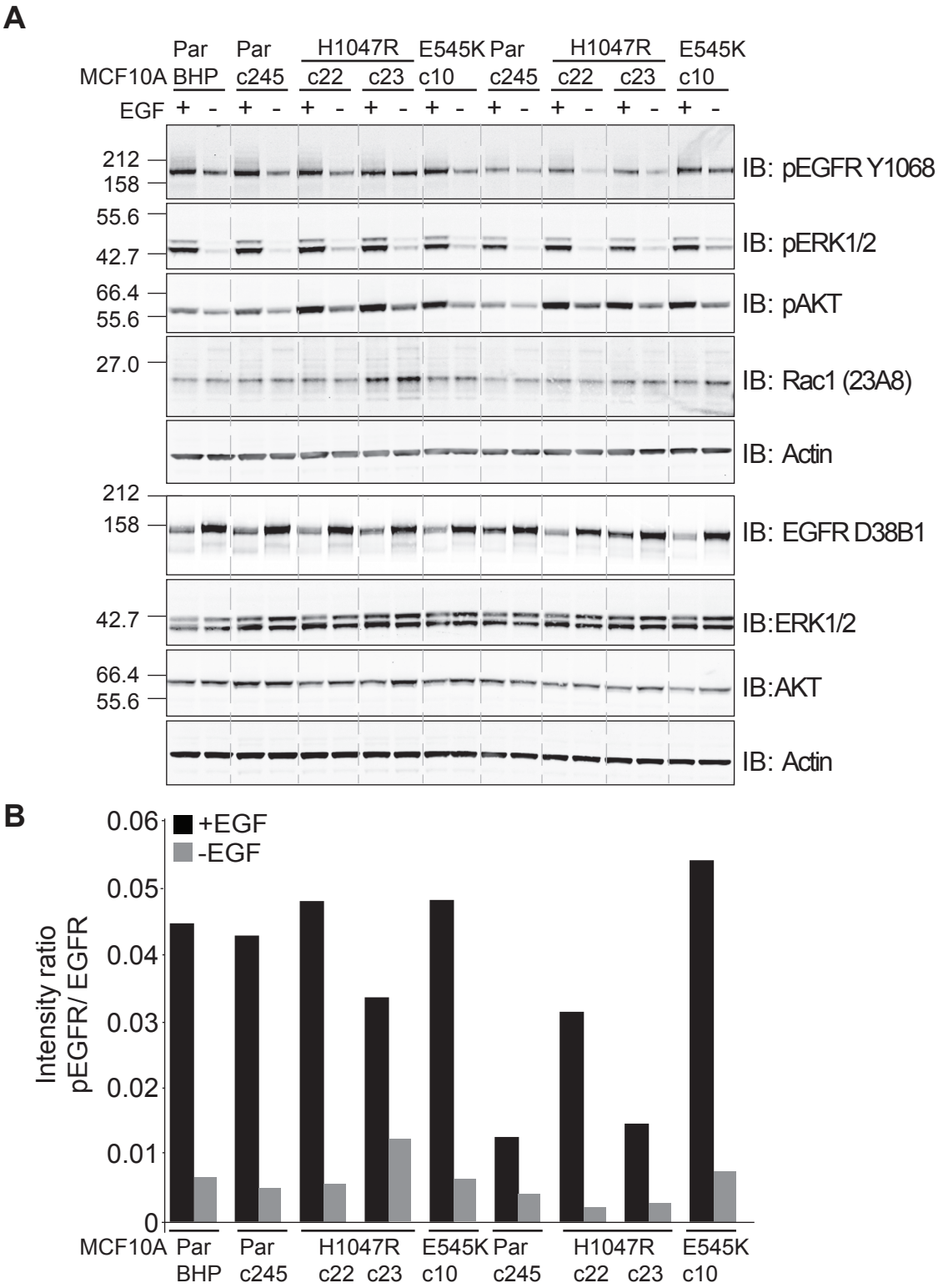


**Figure 3.9. EGFR associated profiles of MCF10A parental, PI3K H1047R and E545K mutants of different clones.** (A) Duplicate lanes were biological repeats of the same cells. MCF10A cells were cultured in complete growth medium ±EGF for 65-72hrs. 12.5µg of MCF10A cell lysates were loaded onto each lane. (B) The intensity of the bands quantified with the Odyssey software for pEGFR Y1068 were normalised to the total EGFR levels of each lane.c, clone; par, parental.

This indicates that the gain-of-function mutations of the isogenic cells do not affect EGFR and Rac expression levels.

## 3.3 Three-dimensional characterisation of MCF10A cells

### *3.3.1 Morphological characterisation of MCF10A cell acini in 3D culture*

MCF10A cells form acinar structures with a hollowed lumen when grown in 3D culture for at least 14 days (Debnath et al., 2003). Bright field microscopy images were used to visualise the general morphology and to quantify the cross sectional surface area (CSA) of the spheroids (Figure 3.10). Using confocal IF microscopy, Golgi apparatus (GM130), actin-membrane linker (p-ERM) and nuclear (DAPI) stains were used to visually dissect the acini in 3D culture (Figure 3.10). This experiment was done in parallel with a colleague, Rebecca Eccles to establish the 3D morphology of these cells in the laboratory. Using bright field microscopy, the structure of MCF10A parental, PTEN WT, PTEN null acini showed similar spheroidal architecture and size (Figure 3.10). H1047R (clone 1) cells showed two populations of irregularly shaped acini: very large and very small in size. These cells were paired with the MCF10A parental cells as control. Similar homologously recombined WT control cells for this mutation were not available at the time of experiment.

GM130 marks the cis-Golgi of cells which polarise towards the lumens of the MCF10A spheroids. pERM was used to mark the cell boundaries within the acini (Debnath et al., 2003; Debnath et al., 2005). On day 14, IF images of MCF10A parental acini showed organised cells in the outer layer. Lumens of acini were evident by the lack of DAPI stain. In contrast, the very large representative H1047R acinus was irregularly shaped, had an apically orientated Golgi apparatus and no visible lumen (Figure 3.10). The very small acinus consisted of tight clumps of cells. This correlated with the 2D microscopy results where two distinct populations of H1047R (clone 1) cells were previously seen (Figure 3.6). PTEN WT spheroids showed a thicker outer layer of cells with an organised GM130 stain. PTEN null acini had the thicker outer layer and the Golgi apparatus were disorganised. The lumens were also less evident compared to PTEN WT acini.

### *3.3.2 Cross-sectional surface area (CSA) distribution of MCF10A isogenic acini*

The bright field images of MCF10A isogenic acini were analysed using Image J software. The outline of each spheroid was individually traced electronically and the

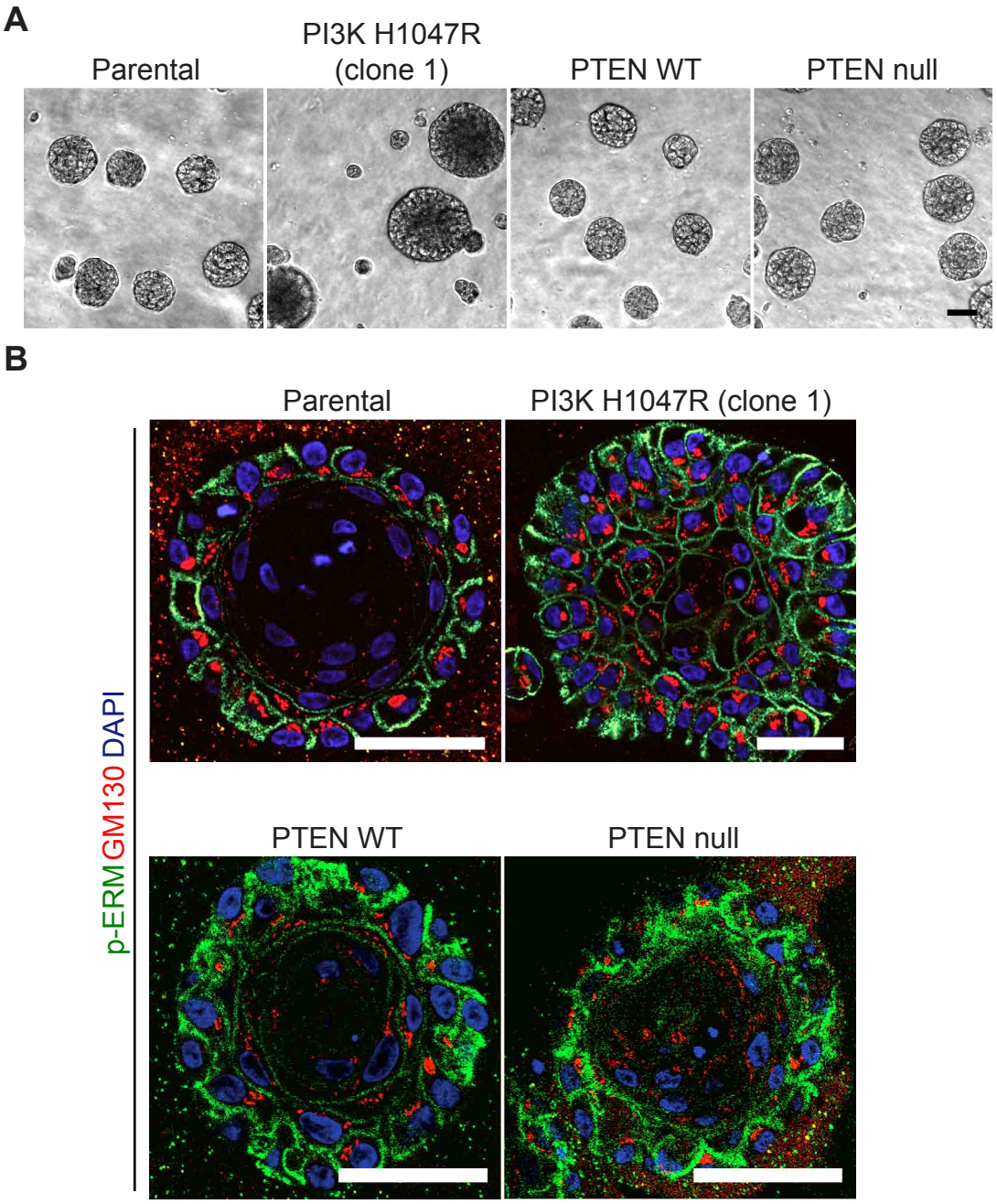


**Figure 3.10. MCF10A spheroidal acinar structures.** (A) Representative images of the MCF10A acinar structures in 3D culture. PI3K H1047R (clone 1) cells show distinct populations with very large and very small acini (second from left). PTEN null acini were larger than PTEN WT acini. (B) Parental and PTEN WT acinis show apical orientated cis-Golgi apparatus (red) and organised actin linker (green). Lumens of acini were hollowing out as seen from DAPI stains (blue). PI3K H1047R (clone 1) show distinct populations of contrasting sizes as seen in (A). Representative spheroids were visualised on day 14 using (A) bright field microscopy at 10x magnification, scale; 75µm. (B) Coverslips were fixed with 2% PFA and stained with p-ERM (green), GM130 (red) and DAPI (blue). Stained spheroids were visualised using confocal immunofluorescence microscopy at 63x magnification, different zooms. Scale; 40µm.

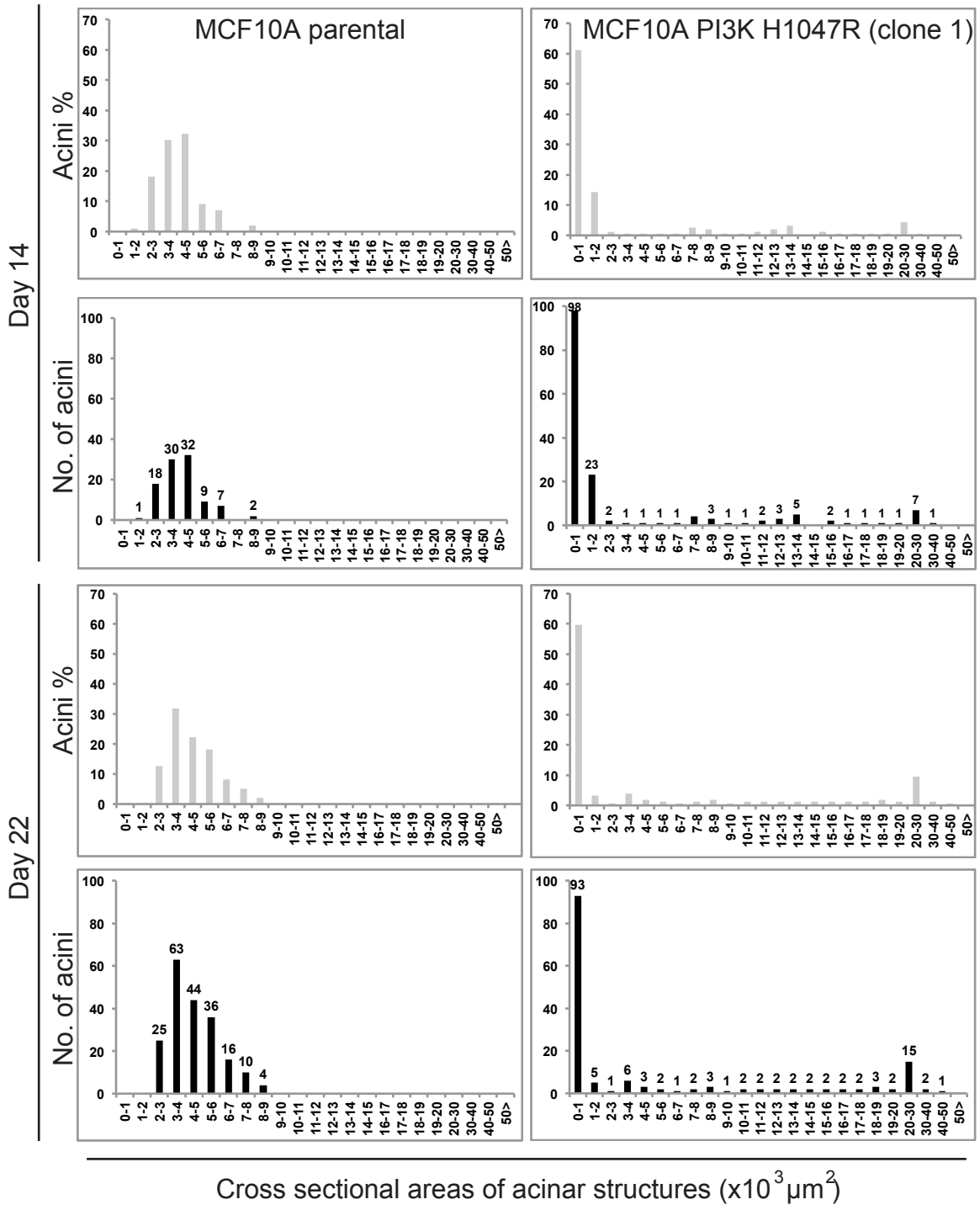


**Figure 3.11. Similar cross sectional area distributions of MCF10A parental and PI3K H1047R acini.** Areas of acini were measured and compared on day 14 and day 22 using 10x bright field microscopy images and Image J. A total of 99-198 acini were counted for each cell type.

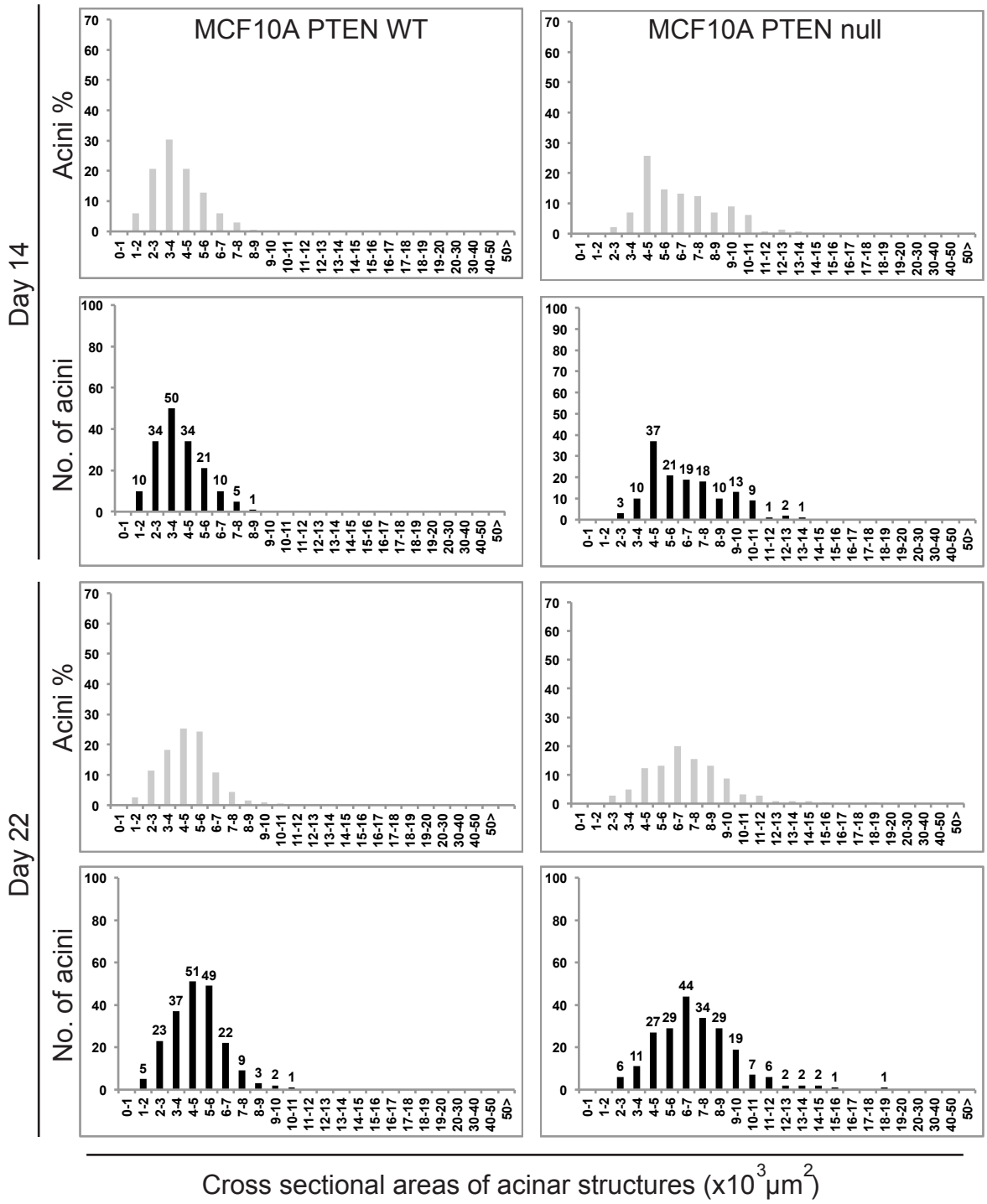


**Figure 3.12. Cross sectional areas of MCF10A PTEN WT and PTEN null acini show similar distribution.** Cross sectional areas of acini were measured and compared on day 14 and day 22 using 10x bright field microscopy images and Image J. A total of 144-220 acini were counted for each cell type.

CSA of each was translated from pixels to $\mu m^2$. The MCF10A parental line showed a normal distribution with the majority of acini around $3000\mu m^2$- $5000\mu m^2$ when measured on day 14 and day 22 (Figure 3.11). The distinct populations of the isogenic PI3K H1047R (clone 1) acini varied in CSA from $\leq 1000\mu m^2$ (59-63%) and up to $50{,}000\mu m^2$ (37-51%). CSA quantitation of the MCF10A parental and H1047R (clone 1) acini revealed no obvious change in trend when left in culture for either 14 or 22 days (Figure 3.11).

The MCF10A PTEN null (-/-) acini, which were paired with the PTEN WT control acini showed similar spheroidal morphology albeit with less lumen clearance (Figure 3.10). The overall CSA of PTEN WT speroids on day 14 and day 22 were comparable to that of MCF10A parentals (Figure 3.11, 3.12). Importantly, the majority of PTEN null acini were on average 28% and 44% larger in CSA compared to most PTEN WT acini controls on day 14 and 22.

### *3.3.3 Effect of culture duration on the size distribution of MCF10A acini*

More than 90% of PTEN null mutant spheroids showed a CSA of $\geq 4000\mu m^2$ compared to 43% of PTEN WT on day 14. On day 22, the majority of PTEN null spheroids were larger than $6000\mu m^2$ in CSA whilst PTEN WT spheroid were predominantly at $2000\ \mu m^2$-$6000\mu m^2$. Overall the MCF10A parental and PTEN WT spheroids showed comparable distributions of CSA on day 14 and day 22 ($3000$-$6000\mu m^2$). The CSA distributions have also been compared to the biological repeat carried out separately by a colleague, Rebecca Eccles, which showed similar trends (not shown).

### *3.3.4 MCF10A parental spheroids cultured ±EGF*

Previously in 2D culture, interdigitations between neighbouring cells were visible in a confluent monolayer. I have preliminarily tested the prevalence of this phenomenon in the 3D context. Spheroids were left to grow in complete growth medium for 4 days before medium was exchanged to medium ±EGF (Figure 3.13). The majority of the spheroids in complete growth medium observed on day 8 and day 14 were qualitatively larger (Figure 3.13). Lumens were surrounded by an organised outer layer stained positive with E-cadherin and pERM. Despite being in complete growth medium for 4 days initially, most spheroids subsequently cultured in -EGF medium remained undeveloped when compared to the +EGF controls. The majority of the cells within the –EGF spheroids also appeared with less lumenal clearance on day 14. According to the manufacturer's datasheet, traces of EGF (<0.5ng/ml) remain in

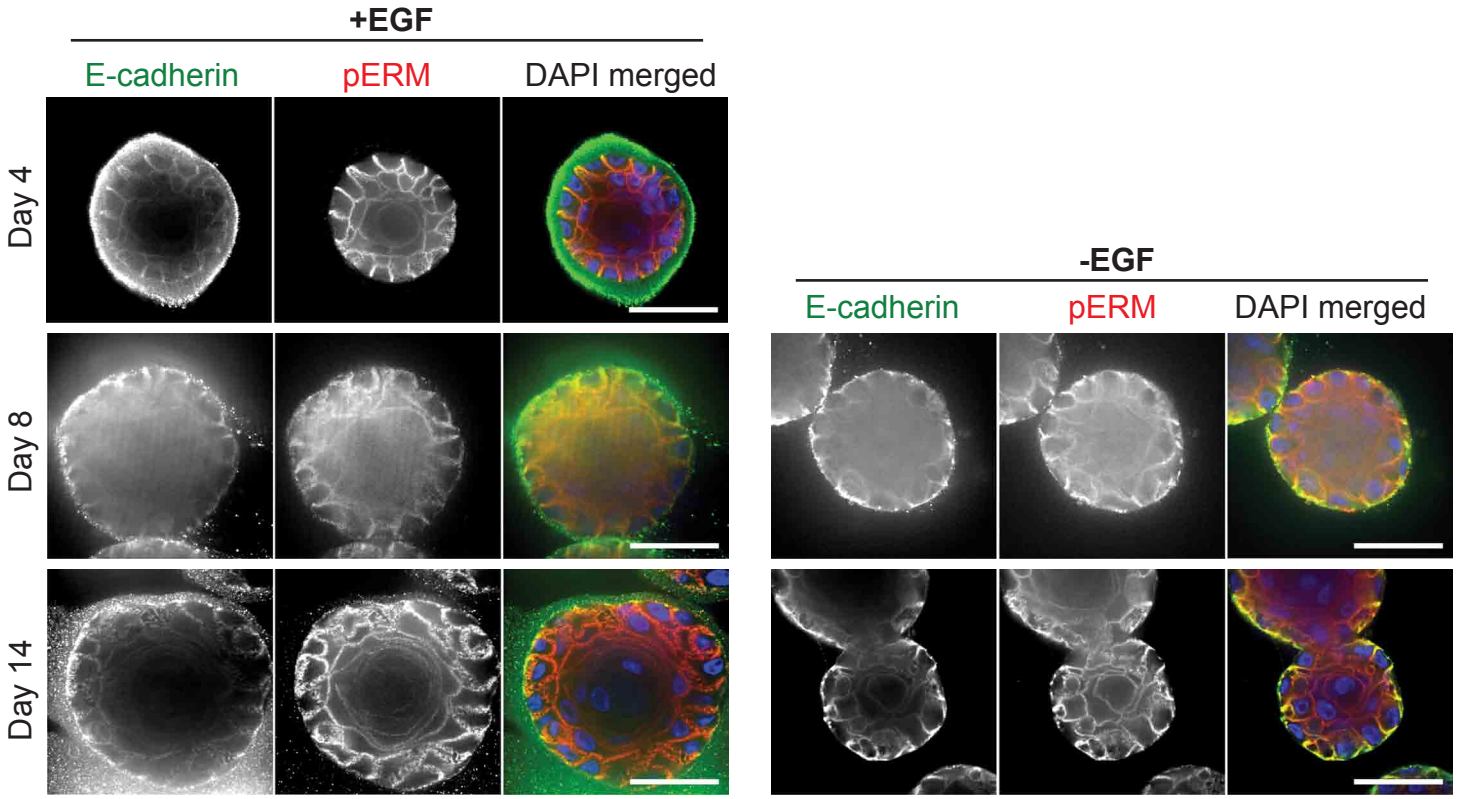


**Figure 3.13. EGFR signalling retards growth of MCF10A acini.** MCF10A parental acini were cultured in complete growth medium until day 4. Medium was exchanged on day 4 to medium with or without 5ng/ml EGF (HS). Medium was refed every 4 days. Spheroids were fixed with 2% PFA and permeabilised on days indicated. Acini were co-stained with E-cadherin (green), pERM (red) and DAPI (blue). Images were visualised using spinning disk confocal immunofluorescence microscopy at 63x magnification. Scale; 40μm. HS, horse serum assay medium. Medium recipes are listed in Methods: Table 2.7.

the Matrigel although acini were cultured without EGF. This may have been sufficient to suppress formation of interdigitations in the 3D environment.

## 3.4 Discussion

**Main chapter findings**

- EGF suppresses the formation of interdigitations in MCF10A cells in 2D culture.
- This phenotype is recapitulated in another clone of MCF10A parental cells and MCF10A PI3K E545K mutant isogenic cells.
- Interdigitations are visibly stained using E-cadherin in confluent monolayers, near the top of cells (less than 3μm depth of cells).

### *3.4.1 Two-dimensional characterisation of MCF10A cells*

The removal of EGF but not insulin in confluent monolayers allowed the formation of interdigitations in MCF10A cells. This suggests that EGF suppresses the process of interdigitation. Most common signalling pathways associated with EGFR activation include the PI3K and the MAPK pathways which are differentially activated by both insulin and EGF (Borisov et al., 2009). Based on computational modelling, insulin and EGF signaling have been proposed to converge upstream of Ras, at the level of adaptor protein, Gab1 (Borisov et al 2009). One may deduce that regulators of the interdigitated phenotypes may lie above this postulated convergence point of the PI3K and MAPK signalling levels due to the inability of insulin removal to recapitulate this process. Interestingly, EGF treatment has been shown to inhibit mammary duct formation *in vivo* in pre-pubertal mouse (Coleman and Daniel, 1990). Unlike the MCF10A cells, the addition of EGF also reduced the proliferative abilities of the ductal epithelial cells. The authors suggested that the preference for EGF at different stages of mammary development varied and is tightly regulated *in vivo*, overlapping with the need for different hormones. Henceforth, further experiments were undertaken in complete growth medium with EGF as the only unique variable tested for its role in the further characterisation of interdigitation in MCF10A parental cells.

Since the first characterisation of MCF10A cells in laboratory culture, many groups have assessed the relevance of culture medium components to the growth and proliferation (Ethier et al., 1993; Park et al., 2004; Soule et al., 1990). Consistently in serum free conditions, EGF, hydrocortisone and insulin provide the strongest stimuli for proliferation of non-tumorigenic human mammary epithelial cells in monolayer culture (McGrath and Soule, 1983; Park et al., 2004). In my hands, EGF removal did

slow the growth of subconfluent MCF10A cells in culture. Subconfluent MCF10A cells changed morphology adversely when hydrocortisone was removed from medium. Additionally, insulin and cholera toxin have been shown to promote differentiation into luminal human mammary epithelial cells on collagen (Ethier et al., 1993). However, cell differentiation remains outside the scope of this thesis.

Cholera toxin raises intracellular cyclic AMP (cAMP) concentrations to positively regulate the polarisation of outer cells and lumen clearance of MCF10A cells in 3D culture (Nedvetsky et al., 2012). Without cholera toxin, the subconfluent EGFR mutant cells exhibited a very mesenchyme-like phenotype compared to control. Presumably, the subconfluent culture of EGFR ΔE746-A750 allowed the cells to exhibit mesenchyme-like characteristic that resembles the epithelial-to-mesenchymal (EMT) phenotype as the cells were not yet contact inhibited. In the presence of an EGFR activating mutation, cholera toxin appears to suppress EMT. EMT has been linked to increased risk of resistance to small molecule tyrosine kinase inhibitors of the EGFR, gefitinib and erlotinib in lung cancer cells that harbours the EGFRΔE746-A750 mutation (Suda et al., 2011). In contrast to my observations, inhibition of the PKA activity downstream of cAMP signalling pathway suppressed EMT in human lung adenocarcinoma A549 cells (Shaikh et al., 2010).

In confluent monolayers, MCF10A parental and EGFR mutant cells remained cobblestone-like. Cholera toxin appears to mildly suppress EGF action as the combinatorial removal of EGF and cholera toxin presented a mild interdigitated phenotype. This reflects the tight regulation of cell morphology by different supplements in different spatial context. The role of cholera toxin and the downstream cAMP pathways in the plasticity of EGFR mutant cells although interesting, was not pursued further. Cholera toxin was kept in the medium to maintain a standard growth medium for both culture and experiments using the MCF10A isogenic cells.

***Morphological characterisation of MCF10A PIK3CA mutant cell clones***

The PIK3CA gain-of-function ‘hotspots’ at H1047R (kinase domain) and E545K (helical domain) result in constitutively active enzymes with differential oncogenic potential (Isakoff et al., 2005; Meyer et al., 2013). The latter has been reported to be less potent in inducing heterogenous mammary tumour in mouse xenograft models which sustained a longer tumour latency period. Accordingly, the E545K mutation is seen in only ~5% of human breast cancers compared to the more frequent H1047R

at ~15% (Meyer et al., 2013). Under control +EGF conditions, different clones of H1047R and E545K cells show characteristic cobblestone monolayers. Control treated WT cells for this mutant were not available. The recommended medium for the PIK3CA mutants (H1047R clone 1 and clone 23) is without EGF. However, in my hands, the PIK3CA clones exhibited varied phenotypes when cultured ±EGF. The H1047R clone 1, clone 22 and clone 23 did not interdigitate in -EGF. The E545K clone 10 showed interdigitations comparable to the MCF10A parental cells. The less-tumour inductive potency of the E545K mutation in MCF10A cells may have sustained the non-malignant ability to interdigitate in the absence of EGF better than the more oncogenic H1047R mutated cells. This would suggest that the ability to interdigitate in confluent monolayers remains within the remit of non malignant mammary epithelial cells. The increase in pAKT witnessed across the PIK3CA isogenic MCF10A cells remained independent of the levels of AKT, which is consistent with reports by other groups (Wallin et al., 2012; Isakoff et al 2005).

### *3.4.2 Three-dimensional characterisation of MCF10A cells*

Subsequently, the PIK3CA H1047R (clone 1) and PTEN null mutants were cultured in the 3D Matrigel assay. The phosphatase and tensin homolog (PTEN), a tumour suppressor antagonises PI3K-AKT signalling by dephosphorylation of phosphatidylinositol 3,4,5-triphosphate ($PIP_3$) to phosphatidylinositol 4,5-biphosphate ($PIP_2$), the secondary messenger that is generated by PI3K (Leslie and Brunton, 2013; Wallin et al., 2012). Presumably, the PIK3CA H1047R and PTEN null acini may show similar morphologies in a 3D Matrigel assay. The MCF10A PI3K H1047R and PTEN null acini lacked lumen clearance when compared to the parental and PTEN WT spheroids. Other studies of similar MCF10A H1047R cells by Genentech Inc. and Horizon Discovery Ltd. show that these cells in short term (1-2 days) Matrigel culture grew into ‘highly elongated network of branches’ suggestive of an invasive phenotype while PTEN null cells displayed minimally invasive behaviour (Wallin et al., 2012, Rigby et al., 2010 [poster]). This would support the subtler phenotype of the PTEN null acini when compared to the PI3K H1047R spheroids. In prolonged 3D culture, I saw two distinct populations of irregularly shaped PI3K H1047R (clone 1) acinar structures that were either very large or very small. This may correspond to the mixed epithelial and mesenchymal phenotype seen in 2D culture. Brugge’s team reported that stably transfected MCF10A PIK3CA (H1047R and E545K) mutant cells have abnormally proliferative acini that did not invade surrounding Matrigel basement membrane but grew in soft agar indicating transformation. They proposed that this is synonymous to pre-malignant, non-

invasive mammary tumour growth (Isakoff et al., 2005). The loss of PTEN in PTEN null cells may have contributed to the enhanced survival of cells within the acinar lumen due to the constant activation of the AKT pathway (Vitolo et al., 2009).
Notably, in my hands, most acini did not exhibit complete lumen clearance on day 14. The low concentration of Matrigel used (8.9mg/ml) may have delayed this process. I also did not discriminate between acini that were embedded either fully or overlaying the surface of Matrigel. Overlaying acini may stain with fluorescent-conjugated antibody more efficiently but may have developed quicker, limiting the cells' ability to form a hollow lumen (Debnath et al., 2003). Due to time limitation, I did not characterise the EGFR signalling profiles within the 3D acini. The comparable CSA distribution of MCF10A parental, PTEN WT and PTEN null acini would allow subsequent experiments to be ended on day 14 to simplify the experimental protocol. However, if changes in CSA of the PTEN null acini are relevant outputs, the experiment may have to be extended to allow PTEN null cells to continue growing to show a more noticeable difference in CSA when compared to PTEN WT.

The majority of MCF10A acini in prolonged culture without EGF were similar in size to the day 4 controls indicative of the lack of growth. Previously sialodectomised (removal of submandibular gland) pregnant mice have reduced the size and weight mammary gland that was reversed by EGF treatment (Okamoto and Oka, 1984). Indirectly, this infers that EGF can positively regulate the size and weight of mammary glands *in vivo*. The size and weight gain of the mammary gland may be due to EGF-stimulated ductal growth as seen in ovariectomised pubertal mice (Coleman et al., 1988). Technically, reduced growth factor Matrigel was used but residual EGF (<0.5ng/ml) listed in the manufacturer's datasheet may have continued to suppress interdigitation in MCF10A cells even when cultured without EGF in the assay medium. This level of EGF is within the range found in human plasma at 0.2-0.8 ng/ml (Hayashi and Sakamoto, 1987). The lack of lumen clearance in the -EGF MCF10A acini may indicate lack of cell polarisation and acini maturation. MCF10A cells incubated in medium lacking EGF in collagen cultures form horizontally spread cell sheets forming 'duct-like' structures as opposed to single cell clumps of control +EGF cells (Soule et al., 1990). Inversely, EGF treatment reduced the number of ducts per mammary gland in the highly proliferative glands of pubertal mice (Coleman and Daniel, 1990). These studies may highlight the role of EGF in suppressing the formation of ductal structures in collagen cultures and *in vivo*. Rationally, the MCF10A acini seen in Matrigel culture may not be the most optimal

assay to visualise the formation of mammary ducts. Further investigation of the interdigitated sheets of MCF10A cells in -EGF should be undertaken in more appropriate cultures such as the collagen cultures as published by Soule et al. (1990).

# Chapter 4
# Detailed characterisation of the interdigitated phenotype

## 4.1 Introduction

To further characterise the interdigitated phenotype previously described in 2D culture, I continue to optimise experimental protocols to induce the formation of interdigitations in MCF10A cells. Building on the knowledge that EGF suppresses interdigitations, the localisation of the EGF receptors was investigated in cells cultured with and without EGF. Further mechanism-related questions explored include:

i) How long does it take to form interdigitations in a monolayer?

ii) Which EGFR associated signalling cascades are involved?

iii) Is the process of interdigitation reversible?

iv) If so, which EGFR associated signals are involved in the reversible process?

Small molecule inhibitors were used to inhibit canonical downstream integrators of the EGFR signals to delineate mechanisms involved in the formation and reversal of digits. Biochemical readouts of phosphorylated and total proteins were coupled with immunofluorescent outputs to establish a link between the interdigitated phenotype and the different signalling cascades.

Previously, the formation of interdigitations required the cells to be cultured without EGF. One would expect that exchange to medium without EGF would fail to resolve digits of the confluent cells. Surprisingly, subsequent optimisation experiments led to the discovery that complete growth medium lacking EGF transiently reversed the interdigitations. This was investigated further by forming two separate hypotheses: i) Do the MCF10A cells secrete an autocrine factor that stabilises/ favours interdigitations? ii) Is there an exhaustible factor in FBS that transiently substitutes for EGF to resolve the interdigitations? These questions were tested in the reversal of interdigitation ±FBS and also by the use of conditioned medium.

It is also possible that the reversal of interdigitations could be due to the presence of another factor in the FBS that may have overlapping effectors as the EGF. The EGFR can be activated by different ligands containing the EGF motif which includes EGF, transforming growth factor-α (TGFα), heparin-binding EGF-like growth factor (HB-EGF), betacellulin (BTC), amphiregulin (AREG), epiregulin (EREG), epigen (EPGN) and neuregulins (Schneider and Wolf, 2011). The ligands are differentially expressed depending on tissue type (Yarden and Sliwkowski, 2001). EGFR can also be transactivated by other signalling receptors such as Met receptor and insulin receptor both activated by non-ErbB family ligands, hepatocyte growth factor (HGF) and insulin to activate the PI3K-pAKT cascades downstream of EGFR (Borisov et

al., 2009; Boyer, 2008; Hammond et al., 2010; Zielinski et al., 2009). Therefore, I investigated if the reversal of interdigitations is specific to EGF or if it may be substituted by other EGF-like ligands that allow EGFR transactivation to relay overlapping downstream signalling.

I have investigated if this phenomenon is applicable to other mammary epithelial cells. Breast cancer cells such as MCF7 maintain smooth boundaries between neighbouring cells and do not require EGF in the culture medium. Another non-malignant mammary epithelial cell line, HMT3522 S1 was reported to form finger-like interdigitations when cultured without EGF but had not been characterised further (Holm et al., 1993). Like MCF10A cells, they also require the presence of EGF in a complex cocktail of medium. Subsequently, I cultured and recapitulated this dynamic phenotype in these cells.

## Results

### 4.2 Formation of interdigitations in MCF10A cells

#### *4.2.1 EGFR distribution along interdigitations*

E-cadherin used as a plasma membrane marker illustrates the smooth boundaries between neighbouring cells within a monolayer cultured in routine growth medium. When EGF was removed, MCF10A cells continued to grow into monolayers but developed 'finger-like' protrusions between cells. EGFR is a transmembrane protein that is internalised into endosomal vesicles upon EGF stimulation (Roepstorff et al., 2008). The EGFRs in control MCF10A (+EGF) cells were internalised. This is consistent with the findings of Duan et al. (2011) who reported EGFR internalisation in MCF10A cells acutely stimulated with EGF. In contrast, EGFRs remained on the membranes in -EGF condition and showed similar staining pattern to E-cadherin, along the folds of the interdigitations (Figure 4.1). Duan et al. (2011) did not record an interdigitated phenotype in their experiments most likely because their observations were limited to subconfluent cells grouped in small islands. Instead they reported that EGFR activation stimulated downstream actin regulators to remodel adherens junctions. Their observation supports the earlier phase contrast results of MCF10A cells in subconfluent culture that did not display the interdigitated phenotype (Figure 3.1).

#### *4.2.2 Timecourse of formation of interdigitations*

Initially I seeded 100,000–150,000 cells per well of a 6 well plate and left the MCF10A cells to proliferate in complete growth medium for 72 hours. Figure 4.1 shows that interdigitations formed under -EGF condition. To determine the minimal time needed for the cells to form digits within the monolayer, I designed separate experimental configurations by asking: i) how long does it take for cells to interdigitate when seeded from a fully dissociated state at low density? ii) Can interdigitations be induced after cells have achieved confluent monolayers? In growth medium lacking EGF, the prominence of E-cadherin stained interdigitations increased from 38-70 hours, when cells were seeded from subconfluence and left to grow into a confluent monolayer (Figure 4.2). Control (+EGF) cells appeared smaller as the cells proliferated to become more crowded in the monolayer. Next, to circumvent the time needed for cells to proliferate and form a monolayer, interdigitations were induced by exchanging the medium after the MCF10A cells were confluent. With this experimental configuration, it took less than 22 hours to induce the interdigitations (Figure 4.2). Using time-lapse microscopy, this time frame

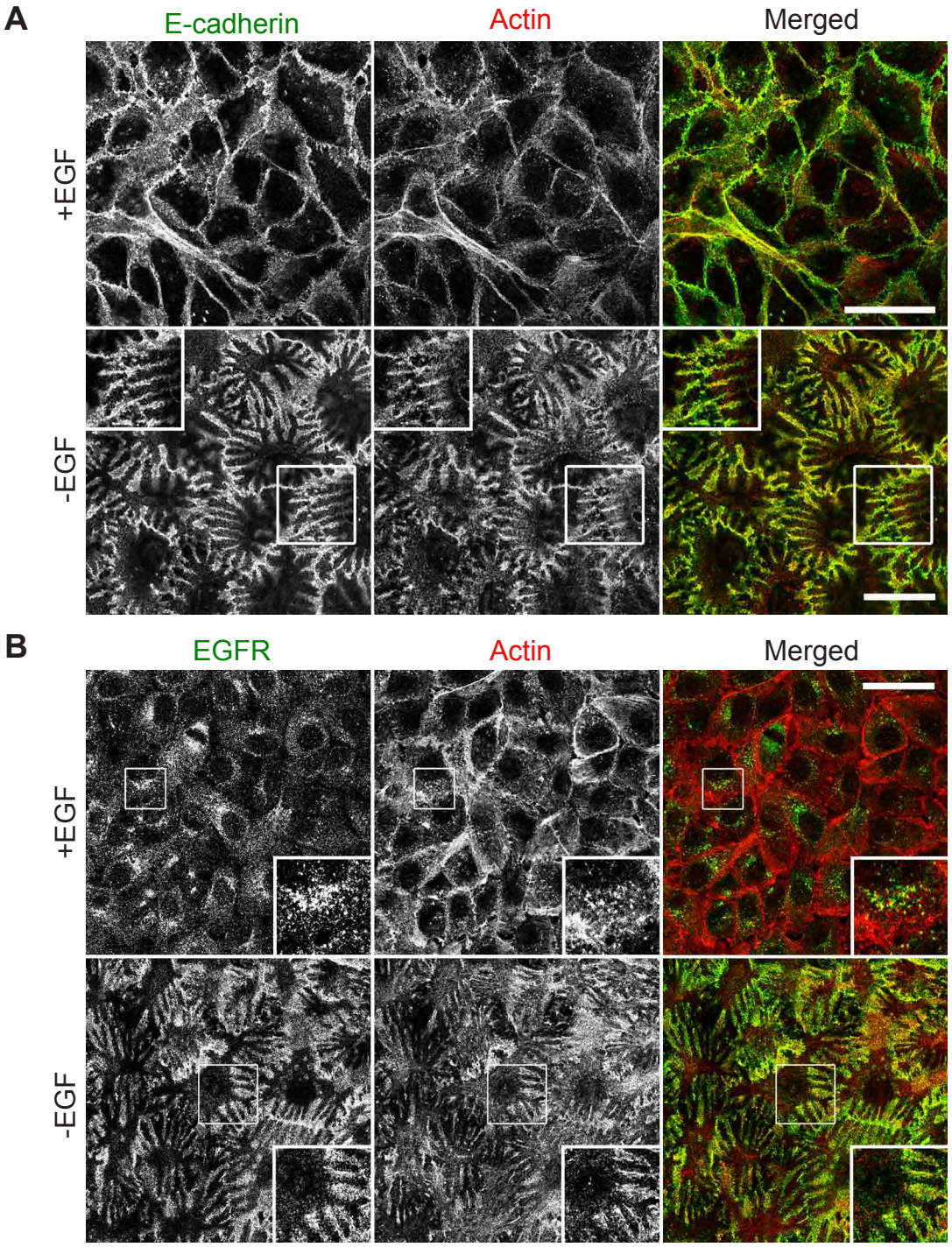


**Figure 4.1. EGF Receptor, E-cadherin and actin stains along interdigitated monolayers of MCF10A cells.** Complete growth medium was exchanged to medium ±20ng/ml EGF six hours post seeding. After 72 hours, cells were fixed with 4% PFA and stained for (A) E-cadherin (green), (B) EGFR (green) and F-actin (red). EGFR remained along the interdigitations when cultured in growth medium without EGF. Cells were visualised using confocal microscopy at 63x magnification (zoom 1.5 and 1.9). Scale; 40µm.

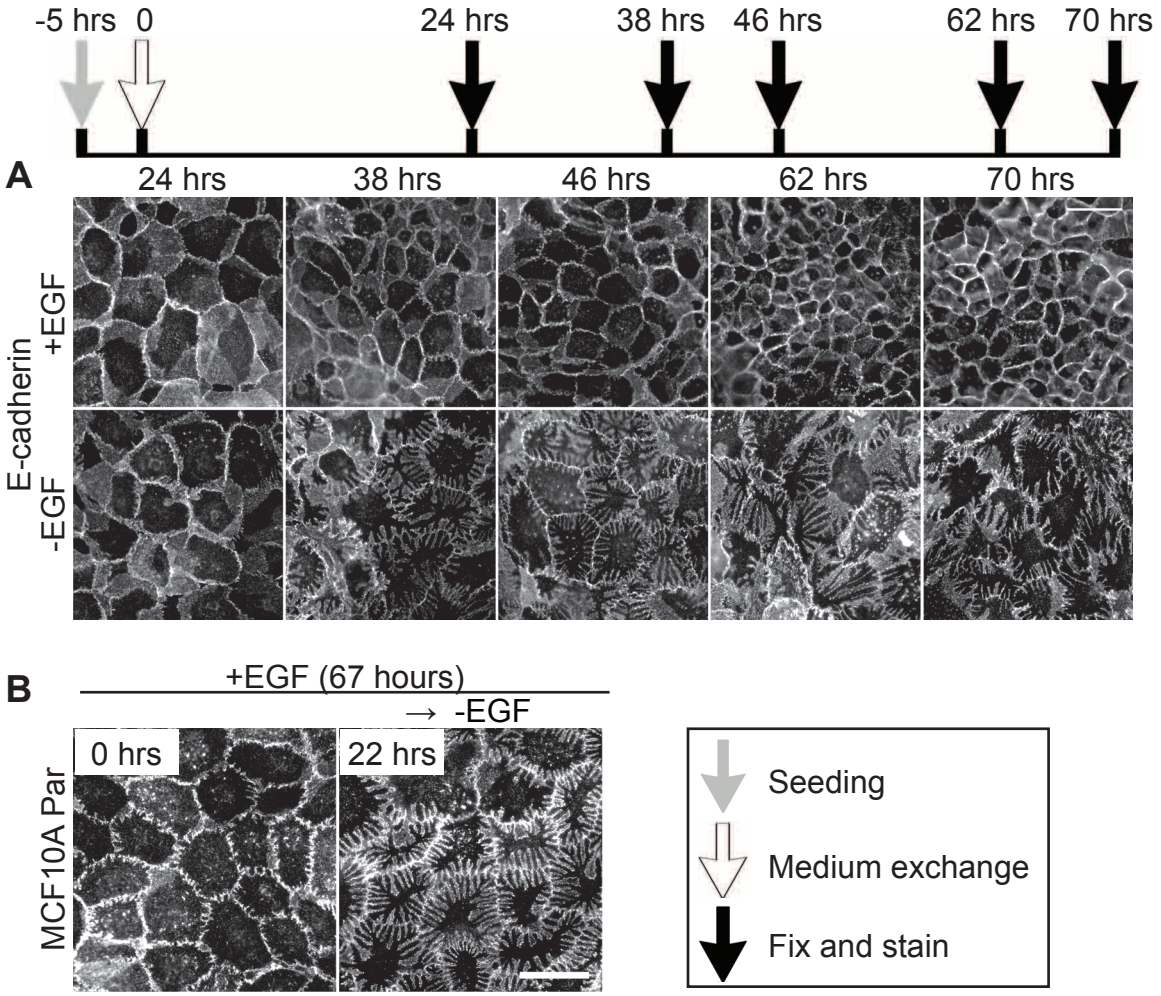


**Figure 4.2. Timecourse for the formation of interdigitations.** (A)The prominence of E-cadherin stained interdigitations on the membrane of MCF10A parental cells gradually increased from 38-70 hours after medium exchange when seeded from subconfluence. Medium lacking EGF was replaced for complete growth medium, 5 hours post seeding. (B) Interdigitations were induced in confluent MCF10A monolayers within 22 hours. Cells were cultured to confluence in complete growth medium (67 hours) before EGF was removed by medium exchange (22 hours). Coverslips were fixed with 4% PFA and stained with E-cadherin. Cells were visualised using immunofluorescence microscopy at 40x magnification. Scale; 40µm.

was narrowed down to between 12-17 hours after medium exchange to remove EGF (Movie 4.1). It was also apparent that the cells became relatively immobile within a monolayer after interdigitations have been induced (Movie 4.1).

### *4.2.3 The EGFR inhibitor, Gefitinib phenocopies the induction of interdigitations in the presence of EGF*

Next I tested if EGFR inhibition would recapitulate this phenotype. Previously, cultures of MCF10A cells with constitutively active EGFR (EGFR∆E746-A750) suppressed interdigitation in medium without EGF (Figure 3.2). Gefitinib inhibits EGFR by competitively binding to the ATP binding pocket of the kinase domain (Jain el al., 2005). Cells treated with Gefitinib recapitulated the formation of interdigitations (Figure 4.3) when cultured for 48 hours in complete growth medium (+EGF). However, using Gefitinib, confluent cells needed between 24-48 hours to form interdigitations in a monolayer. This was longer than required following the removal of EGF (12-17 hours). Subsequently, I asked if Gefitinib decayed in prolonged culture of up to 48 hours (Figure 4.3). When Gefitinib was only added once on seeding day (*) the levels of pEGFR Y1068, pAKT and pERK increased in +EGF condition in contrast to reduced expression when Gefitinib was added daily. When Gefitinib was added daily, the pEGFR Y1068 and p44 of pERK levels were reduced but remained higher than basal levels without EGF stimulation. The reduction of pY1068, pERK and pAKT by Gefitinib treatment was not absolute. Jain et al. (2005) found that Gefitinib treatment only reduced but did not inhibit tumour volume of prostate cancer xenograft in mice as the inhibitor binds only at a few key phosphorylation sites such as Y845 on the kinase domain of EGFR. They attributed the continued tumour growth to EGFR signals propagated via other tyrosine sites as EGFR can be phosphorylated at alternative tyrosine sites such as pY1068 (Guo et al., 2003; Jain et al., 2005). The residues of phosphorylated EGFR (Y1068), AKT and ERK seen in MCF10A cells treated with Gefitinib agree with this view (Figure 4.3).

The levels of pAKT were slightly reduced but remained fairly constant when cultured without EGF for 48 hours (Figure 4.3). In line with previous observations by Boyer, (2008), ERK and AKT levels remained constant, fitting with their extended half-lives of over 27 hours (Schwanhaeusser et al., 2011). As expected, the presence of EGF that stimulated phosphorylation of EGFR at Y1068 and reduced total levels of EGFR.

### *4.2.4 Effect of EGFR associated signalling pathway inhibitors in the induction of interdigitations*

Small molecule inhibitors were used to inhibit canonical signalling pathways downstream of EGFR, orchestrated by PI3K and MEK. Pan class 1A PI3K inhibitor, PI103 and MEK inhibitor, AZD6244 were applied to confluent MCF10A monolayers to suppress these pathways for 6 and 24 hours. IF images show that the application of these inhibitors for 24 hours failed to induce interdigitation (Figure 4.4). Gefitinib only induced mild interdigitations in 24 hours as compared to the prominent digits seen in 48 hours (Figure 4.3, 4.4). Control cells demonstrated obvious interdigitations 24 hours after EGF was removed from the confluent monolayer as expected. The downstream effector pAKT was not reduced by PI103 in the presence of EGF. Basal pAKT levels remained similar regardless of EGF when cultured for 24 hours as seen previously (Figure 4.4, 4.5).

AZD6244 is a MEK1/2 kinase inhibitor that selectively inactivates ERK1/2 phosphorylation in sensitive cancer cell lines, HCT116, SW620 (colon cancers) and WM793 (melanoma) (Yang et al., 2010). In my hands, AZD6244 abrogated pEGFR and pERK levels better than Gefitinib at both timepoints (Figure 4.4). The reduction in pEGFR levels was surprising as this inhibitor functions to block downstream MEK1/2 at a unique pocket structure adjacent to the ATP binding site (Zhao et al., 2014). At the time of writing, AZD6244 is still being evaluated in phase II clinical trial as adjuvant to Erlotinib, an EGFR inhibitor used in KRAS mutated non-small cell lung (NSCLC) cancer patients to mitigate resistance mechanisms (Zhao et al., 2014). Previous experiments using Her2 and EGFR driven cancer cells, BT474 and HCC827 reported that the reduction of pERK signalling by AZD6244 treatment was compensated by the increase in phosphorylation of ErbB3 to stimulate the pro-survival pAKT pathway (Turke et al., 2012). Such response illustrates the ability of tumorigenic cells to resist small molecule inhibition that remains a caveat to personalised medicine. To my knowledge, such experiments have not been conducted in non-malignant cells lacking hyper-activated EGFR. It appears that in non-malignant MCF10A cells, pEGFR at Y1068 is also reduced, and cells proliferated less. This could represent inhibition of a positive feedback loop on the EGFR by the MAPK, in contrast to the situation described for BRAF inhibitors in colon cancer cells (Prahallad et al., 2012). In my hands, pAKT expression remains unchanged, which speaks against the same positive feedback seen in Her2 and EGFR driven cancers.

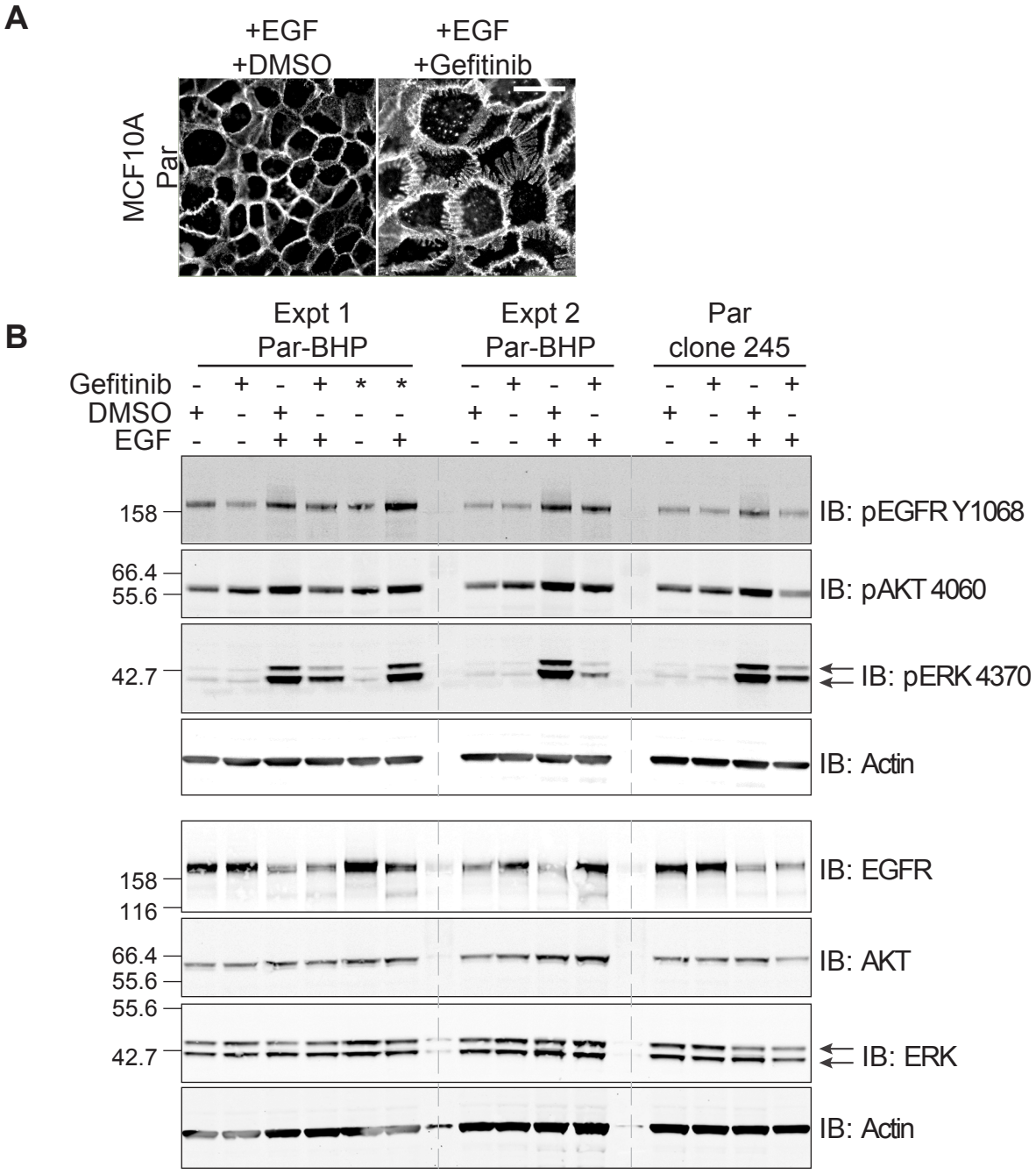


**Figure 4.3. Gefitinib induces interdigitations in the presence of EGF.** (A) Cells were treated with Gefitinib (300nM) from seeding and were fixed 48 hours after medium exchange. Cells stained with E-cadherin were visualised using immunofluorescence microscopy at 20x magnification. Scale; 40µm.
(B) Duplicate lanes of parental cells clone BHP were biological repeats. Cells were cultured in complete growth medium ±EGF for 46.5-49.5 hrs. EGF refers to the presence of EGF in growth medium. Gefitinib was added on seeding day only (*) or daily until lysis. 10µg of MCF10A cell lysates were loaded onto each lane. Expt, experiments repeated.

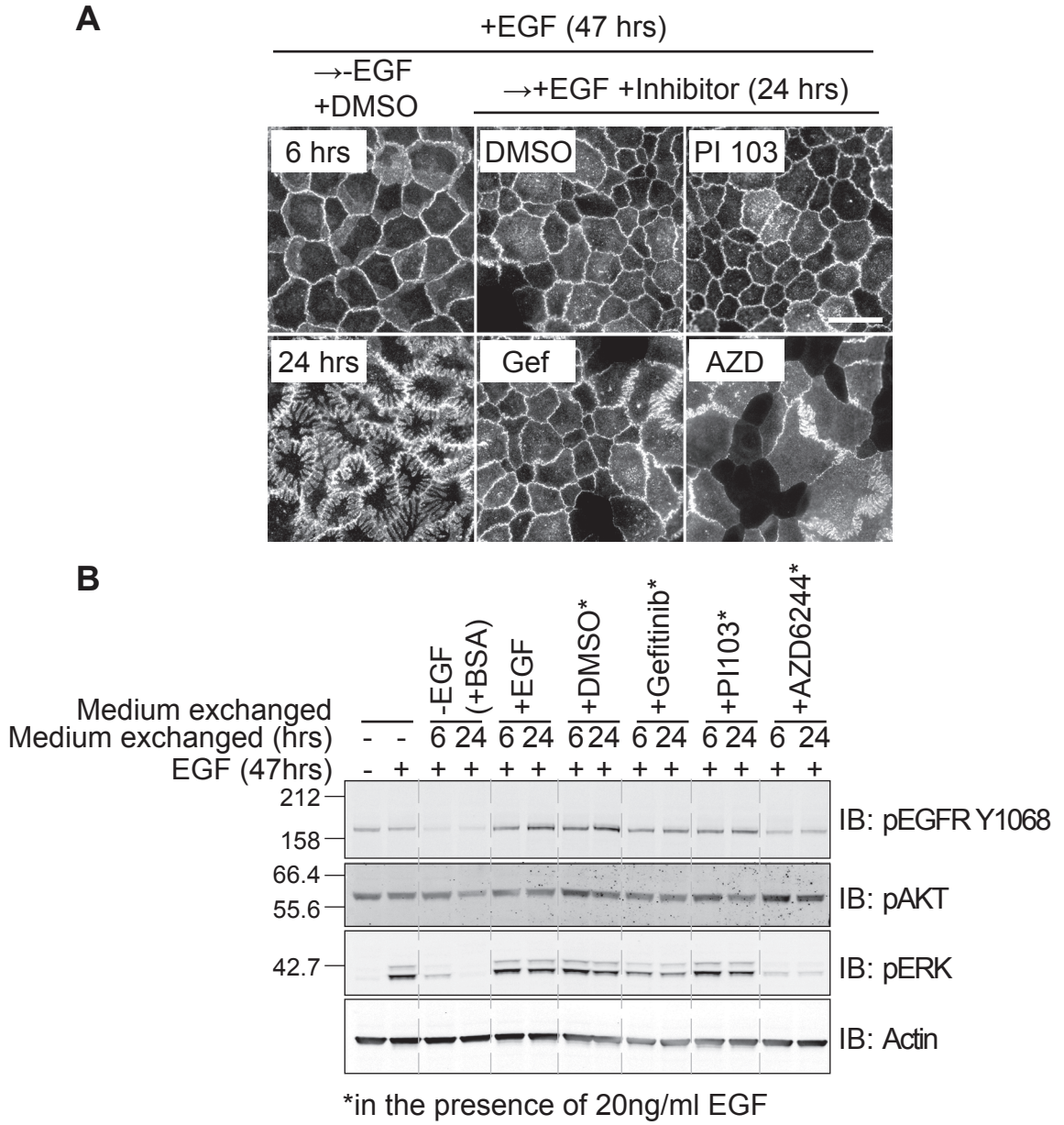


**Figure 4.4. Formation of digits independent of short-term inhibition of EGFR and canonical downstream targets.** MCF10A cells were cultured in complete growth medium (+EGF) for 47 hours after seeding. Medium was then exchanged to include either Gefitinib (300nM, EGFR inhibitor), PI103 (100nM, PI3K inhibitor) or AZD6244 (300nM, MEK inhibitor) for 6 or 24 hours. (A) Coverslips were fixed with 4% PFA and stained with E-cadherin. Cells were visualised using immunofluorescence microscopy at 40x magnification. Scale; 40μm. (B) 10μg of MCF10A cell lysates were loaded onto each lane.

On glass coverslips, AZD6244 treated cells failed to form a coherent monolayer and the larger cells observed indicated lower confluence. Only mild interdigitations were observed. Clearly, 24 hours was not sufficient to induce interdigitated monolayers of MCF10A cells using Gefitinib, PI103 and AZD6244.

An alternative PI3K inhibitor, LY294002 was compared to PI103. There was a slightly better reduction in pAKT levels at 4 hours in the presence of EGF compared to PI103 treatment (Figure 4.5). In ZR-75-1 breast cancer cells, LY294002 suppressed pAKT transiently but levels recovered within 24 hours although growth of cells was halved and they remained viable in culture for up to 6 days (Ripple et al., 2005). Although not formally tested, inhibitors may need to be added daily as Gefitinib (Figure 4.3). Thus, when inhibitors were added daily and in combination for longer (48 hours), digits were induced in confluent monolayers. Interdigitations provoked by Gefitinib treatment was less penetrant compared to the application of AZD6244 that produced more widespread interdigitating structures. This was further elaborated when used in combination with Gefitinib or LY294002 (Figure 4.5). Treatment with AZD6244 or LY294002 alone led to shorter fingers structures compared to the removal of EGF. However, combining all 3 inhibitors recapitulates the prominence of interdigitations seen with the removal of EGF. Thus EGF tonically suppresses interdigitations in confluent monolayers via the combined outputs of EGFR, PI3K and MAPK signalling pathways. It is possible that other downstream EGFR activated components are involved that remain to be determined. It is noteworthy that neither of the EGFR associated inhibitors impeded the induction of interdigitations in the absence of EGF. This demonstrates that neither pathways is critical to induce interdigitations.

Alternative EGFR, ErbB2 and PI3K small molecule inhibitors were also applied to induce interdigitations in MCF10A cells. Accordingly, daily addition of the EGFR inhibitors; Erlotinib and Gefitinib reduced pERK significantly at 48 hours (Figure 4.6). EGFR/ ErbB2 inhibitor; Lapatinib reduced pERK at 4 and 48 hours albeit to a lesser extent. All 3 ErbB inhibitors induced interdigitations in confluent monolayers of MCF10A cells (Figure 4.6). The PI3K inhibitor, GDC0941 significantly reduced pAKT levels at 4, 24 and 48 hours and induced more prominent interdigitations compared to the previously used PI103 and LY294002 inhibitors (Figure 4.4, 4.5, 4.6). Rac-GEF(Trio/ Tiam1) inhibitor, NSC23766 did not affect pERK or pAKT levels as expected (Akbar et al., 2006).

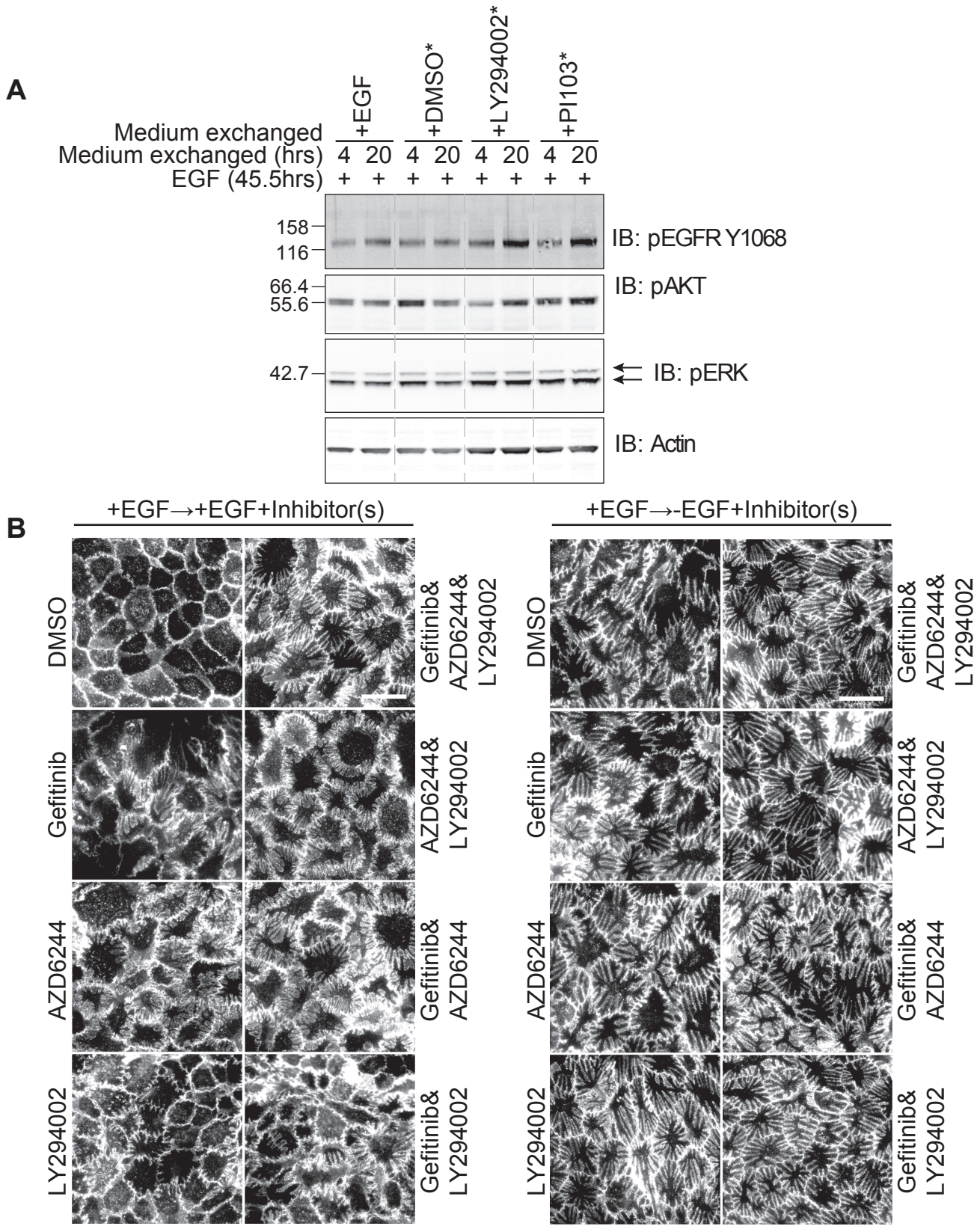


**Figure 4.5. Long-term inhibition of EGFR and canonical downstream targets recapitulates the phenotype induced by EGF removal.,**Cells were cultured in complete growth medium +EGF for 45.5-47 hours. Medium was exchanged to include the inhibitors as annotated for (A) 4, 20 hours and (B) inhibitors were added daily for 48 hours. (A) 10µg of MCF10A cell lysates were loaded onto each lane. * indicates presence of EGF in medium. (B) Combinations of Gefitinib (300nM), AZD 6244 (300nM) and LY294002 (20µM) added to confluent MCF10A cells in the presence of EGF, induced highly developed interdigitations. Formation of fingers by EGF withdrawal was not impeded by the presence of the same inhibitors. Coverslips were fixed with 4% PFA and stained with E-cadherin. Cells were visualised using immunofluorescence microscopy at 40x magnification. Scale; 40µm.

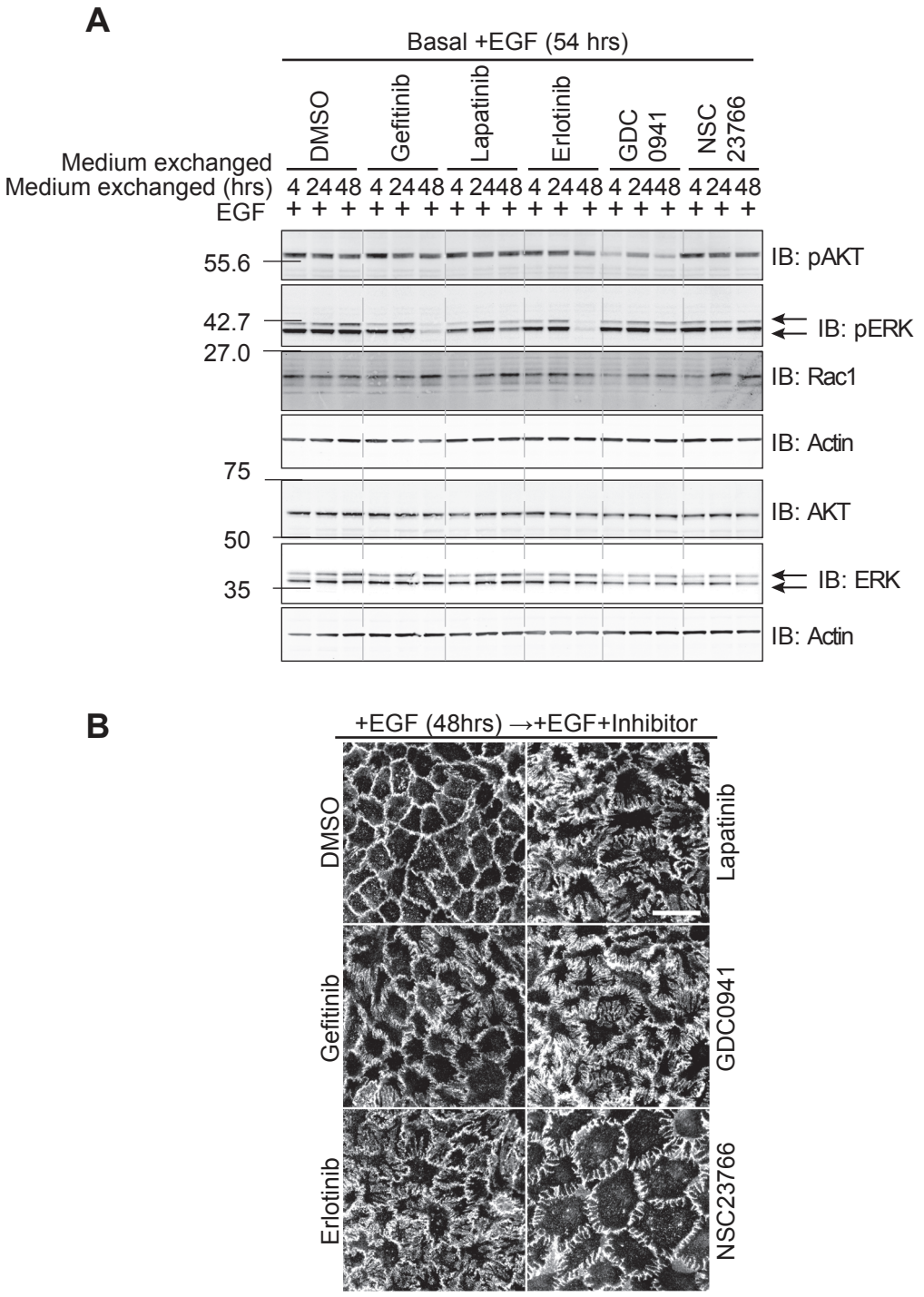


**Figure 4.6. Alternative ErbB family and PI3K inhibitors induces interdigitations at 48 hours.** (A) Treatment with EGFR inhibitors, Gefitinib (300nM) and Erlotinib (100nM) reduced pERK levels at 48hrs. EGFR and ErbB2 inhibitor, Lapatinib (1μM) only reduced pERK slightly. PI3K inhibitor, GDC0941 (500nM) reduced pAKT. Rac-GEF inhibitor, NSC23766 (50μM) did not affect levels of EGFR signalling or Rac1 proteins. 10μg of MCF10A cell lysates were loaded onto each lane. All inhibitors were added in +EGF medium. MCF10A cells were cultured 48-54 hours before exchange of medium to include the inhibitors for (A) 4, 24 and (A & B) 48 hours. Inhibitors were added daily after cells have achieved confluence in the presence of EGF. (B) Coverslips were fixed with 4% PFA and stained with E-cadherin. Cells were visualised using immunofluorescence microscopy at 40x magnification. Scale; 40μm.

## 4.3 Resolution of interdigitations in MCF10A cells

### *4.3.1 Interdigitations resolve upon exchange to medium containing EGF*

Knowing that interdigitations are inducible, naturally I wanted to investigate if these structures are reversible. MCF10A cells were cultured without EGF for up to 70 hours to form interdigitated monolayers. Interdigitations in MCF10A resolved within 24 hours in medium with EGF (Figure 4.7). Resolution of these structures was apparent in MCF10A cells within 1.5 hours after EGF administration, which was relatively rapid compared to the induction (Movie 4.2). Motility of the cells within a monolayer also increased following resolution of interdigitations, accompanied by ruffling on the cell membranes (Movie 4.2). The relatively rapid resolution of interdigitations compared to the induction hints at a separately regulated mechanism, which will be discussed later in this chapter.

### *4.3.2 Experimental optimisation for the reversal of interdigitations*

Initially, I tested if the duration of the experiment can be reduced to 3 hours after exchange to medium containing EGF or addition of EGF as previous experiments resolved interdigitations from 1.5 hours onwards (Movie 4.2). The assumption is that EGF reverses the interdigitations. Unexpectedly, interdigitations also transiently reversed when exchanged to medium lacking EGF (Figure 4.8). At the extended 24 hour time period, interdigitations reformed under these conditions in contrast to the +EGF condition. This led to the formulation of two potential explanations: i) If exchange to fresh medium without EGF transiently reverses interdigitations, do the cells secrete an autocrine factor that is required for maintenance and allows the re-formation of interdigitations within 24 hours? ii) If exchange to fresh medium without EGF transiently reverses interdigitations, does the medium contain an exhaustible factor that transiently substitutes for EGF to supress interdigitations? (Figure 4.9).

To test if cells secrete an autocrine factor, I have compared the exchange of fresh for conditioned medium using the resolution of interdigitations as a readout. Conditioned medium was derived from parallel dishes of cells cultured with ±EGF medium for 68 hours prior to being used. MCF10A cells were cultured to form confluent interdigitated monolayers and digit resolution was observed following medium exchange. Interdigitations remained in conditioned medium without EGF (Figure 4.10). In contrast, exchange to fresh medium without EGF transiently resolved the interdigitations as previously observed (Figure 4.8, 4.10). As expected, exchange to either fresh or conditioned medium containing EGF completely reversed the interdigitations. It is possible that conditioned medium may contain

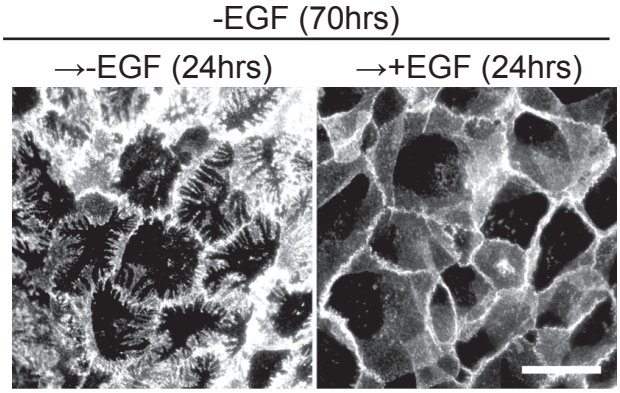


**Figure 4.7. Reversibility of interdigitations in MCF10A cells.** Interdigitations resolved within 24 hours when 20ng/ml EGF was readded to the MCF10A parental cells. Cells were cultured in medium lacking EGF for up to 70 hours. Medium was then exchanged to complete growth medium ±EGF for another 24 hours. Coverslips were fixed with 4% PFA and stained with E-cadherin. Cells were visualised using immunofluorescence microscopy at 40x magnification. Scale; 40µm.

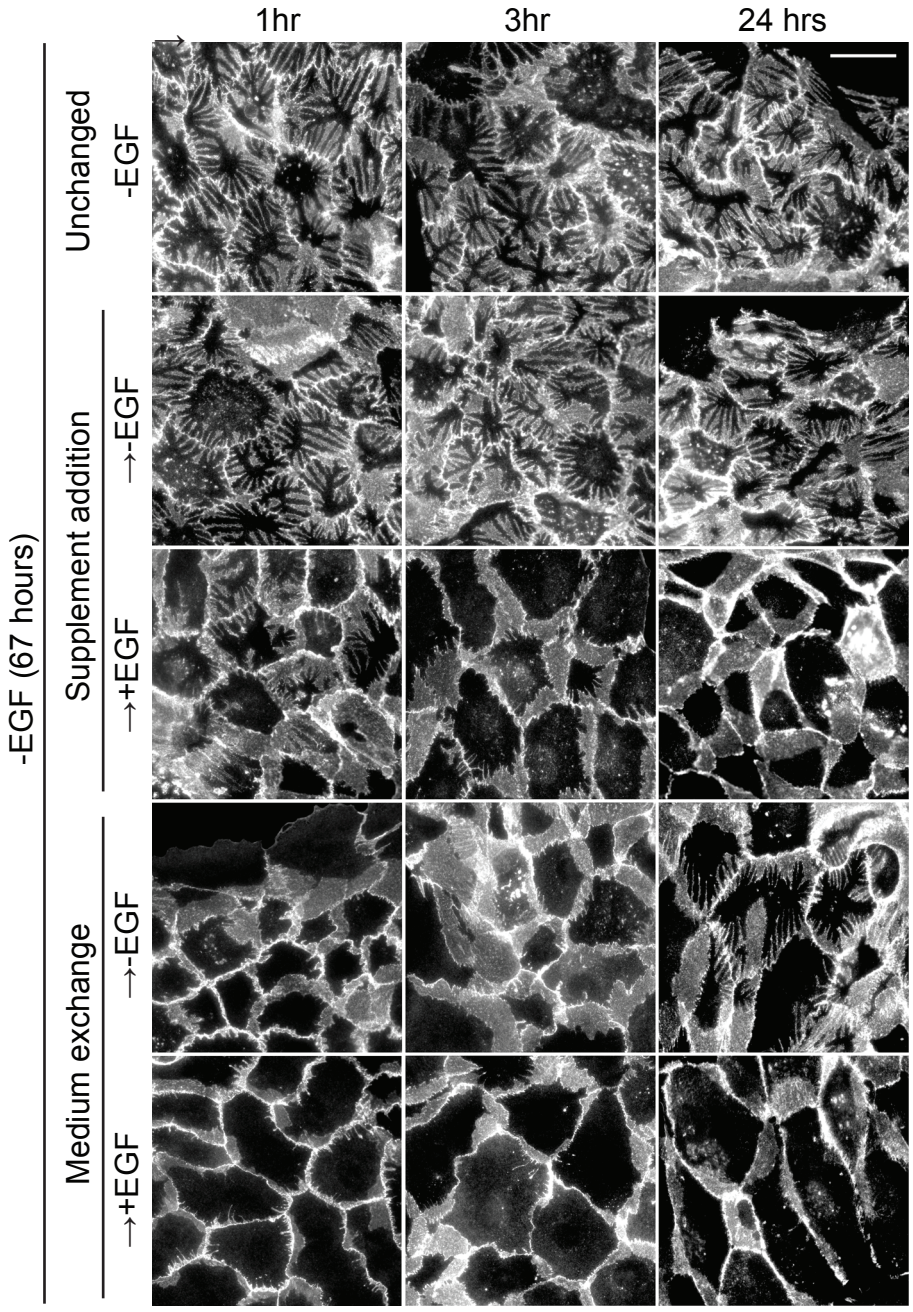


**Figure 4.8. Transient reversal of interdigitations upon exchange to fresh medium.** Interdigitations resolved transiently upon fresh medium exchange regardless of EGF (1 hour, 3 hours). Interdigitations reformed within 24 hours in the absence of EGF. Direct addition of EGF resolved interdigitation at all points. Cells were cultured for 67 hours in -EGF medium before either addition of supplements or exchange to fresh medium ±EGF. 0.5mg/ml BSA was added in the -EGF condition as negative control. Coverslips were fixed with 4% PFA and stained with E-cadherin. Cells were visualised using immunofluorescence microscopy at 40x magnification. Scale; 40μm.

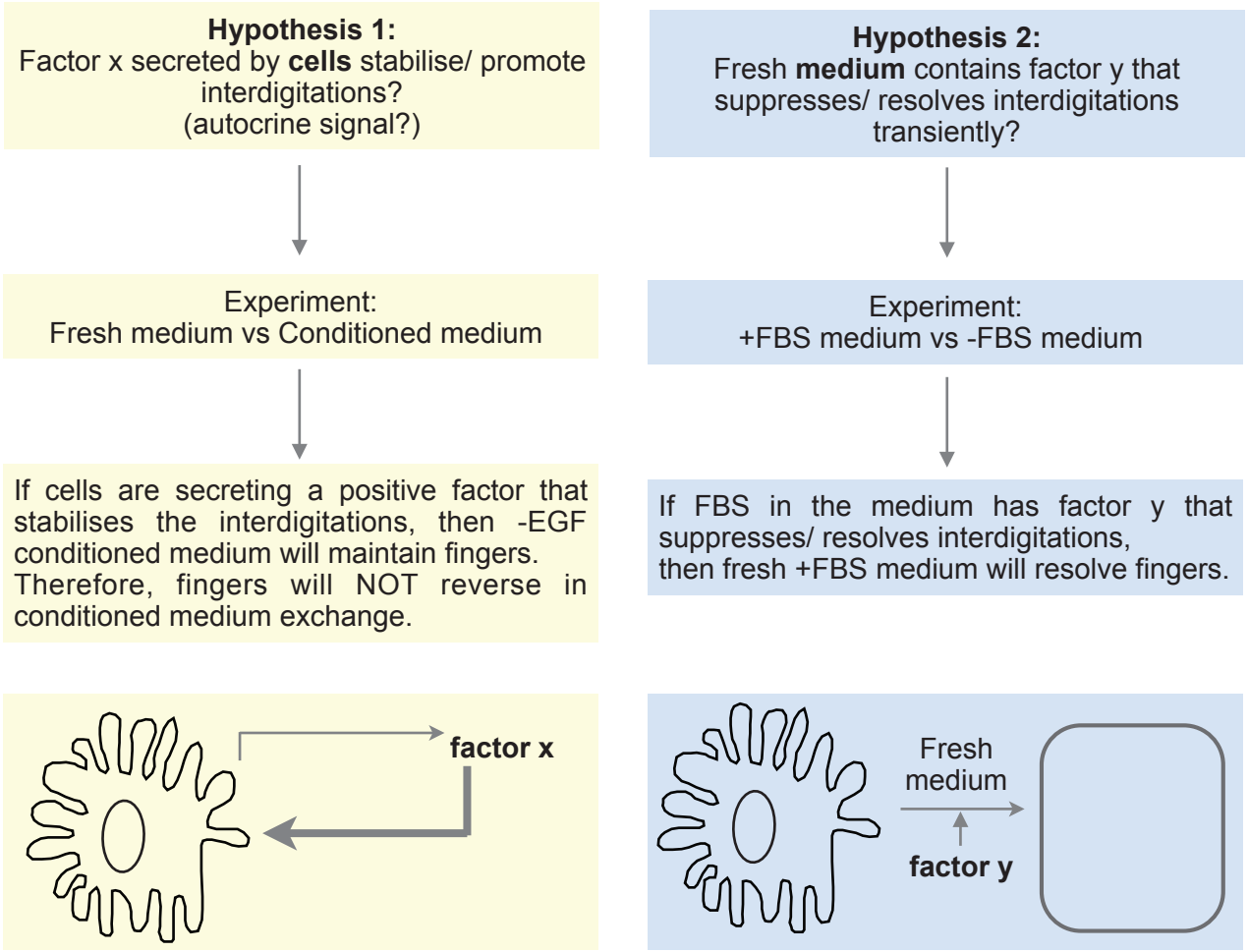


**Figure 4.9. Hypotheses for the transient reversal of interdigitations.** Flowcharts indicate the hypotheses and experiments undertaken with MCF10A cells to investigate the transient reversal of interdigitations seen in fresh medium exchange.

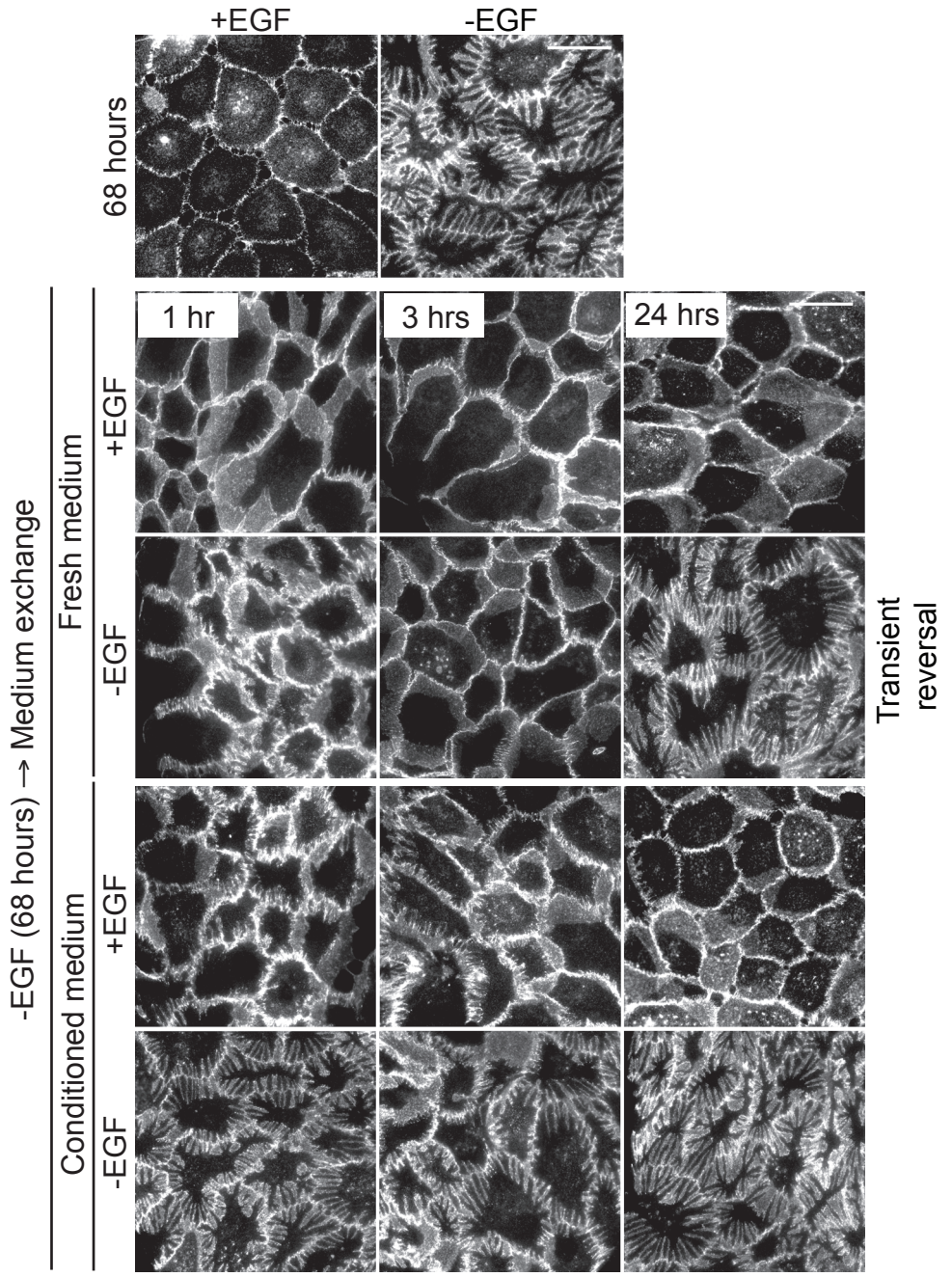


**Figure 4.10. Conditioned medium without EGF maintains interdigitations.** Interdigitations resolved transiently upon fresh medium exchange regardless of EGF (1 hour, 3 hours) and reformed within 24 hours in the absence of EGF. MCF10A cells were cultured for 68 hours in -EGF medium to form interdigitated monolayers before exchange to fresh or conditioned medium ±20ng/ml EGF. Coverslips were fixed with 4% PFA and stained with E-cadherin. Cells were visualised using immunofluorescence microscopy at 40x magnification. Scale; 40µm.

secreted autocrine factor(s) that promotes interdigitations. Hence resolved interdigitations reform within 24 hours of exchange to fresh medium -EGF.

To test if fresh medium contained an exhaustible factor, which transiently suppressed interdigitations, I compared medium ±FBS in their abilities to resolve interdigitations. It is in the FBS that many factors are introduced to the medium. In +FBS-EGF medium, interdigitations resolved transiently as previously seen with fresh medium exchange (Figures 4.8, 4.10, 4.11). In control medium, -FBS-EGF, interdigitations remained after exchange. Medium -FBS+EGF proceeded to resolve interdigitations although this was slightly delayed. Therefore, FBS or components in FBS temporarily substituted for EGF to suppress interdigitations. Henceforth, experiments investigating the resolution of interdigitations were performed with direct addition of EGF without medium exchange. This is to eliminate the effects of FBS, which may act synergistically to EGF to suppress interdigitations.

### *4.3.3 Differential abilities of growth factors to reverse interdigitations*

To follow up further, I asked: What factor in the FBS could account for the transient suppression of interdigitations? Ligands for various RTKs were added separately to monolayers of interdigitated MCF10A cells to mimic the presence of an 'EGF-like' factor present in the FBS (Figure 4.12).

Common ligands implicated in cell signaling related to the ErbB and Met receptor families were tested in their abilities to oppose interdigitations. Insulin that was routinely present in growth medium did not suppress interdigitations (Figure 3.2). TGF-α, which activates EGFR transiently, suppressed the interdigitations at 3 hours, which reformed within 24 hours as seen with the exchange of medium containing FBS (Figure 4.11, 4.12). This correlated with the transient activation of pERK that increased upon TGF-α addition at 15 minutes, 1 hour and 3 hours but reduced to basal non-stimulated cell levels within 24 hours (Figure 4.12). EGFR was continually degraded with EGF but levels were restored within 24 hours of TGF-α stimulation. The downregulation of EGFR may be crucial for the complete resolution of the interdigitations. Here, Neuregulin 1 (NRG1), which binds to ErbB3 and ErbB4, did not resolve the interdigitations. The enhancement of pAKT was sustained throughout 24 hours of NRG1 stimulation as compared to the short-lived phosphorylation of AKT, which terminated at 3 hours after stimulation with EGF or TGF-α. Instead, the pERK levels only spiked within 15 minutes but were

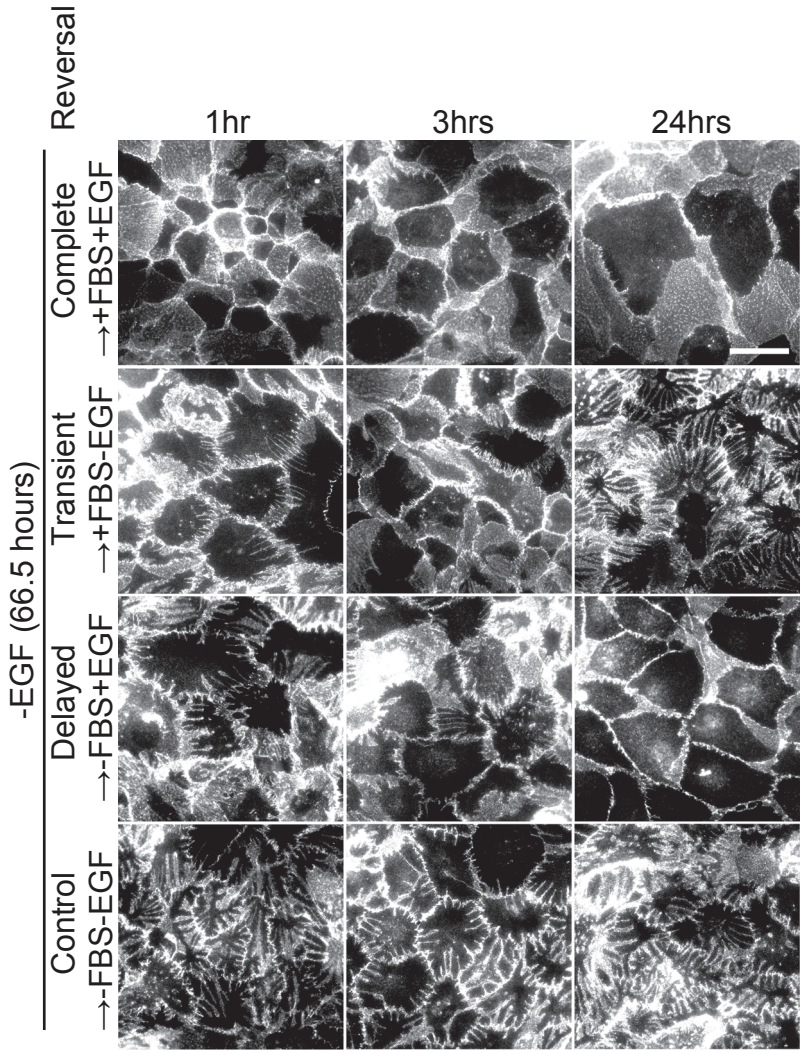


**Figure 4.11. FBS transiently resolves interdigitations.** In the absence of EGF, interdigitations reversed transiently when medium was exchanged to +FBS-EGF medium. Interdigitations reversed completely when exchanged to +FBS+EGF medium. Reversal was slightly delayed when medium was exchanged to -FBS+EGF medium. MCF10A cells were cultured in -EGF medium for 66.5 hours to form interdigitated monolayers before exchange of medium containing DMSO. Coverslips were fixed with 4% PFA and stained with E-cadherin. Cells were visualised using immunofluorescence microscopy at 40x magnification. Scale; 40μm.

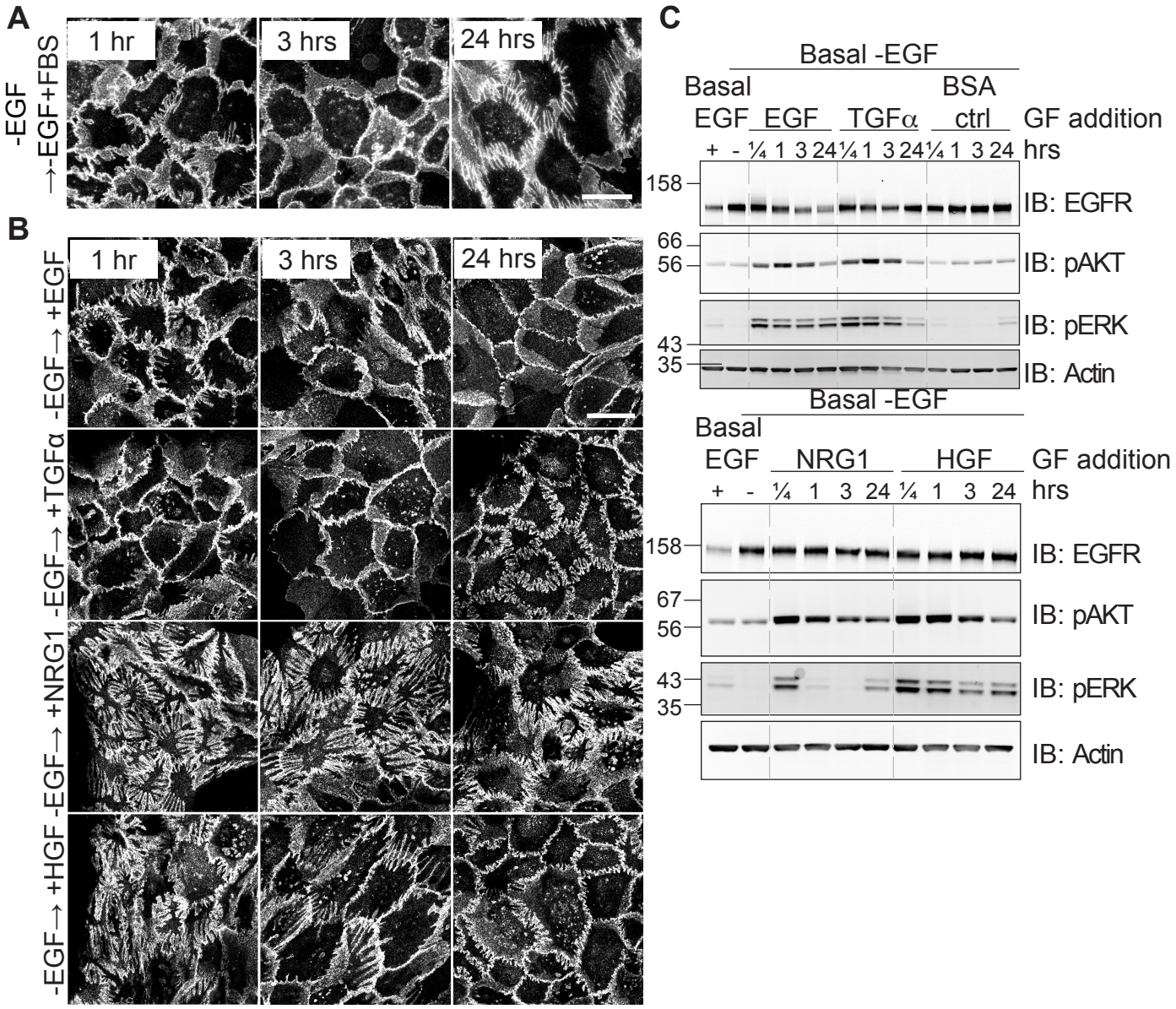


**Figure 4.12. Differential abilities of ligands to reverse interdigitations.** (A) Transient reversal of interdigitations in MCF10A cells (1-3 hours) when medium was exchanged to fresh +FBS-EGF medium. (B) Status of interdigitations at 1, 3 and 24 hours after addition of ligands: EGF (20ng/ml), HGF (20ng/ml), NRG1 (6ng/ml) or TGFα (20ng/ml). Cells were fixed with 4% PFA, immuno-stained with antibody directed at the extracellular domain of E-cadherin before visualisation using immunofluorescence confocal microscopy at 63x magnification, zoom 1.5. Scale; 40μm. (C) MCF10A cell lysates [8μg] following addition of ligands for the indicated times. Cells were cultured in growth medium lacking EGF for 69.5 hours before addition of ligands.

immediately reduced to non-stimulated levels within an hour of NRG1 stimulation in contrast to the sustained pERK signals upon EGF stimulation.

The hepatocyte growth factor (HGF), mediator of the 'HGF-cell scattering' programme failed to resolve the interdigitations at 3 hours despite shortening of the interdigitations apparent after 24hrs. The HGF cell–scattering programme is known to dissociate cell-cell contact when space is available (Birchmeier et al., 2003; Leroy et al., 2006). Western blots show that EGF and HGF elicit similar downstream activation of pERK of the MAPK pathway and pAKT of the PI3K pathway MCF10A cells at the timepoints tested (Figure 4.12). This observation agrees with the overlapping cell signalling networks reported in A549 lung adenocarcinoma cells (Hammond et al., 2010). The inability of NRG1 and HGF to completely resolve the interdigitations implies that this process is defined by a single cue, activation of EGFR. In MCF10A cells, addition of EGF downregulated EGFR levels gradually over 24 hours. (Figure 4.12). The levels of pAKT gradually reduced over 24 hours regardless of ligand stimulation. Insulin in the medium may have been exhausted as cells were cultured in the same medium without replenishment of supplements for up to 93.5 hours.

### *4.3.4 Effect of small molecule inhibitors in the resolution of interdigitations*

Previous experiments showed that the PI3K and the MAPK signalling pathways although not critical, acted synergistically in the formation of interdigitations (Figure 4.5). Inversely, I investigated if this is true to maintain digits following application of EGFR, PI3K and MEK inhibitors. At 24 hours, Gefitinib (EGFR inhibitor), AZD6244 (MEK1/2 inhibitor) and CP724214 (ErbB2 inhibitor) reduced pEGFR and pERK levels but failed to inhibit the resolution of interdigitations (Figure 4.13). AZD6244 suppressed levels of pEGFR Y1068 and pERK significantly compared to other inhibitors as seen in Figure 4.4. The correlating IF image showed less crowded cells on the coverslips when interdigitations reversed in 24 hours (Figure 4.13). This confirms that the inhibition of EGFR, MEK and ErbB2 does not impede the reversal of interdigitations. The resolution of interdigitations induced by EGF was unaffected by treatment with either the PI3K inhibitor, LY294002 or MEK1/2 inhibitor, AZD 6244 (Figure 4.14). This discounts the involvement of these canonical EGFR associated signalling pathways in the reversal process. Presumably, signalling cascades involved in the remodelling of the cell cytoskeleton are independent of the common pro-survival signal integrators downstream of the EGFR. This will be further explored in Chapter 5.

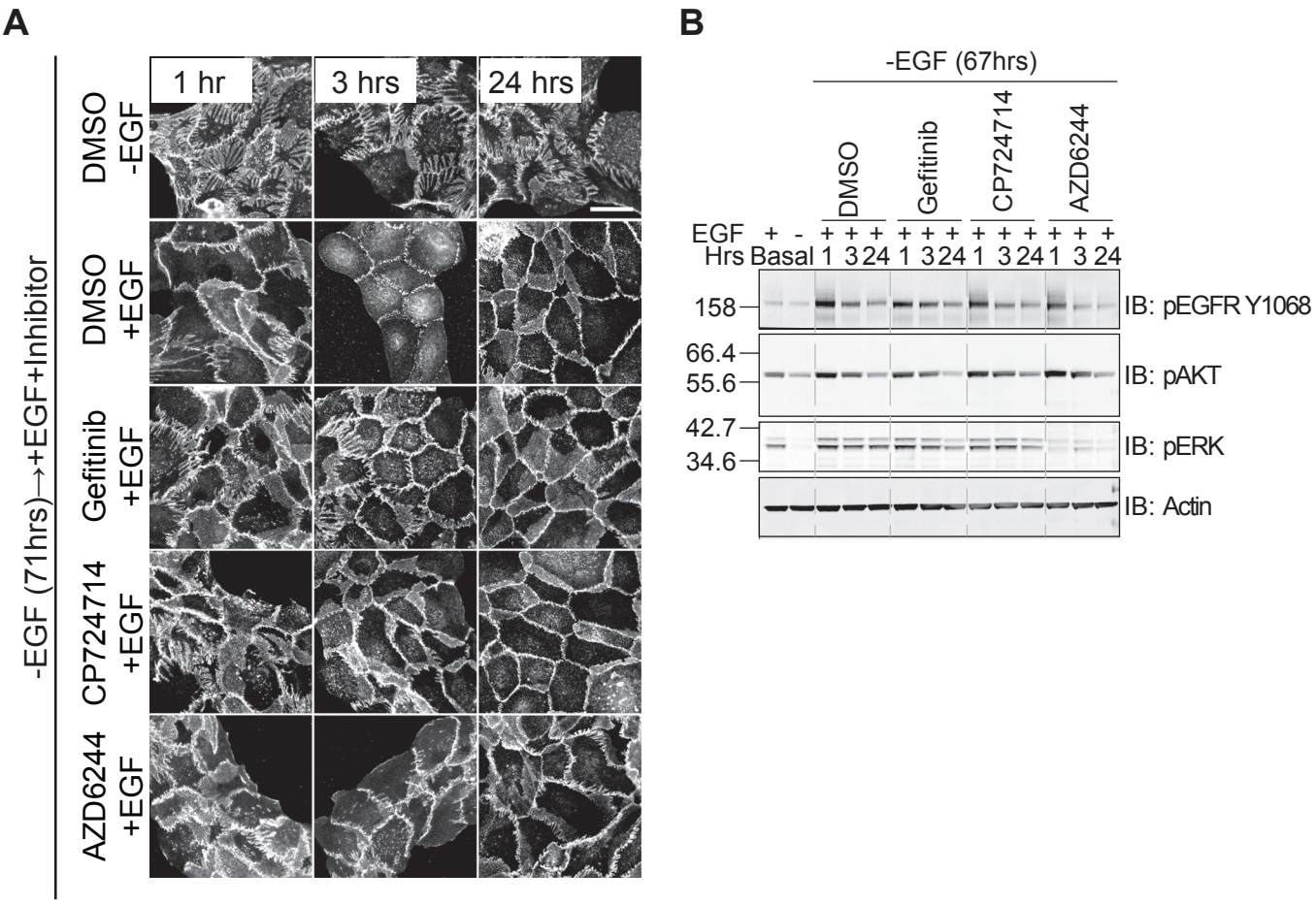


**Figure 4.13. Resolution of interdigitations independent of ErbB family and MEK signaling pathways.** (A) Reversal of interdigitations in the presence of EGFR inhibitor (300nM Gefitinib), ErbB2 inhibitor (250nM CP724714) and MEK inhibitor (300nM AZD6244). MCF10A cells were cultured in medium without EGF for 67-71 hours before addition of EGF and inhibitors as annotated. (A) Coverslips were fixed with 4% PFA at the indicated times after EGF and inhibitor addition, immuno-stained with E-cadherin before visualisation using immunofluorescence confocal microscopy at 40x magnification. Scale; 40μm. (B) Lysates were harvested at the times indicated after addition of EGF and inhibitors to resolve digits. 10μg MCF10A cell lysates were loaded onto each lane, following addition of EGF and inhibitors at the indicated times.

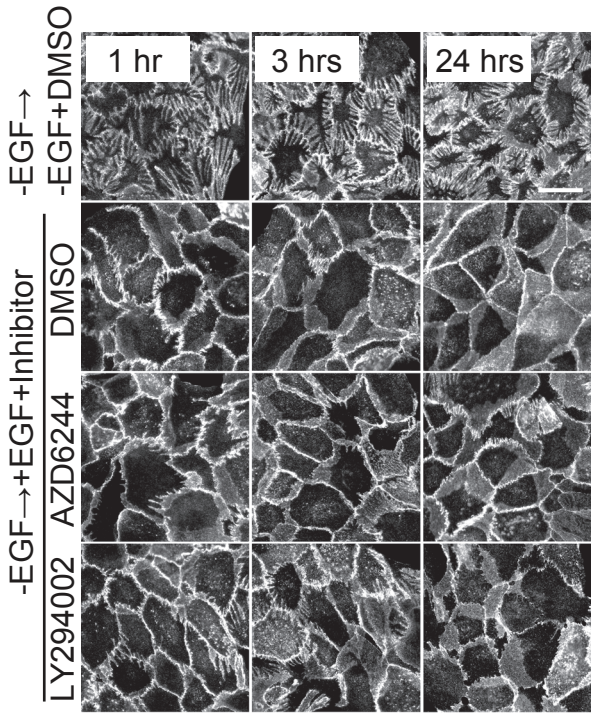


**Figure 4.14. Resolution of interdigitations independent of PI3K and MEK signalling pathways.** Dissolution of interdigitation proceeded normally in the presence of MEK (300nM AZD6244) and PI3K (20μM LY294002) inhibitors in the presence of EGF. Coverslips were fixed with 4% PFA, immuno-stained with E-cadherin before visualisation using immunofluorescence microscopy at 40x magnification at the time points indicated. Scale; 40μm.

### 4.4 HMT 3522 cells interdigitate reversibly dependent on status of EGFR activation

When a separate non-malignant mammary cell line, HMT 3522 S1, was cultured from confluence without EGF, the ability to interdigitate was recapitulated (Figure 4.15). This mimicked the interdigitations seen in MCF10A cells and confirmed a previous report in the literature (Holm et al., 1993). However, the process took longer in these cells (70 hours onwards) that are routinely cultured in serum free medium that are heavily supplemented with other growth factors (Briand et al., 1987; Methods: 2.1.2). Accordingly, cells proliferated in the presence of EGF and became more crowded as compared to the less proliferative cells under -EGF conditions (Figure 4.15). In reverse, addition of EGF resolved most interdigitations within 24 hours resembling the process seen in MCF10A cells (Figure 4.15, 4.12).

### 4.5 Discussion

In this chapter, I have presented a detailed characterisation of the dramatic reversible changes in epithelial cell boundaries within a confluent monolayer that is elicited with a single defined cue, EGF. To my knowledge, the formation of the interdigitated MCF10A monolayers upon EGF removal has not been characterised elsewhere. I have recapitulated this reversible phenomenon in an independent clone of MCF10A cells and also in another non-malignant mammary epithelial cell line, HMT 3522 S1. Collectively, these results illustrate that non-malignant mammary epithelial cells in culture are able to form reversible interdigitation defined by the status of EGFR activation. In contrast, this ability is abrogated in EGFR∆E746-A750 cells with oncogenic activation of EGFR that continually suppress the formation of digits in the absence of EGF.

The assembly of interdigitations in the absence of EGF is slow (>12 hours) when compared to the relatively rapid reversal (1-3 hours). Formation of the interdigitations may reflect the requirement for an altered cellular transcriptome and proteome following EGF withdrawal. One hypothesis could be that cells have to alter transcription and expression of proteins downstream of the EGFR to assemble the interdigitations. To approach this hypothesis, genome wide mRNA expression profiles of confluent MCF10A and EGFR mutant cells in ±EGF conditions can be screened using next-generation sequencing technology (RNAseq). The induction of finger-like protrusions using inhibitors of the EGFR, PI3K and MEK pathways confirms that EGFR signalling mediated by these pathways suppress digits

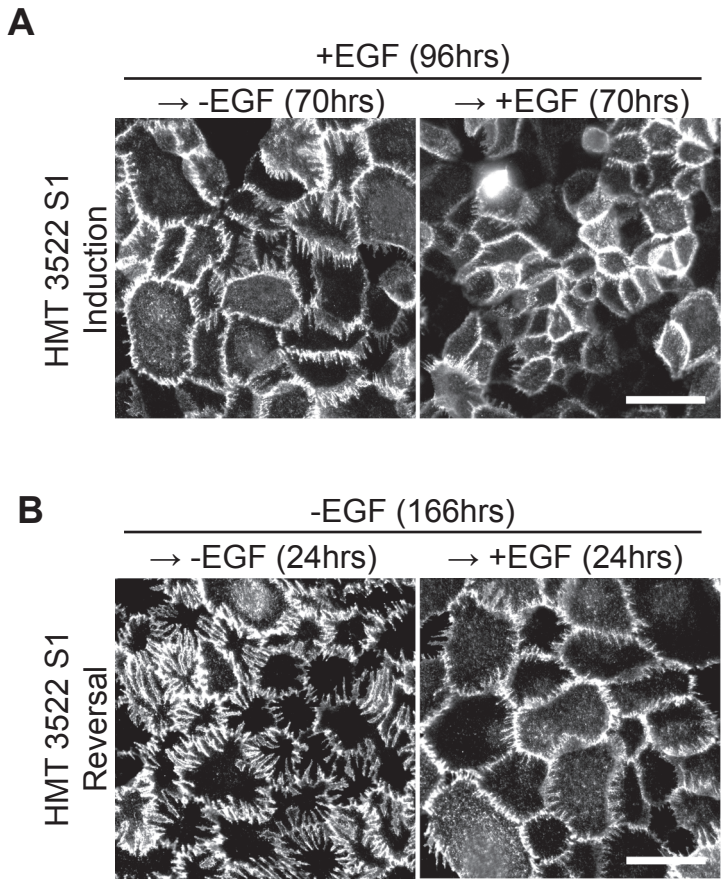


**Figure 4.15. Reversibility of interdigitations in non-malignant mammary epithelial HMT 3522 S1 cells.** HMT 3522 S1 cells were grown to confluence in complete growth medium (10ng/ml EGF) for 96 hours and interdigitations were induced by exchange to medium lacking EGF for a further 70-166 hours. (A) Induction of interdigitations from confluent monolayers of HMT3522 cells. (B) Reversal of digits upon addition of EGF. 20ng/ml EGF was either added or not for another 24 hours. Coverslips were fixed at the indicated times with 4% PFA and stained with E-cadherin. Cells were visualised using immunofluorescence microscopy at 40x magnification. Scale; 40μm.

formation. The tonic suppression of interdigitations requires the combined outputs of the PI3K and MAPK pathways but these are not essential to form digits when EGF is removed.

The resolution of interdigitations is specific to ligands that bind to the EGFR, leading to their downregulation. It was shown that TGF-α transiently mimics EGF in the ability to resolve interdigitations. This can be explained with the transient binding of TGF-α to the EGFR that preferentially dissociates from the receptor due to the pH changes in the endosome. Thus, EGFR is recycled rather than degraded when compared to EGF stimulation (Roepstorff et al., 2009; Lax et al., 1988). In my studies, I have not disproved the possibility that cells may secrete positive autocrine factors that transiently suppress interdigitations. Previous groups have reported the presence of TGF-α in serum and also in secretions from MCF10A cells (Ciardello et al., 1990; Moskal et al., 1995). The secretome of cells in conditioned medium can be compared to fresh medium to identify EGF sensitive secretion that may contribute to the suppression of interdigitated phenotype. However, this falls outside the scope of this thesis. Stimulation of ErbB3 and c-Met by NRG1 and HGF respectively failed to resolve interdigitations. This is accompanied by the observation that interdigitated cells remain shackled with minimal mobility within a monolayer. The mechanical implications will be explored further in Chapter 5.

Although independent of the PI3K and MAPK signalling outputs, the time course for digits reversal following EGF application (initiated within1.5 hours) is consistent with altered post-translational modifications such as phosphorylation (Amit et al., 2007; Avraham and Yarden., 2011; Tarcic et al., 2012). Non-biased systematic phospho-proteome and proteome analysis using SILAC (Stable Isotope labelling by amino acids in culture) based quantitative proteomics can be applied in the future. This would allow understanding of proteins downstream of the EGFR that could mediate the resolution of interdigitations to restore their motility within monolayers. Together, these data would allow unbiased clustering of relevant components to molecularly dissect the mechanisms involved in this reversible phenomenon. A more direct but biased approach would be to investigate the involvement of junctional profiles and the actin cytoskeleton in both processes. This will be further explored in Chapter 5.

# Chapter 5
# Mechanical functions linked to the ultrastructure, cytoskeleton and junctions of interdigitations

## 5.1 Introduction

In this chapter, the characterisation of the interdigitated monolayers is extended to explore the ultrastructure, cytoskeleton and junctions associated with the interdigitated phenotype. Transmission electron microscopy (TEM) work was undertaken to visualise the interdigitations at the ultrastructural level. Filaments resembling actin cables were observed projecting into the tips of the interdigitations. Subsequently, I have evaluated the need for actin polymerisation and actomyosin contractility by treating the cells with relevant inhibitors. The morphology of cells in confluent monolayers was observed using IF microscopy as an assay to determine the role of the actin cytoskeleton in the dynamic reversible action of interdigitations.

In relation to the signal regulation at the actin cytoskeleton, the role of Rac1 GTPase in the formation and reversal of interdigitations was investigated. Rac1 signalling has been associated with actin nucleation and polymerisation via downstream actin regulators within the lamellipodia at the leading edge of mobile cells (Ridley, 2011). In addition, hyperactivation and overexpression of Rac1 have been implicated in breast cancer progression (Wertheimer et al., 2012). Hence, I have evaluated the activity of endogenous Rac1 in MCF10A cells using Glutathione-sepharose beads conjugated to the Rac1/CDC42 p21 binding domain of human p21 activated kinase 1 (GST-PBD) in pull down experiments (Pellegrin and Mellor, 2008).

Observations using the TEM also revealed an increase in desmosomal junctions along the interdigitations. Desmosomal junctions are normally assembled after adherens junctions to strengthen the integrity of cell-cell contact (Garrod, 2010; Chapter 1: Figure 1.8). Biochemical studies were also undertaken. This observation led to two conflicting hypotheses concerning their role in interdigitations: i) Do desmosomal proteins undergo increased clathrin mediated or non-clathrin mediated endocytosis in monolayers of cells with smooth boundaries? ii) Does the synthesis of desmosomal proteins increase during the formation of interdigitations? Both scenarios were explored via co-localisation IF microscopy using relevant antibodies.

Together, these observations raised more questions as to the mechanical function of actin and desmosomal rich interdigitations. In other studies, actin rich lamellipodia have been implicated to aid mobility of cells across substrates while desmosomal junctions have been shown to strengthen cellular sheets of keratinocytes (Garrod, 2010; Kimura et al., 2007; Ridley, 2011). I have proceeded to use a wound-healing assay to compare the ability of control and interdigitated cells to roam and seal a

scratched region in confluent monolayers. The strength of cell-cell adhesion was measured using the dispase-based mechanical assay. Fragments obtained were quantified to indirectly assess resistance to external shear stresses. Preliminary time-lapse imaging recorded the capacity of interdigitated monolayers to withstand induced osmotic stress. Combined, these assays inform on the physiological functions of interdigitations.

## Results

### 5.2 Ultrastructural and cytoskeletal characterisation: Formation and maintenance of interdigitations

#### *5.2.1 Actin cables project to digit tips*

Seeing the dramatic architectural changes upon EGF removal, I hypothesised that actin may be structurally remodelled in this process. When MCF10A monolayers were transiently transfected with GFP-Actin (GFP-LifeAct), interdigitations were seen to contain actin (Figure 5.1). This was also previously seen when boundaries of MCF10A cells were co-stained with E-cadherin and actin (Chapter 4: Figure 4.1). Actin drugs were used to assess the roles of actin polymerisation and actomyosin contraction in the reversible phenomenon of digit-formation. This will be discussed later in this chapter.

To elucidate the ultrastructure of the interdigitations, we collaborated with the Transmission Electron Microscope (TEM) Unit at the University of Liverpool. Plasma membranes of MCF10A cells within monolayers were stained with Ruthenium Red to enhance visibility as described by Deneka et al., (2007). Remnants of interdigitations survived the fixation and presented as protrusions into neighbouring cells that were absent in cells cultured with EGF (Figure 5.1). To note, the presence of interdigitations were only captured at the top of the cells (~2-3μm) and not elsewhere. Transverse sections showed prominent actin cables that projected from the electron dense digit tips. This resembles actin bundles seen in the filopodia of *Dictyostelium* cells (Medalia et al., 2007; David Garrod [personal communication]).

#### *5.2.2 Formation of interdigitations is independent of actomyosin contraction*

The presence of actin filaments in the digits prompted the next question: Is actomyosin contraction required to induce interdigitations? Myosin II motor protein isoforms crosslink actin filaments of the cell cortex to regulate cell stiffness and actomyosin contracts to confer force allowing cells to attach to the substratum in culture (Even-Ram et al., 2007; Stevenson et al., 2012). Blebbistatin inhibits the

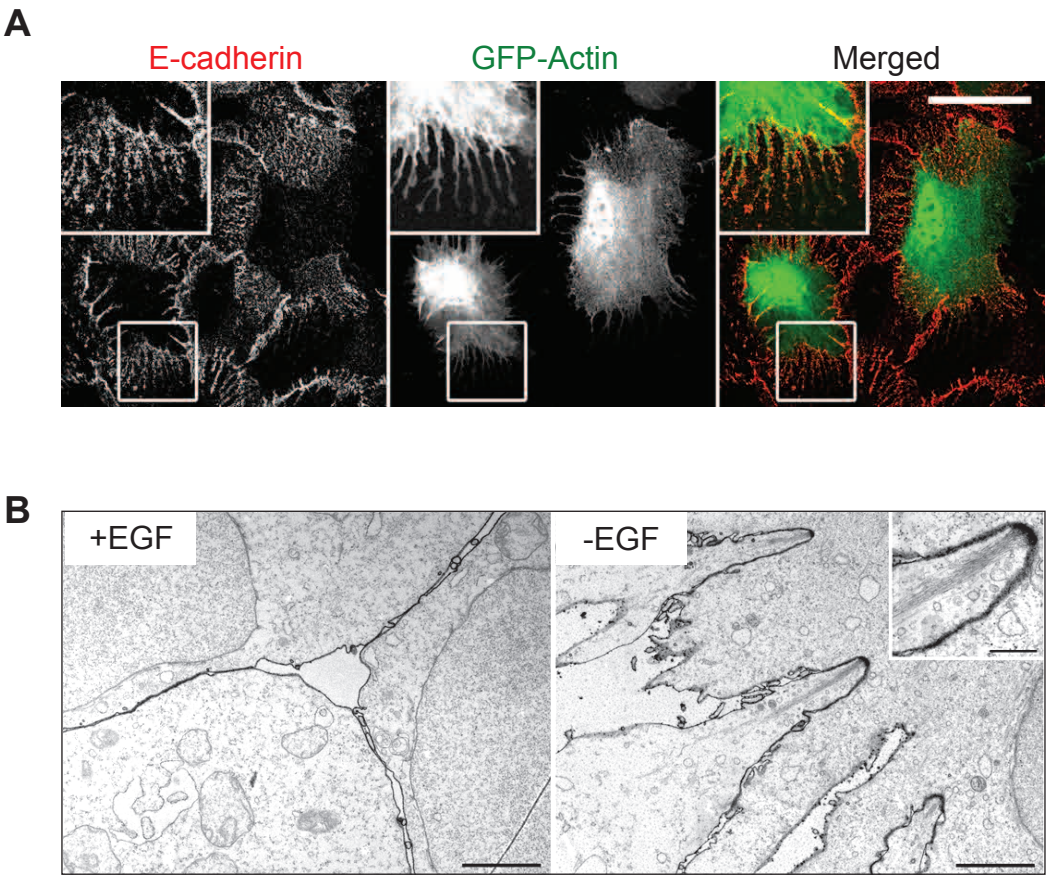


**Figure 5.1. Ultrastructural and confocal evidence that show interdigitations contain actin.** (A) Complete growth medium was exchanged for medium ±20ng/ml EGF six hours post seeding. After 72 hours, cells were transfected with GFP-LifeAct and counter-stained for E-cadherin. Cells were visualised using confocal microscopy at 63x magnification. Scale; 40µm.(B) Control MCF10A cells (left) show smooth membranes between adjacent cells compared to the cells grown in medium lacking EGF (right), which show residual finger-like structures. Actin cables project from tips of the protrusions. Cells were cultured in medium ±EGF and fixed 62 hours later. Scale 2µm and 0.5µm (inset).

magnesium dependent ATPase activity of non-muscle Myosin II thereby uncoupling it from the actin cytoskeleton (Limouze et al., 2004). I undertook a time-lapse imaging experiment to approach this question. Confluent monolayers in complete growth medium were subjected to medium exchange to remove EGF. After 16 hours, cells were treated with Blebbistatin (Myosin II inhibitor) just before interdigitations form. By applying the drug at this timepoint, I was able to determine if actomyosin contraction affects the formation of interdigitations. In control monolayers continually cultured with EGF, blebbistatin treatment gradually induced 'blebbing' of cells and eventually monolayers were disrupted (Figure 5.2, Movie 5.1). In contrast, monolayers in –EGF were maintained and interdigitations were induced within the 8 hours of imaging. Induction of interdigitations is independent of actomyosin contractility and overrides the need to maintain actomyosin-associated attachment of monolayers to substratum.

### *5.2.3 Maintenance of interdigitated monolayers is independent of actin polymerisation and actomyosin contractility*

Once formed, interdigitations were maintained over 1.5 hours when treated with actin depolymerising agents, Cytochalasin D and Latrunculin A (Figure 5.3). Effects of these inhibitors on the induction of interdigitations were not assessed due to their toxicity within the time frame required for this process (>12 hours). Blebbistatin, which did not impede the induction of digits also failed to disrupt the pre-formed interdigitated monolayers for up to 3 hours (Figure 5.3). To further investigate the relevance of the actin cytoskeleton in this process, I have probed for actin-associated proteins, ERM (actin-plasma membrane linker), Abi1 (actin polymerisation regulator) and ArpC2 p34 (actin nucleator) as these have been reported to organise membrane domains via the regulation of actin cytoskeleton (Fehon et al., 2010; Ridley, 2006). The levels of these proteins remained unchanged along with actin in ±EGF condition (Figure 5.4). Subcellular localisation of these proteins has not been explored due to time restriction but may provide visual clues as to their involvement in the formation and maintenance of interdigitated monolayers.

### *5.2.4 Activated Rac1 oppose interdigitations*

Organisation of the actin cytoskeleton to form lamellipodia and membrane ruffles requires signals relayed by Rac1 to co-ordinate the actin cytoskeleton regulators (Ridley, 2006; Ridley, 2011; Wertheimer et al., 2012). EGF can activate Rac1 by conveying signals to the guanine nucleotide exchange factors (Rac-GEFs) which

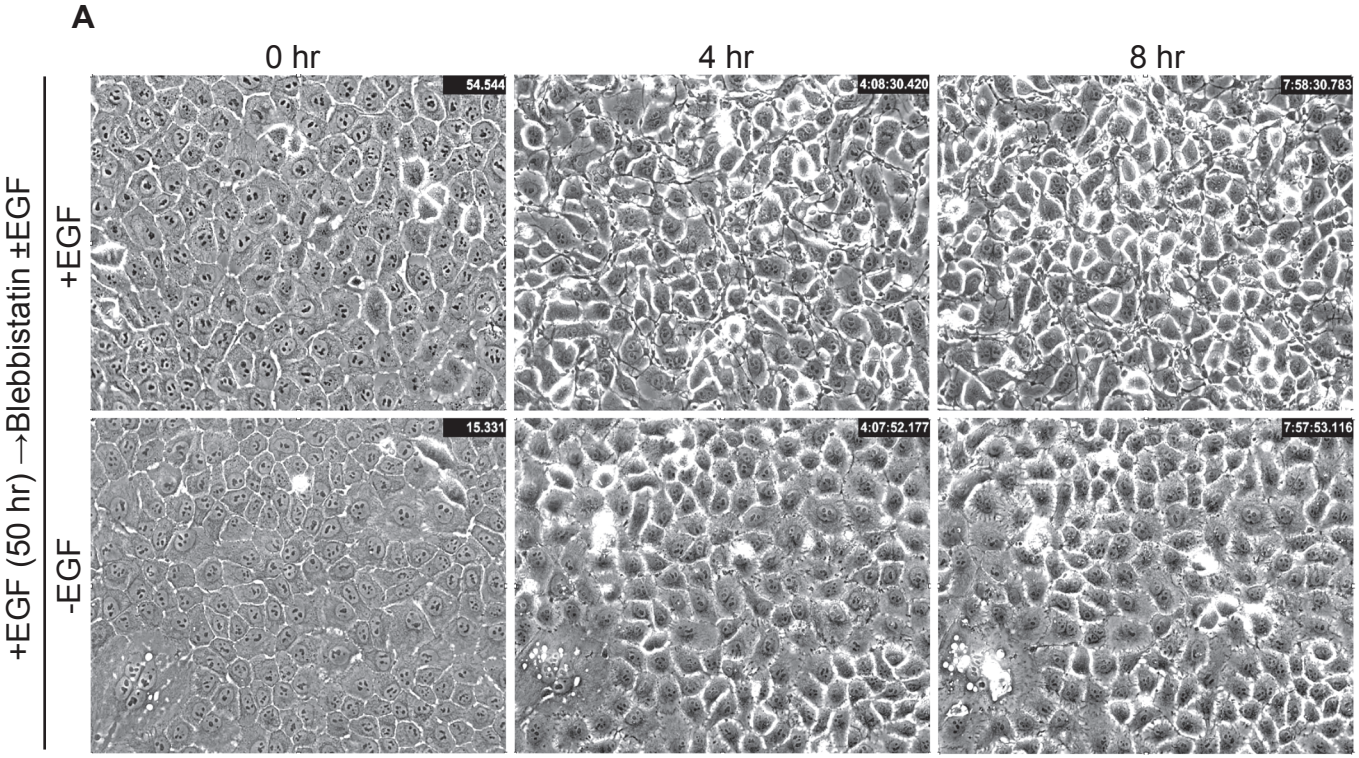


**Figure 5.2. Interdigitations are independent of actomyosin contractility.** (A) MCF10A cells were cultured in complete growth medium for 50 hours before medium exchange to ±20ng/ml EGF. Blebbistatin (25μM) was added 16 hours after medium exchange before digits were induced. Cells were imaged every 10 minutes for 8 hours after addition of Blebbistatin using bright field time-lapse microscopy at 20x magnification. (B) Control cells treated with DMSO vehicle cultured under the same conditions, are included in the next page. These are still images from Movie 5.1.

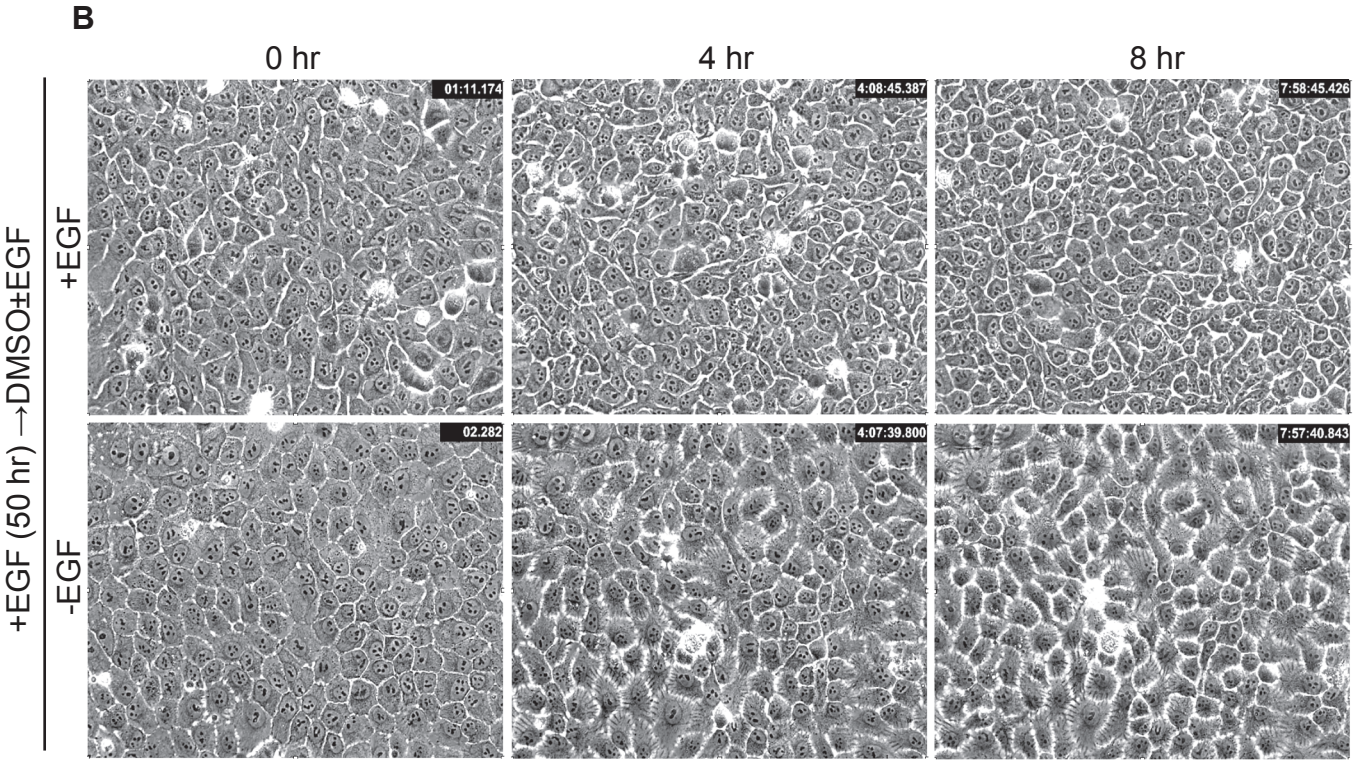


**Figure 5.2. Interdigitations are independent of actomyosin contractility.** (B) MCF10A cells were cultured in complete growth medium for 50 hours before medium exchange to ±20ng/ml EGF. DMSO vehicle was added as control to (A) 16 hours after medium exchange before digits were induced. Cells were imaged every 10 minutes for 8 hours after addition of Blebbistatin using bright field time-lapse microscopy at 20x magnification. These are still images from Movie 5.1.

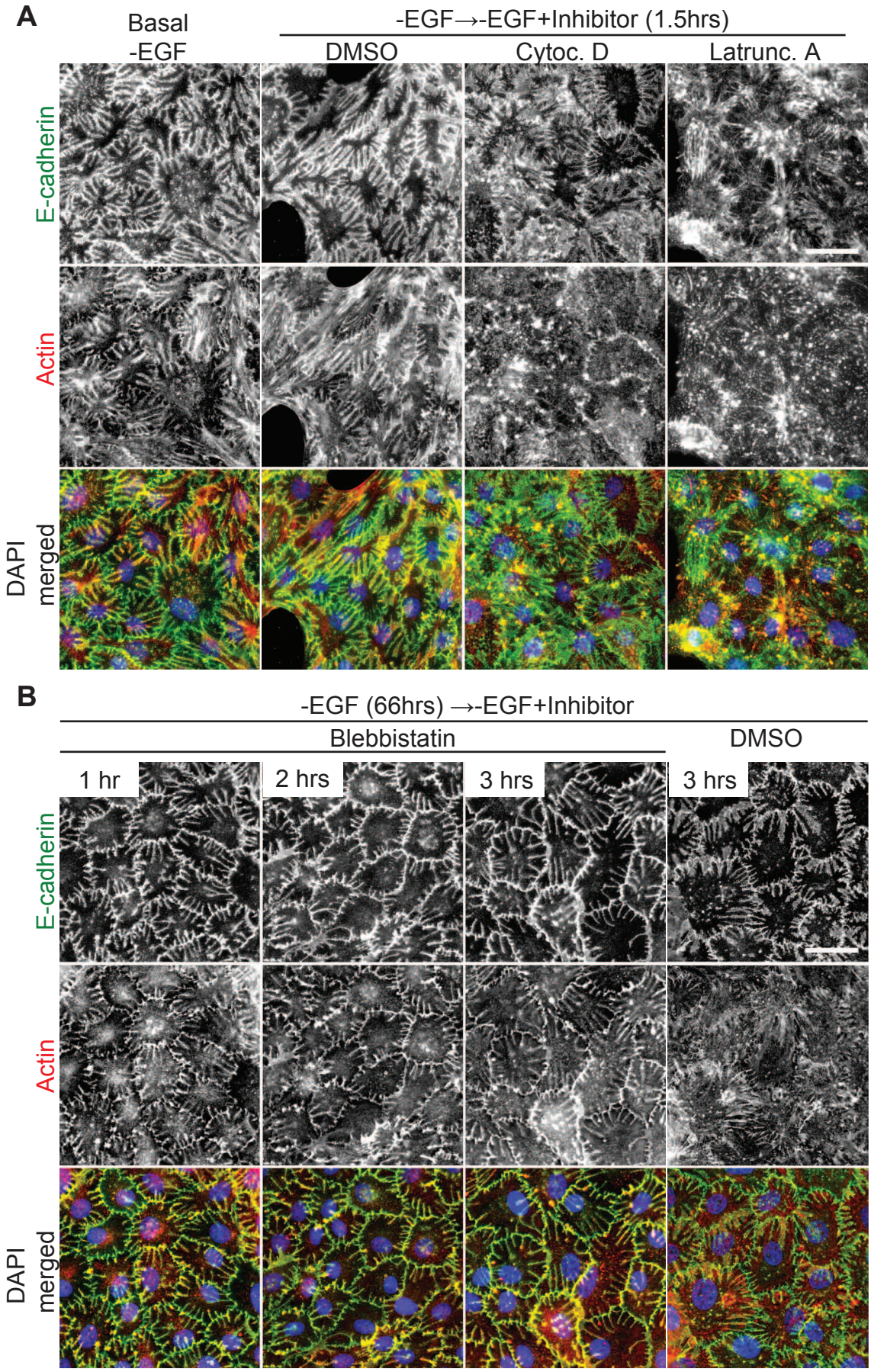


**Figure 5.3. Maintenance of interdigitation does not require actin polymerisation or contraction.** MCF10A cells were cultured in growth medium lacking EGF for 67 hours before treatment with vehicle (DMSO) (A) Cytochalasin D (5μM), Latrunculin A (5μM) or (B) 25 μM Blebbistatin. Cover slips were fixed with 4% PFA at indicated times and stained for E-cadherin, F-actin and with DAPI. Cells were visualised using immunofluorescence microscopy at 40x magnification. Scale; 40μm.

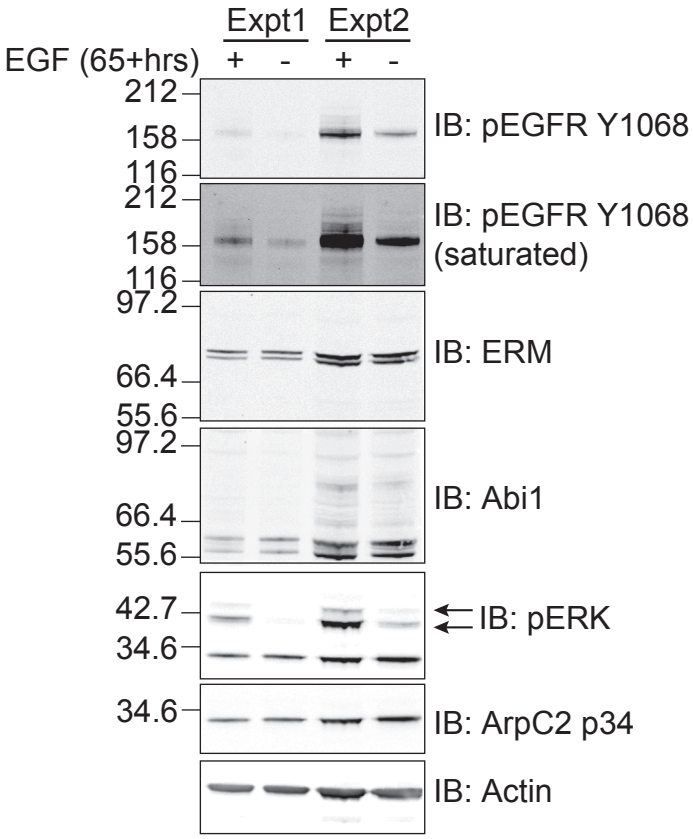


**Figure 5.4. Levels of select actin associated proteins independent of EGF withdrawal.** Immunoblot analysis of 10µg of MCF10A cell lysates harvested from 2 independent experiments, where MCF10A cells were cultured in growth medium lacking EGF for 65-67 hours before lysis with RIPA buffer. Lysates were probed for pEGFR Y1068, pERK and actin associated proteins. ERM, Ezrin, Radixin, Moesin; Abi1, Abl interactor 1; and ArpC2 p34, Actin-related protein 2/3 complex, subunit 2, 34kDa; Expt, experiment.

promote the exchange of Rac-GDP to Rac-GTP (Ridley, 2011; Schmidt and Hall, 1998; Wertheimer et al., 2012). Expression of constitutively active Rac1 (pEGFP-RacV12) in preformed interdigitated monolayers of MCF10A opposed the digit formation (Figure 5.5). In interdigitated monolayers, 33-35% of the cells that were successfully transfected with GFP-RacN17 (Rac1 negative mutant) and pEGFPC1 control vector showed interdigitations. None of the constitutively active Rac1-GTPase cells showed interdigitations (Figure 5.5).

Conversely, I used different Rac1 GEF inhibitors to ascertain if the inhibition of Rac activity may induces interdigitations as previously seen with Gefitinib (EGFR inhibitor) in this configuration (Figure 4.3, Figure 5.6). Treatment with EHop-016 (Vav2 GEF-Rac1 interaction inhibitor) and Gefitinib failed to induce interdigitations over 48 hours (Figure 5.6). Inhibitors may bind to serum proteins and become limiting in the prolonged treatment (Hickman et al., 2004). In these experiments, I have only added them once rather than twice within the 48 hours (in contrast to experiments described in Chapter 4). Rac1 inhibition via EHT1864 induced a mild interdigitated phenotype but was accompanied by anomalously shaped nuclei that resemble nuclear blebs (Figure 5.6). Digits remained indifferent to the Rac1 inhibitors added after their formation. Treatment with the NSC23766 (RacGEFs: Tiam/Trio inhibitor) caused cell death in the absence of EGF (Figure 5.6). Experiments with these inhibitors need to be repeated and have been included here as a record for future reference.

In addition, I have also checked the activation status of Rac1 in MCF10A monolayers under ±EGF conditions with or without prior serum starvation (Figure 5.7). Previous literature has measured Rac1 GTPase activation of growth factor starved MCF10A cells acutely stimulated with 100ng/ml EGF in intervals for up to 90 minutes (Duan et al., 2011). Active endogenous Rac1 and CDC42 were pulled down using GST-PBD beads (Methods: Section 2.4.3). Under basal conditions, monolayers cultured ±EGF with serum showed similar residual Rac1 activity (Figure 5.7). Stimulation with EGF (3 minutes) following serum starvation induced Rac1 and to a lesser degree CDC42 activity. Duan et al. (2011) also reported the increase in Rac1 activity in growth factor starved (72 hours) subconfluent MCF10A cells stimulated with 100ng/ml EGF (10 minutes). The activation of Rac1 in the EGF mediated resolution of interdigitations will be explored later in this chapter.

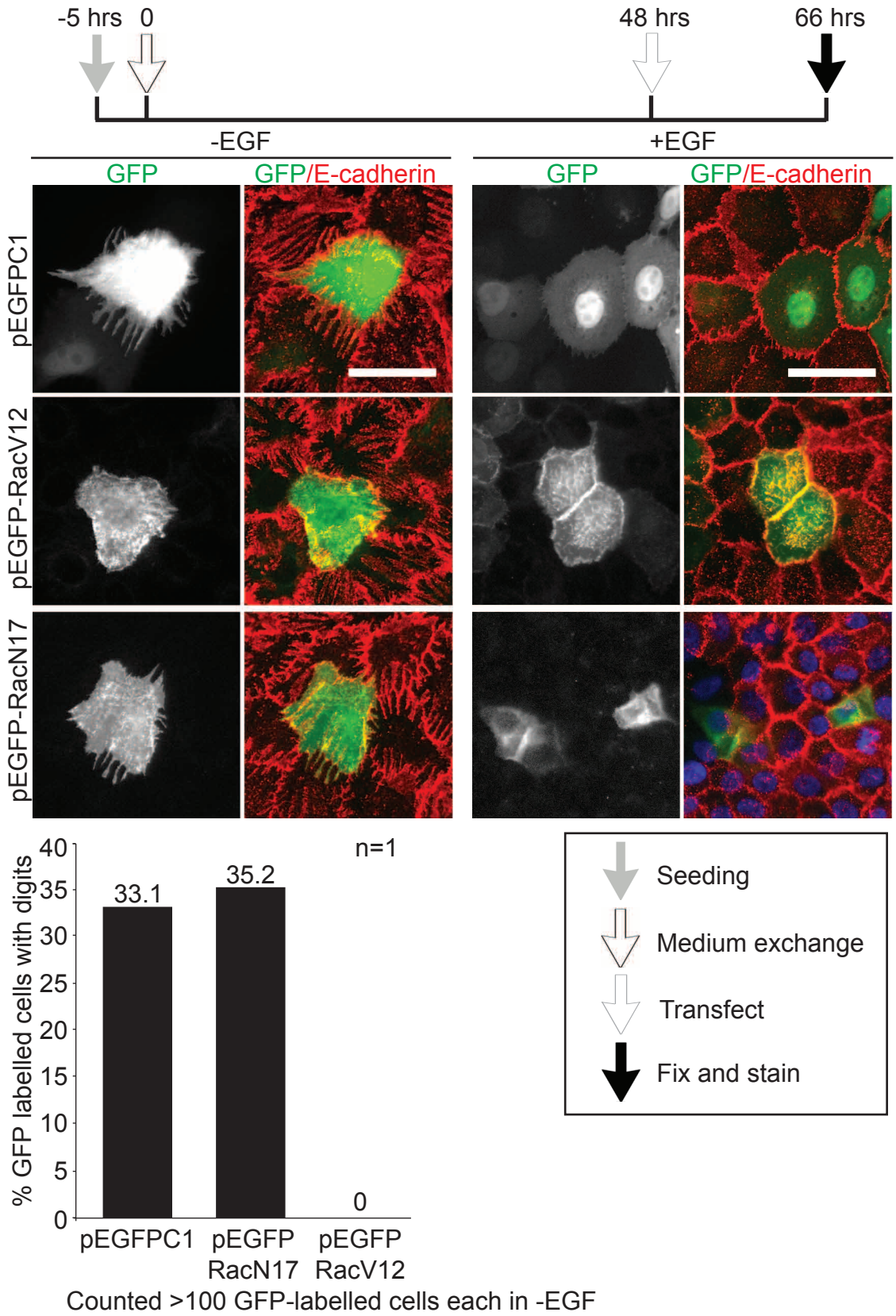


**Figure 5.5. Transient transfection of constitutively active GFP-RacG12V negates the interdigitations invoked by EGF withdrawal.** MCF10A cells were cultured in the absence of EGF for 48 hours then transfected for 18 hours [0.5µg DNA+ 0.5µg pBlueScript vector]. Coverslips were fixed with 4% PFA and stained with E-cadherin. GFP-labelled cells were counted in the -EGF condition and scored for interdigitations. Cells were visualised using immunofluorescence microscopy at 40x magnification. Scale; 40µm.

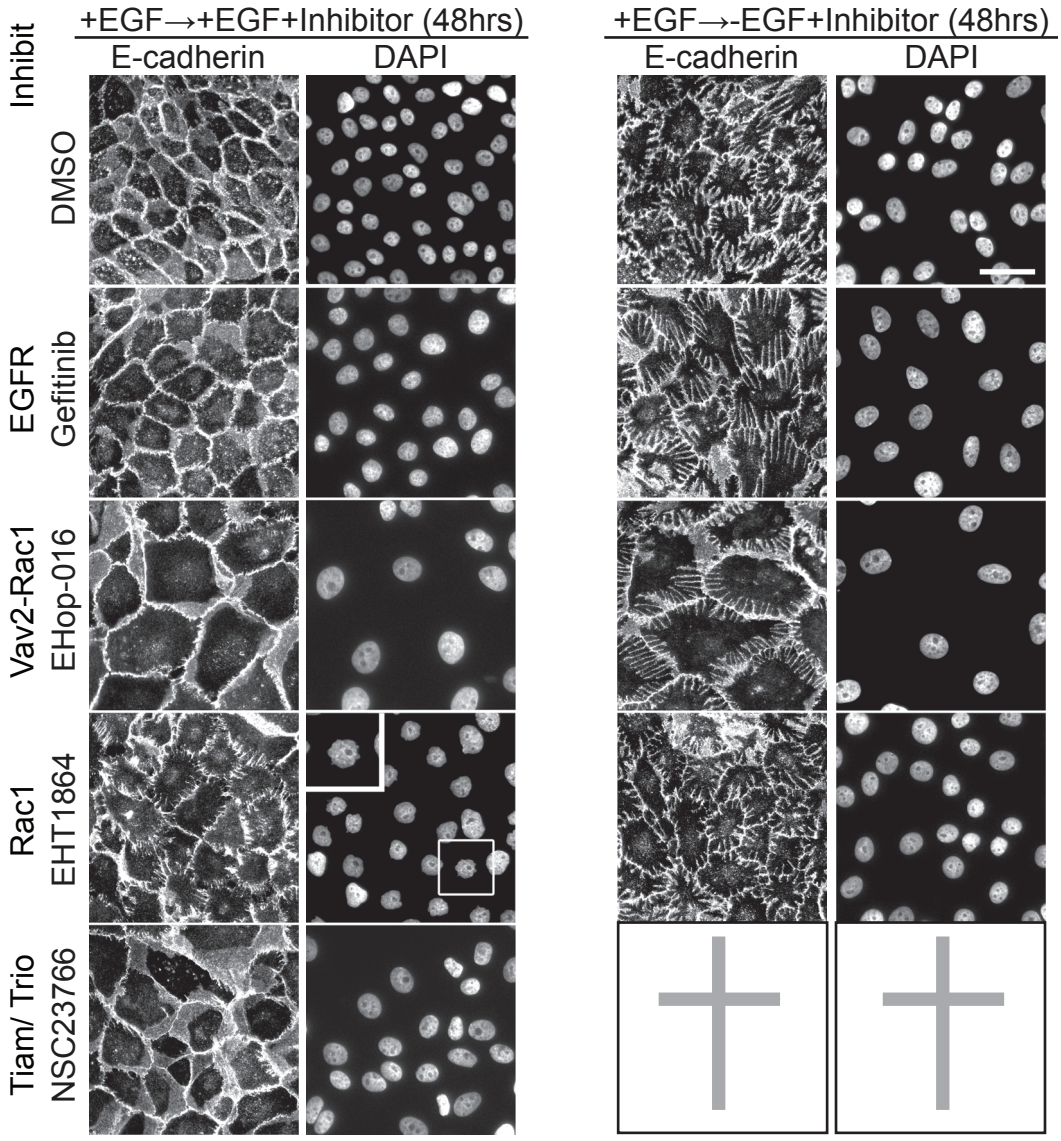


**Figure 5.6. Induction of interdigitations independent of Rac1 inhibition.** MCF10A cells were grown to confluence for 43 hours before exchange of medium to include the inhibitors at these concentrations: Gefitinib (300nM), EHop-016 (5μM), EHT1864 (5μM) and NSC23766 (50μM). The inset shows the nuclear 'blebs' seen. Panel without images indicate cell death. Confluent cells were treated with the inhibitor for 48 hours before coverslips were fixed with 4% PFA and stained with E-cadherin and DAPI. Images were taken using the immunofluorescence microscope at 40x magnification. Scale; 40μm.

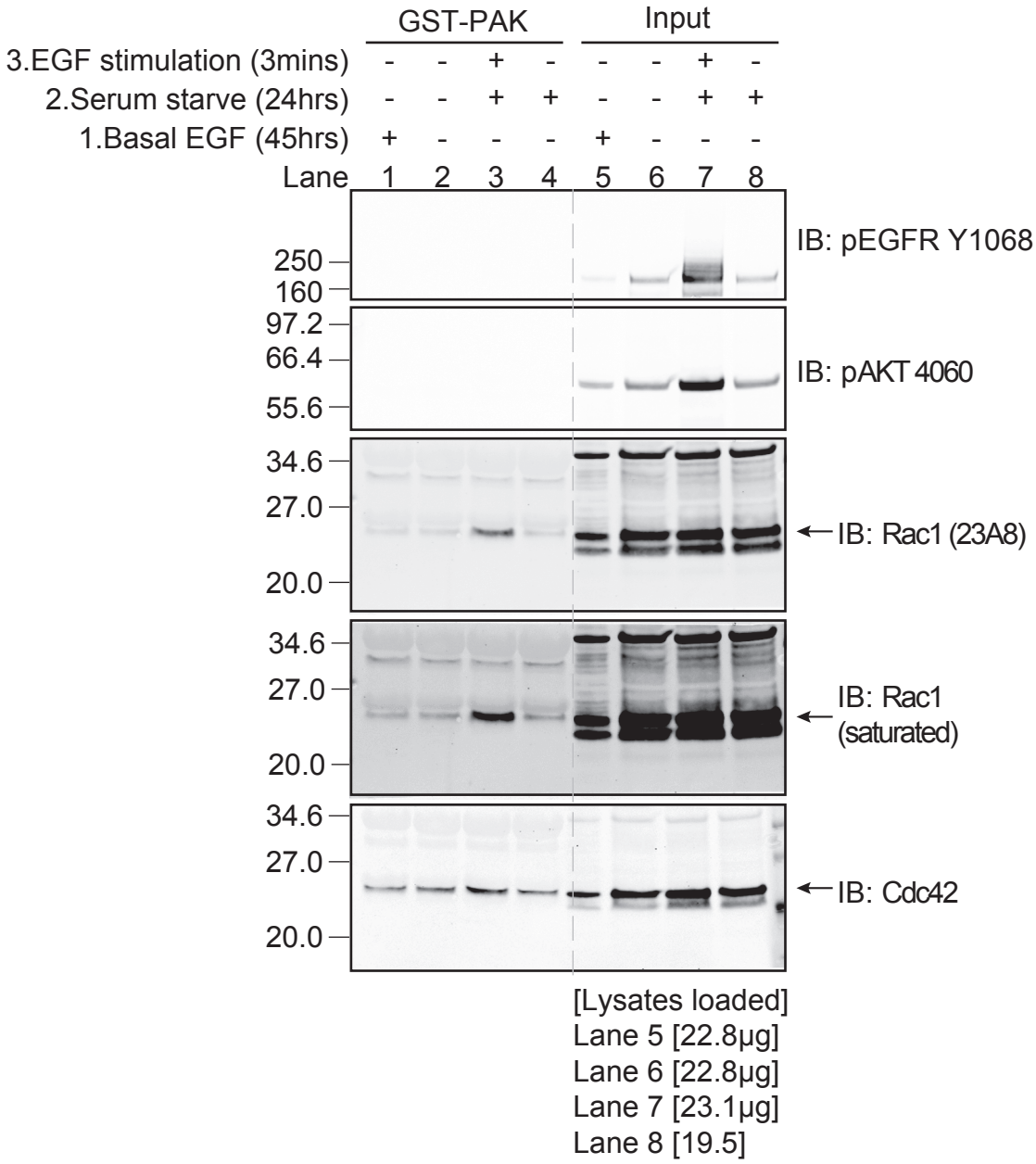


**Figure 5.7. EGF activates Rac1.** MCF10A cells were cultured in ±EGF medium for 45 hours. Serum starved cells were cultured in -FBS-EGF medium for 24 hours. Cells were stimulated with 20ng/ml EGF for 3 minutes. Cells were lysed and endogenous active Rac1 was pulled-down using GST-PAK beads. Input lanes were loaded with 4.6% input of total lysates and each pull down lane was loaded with material from 30µg GST-PAK beads.

## 5.3 Cytoskeletal characterisation: Resolution of interdigitations

### *5.3.1 Resolution of interdigitations requires actin polymerisation and actomyosin contractility*

In tandem, I investigated if the actin cytoskeleton is required in the reversal of digits. As this process is relatively rapid (1.5 hour onwards, Figure 5.8), it is receptive to actin depolymerising agents, Cytochalasin D and Latrunculin A. In interdigitated monolayers, addition of either inhibitor with EGF impeded the ability of cells to resolve digits within 1.5 hours (Figure 5.8). Blebbistatin (Myosin II inhibitor) similarly inhibited the resolution of interdigitations in the presence of EGF. Note that from 1.5 hours onwards, cells started to detach and die owing to the toxicity of the drugs.

### *5.3.2 Residual pool of Rac1 resolves interdigitations*

Rac1 activation relays signals to reorganise the actin cytoskeleton during the formation of lamellipodia in cells (Ridley, 2011). The previous thread of evidence showing that EGF stimulates Rac1 activity (Figure 5.7) was further investigated in the context of digit reversal to smooth membrane boundaries between neighbouring MCF10A cells. Rac1 activity was measured as described previously using GST-PBD beads after fully interdigitated monolayers were stimulated with EGF (3 minutes). Activity of Rac1 increased while that of another small G protein, CDC42 remained indifferent to EGF stimulation (Figure 5.9). One would suspect that Rac1 activation correlates with the reversal of digits. However, inhibition of Rac1 activity using inhibitors; EHT1864 (Rac1 inhibitor), NSC23766 (RacGEFs: Tiam1/Trio inhibitor) and EHop-016 (RacGEF Vav2-Rac1 inhibitor) failed to maintain the interdigitated monolayers upon addition of EGF (Gao et al., 2004; Montalvo-Ortiz et al., 2012; Shutes et al., 2007). Control, pre-formed interdigitated monolayers remained unperturbed in the presence of these inhibitors (Figure 5.10).

These results indicate that the induction and resolution of interdigitations is independent of small molecule inhibition of Rac1, Tiam1/ Trio and the Vav2-Rac1 interaction. When tested, EHT1864 but not NSC23766 treated cells showed reduced Rac1 activity under EGF stimulation (Figure 5.11). Although EHT1864 is supposed to displace guanine nucleotide association in vitro, a low level of Rac activity remains in the MCF10A cells treated with this inhibitor (Shutes et al., 2007). This could be because EHT 1864 only binds at high affinity to Rac1 but does not induce nucleotide loss from Rac2 and Rac3, allowing the latter two to relay basal Rac activity detected by the PAK-PBD beads (Shutes et al., 2007). On the other hand, the lesser reduction of Rac activity by NSC23766 can be explained as this

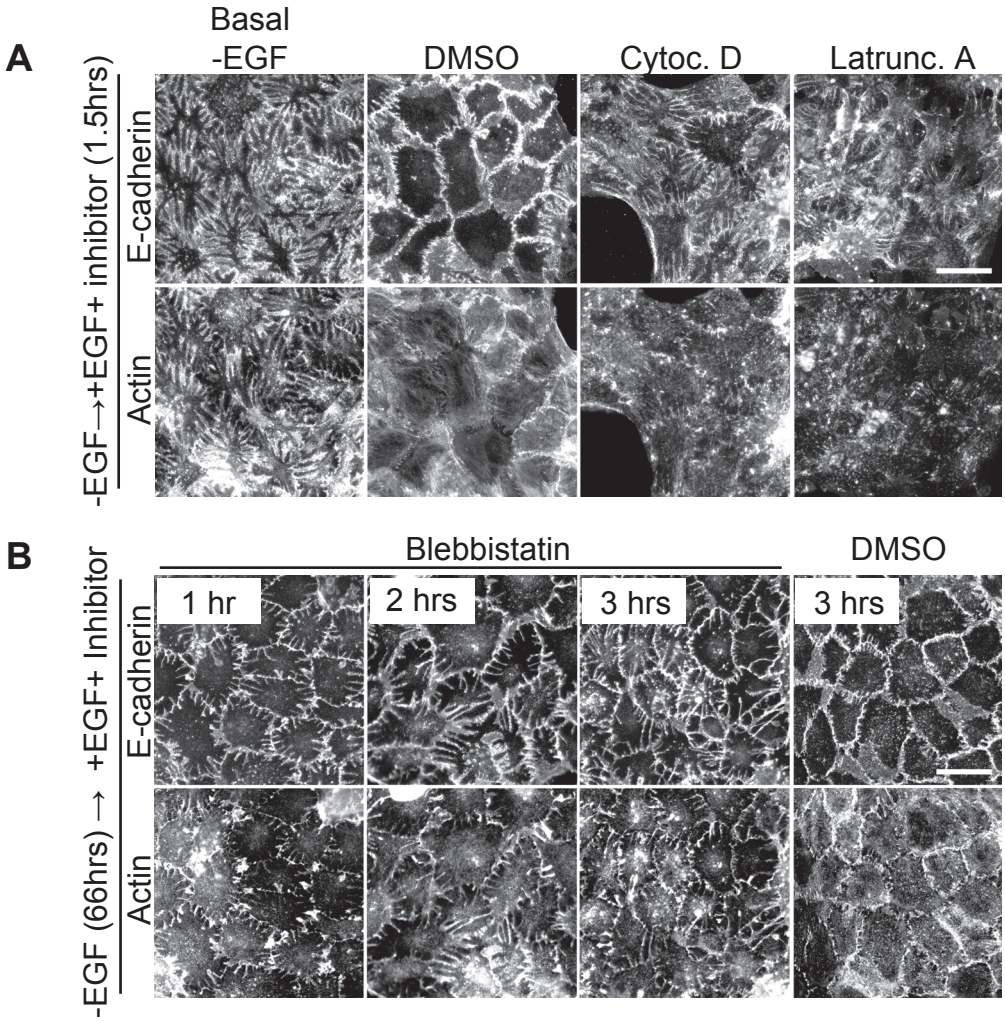


**Figure 5.8. Resolution of interdigitations requires actin polymerisation and actomyosin contraction.** MCF10A cells were cultured in the absence of EGF for 66 hours before treatment with vehicle control (DMSO) and (A) 5μM Cytochalasin D or 5μM Latrunculin A or (B) 25μM Blebbistatin. Coverslips were fixed at indicated time points when significant reversal of interdigitation is evident in control cells, but not those which have been drug treated. Cells were fixed with 4% PFA and stained for E-cadherin, F-actin and visualised using immunofluorescence microscopy at 40x magnification. Scale; 40μm.

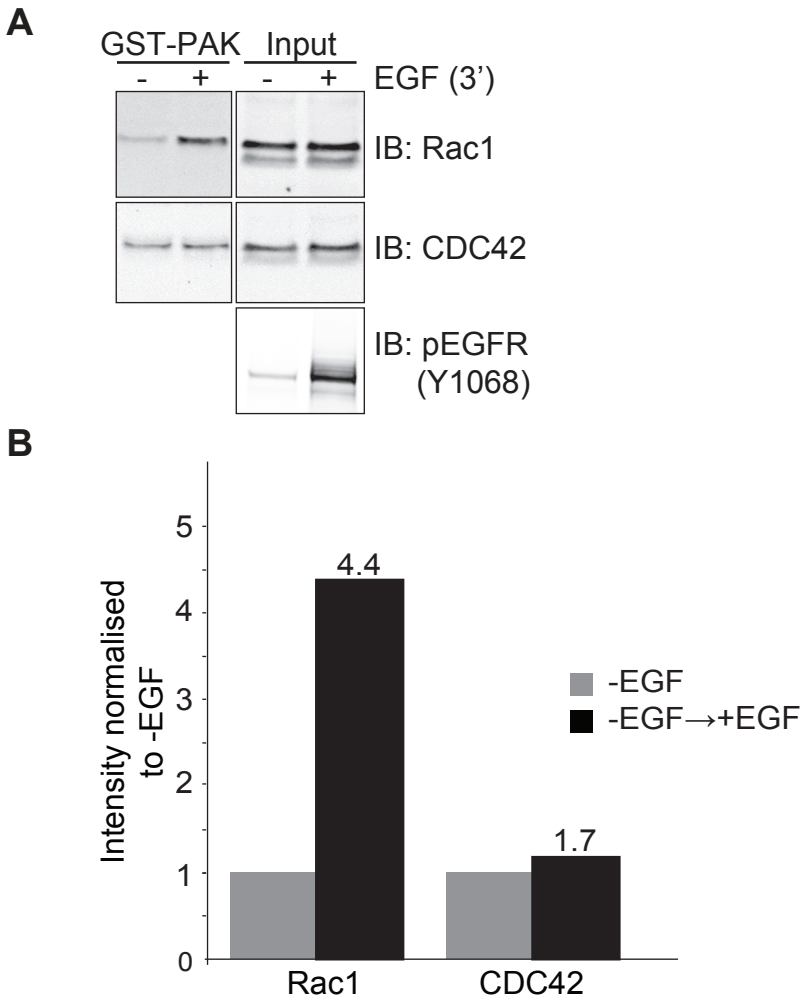


**Figure 5.9. EGF activates Rac1 but not CDC42.** (A) MCF10A cells were cultured without EGF for 62 hours then stimulated for 3 minutes with 20ng/ml EGF. Lysates were probed with anti-Rac1, anti-CDC42 and anti pY1068 EGFR. Lanes were loaded with 4.6% input of total lysates and with material from 30µg GST-PAK beads in each pull down lane. (B) Intensity of the bands were normalised within the same antibody. Intensity of the top bands of Rac1 and CDC42 were quantified using the Odyssey software.

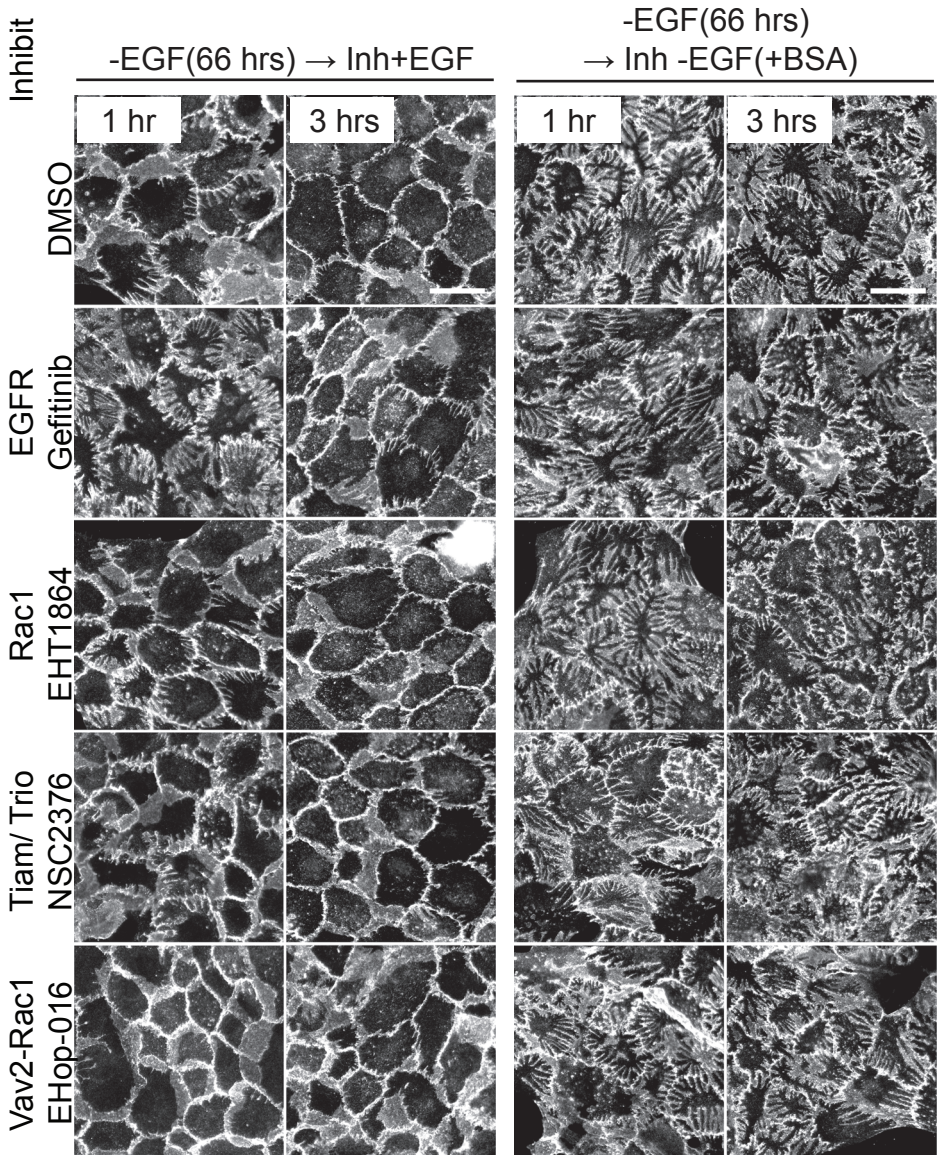


**Figure 5.10. Maintenance and reversal of interdigitations independent of Rac1 inhibition.** (A) MCF10A cells were cultured without EGF for 66 hours and pretreated with inhibitors for 30 mins at these concentrations; Gefitinib (300nM), EHT1864 (5μM), NSC23755 (50μM) and EHop-016 (5μM). Coverslips were PFA fixed 1 and 3 hours after addition of of 20ng/ml EGF or 0.5mg/ml BSA (control) and stained for E-cadherin. IF images were taken using immunofluorescence microscopy at 40x magnification. Scale; 40μm. Inh, inhibitor.

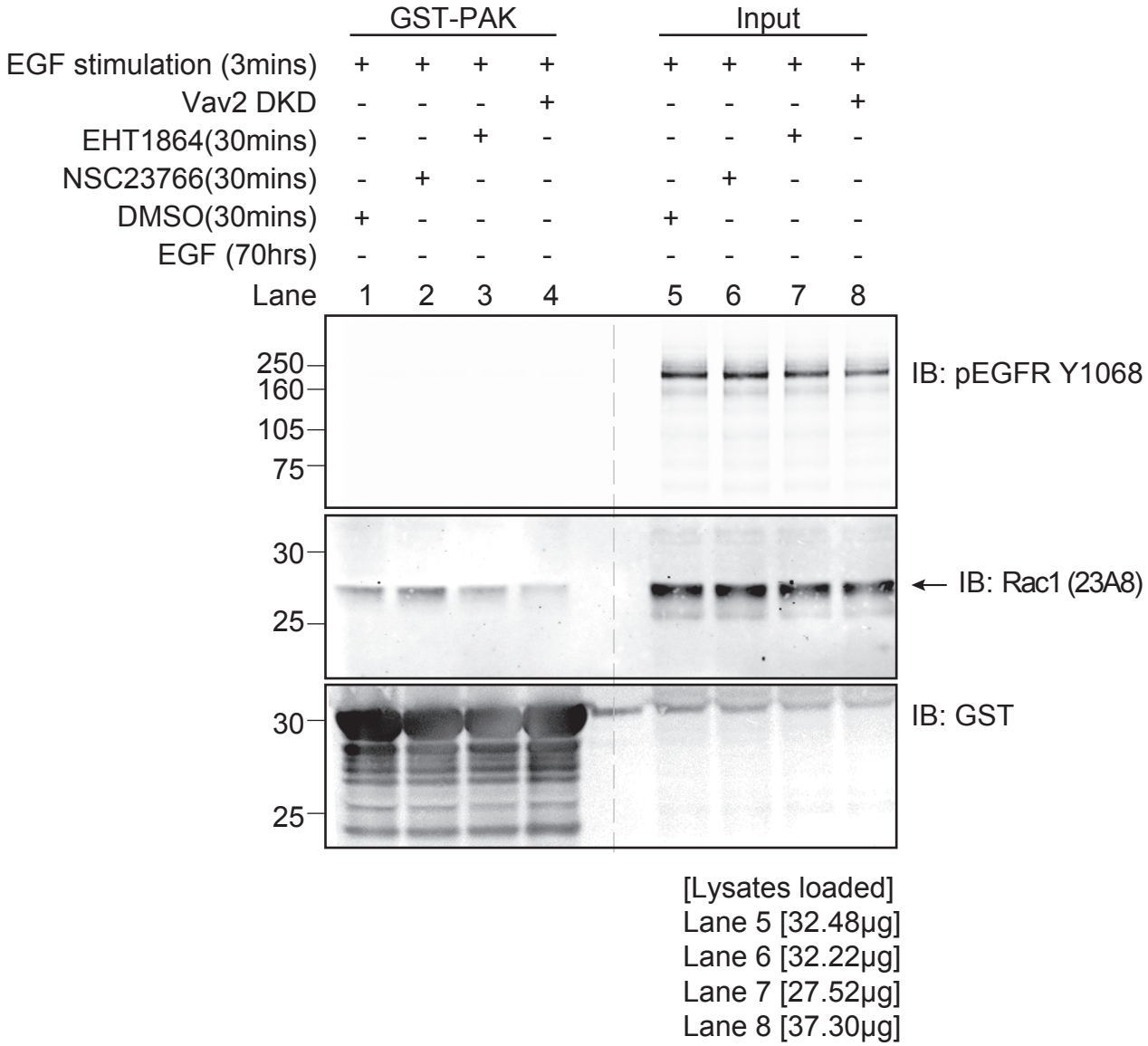


**Figure 5.11. Rac1 activity reduced by inhibitors and RacGEF knock-down. (**A) MCF10A cells were cultured without EGF for 70 hours and pretreated with inhibitors for 30 mins at these concentrations; EHT1864 (5µM) and NSC23766 (50µM). Cells were transfected with pooled siVav2 oligonucleotides on seeding day and on the second day. Cells were then stimulated for 3 minutes with 20ng/ml EGF. Lysates were probed with anti-pY1068 EGFR, anti-Rac1 and anti-GST. Lanes were loaded with 4.6% input of total lysates and with material from 30µg GST-PAK beads in each pull down lane. DKD, double siRNA knockdown; GEF, guanine nucleotide exchange factor.

inhibitor only binds the RacGEF recognition grove that is specific to Tiam1 and Trio. Therefore, other members of the GEF family such as Vav can still stimulate Rac1 activity in MCF10A cells (Gao et al., 2004; Sosa et al., 2010). The double siRNA knockdown (DKD) of Vav2 in MCF10A cells reduced Rac1 activity most efficiently when compared to EHT1864 and NSC23766 treatment possibly because Vav2 is an abundant GEF in MCF10A cells (Figure 5.11; Sosa et al., 2010).

Subsequently, I targeted Rac1 using siRac1 (Methods: Section 2.1.4) oligonucleotides and asked if this would affect interdigitations in monolayers. Firstly, MCF10A cells were cultured and transfected with pooled siRac1 oligonucleotides once in 48, 65 hours and twice in 65 hours in complete growth medium (Figure 5.12). The expression of Rac1 was only slightly reduced in this configuration (Induction). Double knockdown of Rac1 over 67 hours did not affect the ability of cells to form interdigitations upon removal of EGF (Figure 5.13). To test if siRac1 would antagonise the ability of cells to resolve digits, EGF was added to preformed interdigitated monolayers transfected with the oligonucleotides. Rac1 levels were adequately reduced by siRac1 in this configuration (Figure 5.12- Reversal) yet digits continued to reverse within 24 hours (Figure 5.13). The induction and reversal of digits remained indifferent to the partial reduction of Rac1 levels

As an alternative approach, I used pooled siVav2 oligonucleotides as others have shown reduced Rac1 activation via this GEF that is dominant in MCF10A cells (Duan et al., 2011; Sosa et al., 2010). Knockdown of Vav2 in MCF10A cells showed significant reduction of endogenously active Rac1 (Figure 5.14). Then, I investigated if the reduced Rac1 activity would disable the resolution of interdigitations. Interdigitations continued to resolve even though Vav2-knockdown reduced Rac1 activity. Together, although actin polymerisation and actomyosin contractility are required to dissolve interdigitations, reduction in Rac1 activity is insufficient to override this cytoskeletal remodelling process. This was unexpected as Rac1 activation co-ordinates the organisation of the actin cytoskeleton during lamellipodia formation (Ridley, 2006; Ridley, 2011).

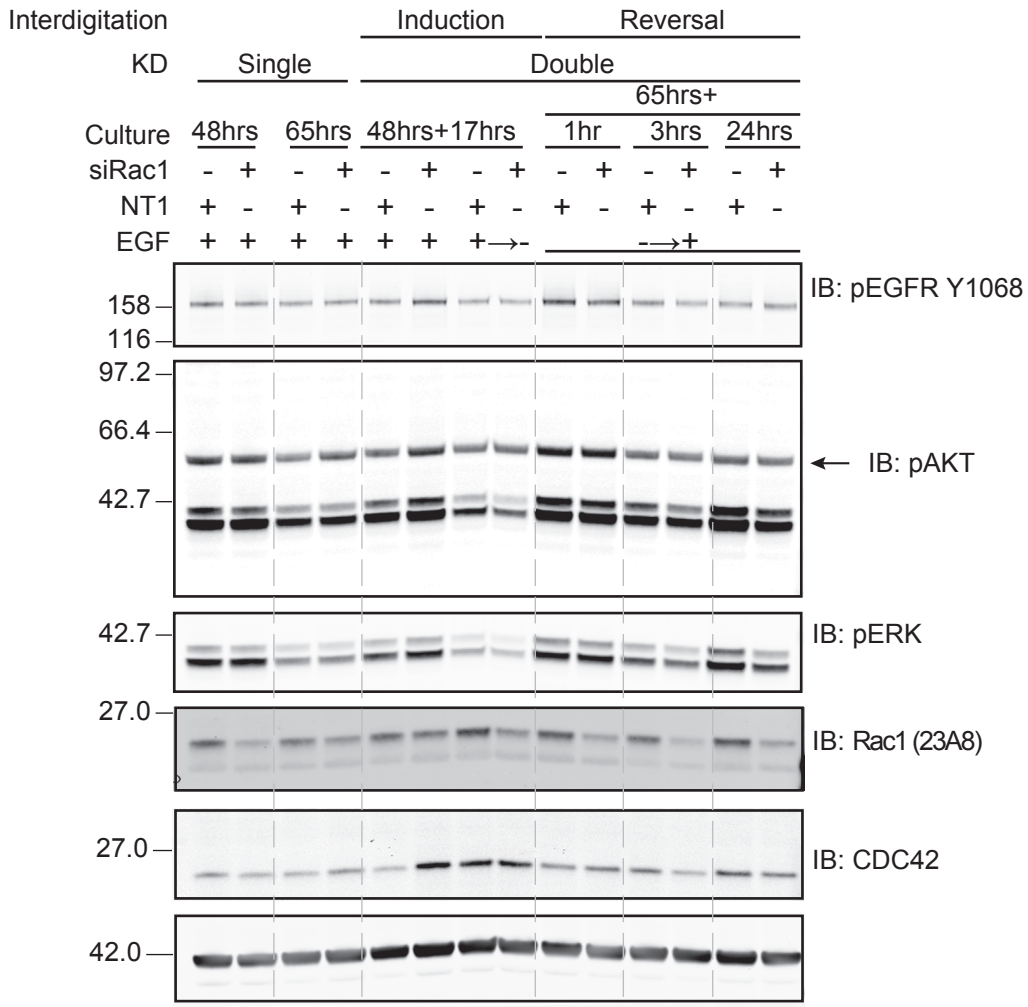


**Figure 5.12. Optimisation of Rac1 knockdown in the induction and reversal of interdigitations.** MCF10A cells were cultured in complete growth medium (48 hours and 65 hours) transfected with pooled siRac1 oligonucleotides once. Medium was exchanged to -EGF and transfected with pooled siRac1 oligonucleotides again to induce interdigitations for 17 hours. 20 ng/ml of EGF was added to reverse pre-formed interdigitations (65+ hours) for 1, 3 and 24 hours. Each lane was loaded with 10µg lysates. Lysates were probed with anti-pY1068 EGFR, anti-pAKT, anti-pERK, anti-Rac1 and anti-CDC42. KD, knockdown by siRNA oligonucleotides.

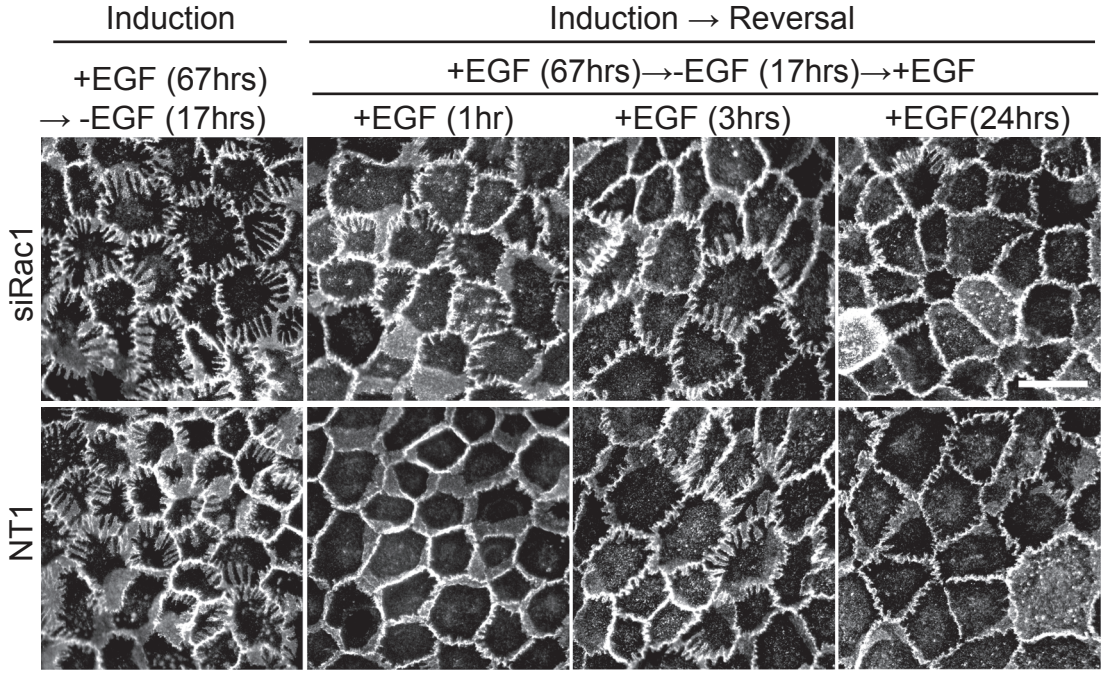


**Figure 5.13. Reversal of interdigitations independent of Rac1 knock-down.** MCF10A cells were cultured in complete growth medium (48 hours) and transfected with pooled siRac1 oligonucleotides on seeding day. Medium was exchanged to -EGF and cells were transfected again with pooled siRac1 oligonucleotides to induce interdigitations for 17 hours. 20 ng/ml of EGF was added to reverse interdigitations at 1, 3 and 24 hours. Cells on coverslips were fixed with 4% PFA and stained with E-cadherin. Images were visualised using immunofluorescence microscopy at 40x magnification. Scale; 40μm. Induction and Reversal refers to the configurations of experiment as denoted in Methods: Table 2.6.

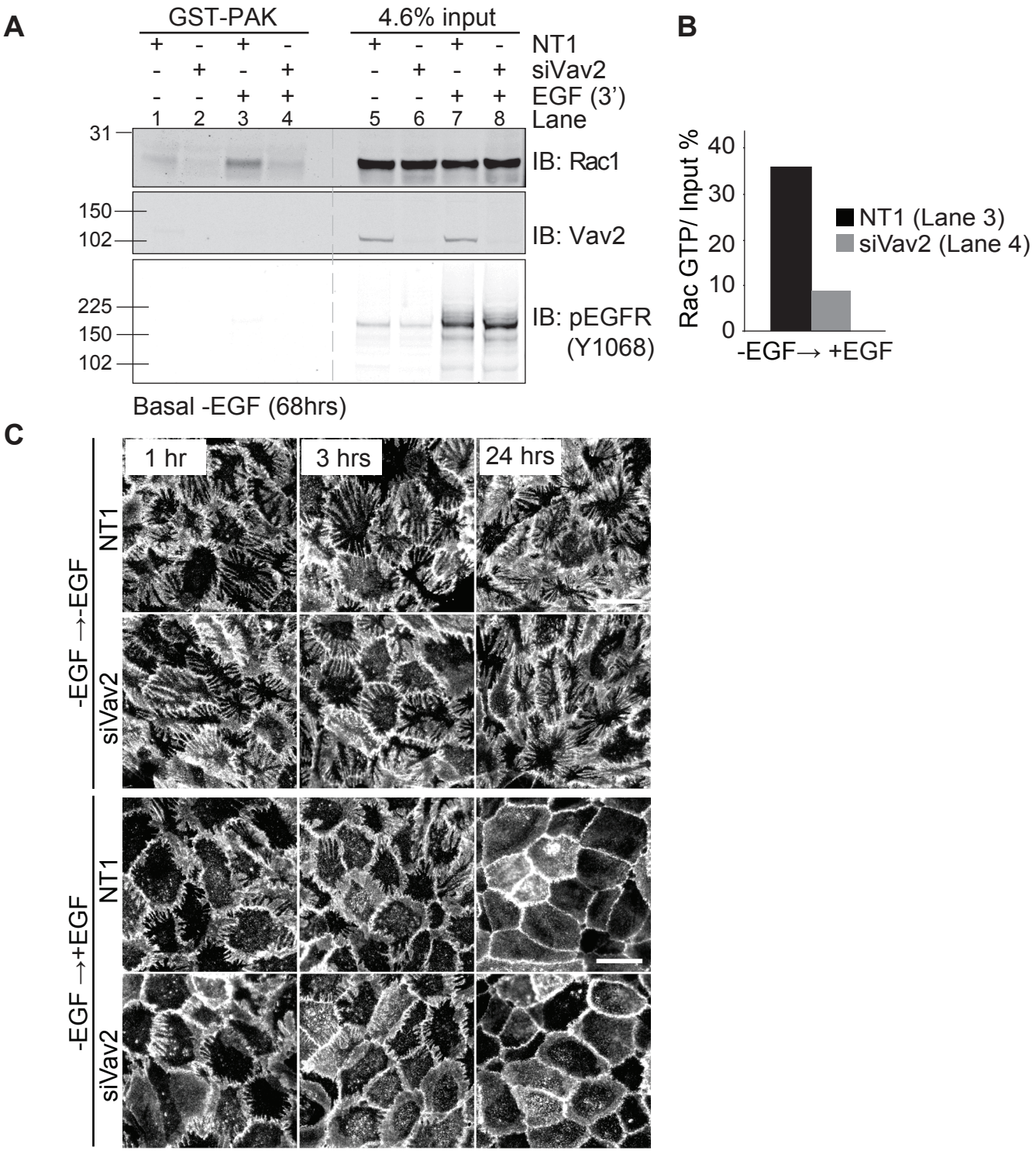


**Figure 5.14. Vav2 activated Rac1 is not required for reversal of interdigitations.** (A) Rac1 activity is substantially reduced by Vav2 depletion. MCF10A cells were cultured in -EGF growth medium (68 hours) and transfected with 40nM siRNA specific for Vav2 on seeding day and day 2. 20 ng/ml of EGF was added (3 mins). Lysates were probed with anti-Y1068 EGFR, anti-Vav2 and anti-Rac1. Lanes were loaded with 4.6% input of total lysates and with material from 30µg GST-PBD beads in each pull down lane. (B) Intensity of the bands pulled down by GST-PBD beads were normalised to input. Band intensities of Rac1 was quantified using the Odyssey software. (C) Reversal of interdigitation is unaffected by Vav2 depletion. Cells were cultured in growth medium lacking EGF for 67 hours to induce interdigitations and treated as (A) and incubated with EGF for the indicated times. Coverslips were fixed after 1 hour, 3 hours and 24 hours with 4% PFA and stained with E-cadherin. Cells were visualised using immunofluorescence microscopy at 40x magnification. Scale; 40µm.

## 5.4 Ultrastructural and junctional characterisation: Formation of interdigitations

### *5.4.1 Interdigitations display increased desmosome numbers*

From TEM micrographs, we observed the accumulation of electron dense regions along the folds of protrusions in interdigitated monolayers (Figure 5.15). In TEM micrographs, adherens junction may form electron dense areas due to the interaction of E-cadherin molecules on the surface of adjacent cells (Kobielak and Fuchs, 2004). These junctions are normally connected to the polarised actin network across epithelial sheets (Figure 1.4). Paired electron dense strips on apposing membranes seen were distinctly surrounded by a haze of intermediate filaments, analogous to desmosomal plaques (Figure 5.15 inset; Green and Gaudry, 2000). Intermediate filaments present in cells are persistently shorter at 0.5μm compared to actin filaments, 13.5μm that allows intermediate filaments to confer more flexibility in cells (Fletcher and Mullins, 2010). This shorter length and the lack of polarity of intermediate filaments are characteristically viewed as a 'haze' in TEM micrographs (Figure 5.15 inset). Desmosomes succeed adherens junctions during the assembly of cell-cell adhesion to strengthen the mechanical integrity of cell layers (Garrod, 2010; Green and Gaudry, 2000). These 'spot welds' are commonly associated to epithelia and other stress bearing tissues and are tethered to the plasma membranes via intermediate filaments. Intriguingly, desmosomal proteins are often mutated or silenced in invasive and/or metastatic breast cancer specimens (Oshiro et al., 2005, Klus et al., 2001)

Quantification of desmosomes per unit length of plasma membrane revealed a 10-fold increase in EGF starved cells. In agreement, expression of the desmosomal protein, Desmoglein and the adaptor molecule, Desmoplakin showed notable increases in MCF10A cells that formed interdigitated monolayers (Figure 5.15). In contrast, levels of Desmoplakin in constitutively active EGFR mutant cells remained indifferent to the presence of EGF in the medium (Figure 5.15). No changes in E-cadherin or selected tight junction markers (ZO-1, Claudin-1) were seen in the MCF10A parental and EGFR mutant monolayers. In the absence of EGF, Desmoplakin continued to stain close to E-cadherin along digits, redolent of the interdigitating cell processes described in another non-malignant breast epithelial cell line, HMT 3522 (Figure 5.16, Holm et al., 1993).

### *5.4.2 Co-localisation of Desmoplakin with Early Endosomal auto-Antigen 1 (EEA1)*

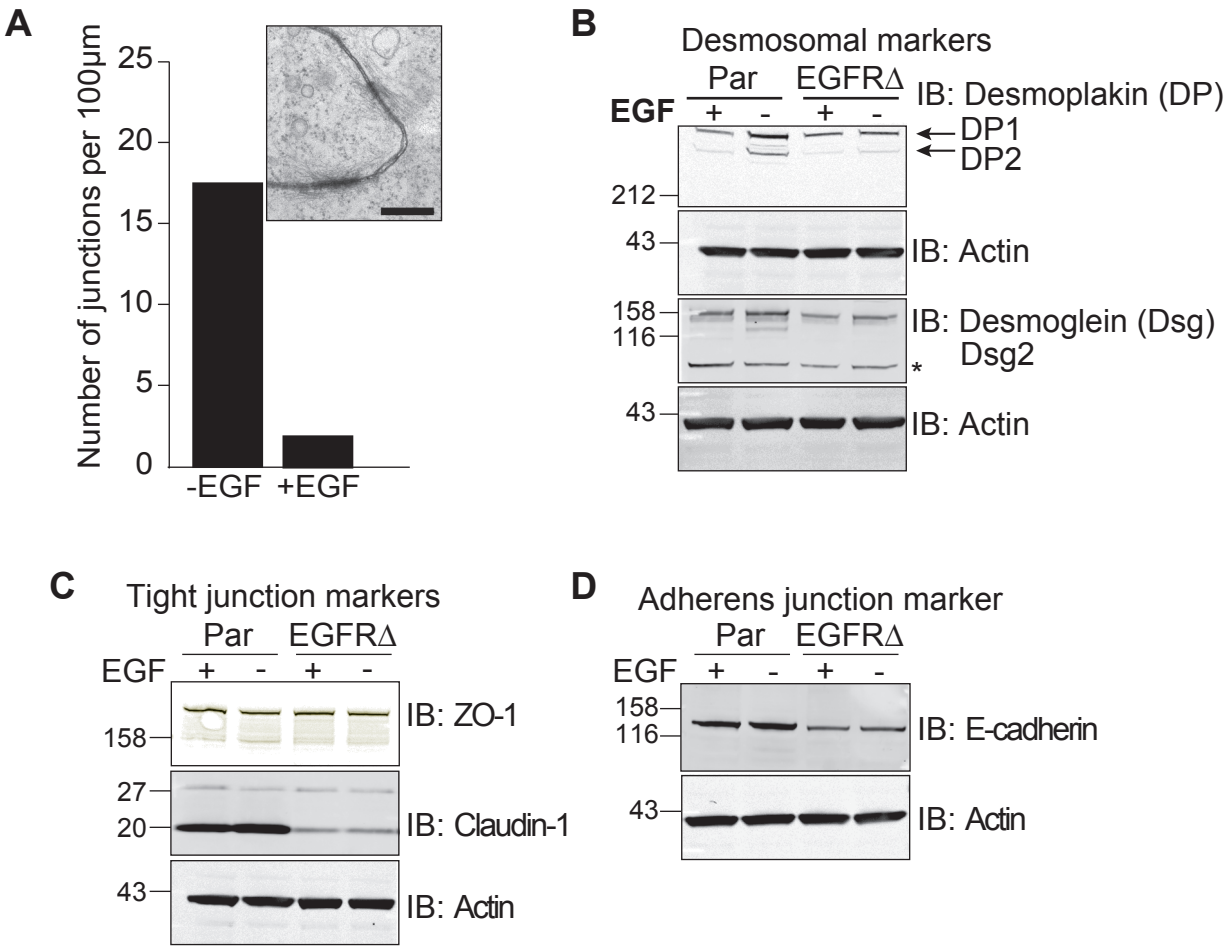


**Figure 5.15. Interdigitations are accompanied by an increase in the number of desmosomes.** (A) MCF10A cells were cultured in ±EGF growth medium and fixed 62 hours later for TEM as Figure 5.1B. Quantification of the number of desmosomes per unit length of plasma membrane indicates ten fold more junctions in cells cultured in medium without EGF. Data are aggregated from 33 micrographs per condition (~500µm) as described in Methods:2.3.3. (B) Immunoblot analysis of 12.5µg of MCF10A cell lysates from parental and EGFRΔE746-A750 cells cultured in medium with or without EGF for 65 hours and probed for desmosomal markers (Desmoplakin 1 & 2, Desmoglein 2), tight junction markers (ZO-1. Claudin-1) and adherens junction marker (E-cadherin). Asterisk indicates a non-specific band. MCF10A parental cells but not the EGFR mutants show increased expression of desmosomal proteins when cultured in medium lacking EGF.

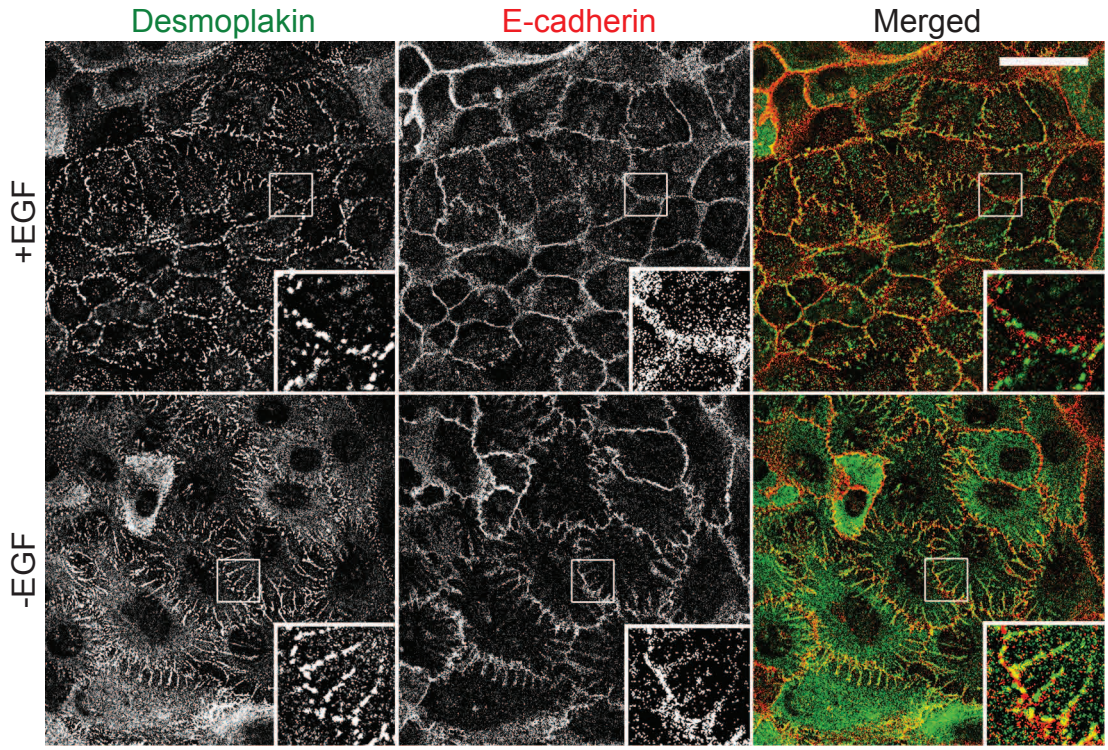


**Figure 5.16. Interdigitated cell processes decorated with Desmoplakin.** Complete growth medium was exchanged for medium ±20ng/ml EGF six hours post seeding. After 72 hours, cells were fixed with 4% PFA and stained for E-cadherin and Desmoplakin. Cells were visualised using confocal microscopoy at 63x magnification. Scale; 40µm.

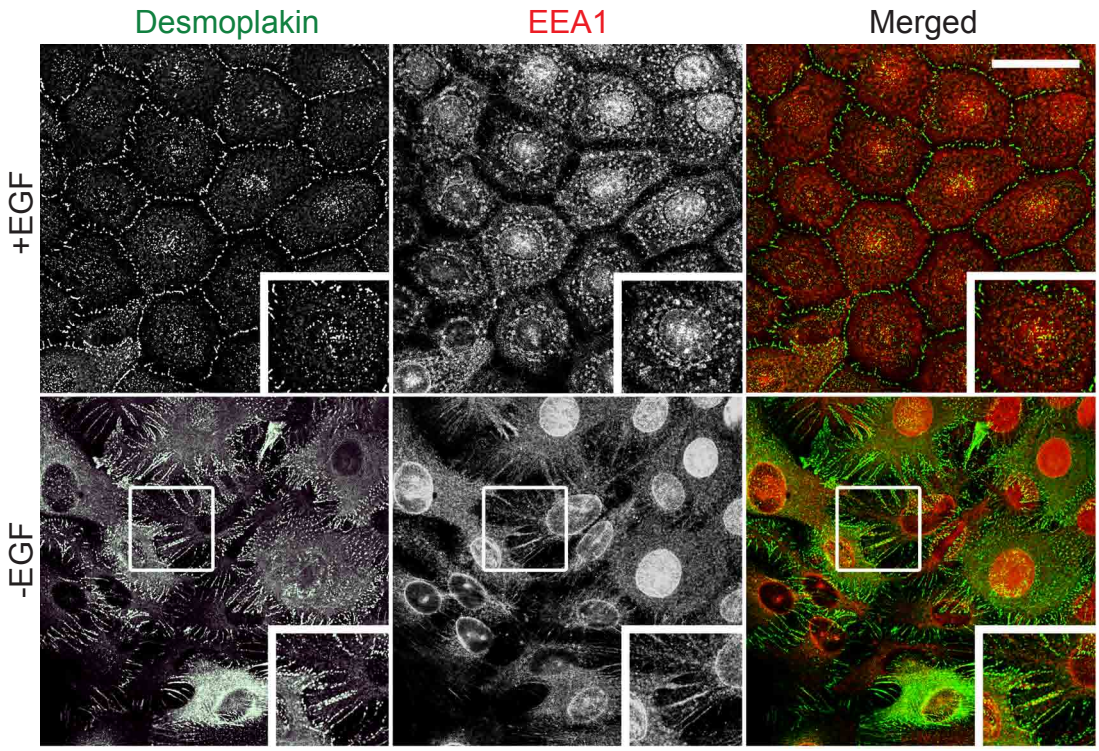


**Figure 5.17. Co-localisation of Desmoplakin and early endosomal marker, EEA1.** MCF10A cells showed diffuse EEA1 stain in -EGF and partially localised with Desmoplakin in both ±EGF conditions. Cells were cultured in growth medium ±EGF for 66.5 hours and coverslips were fixed with ice cold methanol. Cells were stained with Desmoplakin and Early endosomal auto-Antigen 1, EEA1. Images of monolayers were taken using confocal microscopy at 63x magnification (zoom 1.5). Scale; 40µm.

The relative increase in desmosomal proteins in cells cultured without EGF prompted the next question: do Desmoplakins internalise under the influence of EGF from the cell surface leading to their reduction? I approached this question by co-staining desmoplakin with the early endocytic marker (EEA1) to visualise their co-localisation in ±EGF (Figure 5.17). Note the -EGF monolayers previously seen with increased protein expression showed more cells with internalised desmoplakin compared to control (+EGF) cells. In both ±EGF conditions, desmoplakin remained on the borders of cells and showed partial co-localisation with EEA1. No quantification was attempted. Independently, Bo Van Deurs and colleagues reported Desmoplakin endocytosis upon cell dissociation provoked by calcium depletion, which required actin polymerisation but was independent of clathrin-mediated endocytosis in non-malignant mammary epithelial cells, HMT-3522 (Holm et al., 1993).

### *5.4.3 Co-localisation of desmoplakin with Caveolin-1*

As a side observation, the TEM micrograph showed fortuitously recovered caveolae-like invaginations prevalent in digits under the -EGF condition (Figure 5.18; Parton and Simons, 2007). Without positive leads in the canonical endocytic pathway, I wondered whether clathrin-independent, caveolin-dependent endocytosis would contribute to this phenotype. Monolayers of MCF10A cells were cultured ±EGF and stained with a caveolae marker, caveolin-1 (Figure 5.18). Caveolin-1 under -EGF condition appeared dispersed in the cytoplasm and on the membrane, often resembling the outline of interdigitations. In control (+EGF) condition, caveolin-1 localised either in perinuclear pools, along borders of cells or at both locations simultaneously (Figure 5.18, Figure 5.19). These locations reflect the transport of caveolin from the endoplasmic reticulum, to Golgi complex and its subsequent assembly into lipid rafts near plasma membrane (Parton and Simons, 2007; Pol et al., 2005).

### *5.4.4 Organisation of Golgi markers and microtubules induced by EGF removal*

Due to the likeness of caveolin-1 stain to the perinuclear Golgi apparatus and the drastic reorganisation of caveolin-1 to the cell boundaries, I was intrigued if the organisation of Golgi apparatus would be disrupted in the absence of EGF signalling. To visualise the Golgi apparatus, I co-stained caveolin-1 with either GM130 (cis-Golgi marker) or p230 (trans-Golgi marker) (Figure 5.19). Although there was minimal overlap in these stains, there was a distinct rearrangement of the

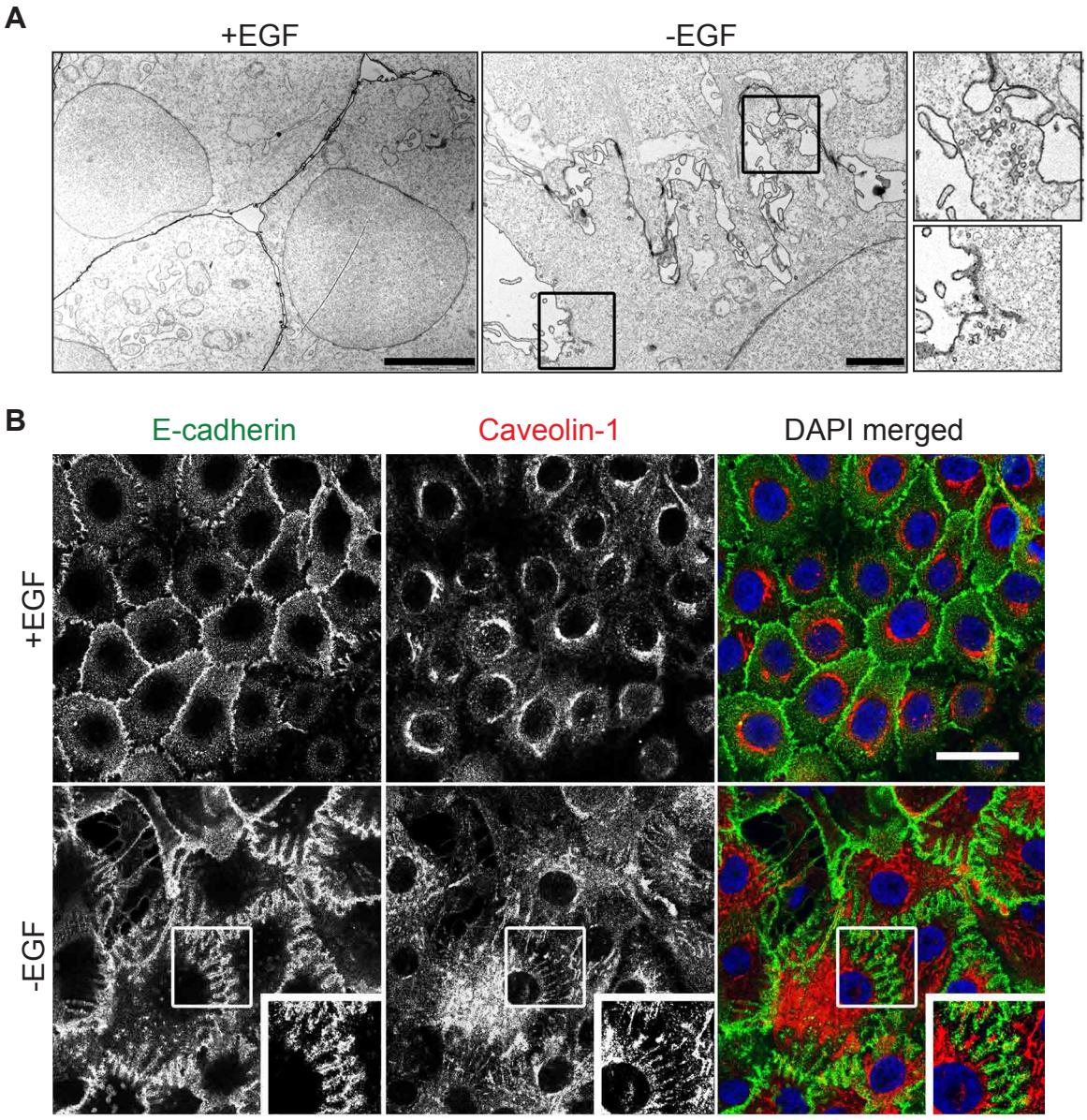


**Figure 5.18. Subcellular localisation of caveolin-1 in MCF10A cells.** (A) Control cells (+EGF) show smooth boundaries between neighbouring cells. This image is the same as Figure 5.1. The caveolae-like structures observed in digits (-EGF) are boxed and enlarged on the right. Cells were cultured in medium ±EGF and fixed 62 hours later for TEM processing. Scale bar, 5 µm and 2µm. (B) MCF10A cells were cultured in ±EGF growth medium and fixed 63 hours later. Coverslips were stained with E-cadherin, caveolin-1 and DAPI. Images were taken using confocal microscopy at 63x magnification, zoom 1.5. Scale; 40µm.

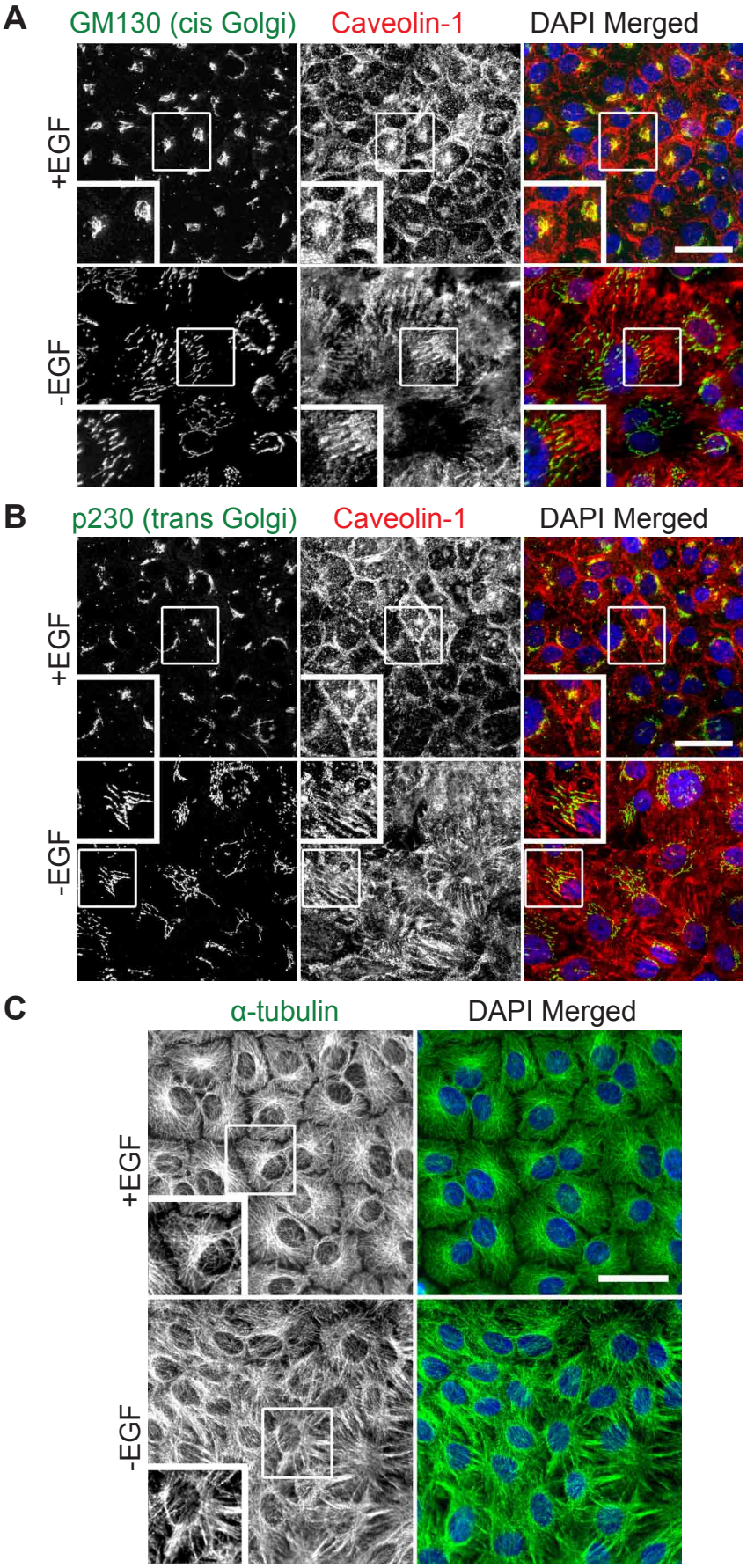


**Figure 5.19. Subcellular localisation of caveolin-1, Golgi markers and mictrotubules.** MCF10A cells were cultured in ±EGF growth medium and fixed 65-67 hours later. Coverslips were stained with DAPI, caveolin-1 and Golgi markers;(A) GM130, (B) p230 and (C) microtubule marker: α-tubulin (DM1A). Coverslips were fixed with (A,B) 4% PFA or (C) ice cold methanol. Images were taken using immunofluorescence microscopy at 40x magnification. Scale; 40μm.

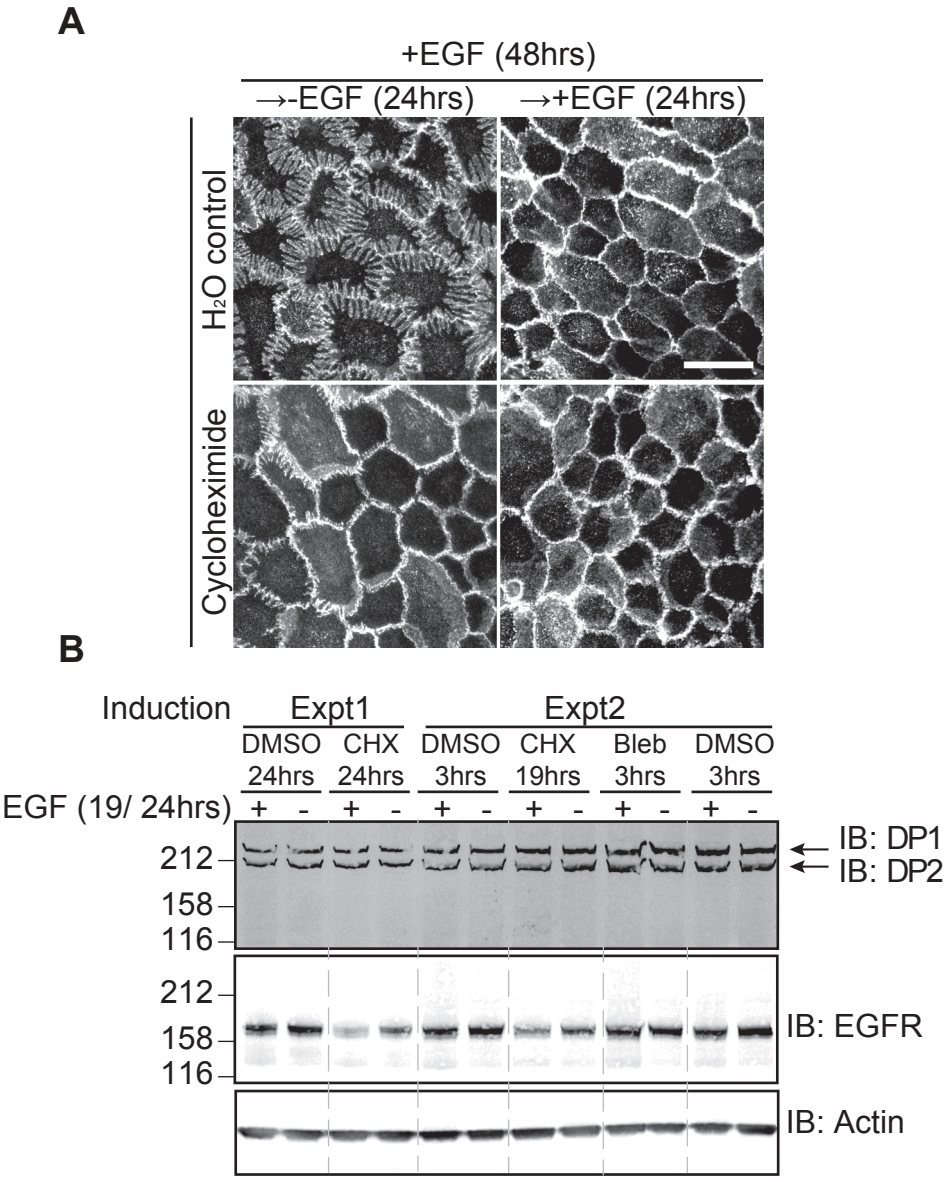


**Figure 5.20. Cycloheximide treatment impedes induction of interdigitations.** (A) MCF10A cells were cultured in +EGF growth medium to achieve confluence at 48 hours before exchange to medium without EGF for 19-24 hours. Cells were treated with either water or 100ng/ml cycloheximide after the medium exchange. Coverslips were fixed with 4% PFA and stained with E-cadherin. Images were taken using immunofluorescence microscopy at 40x magnification. Scale; 40μm. (B) Cells were treated as (A) but lysed and probed for Desmoplakin, EGFR and actin. Each lane was loaded with 10μg of MCF10A cell lysates. Bleb, Blebbistatin; CHX, Cycloheximide; DMSO, vehicle dimethyl sulfoxide; Expt, Experiment.

Golgi apparatus from perinuclear in control (+EGF) cells to dispersed Golgi stacks in the -EGF condition. The Golgi apparatus in mammalian cells is normally positioned near perinuclear microtubule organising centres and this positioning is a dynamic process for which the mechanisms involved are still relatively uncharacterised (Yadav and  and Linstedt, 2011). The scattered Golgi apparatus under -EGF conditions may indicate a lack of cell polarisation and/or inactive secretory pathway as the Golgi and microtubules are known to realign with the leading edge of moving cells to facilitate secretion of proteins that direct cell movement (Yadav and Lindstedt, 2011). This disrupted Golgi localisation may be linked to the reduced mobility of -EGF monolayers when compared to the control (+EGF) monolayers seen in Movie 3.1. Related to this, the polarisation of the Golgi apparatus towards the lumen of MCF10A acini was reported to facilitated rotational movement of cells during acini morphogenesis (Wang et al., 2013).

Golgi stack dispersal has been linked to the disruption of microtubules in Hela cells (Cole et al., 1996). Disruption of microtubules also inhibits the secretion of milk protein, casein in lactating mouse mammary cells (Rennison et al., 1992). Hence, I investigated if the microtubules that organises Golgi positioning would be remodelled upon EGF withdrawal. Fitting with the Golgi dispersal seen under -EGF conditions, microtubules rearranged from a perinuclear localisation (+EGF) to cytoplasmic stains that mimicked the inter-cell protrusions seen with the E-cadherin stained MCF10A cells (Figure 5.19, Figure 4.1). Collectively, these results hints at an EGF induced mechanism that leads to microtubule reorganisation and changes in Golgi apparatus positioning, which may redirect secretory pathway and redistribute caveolin-1. Moreover, the disruption of microtubules has been reported to dephosphorylate EGFR in oesophageal carcinoma cells, rendering microtubules a promising target for cancer therapy (Wu et al., 2013). The involvement of these components in EGF induced membrane remodelling of mammary epithelial cells may provide intriguing mechanisms to be pursued further.

### *5.4.5 Protein synthesis during the induction of interdigitations*

Next, I asked if monolayers of cells need to synthesise additional proteins over at least 12-17 hours to enable the formation of interdigitations? To approach this question, cell monolayers were cultured in complete growth medium for 48 hours. Medium was exchanged to medium ±EGF with or without protein synthesis inhibitor, cycloheximide (CHX) (Figure 5.20, Movie 5.2; Schneider-Poetsch et al., 2010). Overnight treatment of EGF-starved monolayers with CHX failed to induce

interdigitations. However, it is possible that the induction is merely delayed as I did not extend the experiment further at the time.

If inhibition of protein synthesis impaired digits induction, would desmoplakin be a one of the newly synthesised proteins required for interdigitations? MCF10A cells were treated with cycloheximide (CHX) for 19 and 24 hours in ±EGF conditions and cells were lysed to probe for Desmoplakin. The levels of Desmoplakin seen after 19 and 24 hours of EGF removal remained unaffected by 24 hours of CHX treatment although digits failed to form under –EGF condition (Figure 5.20). This indicates that Formation of digits is not dependent on increased Desmoplakin as the digits formed within 24 hours of EGF removal without changing levels of Desmoplakin. It has been reported that a stable pool of Desmoplakin exists in confluent cells with a half-life of 72 hours which may reflect the lack of changes in levels within 19 and 24 hours that have been tested here (Pasdar and Nelson, 1988). This observation with CHX warrants further investigation, as it is possible that synthesis of other proteins that are as yet unidentified is required to induce the digits.

## 5.5 Junctional Characterisation: Resolution of interdigitations

### *5.5.1 Increase of desmoplakin levels downstream of interdigitation formation*

In prolonged culture of MCF10A cells without EGF (60+ hours) expression of the desmosomal adaptor protein, Desmoplakin increased (Figure 5.15, Figure 5.21, Figure 5.22). Conversely, elevated levels of Desmoplakin remained at cell boundaries after interdigitations had been resolved (Figure 5.21, 5.22). Consistent with the unaltered levels of Desmoplakin during the induction of digits (19 & 24 hours, Figures 5.20, 5.21, 5.22), the unchanged levels of Desmoplakin after digits reversal supports the notion that interdigitation itself is unlikely to be caused by desmosomes. Although Desmoplakin levels did not change in within 24 hours of digits induction and reversal, it would be possible for this desmosome adaptor protein to be internalised and relocated within cells to increase or decrease the assembly of desmosomal plaques (Garrod, 2010). To test this possibility, quantitative TEM can be undertaken to compare the numbers of electron-dense desmosomal plaques in the different configurations of induction and reversal of digits that can be induced at different time frames (Methods: Table 2.6).

## 5.6 Mechanical and cell dynamic outputs of interdigitations

### *5.6.1 Reduced wound healing ability of interdigitated monolayers*

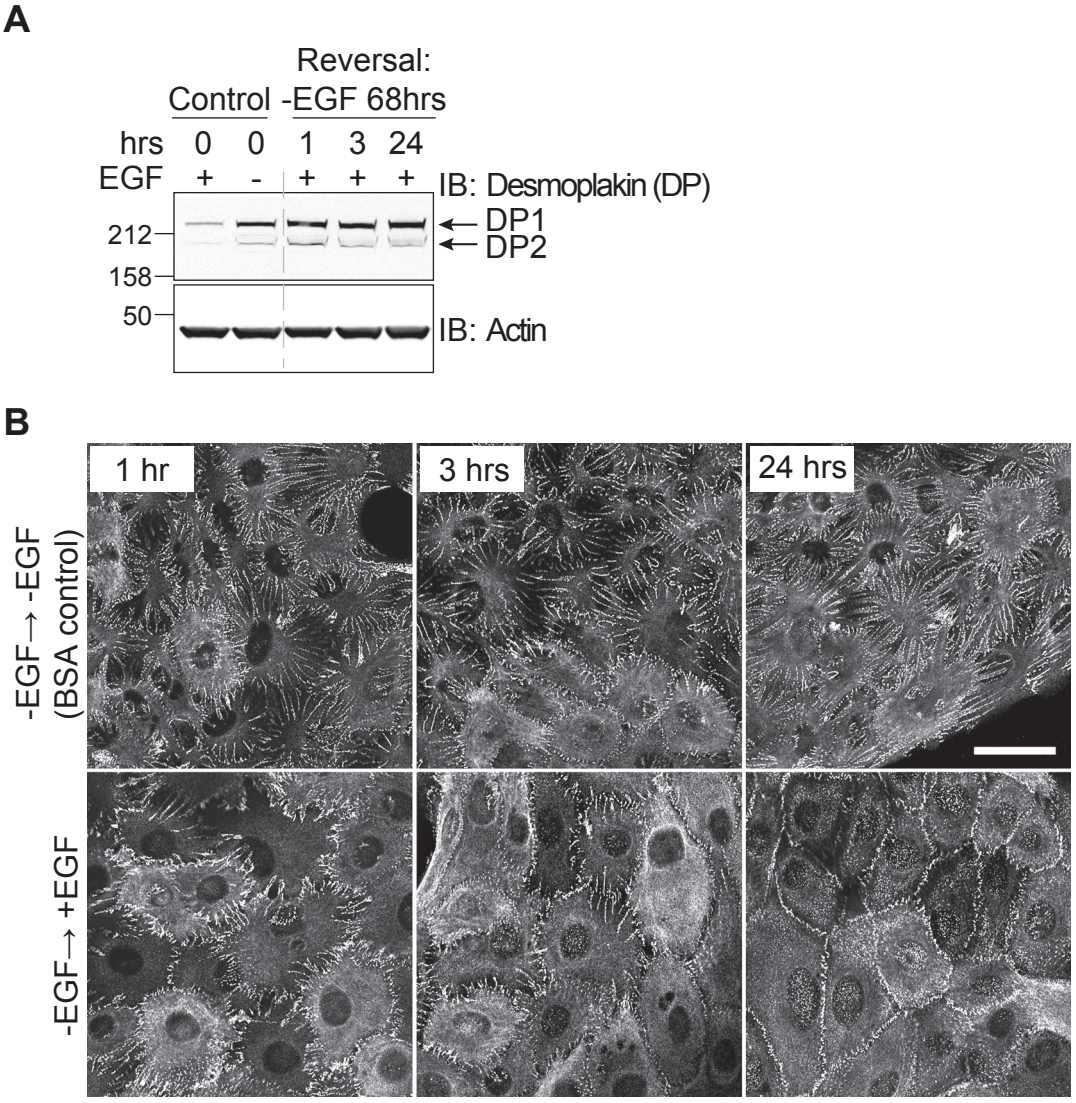


**Figure 5.21. Desmoplakin levels remain elevated after resolution of inter-digitations.** (A) MCF10A cell lysates were prepared from cells incubated for 68 hours in growth medium ±EGF. Other cells were subsequently treated for 1 hour, 3 hours and 24 hours with EGF before lysis. (B) Immunofluoresence images for cells treated as in (A) showing Desmoplakin retention at the cell boundaries during dissolution of interdigitations. Single confocal sections at 63x magnification. Scale bar; 40μm.

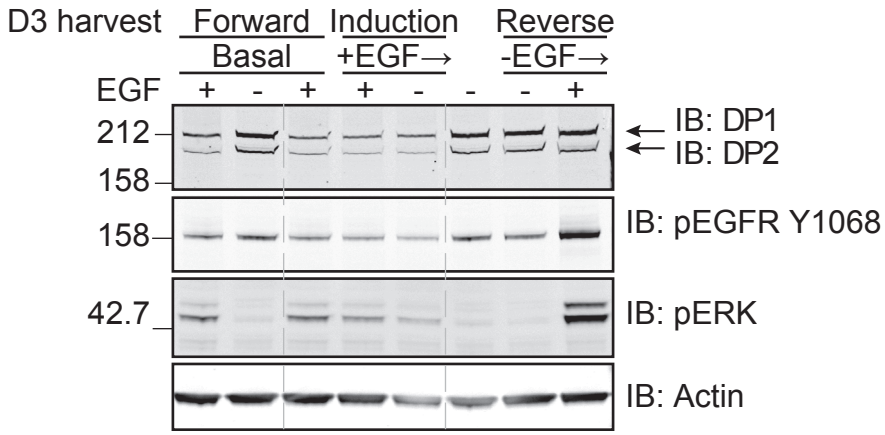


**Figure 5.22. Desmoplakin levels remain basal after interdigitation are induced.** (A) MCF10A cell were cultured in ± EGF medium for 67 hours. Medium was exchanged to -EGF for 24 hours to induce interdigitations. In the reversal experiment, 20ng/ml EGF was added to interdigitated monolayers for 7 hours. Each lane was loaded with 10µg lysates. Lysates were probed for levels of Desmoplakin, Y1068 EGFR, pERK and actin.

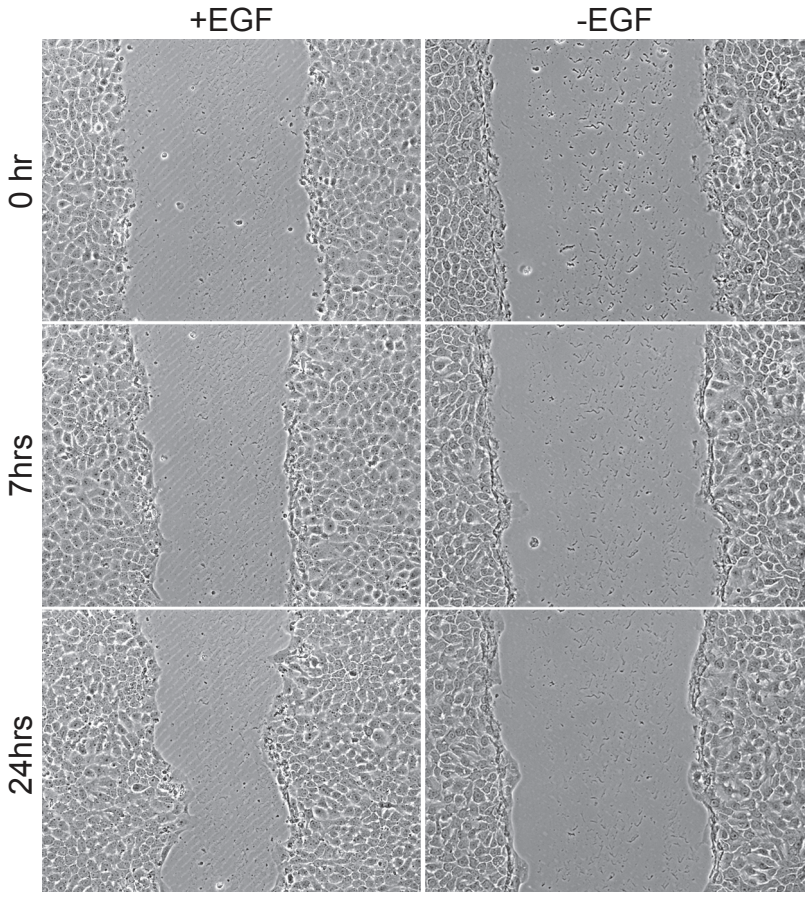


**Figure 5.23. Minimal closure of scratch wounds without ligand stimulation.** A) MCF10A cell were cultured in ± EGF medium for 72 hours. Wound was scratched into confluent monolayers of each well. Preconditioned medium was exchanged into wells to remove debris before phase contrast time-lapse imaging. Area of wounds were imaged every 15 minutes for 24 hours at 10x magnification.

To build on the structural and junctional characteristics, I asked if the interdigitations confer mechanical force and functions in monolayers. Previous observations of interdigitated cells showed restricted mobility within monolayers (Movie 3.1). So, I tested the ability of the interdigitated monolayers to migrate into artificially induced wounds. A pipette tip was used to scratch a wound in each well of the confluent monolayers of MCF10A cells cultured in ±EGF for 72 hours. Without acute ligand stimulation, the scratched wounds failed to fully close (Figure 5.23). However, at the end of imaging (24 hours), the presence EGF in control growth medium allowed the wound to narrow more effectively than the -EGF interdigitated monolayers.

To investigate if the resolution of interdigitations permits the closure of wounds, I added ligands of different receptors (as Figure 4.12) to pre-formed interdigitated monolayers. IF microscopy revealed the inability of the non-EGFR ligands to resolve interdigitations as was previously seen (Figure 5.24, Figure 4.12, Movie 5.3). As expected, acute addition of EGF, HGF and NRG1 all stimulated the phosphorylation of ERK and AKT as previously shown (Figure 5.25, Figure 4.12). HGF and NRG1 did not phosphorylate EGFR at Y1068 as these bind to the c-Met receptor and ErbB3 receptors respectively (Citri et al., 2006; Birchmeier et al., 2003). In parallel, time-lapse imaging revealed that MCF10A cells were unable to seal induced wounds after HGF and NRG1 stimulation (Figure 5.25, Movie 5.3). In contrast, only EGF stimulation allowed effective wound closure within 19 hours by which time interdigitations would have been resolved. This is in agreement with Band and colleagues who observed wound closure within MCF10A monolayers stimulated by EGF (Duan et al., 2011).

### *5.6.2 Increased resistance to external sheer stresses*

If interdigitated cells move less than the control (+EGF) monolayers, do interdigitations confer additional adhesive strength between cells in monolayers? I hypothesised that the interdigitated cells (-EGF) may resist external mechanical shear stresses better than the monolayers with smooth boundaries (+EGF). Typically, confluent sheets of cells were lifted using the dispase enzyme and subjected to shear stress by repeated pipetting (Ishii et al., 2005). The protease, dispase cleaves ECM proteins but preserves molecules of cell-cell adhesions (Lorch et al., 2004). The number of fragments obtained was counted. ‘Fragments’ allude to more than one cell that remains attached to each other. Less fragments were generated from the interdigitated monolayers (-EGF) even when exposed to the same external shear stress as the control (+EGF) monolayers (Figure 5.26). It is

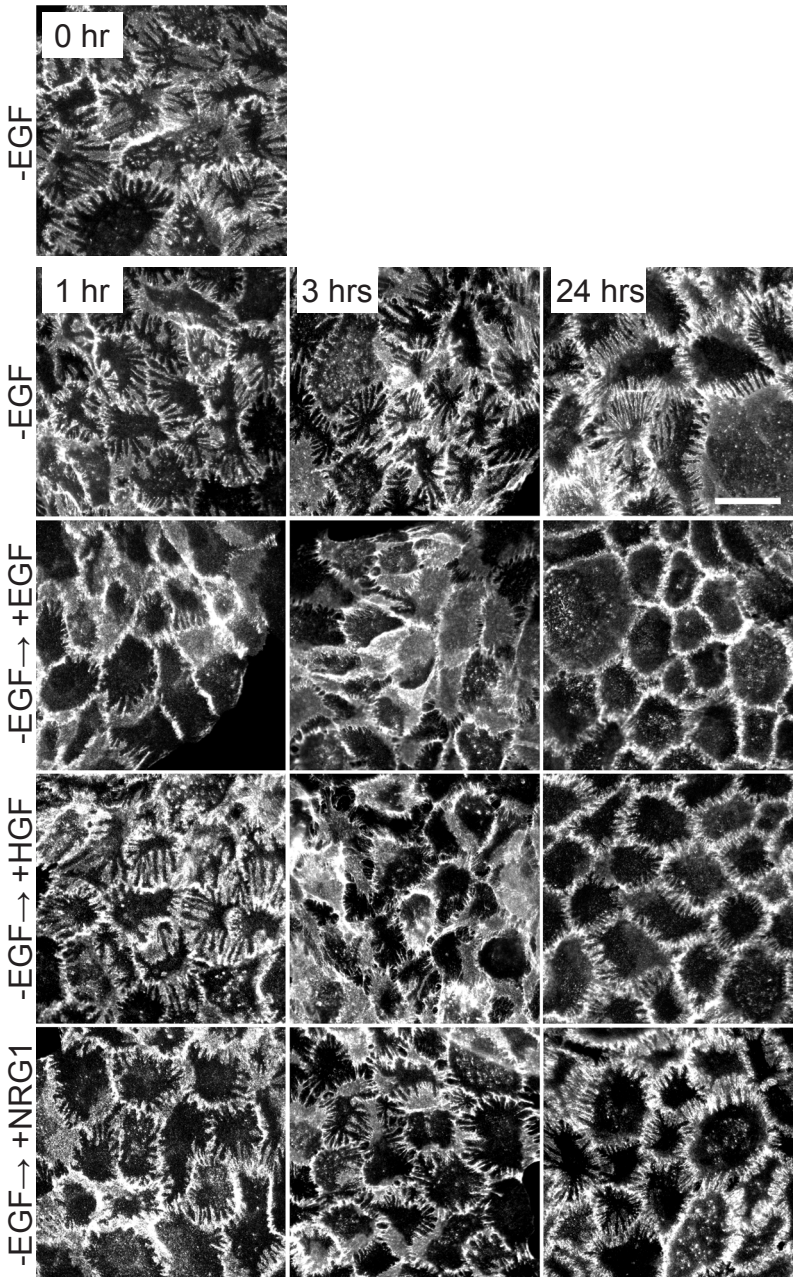


**Figure 5.24. Resolution of interdigitation is specific to EGF.** MCF10A cells were cultured in - EGF medium for 69 hours before addition of growth factors. Coverslips were fixed at the indicated times after ligand addition, with 4% PFA and stained for E-cadherin. Images were taken using immunofluorescence microscopy at 40x magnification. Scale; 40μm.

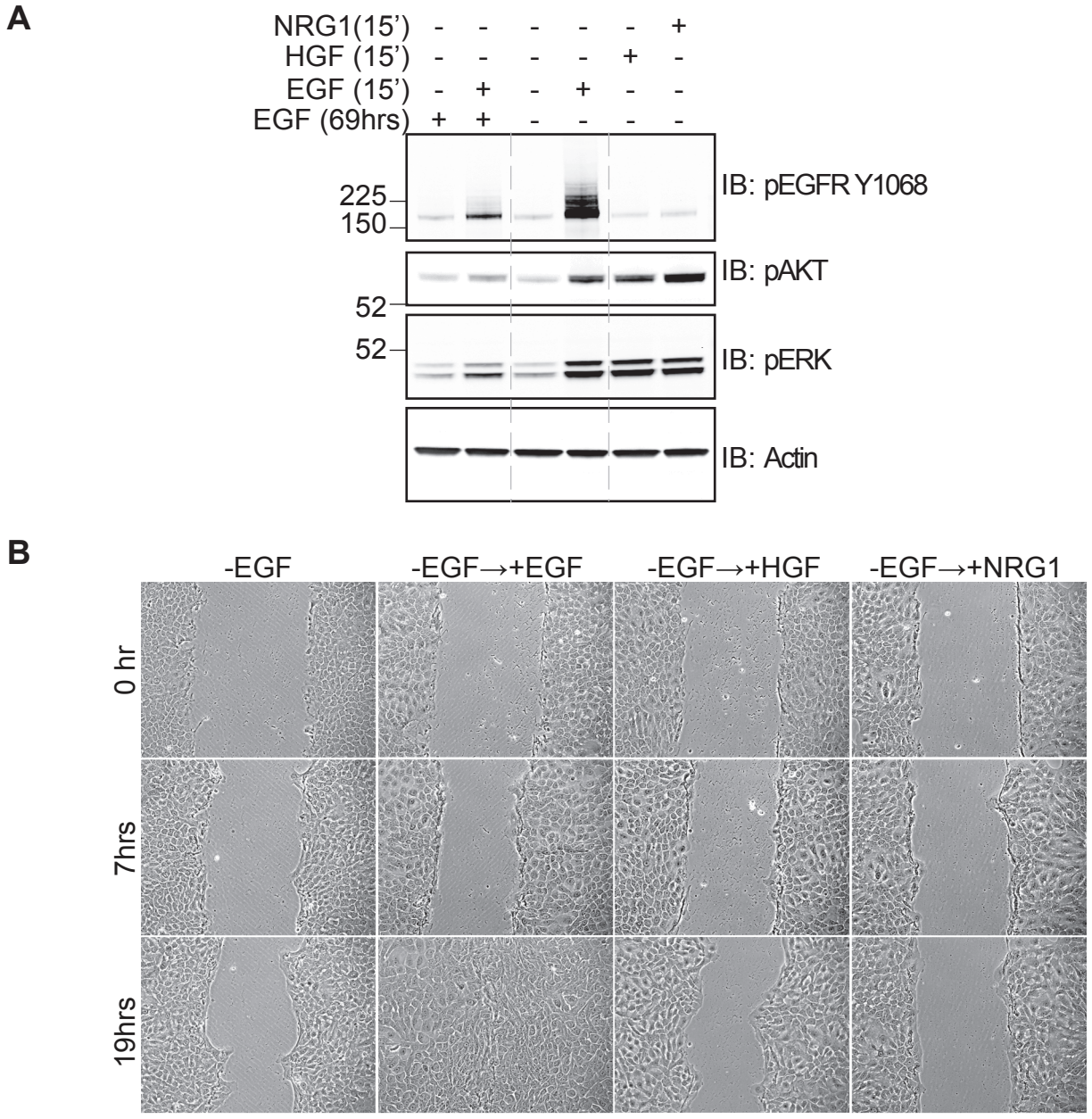


**Figure 5.25. Differential cell migration into scratch wounds.** (A) MCF10A cells were treated as in Figure 5.24 prior to lysis. Each lane was loaded with 10µg of lysates. Lysates were probed for Y1068 EGFR, pAKT, pERK and Actin. (B) Time lapse imaging recorded the ability of monolayers to close wounds when incubated with EGF (20ng/ml), HGF (20ng/ml) and NRG1 (6ng/ml). MCF10A cells were cultured in -EGF medium for 69-72 hours. A wound was scratched onto each well of interdigated monolayers 30-40 minutes prior to phase contrast time-lapse imaging at 10x magnification.

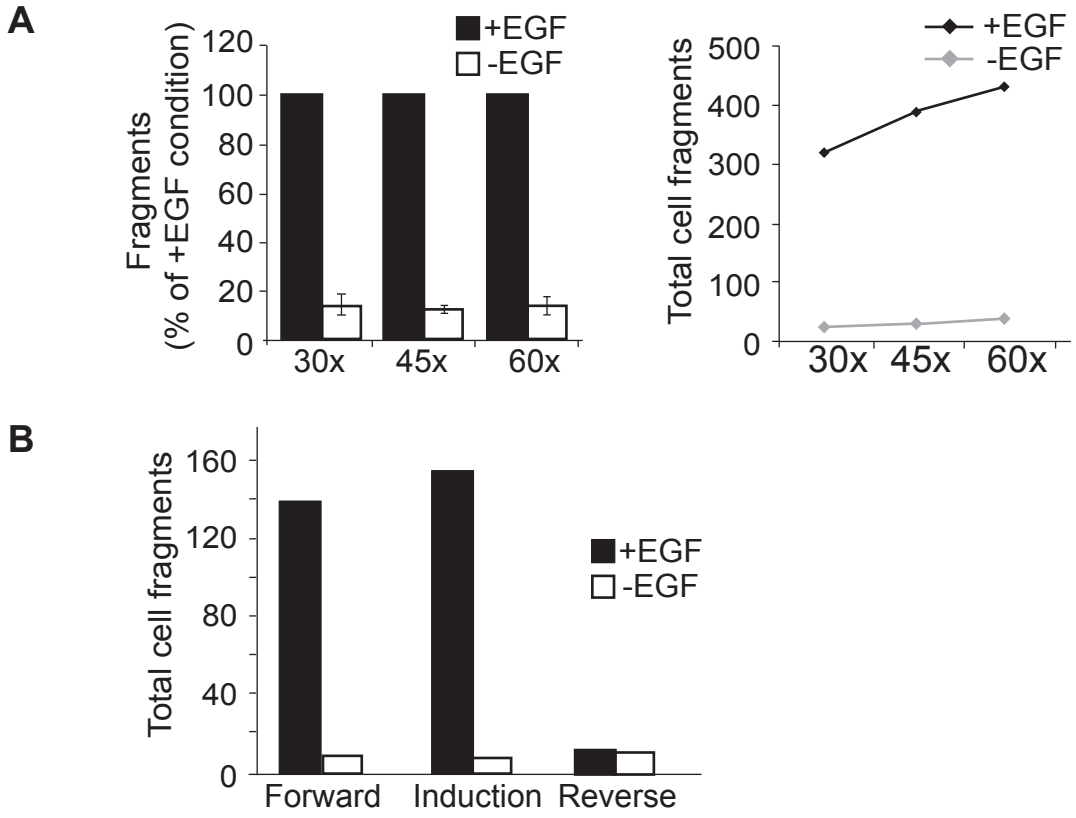


**Figure 5.26 Interdigitated cells resist mechanical shear stress.** (A) MCF10A cells cultured in ±EGF growth medium for 93 hours were subjected to dispase mechanical dissociation assay in triplicates. The number of fragments was assessed sequentially after 30, 45 and 60 pipetting strokes. 'Fragments' refer to more than one cell that remains attached to each other. Left: Shown are the relative fractions of fragments for cells grown ±EGF (average of two independent experiments, error bars indicate range). Right: Cumulative number of fragments of a representative experiment. (B) Cells from these experimental configurations were subjected to the dispase mechanical assay as described above at 30x pipetting strokes. Total cell fragments were counted. Forward (Cells cultured ±EGF for 67 hours); Induction (Cells were cultured +EGF (44 hours)→ ±EGF (24 hours)); Reverse (Cells were cultured -EGF (67hours) → +EGF (7hours). The timelines for the experiments of different configurations, Forward, Induction and Reverse are as denoted in Methods: Table 2.6.

also noteworthy that increasing pipetting shears increased the number of single cells seen in control (+EGF) condition but less was seen in –EGF. Although these single cells were not counted, this suggests that digits protect cell sheets from induced fragmentation. In addition, the monolayers of +EGF sheets continued to fragment with increased shearing but total fragments from interdigitated sheets remained unaltered (Figure 5.26).

I also undertook a preliminary experiment comparing the resistance to shear stresses of the monolayers obtained from different experimental configurations as previously described (Methods: Table 2.6); digits formation from subconfluence (termed 'Forward), digit reversal (termed 'Reverse') and induction from confluent monolayers (termed 'Induction'). Regardless of whether the cells were cultured in -EGF for 24 ('Induction') or 67 hours ('Forward'), the interdigitated monolayers were more resistant to the pipetting shears (Figure 5.26). This would indicate that the increased adhesive strength witnessed in interdigitated cells (-EGF) occurs independent of the levels of adaptor protein, Desmoplakin which are only increased in the 'Forward' configuration (Figure 5.26, compare Figure 5.15 and Figure 5.20).

After reversal of digits for 24 hours ('Reverse), the resistance to fragmentation remained unaffected, corresponding well to the unchanged levels of Desmoplakin observed (Figure 5.26, Figure 5.22). The levels of Desmoplakin in this experimental configuration ('Reverse') resembled the increased Desmoplakin levels in prolonged culture without EGF ('Forward') (Figure 5.22). As discussed earlier (Section 5.5.1), levels of the adaptor protein, Desmoplakin do not inform on the number of assembled desmosomes in cells (Green and Gaudry, 2000). Desmoplakin can be internalised and remain detached from desmosomal plaques. Whether the number of desmosomes contributes to the increased resistance to fragmentation observed in monolayers of MCF10A remains to be determined at the ultrastructural level.

### *5.6.3 Protection against hypotonic osmotic stress*

Previous observation that a caveolae marker (caveolin-1) redistributed from a perinuclear to a generally cytoplasmic localisation upon EGF withdrawal prompted further investigation into the functional relevance of this redistribution (Figure 5.19). Caveolae in cell culture disassemble from the plasma membrane in response to acute mechanical stress such as cell osmotic swelling (Sinha et al., 2012). The interdigitated cells (-EGF) presumably have a higher surface to volume ratio compared to the control (+EGF) cobblestones monolayer (Figure 4.1). Therefore, I

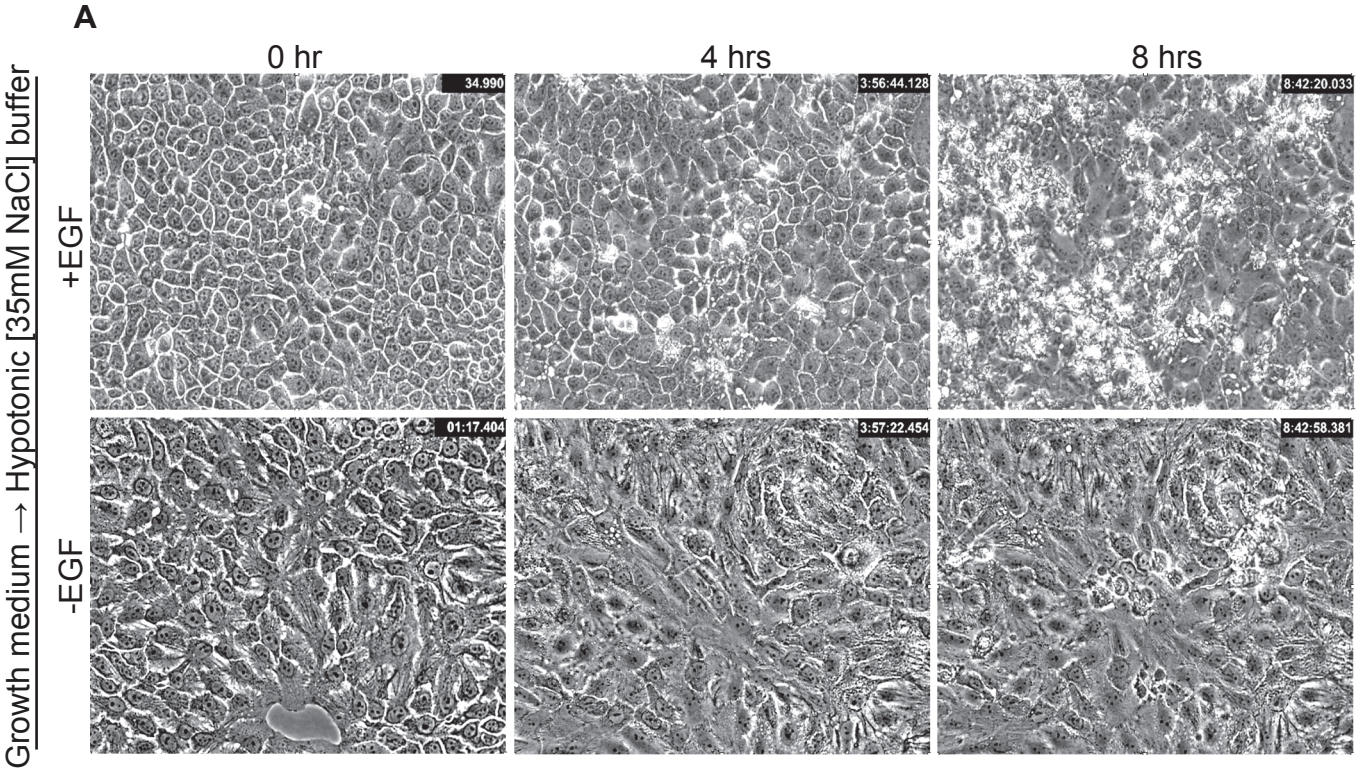


**Figure 5.27. Interdigitated cells withstand hypo-osmotic stress.** (A) MCF10A cells were cultured in growth medium ±EGF for 48 hours before medium exchange to hypotonic buffer [35mM NaCl]. (B) Control cells were exchanged to isotonic buffers at 35mM NaCl shown on the next page. Recipes of buffers are listed in Methods: Table 2.9. Cells were imaged every 5 minutes for 8+ hours after exchange to buffers, using phase contrast time-lapse microscopy at 20x magnification. These are still images from Movie 5.4.

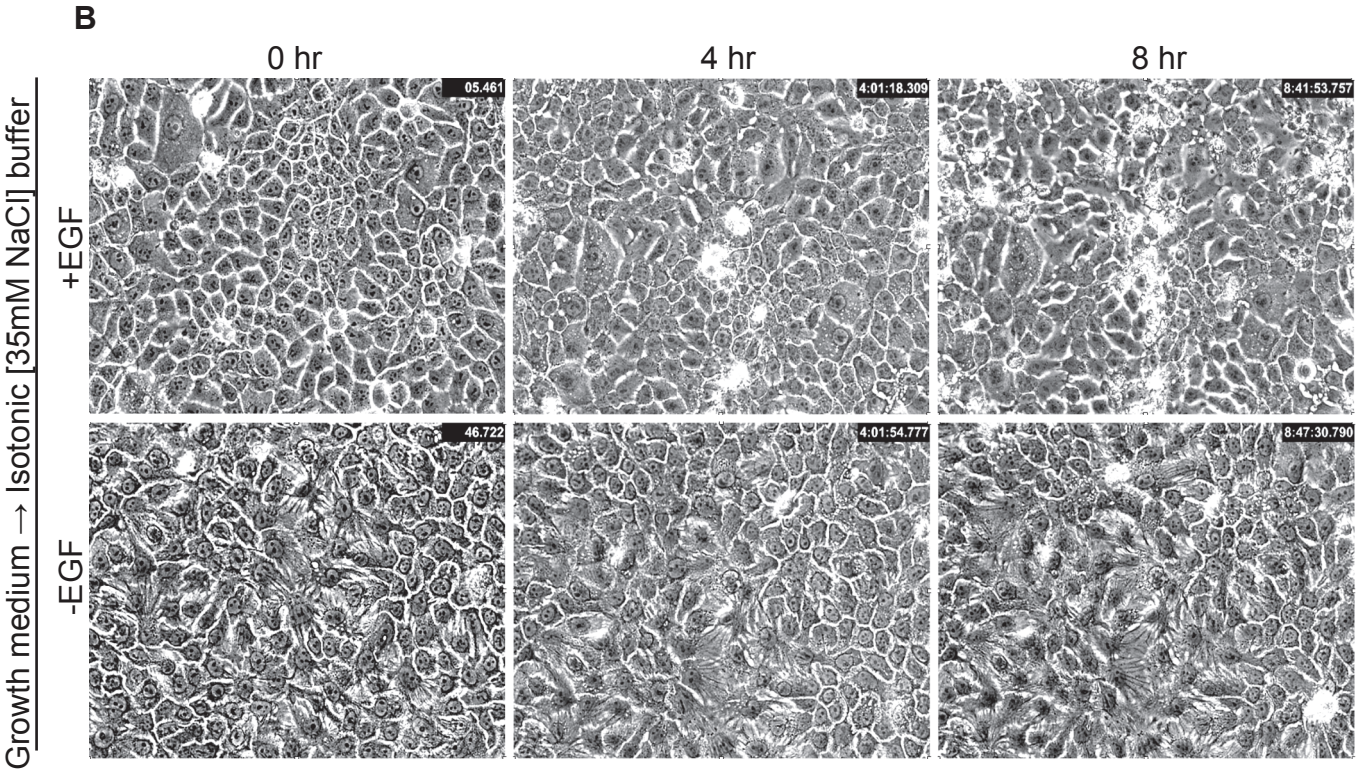


**Figure 5.27. Interdigitated cells withstand hypo-osmotic stress.** (B) MCF10A cells were cultured in growth medium ±EGF for 48 hours before medium exchange to isotonic buffer [35mM NaCl]. These images show control treatment to Figure 5.27A. Recipes of buffers are listed in Methods: Table 2.9. Cells were imaged every 5 minutes for 8+ hours after exchange to buffers, using phase contrast time-lapse microscopy at 20x magnification. These are still images from Movie 5.4.

wondered whether the caveolae seen in digits (-EGF) would allow monolayers to withstand changes in osmolarity more effectively than smooth (+EGF) monolayers? To answer this, I observed the morphology of cells using time-lapse imaging at 5 minute intervals after applying buffers of different osmolarity onto pre-formed monolayers (Movie 5.4, Figure 5.27).

The buffers of different osmolarities tested were hypotonic [35mM NaCl], [77mM NaCl] and isotonic [35mM NaCl] (Methods: Table 2.9). Osmolarity of buffers reflects the concentration of solutes including each ionic species derived from salts (Gold et al., 1987). The osmolarity of isotonic buffer was controlled by the addition of 200mM D-mannitol to mimic iso-osmotic concentrations at 135mM NaCl (Hyzinski-Garcia et al., 2011; Methods: Table 2.9). This provides a control for any effects of ionic strength rather than changes in osmolarity. At the end of the time-lapse imaging experiment, interdigitated monolayers (-EGF) survived better than control monolayers (+EGF) with smooth boundaries in hypotonic buffer [35mM NaCl]. MCF10A monolayers were able to withstand hypotonicity at [77mM NaCl].

## 5.7 Discussion

### *5.7.1 Actin requirement and functional outputs of digits*

In this chapter, I have provided evidence that actin polymerisation and actomyosin contraction is required to resolve interdigitations in confluent monolayers. The EGF induced resolution manifests mechanically to allow closure of wounded monolayers. Rac1 is activated upon EGF stimulation in this process but reduced activation of Rac1 failed to impair digit reversal. Yarden and colleagues have demonstrated that acute stimulation with EGF induced migration of MCF10A cells across Transwell chambers, which is consistent with my observation that EGF prompted cells to move and close scratch wound (Tarcic et al., 2012). They reported the synthesis of EGR1 (Early Growth Response 1) downstream of the EGF induced ERF (E Twenty Six protein family repressor) to sustain migratory ability of cells. It is possible that actin related proteins are also synthesised upon EGF stimulation but they only focused on transcription factors activated downstream of the EGFR signalling. Therefore, EGF dependent adaptors of the actin cytoskeleton remodelling system remain to be explored especially in the rapid reversal of the interdigitations.

The formation and maintenance of the interdigitated state is independent of actin polymerisation and actomyosin contraction. However, data presented in the previous chapter (Chapter 4) have shown that the combined outputs of the PI3K and

MAPK signalling cascades are essential to induce digits in monolayers. Mechanically, the interdigitated monolayers have been shown to remain shackled with restricted ability to close artificially induced wounds in cell culture. In addition, these structures provide superior resistance to external shear stresses by reducing the risk of fragmentation within the monolayers. Interdigitations also allowed cells to remain attached within monolayers when actomyosin contraction was perturbed. The enhanced protection of interdigitated monolayers against physical stresses may reflect its physiological relevance in mammary tissues. For example, mammary glands have to adapt to significant mechanical stresses and volume changes during the menstrual cycle (Nazario et al., 1994).

### *5.7.2 Increased desmosomal numbers as a consequence of digit formation*

The number of desmosomal plaques and levels of desmosomal proteins increased in prolonged culture without EGF (60+hours). However, two strands of evidence suggest that desmosomal adaptor proteins, Desmoplakin do not cause interdigitation: i) Digit induction for 24 hours is not accompanied by an increase in the expression of Desmoplakin, ii) Desmoplakin levels remained elevated after the resolution of digits. However, Desmoplakin can be internalised and detach from desmosomal junctions upon calcium removal (Holm et al., 1993, Garrod, 2010). TEM quantification of the numbers of desmosomal plaques in both the induction and reversal of digits should be compared to establish if assembled desmosomes are required in these processes.

### *5.7.3 Reorganisation of microtubules, Golgi apparatus and caveolae in the absence of EGF*

Surprisingly, monolayers cultured without EGF showed a remarkable reorganisation of β-tubulin (microtubule marker), GM130/p230 (Golgi apparatus marker) and caveolin-1 (caveolae marker). Perinuclear positioning of microtubules, Golgi apparatus and caveolae in control (+EGF) cells was disrupted when cells were cultured without EGF. It is possible that secretion of cargos to the plasma membrane is altered in these cells to induce digits (Yadav and Lindstedt, 2011). The preliminary observation of an increased number of caveolae under -EGF condition in TEM micrographs may relate to the ability of cells to withstand osmotic stresses. However, the link between microtubule, Golgi apparatus, caveolae redistribution and the formation of digits needs to be investigated further by perturbing the microtubules with agents such as Nocodazole to test if this would impair the membrane remodelling witnessed upon EGF withdrawal. Ultrastructural examination to quantify caveolae numbers would establish if there are differences between

smooth and interdigitated membranes. Collectively, these may provide exciting insights into an EGF-dependent mechanism of the dynamic Golgi organisation and membrane remodelling in mammary epithelial cells.

### *5.7.4 Protein synthesis required for the induction of interdigitations*

Inhibition of protein synthesis by CHX impaired the ability of monolayers to induce digits upon removal or interdigitations. This area would warrant further investigation using a more systematic approach to elucidate the EGF-dependent mechanisms involved in the formation of interdigitations. Tarcic et al. (2012) had reported that *de novo* protein synthesis occurs to sustain EGF induced migration of MCF10A cells based on mRNA microarray hybridisation studies. Hence it is rational to assume that cells would have to synthesise a different set of proteins to induce interdigitations and restrict mobility. Changes in the proteome and phospho-proteome can be analysed using stable isotope labelling of amino acids (SILAC) in cell culture to compare the ±EGF conditions. Using this technology, it is possible to systematically unravel the disparate mechanisms and post-translational modifications involved in both the formation and reversal of interdigitations (Hammond et al., 2010, Tarcic et al., 2012).

### *5.7.5 Biological perspectives*

The enhanced protection against mechanical and osmotic stress and the increased cell-cell adhesion of interdigitated monolayers indicates that these structures may be biologically relevant in non-malignant mammary epithelial cells (Chapter 1: Section 1.5). This study provides a simplified *in vitro* system to methodically delineate the mechanisms associated with interdigitations that is widespread in stratified animal tissues. Further investigation is warranted to investigate the involvement of actin associated proteins especially in the rapid resolution of interdigitations. Moreover, the paradoxical requirements for actin remodelling in the reversal but not the formation of digits further indicates that both processes are separately regulated via EGF dependent signalling pathways that are yet to be identified.

# Chapter 6
# Discussion

# Chapter 6: Discussion

## *6.1 Reversibility of interdigitations accompanied by phenotypic and mechanical outcomes*

In this thesis, I have characterised in detail the remarkable changes in non-malignant mammary epithelial cell boundaries within a confluent monolayer, elicited by a single defined cue, EGF (Chapter 1: Figure 1.10). EGFR signalling in this context serves to suppress the ability of confluent MCF10A cell sheets to interdigitate. Confluent monolayers and the absence of EGF are prerequisites to the assembly of interdigitations (>12 hours). This process is recapitulated but requires a longer duration with EGFR, PI3K and MAPK inhibitors (24-48 hours). Interdigitations are inducible from cells seeded in subconfluence or from confluent monolayers with differing time scales at 24-36 hours and 12-17 hours respectively. The appearance of these finger-like protrusions is accompanied by a 10x increase in the number of desmosomes assessed by quantitative electron microscopy and levels of desmosomal proteins, whilst markers of adherens and tight junction proteins remain unchanged. The induction and maintenance of digits in a confluent monolayer does not require actomyosin contraction with actin polymerisation unnecessary in the latter. In monolayers of interdigitated cells, other phenotypic manifestations include dispersed Golgi apparatus with rearrangement of microtubules. This resembles loss of cell polarity congruent with the lack of directional movement within the interdigitated monolayers. As a consequence, interdigitated cells are unable to close an artificially induced wound but display increased cell-cell adhesive strength, resistance to fragmentation and osmotic pressures.

Interdigitations are dynamically resolved upon application of EGF by a relatively rapid process (1-3 hours). Noteworthy is that dissolution is specific to EGF and not amenable to ligands of other RTK receptors, c-MET and ErbB3 despite the strong overlap in downstream signals (Citri and Yarden, 2006; Hammond et al., 2010). Instead reversal is dependent on actin polymerisation and actomyosin contractile forces. Counter-intuitively, this process is independent of the PI3K and MAPK signalling although these are required for the formation. Together, these imply the involvement of signalling pathways unique to EGFR that regulate actin dynamics. Rho GTPases are well known to regulate remodelling of the actin cytoskeleton (Ridley, 2006). Rac1 has been shown to be activated upon EGF stimulation and induce membrane protrusions known as lamellipodia by stimulating actin polymerisation (Duan et al., 2011; Machesky and Hall, 1996; Ridley 2006). In my hands, overexpression of constitutively active pEGFP-RacV12 opposes

interdigitations by forming membrane ruffles. This is consistent with other findings which have shown that hyper-activation of RacV12 oppresses cellular protrusions such as invadopodia in rat mammary adenocarcinoma cells and filopodia in *Dictyostelium* to impair the migratory ability of these cells (Dumontier et al., 2000; Moshfegh et al., 2014). Although membrane ruffling structures such as lamellipodia are known to facilitate movement of cells across substrates, the ruffling cells with constitutively active Rac remain confined to their interdigitating neighbours under -EGF condition (Ridley, 2011). Rac1 overexpression has been found in breast tumours to promote lamellipodia formation allowing oncogenic cells to metastasise (Small et al., 2002; Sahai and Marshall, 2002). Therefore, by elucidating the mechanisms that regulate the formation and maintenance of interdigitations, it may become possible to introduce this phenomenon into malignant breast tissues, to oppose ruffling, metastatic cells.

However, reduction of Rac1 activity via the Rac-GEF, Vav2 is insufficient to maintain interdigitations. One possibility is that the residual pool of Rac1 is sufficient to remains to be explored. The molecular comparisons of interdigitations with other existing subcellular structures such as filopodia and invadopodia may provide additional insights to the mechanism governing the formation and reversal of interdigitations. The activation of CDC42 has been shown to impair EGFR degradation, which reduced the motility of breast cancer cells in culture (Hirsch et al., 2006; Wu et al., 2003). This situation may be synonymous with the formation of interdigitations in MCF10A cells when cultured without EGF that prevents cell movement within confluent monolayers.

Cables of actin filaments seen in the digits resemble filopodia with parallel actin bundles (Ridley, 2006; Stevenson et al., 2012). CDC42 is known to promote the formation of filopodia by binding and stimulating actin nucleating and bundling protein families including diaphanous related formins (DRF), Ena/ VASP proteins and fascin (Ridley, 2006; Stevenson et al., 2012). The actin bundling protein, Fascin has been shown to be highly expressed at the invasive front of epithelia tumours whereas a variant of Mena have been reported to be overexpressed in breast cancer (Machesky and Li, 2010; Di Modugno., 2004). In my hands, actin polymerisation has been shown to be necessary for the reversal of interdigitations. One may hypothesise that Rho-GTPases and clusters of actin bundling proteins such as those mentioned above may alter localisation during digit reversal to allow remodelling of the cytoskeleton.

In future work, we propose to investigate the effects of constitutively active CDC42 as well as its inhibition in the formation of digits. This will be possible by transfecting the cells under -EGF condition with constitutively active CDC42 constructs or using siRNA to knockdown CDC42 or it's related GEFs. It will also be insightful to identify the location of the different actin regulators mentioned above especially in the reversal of digits and to draw comparisons with the actin components known in other types of cellular protrusions. The turnover of actin can also be visualised by transfecting cells with GFP-LifeAct and tracing the dynamic turnover of actin using fluorescence recovery after photobleaching (FRAP) microscopy. The rate of turnover of actin in both the formation and reversal of digits may provide clues as to the stability and modulation of actin polymerisation in these processes.

Desmosomes have been seen to intermingle between interdigitating mammary epithelial cells in 2D and 3D cultures (Ewald et al., 2012; Holm et al., 1993). This supports the TEM quantification that showed increased desmosomal numbers under -EGF condition when cells interdigitate. However, the induction of interdigitations within confluent monolayers appears to form prior to the increase in desmosomal adaptor protein, Desmoplakin. Cells that interdigitated within 24 hours of –EGF culture did not show an increase in Desmoplakin when compared to cells that were in prolonged -EGF culture (60+ hours). Other studies in keratinocytes reported that the levels of desmosomal components did not correlate with the adhesive capabilities of cells in confluent monolayers (Kimura et al., 2007; Mattey and Garrod, 1986). Consistently, separate pools of cytoplasmic or intermediate filament attached Desmoplakin have been reported in cells (Pasdar and Nelson, 1988). This suggests that the number of desmosomes may change even when level of the adaptor protein, Desmoplakin remain stable in the induction and reversal of interdigitations. Therefore, we propose to evaluate and compare the number of electron dense desmosomal plaques by TEM in interdigitated monolayers before and after the resolution of interdigitation to assess if there is a change in the number of desmosomes in these processes.

### *6.2 Physiological relevance of interdigitations in mammary glands*

Mammary gland tissues are subjected to remarkable changes in architecture to accommodate mechanical stresses and volume changes due to fluid and cell transports during physiological events that spans decades in humans (Gjorevski and Nelson, 2011; Nazario et al., 1994). Ultrastructural studies reported interdigitations between cells in i) luminal-like epithelial cells isolated from human post-weaning

fluid (Russo et al., 1975) ii) in the apical portion of human mammary gland alveolar cells in the secretory phase of the menstrual cycle (Nazario et al., 1994). The luminal-like epithelial cells of post-weaning fluid were cultured into confluent interdigitated monolayers without EGF as the MCF10A cells in this report. The interdigitated cells were proposed to line mammary ducts and be removed from the gland during involution (Russo et al., 1975). As discussed earlier in Chapter 5, the interdigitated state confers extra adhesion between cells. Counter-intuitively one would deduce that *in vivo* these cells would be less likely to detach and be removed from the ducts. However, it is possible that digits reverse in the ductal lumen due to the high concentration of EGF (>100ng/ml) found in mammary ductal lumens (Carpenter and Cohen 1979; Roepstorff et al., 2008). These detached epithelial cells could then re-form digits when cultured into monolayers without EGF. In an ultrastructure study of human non-malignant fibroadenomatous tissue, the authors reported interdigitations in the apical portion of the mammary alveolar cells especially in the secretory phase of the menstrual cycle accompanied by desmosomal junctions (Nazario et al., 1994).

Ultrastructural studies of organotypic culture of primary pubertal mouse ductal epithelial cells on Matrigel revealed transient interdigitated 'interior' cells between the lumen and basement membrane upon FGF2 stimulation (Ewald et al., 2012). Using time-lapse microscopy, the authors elegantly demonstrated that these digits only appear transiently during the active branching process by which multilayer epithelia transition into simple bilayered epithelia lining. Cell protrusions allow the cells to move and polarize within the confines of the lumen and basement membrane without dispersion into the extracellular matrix (ECM). It may be possible that the non-branching MCF10A acini do not have cells that interdigitate within the spheroids. Alternatively, Brooks and colleagues reported well-organised duct-like structures when MCF10A cells were cultured without EGF in collagen as opposed to single-cell radiation from clumps when cultured with EGF (Soule et al., 1990). Although they did not report seeing interdigitations, it would be of interest to visualise MCF10A cells in this context as it was previously viewed at low magnification. Furthermore, collagen culture not only facilitates organisation of mammary acini but also monolayers and ductal structures, providing a more relevant surrogate for *in vivo* mammary morphogenetic processes (Dhimolea et al., 2010).

Interestingly, Holm et al. (1993) noted that a non-tumorigenic HMT 3522 cell line form interdigitations remarkably similar to those described here, in medium without EGF. I have recapitulated and reversed this phenotype in these cells. The tonic application of EGF in culture may be similar to the activation of the EGFR observed during the pubertal mammary gland development and paradoxically also in mammary tumours in which EGFR is overexpressed (Yarden and Pines, 2012; Watson and Khaled., 2008). During pubertal development, collective migration may facilitate mammary gland branching (Gjorevski and Nelson, 2011). Prominent interdigitated structures have been observed in intraductal carcinomas, suggesting the possible subversion of this developmental process in cancer (Goldenberg et al., 1969). Therefore, the inability of isogenic ΔE746-A750 cells expressing constitutively active EGFR to interdigitate seen here may lead to enhanced capabilities to detach from monolayers and contribute to metastatic cell migration.

### *6.3 Physiological relevance of interdigitations in non-tumorigenic systems*

The phenomena of interdigitations in MCF10A monolayers provides a simple *in vitro* system to examine a phenomenon that has been described in stratified animal tissues (Introduction: 1.5). Digits that resist shear stresses may reflect a key aspect of its physiological function. The molecular mechanisms governing interdigitations *in vivo* remains obscure although interdigitations are increasingly reported both *in vivo* and in laboratory culture. Other reports of interdigitations very rarely indicate the need or specificity of growth factor signalling (Baluk et al., 2007; Hoelzle and Svitkina, 2012; Russo et al., 1975). Rather, they have been reported in these non-malignant systems as basal phenomena regardless of growth factor stimulation or withdrawal. Interestingly, the interdigitated endothelial cells lining the initial lymphatic vessels function to allow the flow of fluids and cells in developmental and immunogenic instances (Baluk et al., 2007; Yao and McDonald, 2014). This may provide a hint as to the plausible role of interdigitated cells in the ductal structures of mammary gland that have to withstand shear forces of fluid flow and transport of milk proteins necessary during lactation (Gjorevski and Nelson, 2011).

### *6.4 Interdigitated phenotype as an in vitro screening tool*

The integration of phenotypic screens and systematic pathway profiling has been increasingly used to aid the concurrent discovery of disease biomarkers and also as pre-clinical drug evaluation in biological contexts (Carragher et al., 2012). With this multi-dimensional approach, it is now possible to pre-empt drug resistance and

allow a more robust pre-clinical testing to maximise the chances of a developmental drug to benefit patients in the most cost effective manner. A distinguishing feature of the system described here is that interdigitation can be invoked within a pre-formed coherent monolayer. Validation studies of EGFR small molecule inhibitors are currently performed in growth or invasion assays where cells are subconfluent or dispersed. This does not reflect the complex multi-layered cells found in tissues (Ewald et al., 2012). Selected inhibitors once developed often fail in the penultimate or final clinical testing stages, with high attrition rates incurring huge financial losses to the parties involved (Carragher et al., 2012). Therefore, this *in vitro* system may be advantageous to screen for the efficacy of EGFR inhibitors in a more relevant *in vitro* context, ie cell confluency mimicking the multi-layer epithelia strata *in vivo*.

Collectively, the tonic suppression of interdigitation by EGF and the rapid dissolution of established interdigitations by acute addition represent distinct pathways. Previously, other groups have used EGF induced migratory ability of MCF10A cells as an assay to undertake systematic large scale wound healing, proteomic and transcriptomic screens (Simpson et al., 2008; Tarcic et al., 2012). Inversely, systematic proteomic and transcriptomic profiling of the reduced migration of these interdigitated cells when cultured without EGF may offer mechanistic insights in a non-tumorigenic setting. EGF associated components can be validated and cross-referenced to the targets found previously and to allow identification of therapeutic targets in the context of cancer. With the complexity of signalling networks, it is unlikely that one protein downstream of EGFR would dominate this phenotype. Rather, like signal transduction cascades, it will be possible to identify and manipulate clusters of protein or pathway hubs that may be implicated in this EGF defined membrane-remodelling phenomenon.

### *6.5 Mammary morphogenesis linked to mammary oncogenesis*

This remarkable plasticity of mammary boundaries is reserved in non-tumorigenic mammary epithelial cells. The MCF10A and HMT 3522 S1 cells used are distinct from the commonly used breast cancer cells lines, which form smooth boundaries in cultures without EGF (eg. MCF7). Most such cell lines are maintained in simpler media without EGF supplementation. The accompanying physical manifestation of the digits is the shackling of the cells to a fixed position within a confluent monolayer. Tension generated from cell-cell adhesion between mammary luminal epithelial cells has been shown to maintain cell polarisation and facilitate collective cell migration (Ewald et al., 2012; Fata et al., 2007; Gjorevski and Nelson, 2011).

This is important to sort luminal epithelial cells into either the luminal ducts or terminal end buds for correct mammary patterning during pubertal development (Lanigan et al., 2007). One may envision that this also have implications in the initiation, metastasis and invasion of cancers.

### *6.6 Future perspectives*

We have established here an *in vitro* cell system that recapitulates cellular interdigitation in adult non-malignant mammary epithelial cells. This system provides a simple setting to allow the systematic analysis of molecular mechanisms related to this phenotype and also the downstream migration capability in response to prolonged EGF withdrawal. Analyses of the transcriptomic and proteomic profiles associated to this reversible phenomenon may provide the first step to elucidate this tightly regulated yet dynamic restructuring of the cell cytoskeleton. Identification of the clusters of actin regulating proteins and signalling hubs associated to interdigitations can be extrapolated to genetically engineered isogenic cells with cancer-relevant mutations to validate their function and relevance in cancer.

# References

**References**

Abd El-Rehim, D. M., et al. (2004). "Expression and co-expression of the members of the epidermal growth factor receptor (EGFR) family in invasive breast carcinoma." British Journal of Cancer **91**(8): 1532-1542.

Abercrom.M, et al. (1970). "Locomotion of fibroblasts in culture. Ii2. Ruffling." Experimental Cell Research **60**(3): 437-&.

Akbar, H., et al. (2006). "Rational design and applications of a Rac GTPase-specific small molecule inhibitor." Methods in Enzymology, Vol 406, Regulators and Effectors of Small Gtpases: Rho Family **406**: 554-565.

Amit, I., et al. (2007). "A module of negative feedback regulators defines growth factor signaling." Nature Genetics **39**(4): 503-512.

Aoyama, Y. and Y. Kitajima (1999). "Pemphigus vulgaris IgG causes a rapid depletion of desmoglein 3 (Dsg3) from the Triton X-100 soluble pools, leading to the formation of Dsg3-depleted desmosomes in a human squamous carcinoma cell line, DJM-1 cells." Journal of Investigative Dermatology **112**(1): 67-71.

Avraham, R. and Y. Yarden (2011). "Feedback regulation of EGFR signalling: decision making by early and delayed loops." Nature Reviews Molecular Cell Biology **12**(2): 104-117.

Bailly, M., et al. (1998). "Chemoattractant-induced lamellipod extension." Microscopy Research and Technique **43**(5): 433-443.

Bailly, M., et al. (2000). "Epidermal growth factor receptor distribution during chemotactic responses." Molecular Biology of the Cell **11**(11): 3873-3883.

Baluk, P., et al. (2007). "Functionally specialized junctions between endothelial cells of lymphatic vessels." Journal of Experimental Medicine **204**(10): 2349-2362.

Birchmeier, C., et al. (2003). "Met, metastasis, motility and more." Nature Reviews Molecular Cell Biology **4**(12): 915-925.

Borisov, N., et al. (2009). "Systems-level interactions between insulin-EGF networks amplify mitogenic signaling." Molecular Systems Biology **5**.

Boureux, A., et al. (2007). "Evolution of the Rho family of Ras-like GTPases in eukaryotes." Molecular Biology and Evolution **24**(1): 203-216.

Boyer, A. P. (2008). Effects of HER-2 over expression in human mammary epithelial cells: evidence of altered HER-2 signaling and crosstalk between insulin and EGF signaling Wayne State University. [Thesis]

Briand, P. and A. E. Lykkesfeldt (2001). "An in vitro model of human breast carcinogenesis: epigenetic aspects." Breast Cancer Research and Treatment **65**(2).

Briand, P., et al. (1996). "Trisomy 7p and malignant transformation of human breast epithelial cells following epidermal growth factor withdrawal." Cancer Research **56**(9): 2039-2044.

Briand, P., et al. (1987). "A NEW DIPLOID NONTUMORIGENIC HUMAN-BREAST EPITHELIAL-CELL LINE ISOLATED AND PROPAGATED IN CHEMICALLY DEFINED MEDIUM." In Vitro Cellular & Developmental Biology **23**(3): 181-188.

Bryant, D. M. and J. L. Stow (2004). "The ins and outs of E-cadherin trafficking." Trends in Cell Biology **14**(8): 427-434.

Campaner, S. and B. Amati (2012). "Two sides of the Myc-induced DNA damage response: from tumor suppression to tumor maintenance." Cell Division **7**.

Campbell, J. J. and C. J. Watson (2009). "Three-dimensional culture models of mammary gland." Organogenesis **5**(2): 43-49.

Carpenter, G. and S. Cohen (1979). "Epidermal growth-factor." Annual Review of Biochemistry **48**: 193-216.

Carpenter, G., et al. (1978). "Epidermal growth-factor stimulates phosphorylation in membrane preparations invitro." Nature **276**(5686): 409-410.

Carpenter, G., et al. (1975). "Characterization of binding of i-125-labeled epidermal growth-factor to human fibroblasts." Journal of Biological Chemistry **250**(11): 4297-4304.

Carragher, N. O., et al. (2012). "Combining imaging and pathway profiling: an alternative approach to cancer drug discovery." Drug Discovery Today **17**(5-6): 203-214.

Cayrol, C., et al. (2007). "The THAP-zinc finger protein THAP1 regulates endothelial cell proliferation through modulation of pRB/E2F cell-cycle target genes." Blood **109**(2): 584-594.

Chang, L. and R. D. Goldman (2004). "Intermediate filaments mediate cytoskeletal crosstalk." Nature Reviews Molecular Cell Biology **5**(8): 601-613.

Charafe-Jauffret, E., et al. (2006). "Gene expression profiling of breast cell lines identifies potential new basal markers." Oncogene **25**(15).

Charras, G. and E. Paluch (2008). "Blebs lead the way: how to migrate without lamellipodia." Nature Reviews Molecular Cell Biology **9**(9): 730-736.

Chinkers, M., et al. (1981). "Rapid rounding of human epidermoid carcinoma-cells a-431 induced by epidermal growth-factor." Journal of Cell Biology **88**(2): 422-429.

Ciardiello, F., et al. (1990). "Transforming growth factor-alpha expression is enhanced in human mammary epithelial-cells transformed by an activated c-ha-ras protooncogene but not by the c-neu protooncogene, and overexpression of the transforming growth factor-alpha complementary-dna leads to transformation." Cell Growth & Differentiation **1**(9): 407-420.

Citri, A. and Y. Yarden (2006). "EGF-ERBB signalling: towards the systems level." Nature Reviews Molecular Cell Biology **7**(7): 505-516.

Cohen, M. H., et al. (2003). "FDA drug approval summary: Gefitinib (ZD1839) (Iressa (R)) tablets." Oncologist **8**(4): 303-306.

Cohen, S. (1962). "Isolation of a mouse submaxillary gland protein accelerating incisor eruption and eyelid opening in new-born animal." Journal of Biological Chemistry **237**(5): 1555-&.

Cohen, S. and R. Levimontalcini (1957). "Purification and properties of a nerve growth-promoting factor isolated from mouse sarcoma-180." Cancer Research **17**(1): 15-&.

Cole, N. B., et al. (1996). "Golgi dispersal during microtubule disruption: Regeneration of Golgi stacks at peripheral endoplasmic reticulum exit sites." Molecular Biology of the Cell **7**(4): 631-650.

Coleman, S. and C. W. Daniel (1990). "Inhibition of mouse mammary ductal morphogenesis and down-regulation of the egf receptor by epidermal growth-factor." Developmental Biology **137**(2): 425-433.

Coleman, S., et al. (1988). "Ductal morphogenesis in the mouse mammary-gland - evidence supporting a role for epidermal growth-factor." Developmental Biology **127**(2): 304-315.

Cook, D. R., et al. (2014). "Rho guanine nucleotide exchange factors: regulators of Rho GTPase activity in development and disease." Oncogene **33**(31): 4021-4035.

Cowell, J. K., et al. (2005). "Molecular characterization of the t(3;9) associated with immortalization in the MCF10A cell line." Cancer Genetics and Cytogenetics **163**(1): 23-29.

Crouch, M. F., et al. (2000). "Insulin induces EGF receptor clustering and potentiates EGF-stimulated DNA synthesis in Swiss 3T3 cells: A mechanism for costimulation in mitogenic synergy." Molecular Biology of the Cell **11**: 386A-386A.

Debnath, J. and J. S. Brugge (2005). "Modelling glandular epithelial cancers in three-dimensional cultures." Nature Reviews Cancer **5**(9): 675-688.

Debnath, J., et al. (2003). "Morphogenesis and oncogenesis of MCF-10A mammary epithelial acini grown in three-dimensional basement membrane cultures." Methods **30**(3): 256-268.

Deneka M., P.-M. A., Byland R., Ruiz-Mateos E. and Marsh M. (2007). "In Macrophages, HIV-1 assembles into an intracellular plasma membrane domain containing the tetraspanins CD81, CD9 and CD53." The Journal of Cell Biology **177**(2): 329-341.

Denhartigh, J. C., et al. (1992). "The egf receptor is an actin-binding protein." Journal of Cell Biology **119**(2): 349-355.

Dhimolea, E., et al. (2010). "The role of collagen reorganization on mammary epithelial morphogenesis in a 3D culture model." Biomaterials **31**(13): 3622-3630.

Di Modugno, F., et al. (2004). "Human mena protein, a serex-defined antigen overexpressed in breast cancer eliciting both humoral and CD8(+) T-cell immune response." International Journal of Cancer **109**(6): 909-918.

Di Nicolantonio, F., et al. (2008). "Replacement of normal with mutant alleles in the genome of normal human cells unveils mutation-specific drug responses." Proceedings of the National Academy of Sciences of the United States of America **105**(52): 20864-20869.

DiAugustine, R. P., et al. (1997). "EGF-Related Peptides and Their Receptors in Mammary Gland Development." Journal of Mammary Gland Biology and Neoplasia **2**(2): 109-117.

Duan, L., et al. (2011). "Negative Regulation of EGFR-Vav2 Signaling Axis by Cbl Ubiquitin Ligase Controls EGF Receptor-mediated Epithelial Cell Adherens Junction Dynamics and Cell Migration." Journal of Biological Chemistry **286**(1): 620-633.

Dubash, A. D. and K. J. Green (2011). "Desmosomes." Current Biology **21**(14): R529-R531.

Dumontier, M., et al. (2000). "Rac1 GTPases control filopodia formation, cell motility, endocytosis, cytokinesis and development in Dictyostelium." Journal of Cell Science **113**(12): 2253-2265.

Eden, E. R., et al. (2009). "Down-regulation of epidermal growth factor receptor signalling within multivesicular bodies." Biochemical Society Transactions **37**: 173-177.

Engelman, J. A. (2009). "Targeting PI3K signalling in cancer: opportunities, challenges and limitations." Nature Reviews Cancer **9**(8): 550-562.

Ethier, S. P., et al. (1993). "Differential isolation of normal luminal mammary epithelial-cells and breast-cancer cells from primary and metastatic sites using selective media." Cancer Research **53**(3): 627-635.

Even-Ram, S., et al. (2007). "Myosin IIA regulates cell motility and actomyosin microtubule crosstalk." Nature Cell Biology **9**(3): 299-U104.

Even-Ram, S., et al. (2007). "Myosin IIA regulates cell motility and actomyosin microtubule crosstalk." Nature Cell Biology **9**(3): 299-U104.

Ewald, A. J., et al. (2012). "Mammary collective cell migration involves transient loss of epithelial features and individual cell migration within the epithelium." Journal of Cell Science **125**(11): 2638-2654.

Fasano, O., et al. (1984). "New human transforming genes detected by a tumorigenicity assay." Molecular and Cellular Biology **4**(9): 1695-1705.

Fata, J. E., et al. (2007). "The MAPK(ERK-1,2) pathway integrates distinct and antagonistic signals from TGF alpha and FGF7 in morphogenesis of mouse mammary epithelium." Developmental Biology **306**(1): 193-207.

Fehon, R. G., et al. (2010). "Organizing the cell cortex: the role of ERM proteins." Nature Reviews Molecular Cell Biology **11**(4): 276-287.

Fletcher, D. A. and D. Mullins (2010). "Cell mechanics and the cytoskeleton." Nature **463**(7280): 485-492.

Franke, W. W. (2009). "Discovering the Molecular Components of Intercellular Junctions-A Historical View." Cold Spring Harbor Perspectives in Biology **1**(3).

Friedl, P. and D. Gilmour (2009). "Collective cell migration in morphogenesis, regeneration and cancer." Nature Reviews Molecular Cell Biology **10**(7): 445-457.

Fu, Z. and D. J. Tindall (2008). "FOXOs, cancer and regulation of apoptosis." Oncogene **27**(16): 2312-2319.

Fuchs, E. and S. Raghavan (2002). "Getting under the skin of epidermal morphogenesis." Nature Reviews Genetics **3**(3): 199-209.

Fukuoka, M., et al. (2003). "Multi-institutional randomized phase II trial of gefitinib for previously treated patients with advanced non-small-cell lung cancer." Journal of Clinical Oncology **21**(12): 2237-2246.

Gaffney, E. V. and D. Pigott (1978). "Hydrocortisone stimulation of human mammary epithelial-cells." In Vitro-Journal of the Tissue Culture Association **14**(7): 621-624.

Gao, Y., et al. (2004). "Rational design and characterization of a Rac GTPase-specific small molecule inhibitor." Proceedings of the National Academy of Sciences of the United States of America **101**(20): 7618-7623.

Garrod, D. (2010). "Desmosomes in vivo." Dermatology research and practice **2010**.

Gill, G. N., et al. (1984). "Monoclonal anti-epidermal growth-factor receptor antibodies which are inhibitors of epidermal growth-factor binding and antagonists of epidermal growth factor-stimulated tyrosine protein-kinase activity." Journal of Biological Chemistry **259**(12): 7755-7760.

Gjorevski, N. and C. M. Nelson (2011). "Integrated morphodynamic signalling of the mammary gland." Nature Reviews Molecular Cell Biology **12**(9): 581-593.

Gold, V., et al. (1987). "Compendium of chemical terminology iupac international union of pure and applied chemistry recommendations." Gold, V., K. L. Loening, a. D. Mcnaught and P. Sehmi. Compendium of Chemical Terminology: Iupac (International Union of Pure and Applied Chemistry) Recommendations. Viii+456p. Blackwell Scientific Publications Inc.: Oxford, England, Uk; Palo Alto, California, USA. Illus: VIII+456P-VIII+456P.

Goldenbe.Ve, et al. (1969). "Comparative ultrastructure of atypical ductal hyperplasia, intraductal carcinoma, and infiltrating ductal carcinoma of breast." Cancer **24**(6): 1152-&.

Green, K. J. and C. A. Gaudry (2000). "Are desmosomes more than tethers for intermediate filaments?" Nature Reviews Molecular Cell Biology **1**(3): 208-216.

Green, K. J., et al. (2010). "Intercellular junction assembly, dynamics, and homeostasis." Cold Spring Harbor perspectives in biology **2**(2): a000125.

Gschwind, A., et al. (2004). "Timeline - The discovery of receptor tyrosine kinases: targets for cancer therapy." Nature Reviews Cancer **4**(5): 361-370.

Gumbiner, B., et al. (1988). "The role of the cell-adhesion molecule uvomorulin in the formation and maintenance of the epithelial junctional complex." Journal of Cell Biology **107**(4): 1575-1587.

Guo, L., et al. (2003). "Studies of ligand-induced site-specific phosphorylation of epidermal growth factor receptor." Journal of the American Society for Mass Spectrometry **14**(9): 1022-1031.

Gupton, S. L. and F. B. Gertler (2007). "Filopodia: the fingers that do the walking." Science's STKE : signal transduction knowledge environment **2007**(400): re5-re5.

Hammond, D. E., et al. (2010). "Quantitative Analysis of HGF and EGF-Dependent Phosphotyrosine Signaling Networks." Journal of Proteome Research **9**(5): 2734-2742.

Hayashi, T. and S. Sakamoto (1988). "Radioimmunoassay of human epidermal growth-factor - hegf levels in human-body fluids." Journal of Pharmacobio-Dynamics **11**(3): 146-151.

Hendler, F. J. and B. W. Ozanne (1984). "Human squamous-cell lung cancers express increased epidermal growth-factor receptors." Journal of Clinical Investigation **74**(2): 647-651.

Hickman, D., et al. (2004). "Estimation of serum-free 50-percent inhibitory concentrations for human immunodeficiency virus protease inhibitors lopinavir and ritonavir." Antimicrobial Agents and Chemotherapy **48**(8): 2911-2917.

Hirsch, D. S., et al. (2006). "Growth and motility inhibition of breast cancer cells by epidermal growth factor receptor degradation is correlated with inactivation of Cdc42." Cancer Research **66**(7): 3523-3530.

Hoelzle, M. K. and T. Svitkina (2012). "The cytoskeletal mechanisms of cell-cell junction formation in endothelial cells." Molecular Biology of the Cell **23**(2): 310-323.

Holm, P. K., et al. (1993). "Endocytosis of desmosomal plaques depends on intact actin-filaments and leads to a nondegradative compartment." European Journal of Cell Biology **62**(2): 362-371.

Huen, A. C., et al. (2002). "Intermediate filament-membrane attachments function synergistically with actin-dependent contacts to regulate intercellular adhesive strength." Journal of Cell Biology **159**(6): 1005-1017.

Hunter, T. and B. M. Sefton (1980). "Transforming gene-product of rous-sarcoma virus phosphorylates tyrosine." Proceedings of the National Academy of Sciences of the United States of America-Biological Sciences **77**(3): 1311-1315.

Hyzinski-Garcia, M. C., et al. (2011). "Hypo-osmotic swelling modifies glutamate-glutamine cycle in the cerebral cortex and in astrocyte cultures." Journal of Neurochemistry **118**(1): 140-152.

Imai, K. and A. Takaoka (2006). "Comparing antibody and small-molecule therapies for cancer." Nature Reviews Cancer **6**(9): 714-727.

Isakoff, S. J., et al. (2005). "Breast cancer-associated PIK3CA mutations are oncogenic in mammary epithelial cells." Cancer Research **65**(23): 10992-11000.

Ishii, K., et al. (2005). "In vitro keratinocyte dissociation assay for evaluation of the pathogenicity of anti-desmoglein 3 IgG autoantibodies in pemphigus vulgaris." Journal of Investigative Dermatology **124**(5): 939-946.

J, P. (2005). The cadherin superfamily, Wormbook.

Jain, A., et al. (2005). "Epithelial membrane protein-1 is a biomarker of gefitinib resistance." Proceedings of the National Academy of Sciences of the United States of America **102**(33): 11858-11863.

Joslin, E. J., et al. (2007). "EGF-receptor-mediated mammary epithelial cell migration is driven by sustained ERK signaling from autocrine stimulation." Journal of Cell Science **120**(20): 3688-3699.

Kadmiel, M. and J. A. Cidlowski (2013). "Glucocorticoid receptor signaling in health and disease." Trends in Pharmacological Sciences **34**(9): 518-530.

Kadota, M., et al. (2010). "Delineating Genetic Alterations for Tumor Progression in the MCF10A Series of Breast Cancer Cell Lines." Plos One **5**(2).

Kaelin, W. G. (2005). "The concept of synthetic lethality in the context of anticancer therapy." Nature Reviews Cancer **5**(9): 689-698.

Kalluri, R. and R. A. Weinberg (2009). "The basics of epithelial-mesenchymal transition." Journal of Clinical Investigation **119**(6): 1420-1428.

Kang, S. Y., et al. (2005). "Phosphatidylinositol 3-kinase mutations identified in human cancer are oncogenic." Proceedings of the National Academy of Sciences of the United States of America **102**(3): 802-807.

Karakas, B., et al. (2006). "Mutation of the PIK3CA oncogene in human cancers." British Journal of Cancer **94**(4): 455-459.

Katz, M., et al. (2007). "Regulation of MAPKs by growth factors and receptor tyrosine kinases." Biochimica Et Biophysica Acta-Molecular Cell Research **1773**(8): 1161-1176.

Kawamoto, T., et al. (1983). "Growth-stimulation of a431 cells by epidermal growth-factor - identification of high-affinity receptors for epidermal growth-factor by an anti-receptor monoclonal-antibody." Proceedings of the National Academy of Sciences of the United States of America-Biological Sciences **80**(5): 1337-1341.

Kenny, P. A., et al. (2007). "The morphologies of breast cancer cell lines in three-dimensional assays correlate with their profiles of gene expression." Molecular Oncology **1**(1): 84-96.

Kim, J.-H. and A. R. Asthagiri (2011). "Matrix stiffening sensitizes epithelial cells to EGF and enables the loss of contact inhibition of proliferation." Journal of Cell Science **124**(8): 1280-1287.

Kimura, T. E., et al. (2007). "Calcium-independent desmosomes of keratinocytes are hyper-adhesive." Journal of Investigative Dermatology **127**(4): 775-781.

King, N., et al. (2008). "The genome of the choanoflagellate Monosiga brevicollis and the origin of metazoans." Nature **451**(7180): 783-788.

Klessner, J. L., et al. (2009). "EGFR and ADAMs Cooperate to Regulate Shedding and Endocytic Trafficking of the Desmosomal Cadherin Desmoglein 2." Molecular Biology of the Cell **20**(1): 328-337.

Klus, G. T., et al. (2001). "Down-regulation of the desmosomal cadherin desmocollin 3 in human breast cancer." International Journal of Oncology **19**(1): 169-174.

Kobielak, A. and Fuchs, E. (2004) “α-Catenin: At the junction of intercellular adhesion and actin dynamics” Nature Reviews **5**: 614-625.

Kumar, A., et al. (2008). "Structure and clinical relevance of the epidermal growth factor receptor in human cancer." Journal of Clinical Oncology **26**(10): 1742-1751.

Lanigan, F., et al. (2007). "Molecular links between mammary gland development and breast cancer." Cellular and molecular life sciences : CMLS **64**(24): 3159-3184.

Lax, I., et al. (1988). "Chicken epidermal growth-factor (egf) receptor - cdna cloning, expression in mouse cells, and differential binding of egf and transforming growth factor-alpha." Molecular and Cellular Biology **8**(5): 1970-1978.

Lemmon, M. A. and J. Schlessinger (2010). "Cell Signaling by Receptor Tyrosine Kinases." Cell **141**(7): 1117-1134.

Leroy, C., et al. (2006). "HGF/SF regulates expression of apoptotic genes in MCF-10A human mammary epithelial cells." Signal Transduction Pathways, Pt a: Apoptotic and Extracellular Signaling **1090**: 188-202.

Leslie, N. R. and V. G. Brunton (2013). "Where Is PTEN?" Science **341**(6144): 355-356.

Levimontalcini, R. (1952). "Effects of mouse tumor transplantation on the nervous system." Annals of the New York Academy of Sciences **55**(2): 330-342.

Levimontalcini, R. and S. Cohen (1960). "Effects of the extract of the mouse submaxillary salivary glands on the sympathetic system of mammals." Annals of the New York Academy of Sciences **85**(1): 324-341.

Levkowitz, G., et al. (1999). "Ubiquitin ligase activity and tyrosine phosphorylation underlie suppression of growth factor signaling by c-Cbl/Sli-1." Molecular Cell **4**(6): 1029-1040.

Limouze, J., et al. (2004). "Specificity of blebbistatin, an inhibitor of myosin II." Journal of Muscle Research and Cell Motility **25**(4-5): 337-341.

Lorch, J. H., et al. (2004). "Epidermal growth factor receptor inhibition promotes desmosome assembly and strengthens intercellular adhesion in squamous cell carcinoma cells." Journal of Biological Chemistry **279**(35).

Machesky, L. M. and A. Li (2010). "Fascin: Invasive filopodia promoting metastasis." Communicative & integrative biology **3**(3): 263-270.

MacNeill, S. A. (2010). "Structure and function of the GINS complex, a key component of the eukaryotic replisome." Biochemical Journal **425**: 489-500.

Mader, C. C., et al. (2011). "An EGFR-Src-Arg-Cortactin Pathway Mediates Functional Maturation of Invadopodia and Breast Cancer Cell Invasion." Cancer Research **71**(5): 1730-1741.

Masuda, H., et al. (2012). "Role of epidermal growth factor receptor in breast cancer." Breast Cancer Research and Treatment **136**(2): 331-345.

Mattey, D. L. and D. R. Garrod (1986). "Splitting and internalization of the desmosomes of cultured kidney epithelial-cells by reduction in calcium-concentration." Journal of Cell Science **85**: 113-124.

Maxfield, F. R. and T. E. McGraw (2004). "Endocytic recycling." Nature Reviews Molecular Cell Biology **5**(2): 121-132.

McGrath, C. M. and H. D. Soule (1983). "Renewal inhibition of human mammary cell-growth invitro - cortisol and the recruitment of cells to terminal differentiation." Journal of Cellular Physiology **116**(3): 385-396.

Medalia, O., et al. (2007). "Organization of actin networks in intact filopodia." Current Biology **17**(1): 79-84.

Meyer, D. S., et al. (2013). "Expression of PIK3CA mutant E545K in the mammary gland induces heterogeneous tumors but is less potent than mutant H1047R." Oncogenesis **2**: e74-e74.

Montalvo-Ortiz, B. L., et al. (2012). "Characterization of EHop-016, Novel Small Molecule Inhibitor of Rac GTPase." Journal of Biological Chemistry **287**(16): 13228-13238.

Mosesson, Y., et al. (2008). "Derailed endocytosis: an emerging feature of cancer." Nature Reviews Cancer **8**(11): 835-850.

Moshfegh, Y., et al. (2014). "A Trio-Rac1-Pak1 signalling axis drives invadopodia disassembly." Nature Cell Biology **16**(6): 571-+.

Moskal, T. L., et al. (1995). "Serum levels of transforming growth-factor-alpha in gastrointestinal cancer-patients." Cancer Epidemiology Biomarkers & Prevention **4**(2): 127-131.

Motley, A., et al. (2003). "Clathrin-mediated endocytosis in AP-2-depleted cells." Journal of Cell Biology **162**(5): 909-918.

Mundel, P. and W. Kriz (1995). "Structure and function of podocytes: An update." Anatomy and Embryology **192**(5): 385-397.

Nazario, A. C., et al. (1994). "Morphological and ultrastructural aspects of the cyclical changes of human mammary gland during the menstrual cycle." Sao Paulo medical journal = Revista paulista de medicina **112**(2): 543-547.

Nedvetsky, P. I., et al. (2012). "Cyclic AMP regulates formation of mammary epithelial acini in vitro." Molecular Biology of the Cell **23**(15): 2973-2981.

Nekrasova, O. and K. J. Green (2013). "Desmosome assembly and dynamics." Trends in Cell Biology **23**(11): 537-546.

Nelson, C. M., et al. (2006). "Tissue geometry determines sites of mammary branching morphogenesis in organotypic cultures." Science **314**(5797): 298-300.

Neve, R. M., et al. (2006). "A collection of breast cancer cell lines for the study of functionally distinct cancer subtypes." Cancer Cell **10**(6): 515-527.

Nijman, S. M. B. (2011). "Synthetic lethality: General principles, utility and detection using genetic screens in human cells." Febs Letters **585**(1): 1-6.

Nisenholz N, R. K., Dang Q, Chen H, Kemkemer R, Krishnan R, Zemel A (2014). "Active mechanics and dynamics of cell spreading on elastic substrates." Soft Matter **Advance Article**.

Nyati, M. K., et al. (2006). "Integration of EGFR inhibitors with radiochemotherapy." Nature Reviews Cancer **6**(11): 876-885.

Okamoto, S. and T. Oka (1984). "Evidence for physiological-function of epidermal growth-factor - pregestational sialoadenectomy of mice decreases milk-production and increases offspring mortality during lactation period." Proceedings of the National Academy of Sciences of the United States of America-Biological Sciences **81**(19): 6059-6063.

Olayioye, M. A., et al. (2000). "The ErbB signaling network: receptor heterodimerization in development and cancer." Embo Journal **19**(13): 3159-3167.

Oshiro, M. M., et al. (2005). "Epigenetic silencing of DSC3 is a common event in human breast cancer." Breast Cancer Research **7**(5): R669-R680.

Park, S., et al. (2004). "TCDD causes suppression of growth and differentiation of MCF10A, human mammary epithelial cells by interfering with their insulin receptor signaling through c-Src kinase and ERK activation." Journal of Biochemical and Molecular Toxicology **18**(6).

Parton, R. G. and K. Simons (2007). "The multiple faces of caveolae." Nature Reviews Molecular Cell Biology **8**(3): 185-194.

Pasdar, M. and W. J. Nelson (1988). "Kinetics of desmosome assembly in madin-darby canine kidney epithelial-cells - temporal and spatial regulation of desmoplakin organization and stabilization upon cell cell contact .2. Morphological analysis." Journal of Cell Biology **106**(3): 687-695.

Pauley, R. J., et al. (1993). "The MCF10 family of spontaneously immortalized human breast epithelial cell lines: models of neoplastic progression." European journal of cancer prevention : the official journal of the European Cancer Prevention Organisation (ECP) 2 Suppl 3: 67-76.

Pellegrin, S. a. M., Harry. (2008). "Rho GTPase Activation Assays." Current Protocols in Cell Biology Supplement 38: 1-19.

Perrais, M., et al. (2007). "E-cadherin homophilic ligation inhibits cell growth and epidermal growth factor receptor signaling independently of other cell interactions." Molecular Biology of the Cell **18**(6).

Pol, A., et al. (2005). "Cholesterol and fatty acids regulate dynamic caveolin trafficking through the golgi complex and between the cell surface and lipid bodies." Molecular Biology of the Cell **16**(4): 2091-2105.

Prahallad, A., et al. (2012). "Unresponsiveness of colon cancer to BRAF(V600E) inhibition through feedback activation of EGFR." Nature **483**(7387): 100-U146.

Rao, J. Y., et al. (1993). "Alterations in phenotypic biochemical markers in bladder epithelium during tumorigenesis." Proceedings of the National Academy of Sciences of the United States of America **90**(17): 8287-8291.

Rennison, M. E., et al. (1992). "Investigation of the role of microtubules in protein secretion from lactating mouse mammary epithelial-cells." Journal of Cell Science **102**: 239-247.

Ridley, A. J. (2006). "Rho GTPases and actin dynamics in membrane protrusions and vesicle trafficking." Trends in Cell Biology **16**(10): 522-529.

Ridley, A. J. (2011). "Life at the Leading Edge." Cell **145**(7): 1012-1022.

Ridley, A. J. and A. Hall (1992). "The small gtp-binding protein rho regulates the assembly of focal adhesions and actin stress fibers in response to growth-factors." Cell **70**(3): 389-399.

Riedel, H., et al. (1986). "A chimeric receptor allows insulin to stimulate tyrosine kinase-activity of epidermal growth-factor receptor." Nature **324**(6092): 68-70.

Rigby Sue , G. J., Foster Rebecca ,Mead Suzanne ,Chen Zhiqiang, Howes Rob, Torrance Chris and Grimshaw Kyla (2010). The use of PI3K isogenic cell lines in conditions that model the tumor microenvironment provides a relevant system in which to test PI3K inhibitor profiles, Horizon Discovery Ltd. [Poster]

Ripple, M. O., et al. (2005). "Inhibition of either phosphatidylinositol 3-kinase/Akt or the Mitogen/Extracellular-regulated kinase, MEK/ERK, signaling pathways suppress growth of breast cancer cell lines, but MEK/ERK signaling is critical for cell survival." Breast Cancer Research and Treatment **93**(2): 177-188.

Roepstorff, K., et al. (2009). "Differential Effects of EGFR Ligands on Endocytic Sorting of the Receptor." Traffic **10**(8): 1115-1127.

Roepstorff, K., et al. (2008). "Endocytic downregulation of ErbB receptors: mechanisms and relevance in cancer." Histochemistry and Cell Biology **129**(5): 563-578.

Roskoski, R., Jr. (2014). "The ErbB/HER family of protein-tyrosine kinases and cancer." Pharmacological Research **79**: 34-74.

Russo, J., et al. (1975). "Ultrastructural study of normal human mammary epithelial-cells in culture." American Journal of Anatomy **142**(2): 221-231.

Sahai, E. and C. J. Marshall (2002). "RHO-GTPases and cancer." Nature Reviews Cancer **2**(2): 133-+.

Sato, J. D., et al. (1983). "Biological effects in vitro of monoclonal antibodies to human epidermal growth factor receptors." Molecular biology & medicine **1**(5): 511-529.

Schlessinger, J. (1988). "Signal transduction by allosteric receptor oligomerization." Trends in Biochemical Sciences **13**(11): 443-447.

Schmidt, A., et al. (1998). "Signaling to the actin cytoskeleton." Annual Review of Cell and Developmental Biology **14**: 305-338.

Schneider, M. R. and E. Wolf (2009). "The Epidermal Growth Factor Receptor Ligands at a Glance." Journal of Cellular Physiology **218**(3): 460-466.

Schneider-Poetsch, T., et al. (2010). "Inhibition of eukaryotic translation elongation by cycloheximide and lactimidomycin." Nature Chemical Biology **6**(3): 209-217.

Schreiber, A. B., et al. (1981). "Monoclonal-antibodies against receptor for epidermal growth-factor induce early and delayed-effects of epidermal growth-factor." Proceedings of the National Academy of Sciences of the United States of America-Biological Sciences **78**(12): 7535-7539.

Schulze, W. X., et al. (2005). "Phosphotyrosine interactome of the ErbB-receptor kinase family." Molecular Systems Biology **1**.

Schwanhaeusser, B., et al. (2011). "Global quantification of mammalian gene expression control." Nature **473**(7347): 337-342.

Serezani, C. H., et al. (2008). "Cyclic AMP - Master regulator of innate immune cell function." American Journal of Respiratory Cell and Molecular Biology **39**(2): 127-132.

Shaikh, D., et al. (2010). "CAMP-dependent Protein Kinase Is Essential For Hypoxia-mediated Epithelial-mesenchymal Transition, Migration, And Invasion In Lung Cancer Cells." American Journal of Respiratory and Critical Care Medicine **181**.

Shutes, A., et al. (2007). "Specificity and mechanism of action of EHT 1864, a novel small molecule inhibitor of rac family small GTPases." Journal of Biological Chemistry **282**(49): 35666-35678.

Siddle, K. (2011). "Signalling by insulin and IGF receptors: supporting acts and new players." Journal of Molecular Endocrinology **47**(1): R1-R10.

Simpson, K. J., et al. (2008). "Identification of genes that regulate epithelial cell migration using an siRNA screening approach." Nature Cell Biology **10**(9): 1027-1038.

Singha, P. K., et al. (2010). "Transforming Growth Factor-beta (TGF-beta)-Inducible Gene TMEPAI Converts TGF-beta from a Tumor Suppressor to a Tumor Promoter in Breast Cancer." Cancer Research **70**(15): 6377-6383.

Sinha, B., et al. (2011). "Cells Respond to Mechanical Stress by Rapid Disassembly of Caveolae." Cell **144**(3): 402-413.

Small, J. V., et al. (2002). "The lamellipodium: where motility begins." Trends in Cell Biology **12**(3): 112-120.

Sorkin, A. and M. von Zastrow (2002). "Signal transduction and endocytosis: Close encounters of many kinds." Nature Reviews Molecular Cell Biology **3**(8): 600-614.

Sosa, M. S., et al. (2010). "Identification of the Rac-GEF P-Rex1 as an Essential Mediator of ErbB Signaling in Breast Cancer." Molecular Cell **40**(6): 877-892.

Soule, H. D., et al. (1990). "Isolation and characterization of a spontaneously immortalized human breast epithelial-cell line, mcf-10." Cancer Research **50**(18): 6075-6086.

Stevenson, R. P., et al. (2012). "Actin-bundling proteins in cancer progression at a glance." Journal of Cell Science **125**(5): 1073-1079.

Stoorvogel, W., et al. (2004). "Sorting of ligand-activated epidermal growth factor receptor to lysosomes requires its actin-binding domain." Journal of Biological Chemistry **279**(12): 11562-11569.

Suda, K., et al. (2011). "Epithelial to Mesenchymal Transition in an Epidermal Growth Factor Receptor-Mutant Lung Cancer Cell Line with Acquired Resistance to Erlotinib." Journal of Thoracic Oncology **6**(7): 1152-1161.

Tait L, S. H. a. R. J. (1990). "Ultrastructural and Immunocytochemical Characterization of an Immortalized Human Breast Epithelial Cell Line, MCF-10." Cancer Research **50**: 6087-6094.

Tait, L., et al. (1990). "Ultrastructural and immunocytochemical characterization of an immortalized human breast epithelial-cell line, MCF-10." Cancer Research **50**(18).

Tarcic, G., et al. (2012). "EGR1 and the ERK-ERF axis drive mammary cell migration in response to EGF." Faseb Journal **26**(4): 1582-1592.

Turke, A. B., et al. (2012). "MEK Inhibition Leads to PI3K/AKT Activation by Relieving a Negative Feedback on ERBB Receptors." Cancer Research **72**(13): 3228-3237.

Ullrich, A., et al. (1984). "Human epidermal growth-factor receptor cdna sequence and aberrant expression of the amplified gene in a431 epidermoid carcinoma-cells." Nature **309**(5967): 418-425.

Umezawa, H., et al. (1986). "Studies on a new epidermal growth factor-receptor kinase inhibitor, erbstatin, produced by mh435-hf3." Journal of Antibiotics **39**(1): 170-173.

Underwood, J. M., et al. (2006). "The ultrastructure of MCF-10A acini." Journal of Cellular Physiology **208**(1): 141-148.

Vasioukhin, V., et al. (2000). "Directed actin polymerization is the driving force for epithelial cell-cell adhesion." Cell **100**(2): 209-219.

Vehlow, A., et al. (2013). "Endophilin, Lamellipodin, and Mena cooperate to regulate F-actin-dependent EGF-receptor endocytosis." Embo Journal **32**(20): 2722-2734.

Vitolo, M. I., et al. (2009). "Deletion of PTEN Promotes Tumorigenic Signaling, Resistance to Anoikis, and Altered Response to Chemotherapeutic Agents in Human Mammary Epithelial Cells." Cancer Research **69**(21): 8275-8283.

Wallin, J. J., et al. (2012). "Active PI3K Pathway Causes an Invasive Phenotype Which Can Be Reversed or Promoted by Blocking the Pathway at Divergent Nodes." Plos One **7**(5).

Wang, H., et al. (2013). "Rotational motion during three-dimensional morphogenesis of mammary epithelial acini relates to laminin matrix assembly." Proceedings of the National Academy of Sciences of the United States of America **110**(1): 163-168.

Waterman, H., et al. (2002). "A mutant EGF-receptor defective in ubiquitylation and endocytosis unveils a role for Grb2 in negative signaling." Embo Journal **21**(3): 303-313.

Watson, C. J. and W. T. Khaled (2008). "Mammary development in the embryo and adult: a journey of morphogenesis and commitment." Development **135**(6): 995-1003.

Wertheimer, E., et al. (2012). "Rac signaling in breast cancer: A tale of GEFs and GAPs." Cellular Signalling **24**(2): 353-362.

Wiesen, J. F., et al. (1999). "Signaling through the stromal epidermal growth factor receptor is necessary for mammary ductal development." Development **126**(2): 335-344.

Wirtz-Peitz, F. and J. A. Zallen (2009). "Junctional trafficking and epithelial morphogenesis." Current Opinion in Genetics & Development **19**(4): 350-356.

Wong, J. L. (2012). Identification of Deubiquitylases Involved in the Regulation of Adherens Junction Components. Institute of Translational Medicine, University of Liverpool. [Thesis]

Wu, X., et al. (2013). "Microtubule inhibition causes epidermal growth factor receptor inactivation in oesophageal cancer cells." International Journal of Oncology **42**(1): 297-304.

Yadav, S. and A. D. Linstedt (2011). "Golgi Positioning." Cold Spring Harbor Perspectives in Biology **3**(5).

Yaish, P., et al. (1988). "Blocking of EGF-dependent cell-proliferation by egf receptor kinase inhibitors." Science **242**(4880): 933-935.

Yamada, K. M. and B. Geiger (1997). "Molecular interactions in cell adhesion complexes." Current Opinion in Cell Biology **9**(1): 76-85.

Yang, J.-Y., et al. (2010). "Activation of FOXO3a Is Sufficient to Reverse Mitogen-Activated Protein/Extracellular Signal-Regulated Kinase Kinase Inhibitor Chemoresistance in Human Cancer." Cancer Research **70**(11): 4709-4718.

Yao, L.-C. and D. M. McDonald (2014). "Plasticity of Airway Lymphatics in Development and Disease." Developmental Aspects of the Lymphatic Vascular System **214**: 41-54.

Yarden, Y. and G. Pines (2012). "The ERBB network: at last, cancer therapy meets systems biology." Nature Reviews Cancer **12**(8): 553-563.

Yarden, Y. and M. X. Sliwkowski (2001). "Untangling the ErbB signalling network." Nature Reviews Molecular Cell Biology **2**(2): 127-137.

Yin, T. F., et al. (2005). "Mechanisms of plakoglobin-dependent adhesion - Desmosome-specific functions in assembly and regulation by epidermal growth factor receptor." Journal of Biological Chemistry **280**(48).

Yoshida, T., et al. (2010). "Targeting epidermal growth factor receptor: Central signaling kinase in lung cancer." Biochemical Pharmacology **80**(5): 613-623.

Yoshidanoro, C., et al. (1984). "Molecular nature of the calcium-dependent cell cell-adhesion system in mouse teratocarcinoma and embryonic-cells studied with a monoclonal-antibody." Developmental Biology **101**(1): 19-27.

Yu, X., et al. (2012). "N-WASP coordinates the delivery and F-actin-mediated capture of MT1-MMP at invasive pseudopods." Journal of Cell Biology **199**(3): 527-544.

Zhan, L., et al. (2006). "Controlled activation of ErbB1/ErbB2 heterodimers promote invasion of three-dimensional organized epithelia in an ErbB1-dependent manner: Implications for progression of ErbB2-overexpressing tumors." Cancer Research **66**(10): 5201-5208.

Zhao, Y. and A. A. Adjei (2014). "The clinical development of MEK inhibitors." Nature Reviews Clinical Oncology **11**(7): 385-400.

Zielinski, R., et al. (2009). "The crosstalk between EGF, IGF, and Insulin cell signaling pathways - computational and experimental analysis." Bmc Systems Biology **3**.

# Appendices

# Appendix:
# Table 2.1A Chemical structures of inhibitors

| AZD6244 | Blebbistatin | CP724714 |
|---|---|---|
| 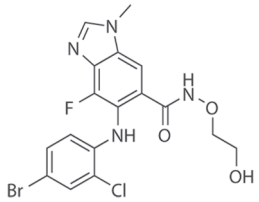 | 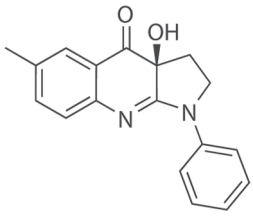 | 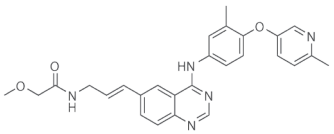 |
| Cycloheximide | Cytochalasin D | EHop-016 |
| 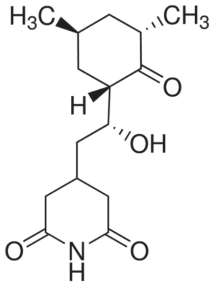 | 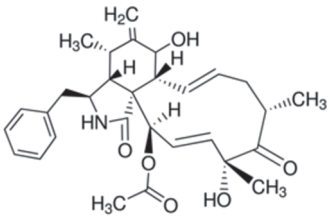 | 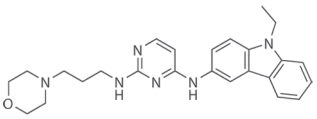 |
| EHT1864 | Erlotinib | GDC0941 |
| 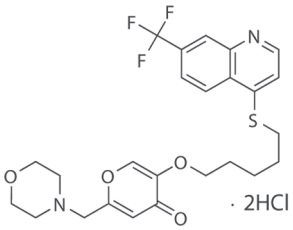 | 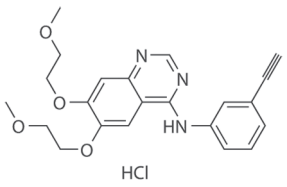 | 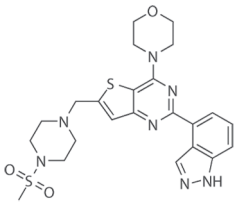 |
| Gefitinib | Lapatinib | Latrunculin A |
| 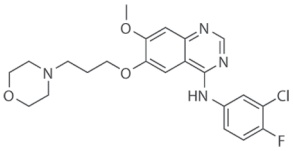 | 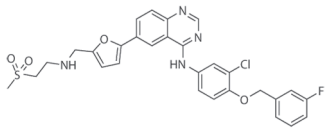 | 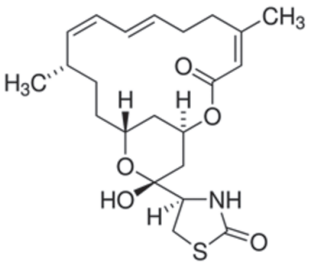 |

**Table 2.1A Chemical structures of inhibitors used.** Structures of inhibitors were obtained from the respective manufacturers' websites. The inhibitors are listed in alphabetical order based on the drug names listed in Methods: Table 2.1.

| LY294002 | NSC23766 | PI103 |
| --- | --- | --- |
| 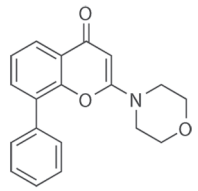 | 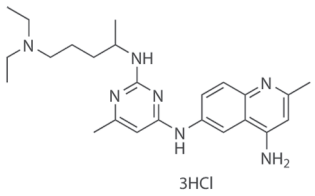 | 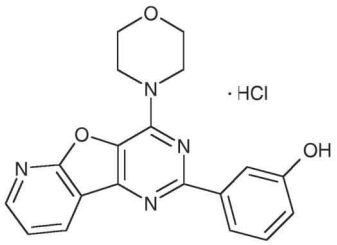 |

**Table 2.1A (continued) Chemical structures of inhibitors used.** Structures of inhibitors were obtained from the respective manufacturers' websites. The inhibitors are listed in alphabetical order based on the drug names listed in Methods: Table 2.1.

# Appendix 1:
# Hard copy of published paper derived from the results in this thesis

Report

Cell Reports

# Plasticity of Mammary Cell Boundaries Governed by EGF and Actin Remodeling

## Graphical Abstract

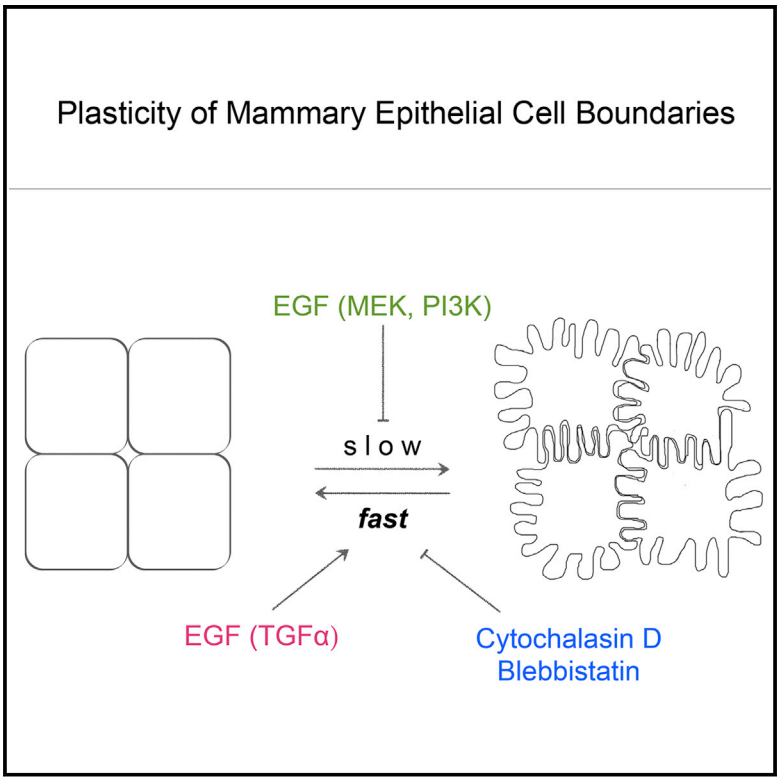


## Highlights

Major reorganization of MCF10A cellular boundaries occurs upon EGFR activation

EGF-responsive interdigitating cell projections restrict cell mobility

Rapid dissolution of interdigitations requires dynamic actin polymerization

Distinct EGF-dependent pathways exist for formation and reversal of interdigitations

## Authors

Wai Ying Yvonne Tang, Alison J. Beckett, ..., Sylvie Urbé, Michael J. Clague

## Correspondence

urbe@liv.ac.uk (S.U.),
clague@liv.ac.uk (M.J.C.)

## In Brief

Tang et al. describe a dramatic reconfiguration of confluent mammary MCF10A cells controlled by EGF signaling. Withdrawal of EGF leads to wide-scale interdigitation of cells and increased desmosome number. Cells thereby become locked into position and unable to migrate within a monolayer. These interdigitations can be rapidly dissolved by reapplication of EGF, through a process that requires actin polymerization and myosin II activity. These convenient phenotypic assays offer a platform for detailed dissection of relevant effector pathways.

Tang et al., 2014, Cell Reports 8, 1–9
September 25, 2014 ©2014 The Authors
http://dx.doi.org/10.1016/j.celrep.2014.08.026

Please cite this article in press as: Tang et al., Plasticity of Mammary Cell Boundaries Governed by EGF and Actin Remodeling, Cell Reports (2014), http://dx.doi.org/10.1016/j.celrep.2014.08.026

Cell Reports
Report



# Plasticity of Mammary Cell Boundaries Governed by EGF and Actin Remodeling

Wai Ying Yvonne Tang,[1] Alison J. Beckett,[1] Ian A. Prior,[1] Judy M. Coulson,[1] Sylvie Urbé,[1,*] and Michael J. Clague[1,*]
[1]Cellular and Molecular Physiology, Institute of Translational Medicine, University of Liverpool, Liverpool L69 3BX, UK
*Correspondence: urbe@liv.ac.uk (S.U.), clague@liv.ac.uk (M.J.C.)
http://dx.doi.org/10.1016/j.celrep.2014.08.026


## SUMMARY

**Defined signals that dictate the architecture of cellular boundaries in confluent cultures are poorly characterized. Here, we report dramatic remodeling, invoked by long-term epidermal growth factor (EGF) withdrawal from mammary-derived MCF10A cells. Such intervention generates an interdigitated, desmosome-rich monolayer, wherein cells project actin-containing protrusions deep into neighboring cells. These changes protect cellular sheets from mechanical disruption and dramatically restrict the freedom of cells to roam within the monolayer. Ectopic expression of activated Rac counteracts interdigitation and induces membrane ruffling, but cells remain confined by their interdigitated neighbors. Interdigitations are rapidly dissolved by acute EGF application in a process that is sensitive to actin depolymerization and myosin II inhibition. These assays for formation and dissolution of interdigitations provide a platform for the dissection of novel signaling pathways that are highly specific to EGF receptor (EGFR) activation.**

## INTRODUCTION

In a physiological setting, boundaries between cells can be smooth or highly interdigitated, such as the visceral epithelia podocytes of the kidney (Mundel and Kriz, 1995). Early morphological studies of mammary epithelial cells isolated from human donor after weaning breast fluids described "a well developed system of cytoplasmic interdigitation and numerous desmosomes" (Russo et al., 1975). During early embryonic development and puberty, the elongated tips of mammary buds form multilayered epithelia, and cells within the interior layers show prominent interdigitation and high levels of desmosomes (Ewald et al., 2012; Nazario et al., 1994). Interdigitated structures are also prominent in intraductal carcinomas, suggesting that they may have acquired characteristics of the normal developmental program (Goldenberg et al., 1969). In keratinocyte and endothelial cell cultures, interdigitated structures are observed as intermediates in the formation of stable cell-cell contacts (Hoelzle and Svitkina, 2012; Vasioukhin et al., 2000). However, defined molecular pathways that can control the decision between smooth or interdigitated cell boundaries have not been substantively dissected in vitro.

The epidermal growth factor receptor (EGFR) is the founding member of the ErbB family of receptor tyrosine kinases that together coordinate complex signaling systems that underpin organogenesis and differentiation of several cell lineages (Citri and Yarden, 2006). Mutation and other mechanisms constitutively activate the network in a variety of carcinomas, rendering it a major target for pharmaceutical intervention. Epidermal growth factor (EGF) stimulation initiates multiple signaling cascades, including the PtdIns3-kinase pathway and several mitogen-activated protein kinase (MAPK) pathways, of which the ERK pathway is best understood (Katz et al., 2007). From a cell biological perspective, the key EGF-mediated responses, so far defined, are mitogenic and motogenic.

MCF10A cells are an immortal nontumorigenic epithelial cell line that arose spontaneously from mortal diploid mammary epithelial cells of extended lifespan (Soule et al., 1990). They have found widespread use in epithelial cell biological studies and are a favored model for the generation of isogenic cell line panels. They form organized monolayers in cell culture, presenting a characteristic "cobblestone" appearance. EGF stimulates invasive properties of these cells but is not required for growth (Tarcic et al., 2012).

The most radical change in cellular adhesive properties occurs during epithelial-to-mesenchymal transition that is important to development, wound healing, and cancer cell metastasis (Kalluri and Weinberg, 2009). For many cancer cell types, this can be promoted by activation of receptor tyrosine kinases such as EGFR and MET. Adherens junctions (AJ) and desmosomes constitute sites of cellular adhesion that link adhesive Cadherin proteins to actin and intermediate filaments (IF), respectively. Together, they contribute synergistically to determine the strength of adhesion between cells (Huen et al., 2002). Desmosomes appear as paired electron dense plaques that align between neighboring cells and contain two types of Cadherin family proteins, Desmogleins and Desmocollins (Dubash and Green, 2011). At both types of adhesive junctions, the armadillo family of proteins connect Cadherins with adaptor proteins, which link to the cytoskeleton. One such, Plakoglobin (PG), is a constituent of both AJ and desmosomes. Another, Desmoplakin (DP), is specific to desmosomes and is required for strong cellular adhesion and integrity of epithelia in vitro and in vivo.

Please cite this article in press as: Tang et al., Plasticity of Mammary Cell Boundaries Governed by EGF and Actin Remodeling, Cell Reports (2014), http://dx.doi.org/10.1016/j.celrep.2014.08.026



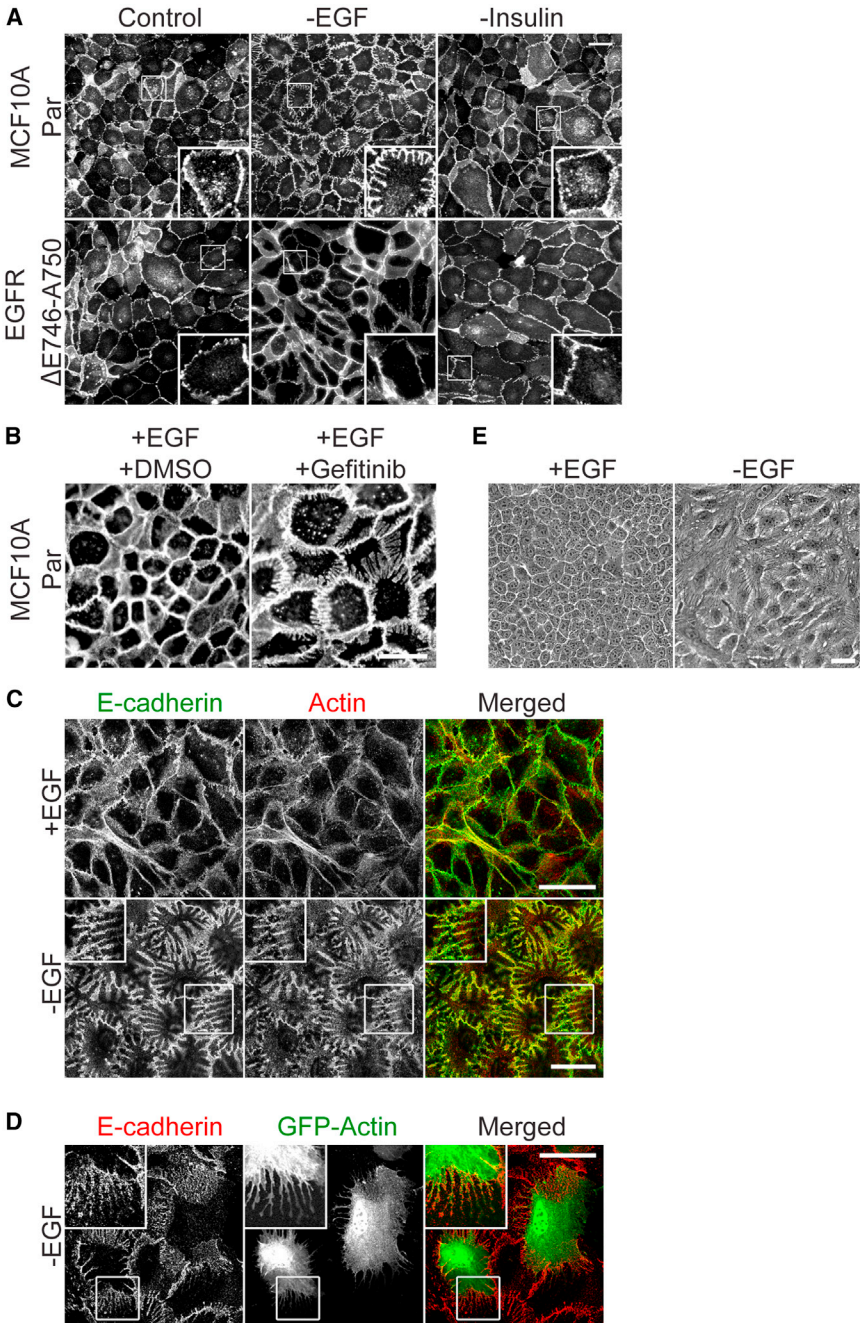


**Figure 1. EGFR Signaling Suppresses Actin-Containing Interdigitations between MCF10A Cells**

(A) Effect of removal of EGF or insulin from growth media of MCF10A cells (top row) or isogenic cells expressing EGFR ΔE746-A750 (bottom row). Control MCF10A cells organize in a confluent monolayer with "cobblestone" morphology. Interdigitations seen following EGF removal are not apparent in EGFR mutant cells.

(B) Phenocopy of the "finger-like" structures when cells are cultured in the presence of EGF and the EGFR inhibitor, Gefitinib. Medium was exchanged 6 hr post seeding in complete growth medium (10% FBS ± EGF, insulin), fixed with 4% PFA 72 (A) or 48 (B) hr later, and immunostained with antibody directed at the extracellular domain of E-cadherin.

(C–E) Complete growth medium was exchanged for medium ± 20 ng/ml EGF 6 hr postseeding (C). After 72 hr, cells were fixed with 4% PFA and stained for E-cadherin (green), and F-actin (red), (D) cells transfected with GFP-LifeAct and counterstained for E-cadherin (red), (E) live cell monolayer grown on a plastic dish. Cells were visualized using conventional immunofluorescence microscopy at 20× magnification (A and B), confocal immunofluorescence microscopy at 63× magnification (C and D), and phase-contrast microscopy at 20× magnification (E). Scale bar, 40 μm.

Here, we show that MCF10A cells within a confluent monolayer setting are capable of major rearrangements to form highly developed interdigitating structures prompted by EGF withdrawal. Our ultrastructural analysis reveals actin cables projecting from the tips of these structures. Such interdigitations can be rapidly reversed by reapplication of EGF in a process that requires dynamic polymerization of actin and cytoskeletal contractility. The presence of interdigitating structures is associated with immobility within confluent monolayers, impaired wound healing, and enhanced mechanical stability.

## RESULTS

### EGFR Signaling Suppresses Interdigitation of MCF10A Cells

The widely accepted culture conditions for MCF10A cells suggest supplementation of the medium with a cocktail of hormones and other factors (EGF, insulin, hydrocortisone, and cholera enterotoxin) together with horse serum (Soule et al., 1990). Our first step was to determine if all these components are necessary for cell growth. In our hands, 2D cell growth was not influenced by insulin or cholera toxin, diminished by EGF withdrawal, and most profoundly impaired by hydrocortisone loss. For the ensuing experiments, cells were routinely cultured with all of these components ±EGF.

Under normal culture conditions, E-cadherin provides a uniform plasma membrane staining, which highlights the smooth boundaries between neighboring cells. However, we noticed a remarkable reorganization upon culturing cells in the absence of EGF. Under these conditions, cells form long finger-like projections into the body of neighboring cells, creating a regular pattern of interdigitation (Figure 1A). Two lines of evidence indicate that EGFR tyrosine kinase activity is required for the suppression of this interdigitated state: (1) isogenic

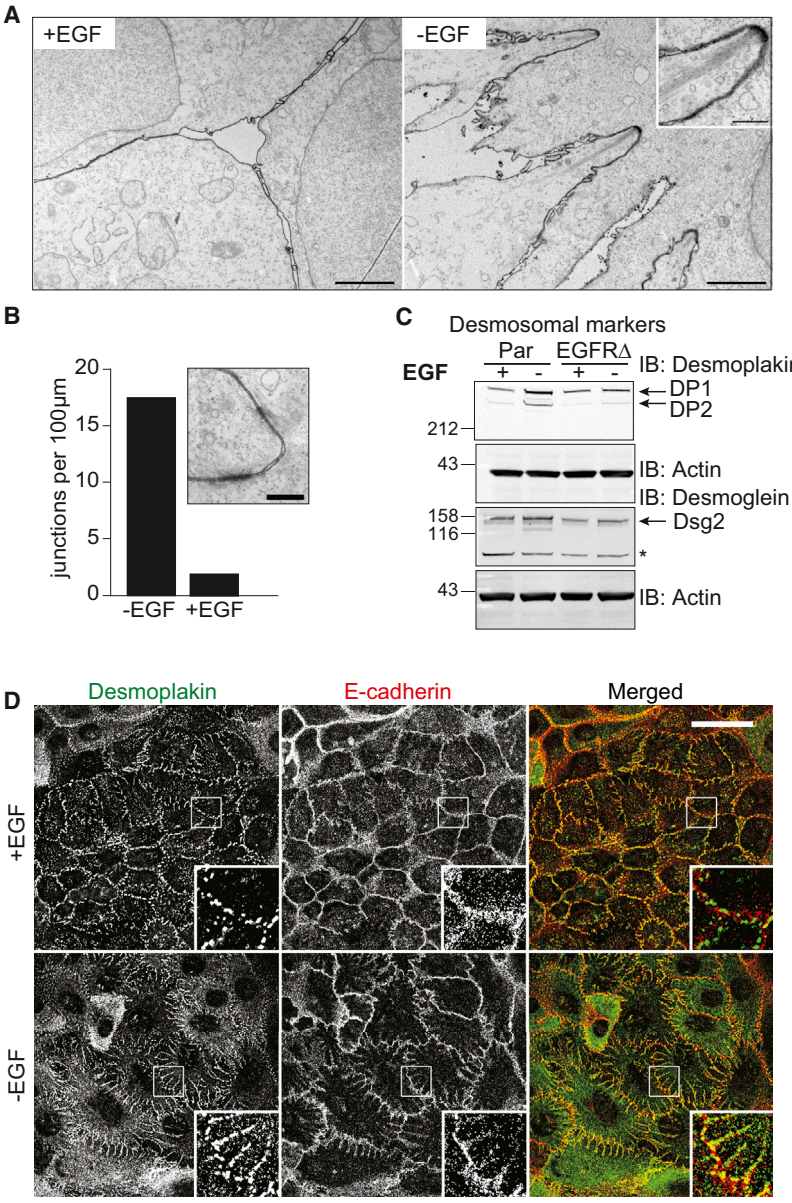


**Figure 2. Ultrastructural and Confocal Visualization of Interdigitations and an Accompanying Increase in the Number of Desmosomes**

(A) Control MCF10A cells (left) show smooth membranes between adjacent cells compared to the cells grown in medium lacking EGF (right), which show residual finger-like structures. Actin cables project from tips of the protrusions. Cells were cultured in medium ±EGF and fixed 62 hr later. Scale bar, 2 μm and 0.5 μm (insets).

(B) Quantification of the number of desmosomes per unit length of plasma membrane indicates 10-fold more junctions in cells cultured in medium without EGF. Data are aggregated from 33 micrographs per condition (~500 μm) as described in Experimental Procedures.

(C) Immunoblot analysis of 12.5 μg of MCF10A cell lysates from parental and EGFRΔE746-A750 cells cultured in medium with or without EGF for 65 hr and probed for Desmoplakin 1 and 2 and Desmoglein 2. Asterisk indicates a nonspecific band. Parental cells, but not EGFRΔE746-A750 cells, show increased expression of desmosomal proteins when cultured in medium lacking EGF.

(D) Confocal immunofluorescence images showing staining patterns of desmoplakin and E-cadherin. Cells were cultured in medium ± EGF and fixed with methanol after 70 hr.

Scale bar, 40 μm.

MCF10A cells, in which one allele of the endogenous EGFR gene has been engineered to express a constitutively active EGFR (ΔE746-A750), do not respond to EGF withdrawal (Figure 1A), and (2) application of the EGFR inhibitor Gefitinib induces interdigitation in the presence of EGF (Figure 1B).

## Actin Cables Project to Digit Tips and Desmosome Numbers Increase

Interdigitations contain actin and can be observed in cells expressing GFP-Actin (Life-Act) or simply by phase-contrast light microscopy (Figures 1C–1E; Movie S1). Once formed, they are maintained over 1.5 hr in the presence of the actin-depolymerizing agent Cytochalasin D (Figure S1A). The myosin II inhibitor, Blebbistatin, also fails to disrupt interdigitation (Figure S1B).

We were not able to assess the effects of these drugs on digit formation itself, owing to their toxicity within the time frame required for this process (>12 hr, see below). We undertook a transmission electron microscopic (TEM) analysis of the cellular morphology induced by EGF withdrawal, using ruthenium red to enhance the plasma membrane staining, as described by Deneka et al. (Deneka et al., 2007). Remnants of interdigitations survive the fixation and present as rough projections into the neighboring cell that are entirely absent in cells cultured with EGF (Figure 2A). In transverse sections, prominent actin cables are observed which project from a dense structure at the digit tip (inset, Figure 2A). Also striking is the accumulation of electron dense desmosomal plaques in cells deprived of EGF. These are recognized as paired electron-dense regions associated with both membranes of neighboring cells and by the intermediate filaments, which project from them (inset, Figure 2B). Desmosomes provide a system of "spot welds," which contribute to the mechanical properties of cell layers. These adhesive structures maintain the mechanical integrity of epithelial and other stress-bearing tissues by tethering intermediate filaments to the plasma membrane. Desmosomal proteins are often mutated or silenced in breast cancer (Klus et al., 2001; Oshiro et al., 2005). EGF withdrawal

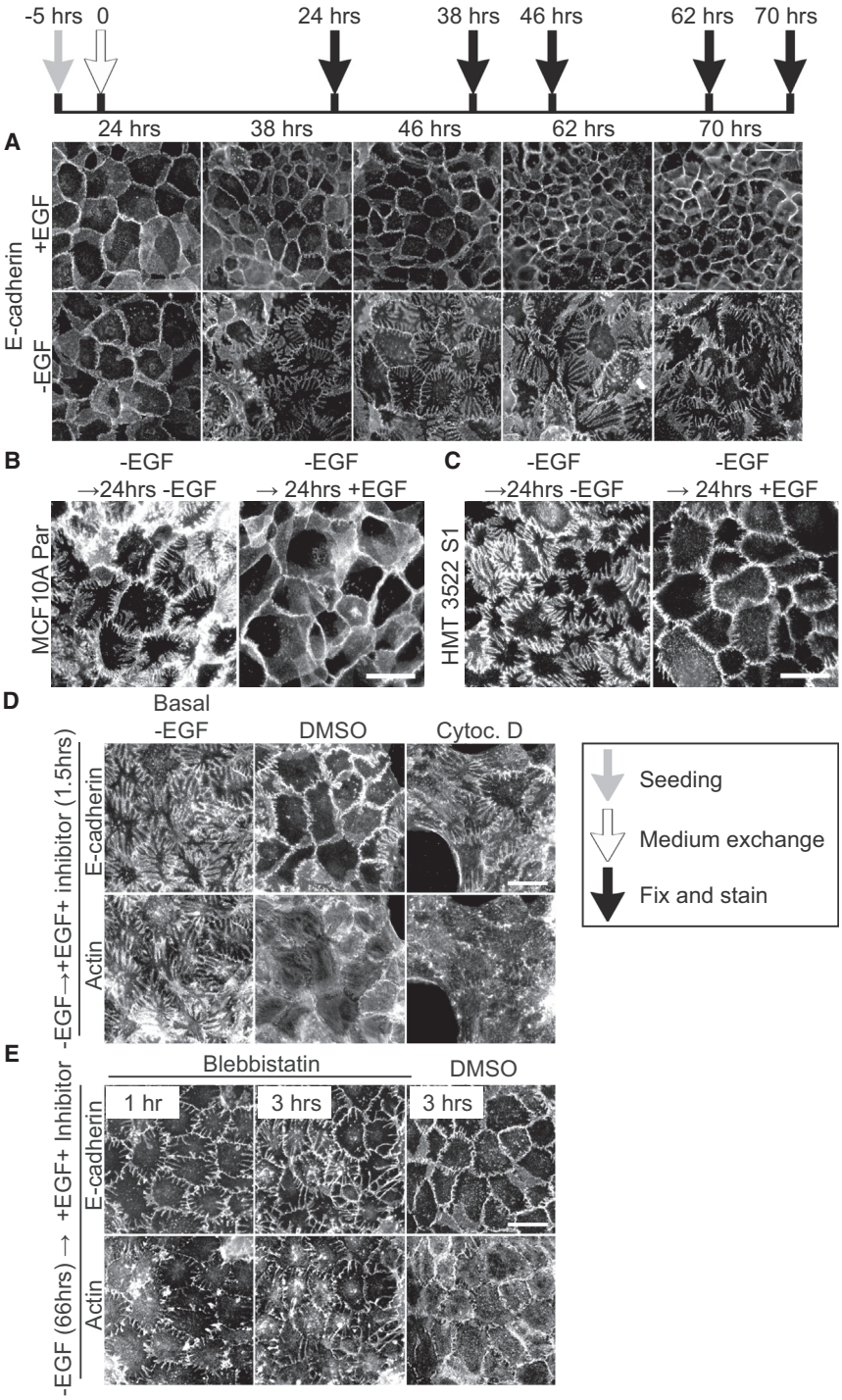


**Figure 3. Time Course of Interdigitation, Reversibility, and the Requirement of Actin Polymerization**

(A) The prominence of E-cadherin stained interdigitations on the membrane of MCF10A parental cells gradually increased from 38 to 70 hr after medium exchange. Medium lacking EGF replaced the complete growth medium 5 hr post-seeding, and cells were fixed with 4% PFA at times indicated after medium exchange (timeline).

(B and C) Interdigitations resolved within 24 hr when 20ng/ml EGF was restored to the MCF10A parental cells or HMT 3522 S1 cells. MCF10A cell coverslips were treated as in (A) up to 70 hr, and medium was then exchanged and left for a further 24 hr ± EGF. HMT 3522 were grown to confluence in full medium containing 10 ng/ml EGF for 96 hr followed by EGF withdrawal for 166 hr, which established interdigitations. Cells were then treated for a final 24 hr ±EGF.

(D and E) Actin polymerization and actomyosin contractility is required for the reversal of interdigitations. Cells were cultured in growth medium lacking EGF for ~67 hr before treatment with vehicle control (DMSO) and 5 μM Cytochalasin D (D) or 25 μM blebbistatin (E; left 1 hr; middle and right, 3 hr). Coverslips were fixed at indicated time points when significant reversal of interdigitation is evident in control cells, but not those that have been drug treated. Cells were stained for E-cadherin and F-actin and visualized using immunofluorescence microscopy at 40× magnification. Scale bar, 40 μm.

leads to a 10-fold increase in desmosomes per unit length of plasma membrane (Figure 2B). This is accompanied by a notable increase in expression of the transmembrane desmosomal protein Desmoglein and the adaptor molecule Desmoplakin (Figure 2C,D), while no changes in E-cadherin levels or of selected tight junctional markers (ZO-1, Claudin) are seen (Figure S2A).

## Differing Time Scales of Formation and Dissolution of Interdigitations Reflect Different Signaling Cascades

Interdigitations can be seen forming 24–38 hr after withdrawal of EGF from newly seeded cells and elaborate over the next day or so (Figure 3A). They can also be induced within an already established confluent monolayer by acute removal of EGF, under which circumstances they become apparent after 12–16 hr (Movie S2). This is accompanied by a remarkable stabilization of cellular position and neighbor associations within a monolayer and loss of all roaming capability (Movies S1 and S2). Ectopic expression of the constitutively active form (V12) of the small GTPase Rac1 (tagged with GFP), which regulates cytoskeletal dynamics and cell motility, suppresses the interdigitation with neighboring cells. However, such isolated cells are held in place by a cordon of interdigitating neighbors (Figure S3; Movie S3).

Importantly, interdigitating structures are reversible; smooth boundaries between cells and mobility within the monolayer are re-established upon addition of medium containing EGF

(Figure 3B; Movie S4). Reversal of fingers is apparent within 1 hr after EGF administration. Another "near-normal" breast cell line, HMT-3522, forms similar interdigitations following EGF withdrawal, and these too are dissolved by application of EGF (Figure 3C; Holm et al., 1993). Remarkably, this reversal process requires actin polymerization, as treatment with the actin depolymerizing agent cytochalasin D inhibits the acute loss of interdigitations (Figure 3D). Uncoupling of myosin II from actin by applying Blebbistatin similarly inhibited the dissolution of interdigitations (Figure 3E). Although there are some intriguing observations reported, linking desmosomal proteins (Plakophilin 1, Desmoglein 3) to actin organization and dynamics (Hatzfeld et al., 2000; Tsang et al., 2012), we propose that interdigitation itself, is unlikely to be caused by increased desmosome number. Desmosomal proteins of mouse keratinocytes and oral squamous carcinoma cells are similarly sensitive to EGF, but no interdigitating structures were reported in these studies (Lorch et al., 2004; Yin et al., 2005). Furthermore, following acute application of EGF, interdigitations dissolve and the cells recover motile properties, but desmosomal proteins remain elevated and distributed at the plasma membrane (Movie S4; Figures S2B and S2C).

Interdigitations readily form if EGF is withdrawn shortly after seeding or after cells have reached full confluency. The first configuration is not amenable to analyzing the effects of drugs, which severely inhibit cell growth, but responds clearly to Gefitinib (Figure 1). However, when starting with established confluent monolayers, the induction of interdigitations by Gefitinib treatment is less penetrant. In fact, under these conditions, the mitogen-activated protein kinase/extracellular signal-regulated kinase 1 inhibitor AZD6244 produced more widespread interdigitating structures, which can be further elaborated by combining with the PtdIns3-kinase inhibitor LY294002. Treatment with LY294002 alone leads to some short finger structures. In both these cases, the finger structures are less fine than those produced by EGF withdrawal, shorter and fatter i.e., stubby. Combining all 3 inhibitors recapitulates the effects of EGF withdrawal at high penetrance (Figure S4A). Thus in confluent cell monolayers the tonic suppression of interdigitation by EGF, requires the combined outputs of PtdIns3-kinase and MAPK pathways, as well as further EGFR-dependent factors. A corollary of these experiments is the finding that the active process of interdigitation induced by EGF withdrawal is not negatively influenced by inhibition of either PtdIns3-kinase or MAPK pathways (Figure S4A).

We noted that simply exchanging the culture medium for fresh medium containing 10% bovine serum, but no added EGF, transiently reversed the interdigitated phenotype (Figure 4A). This implies that bovine serum must contain an exhaustible factor capable of mimicking the effect of EGF. We tested a number of other growth factors for their ability to suppress the maintenance of interdigitations. First of all, insulin, which is routinely included in the culture medium, has no effect (Figure 1). Transforming growth factor alpha (TGF-$\alpha$), which also activates EGFR directly, transiently suppresses interdigitations similar to the effect of fresh serum. However, neuregulin 1 (NRG1), which specifically activates other ErbB family members (ErbB3 and ErbB4), had no effect (Figure 4B). The hepatocyte growth factor (HGF) showed no effect after 3 hr, when the process is essentially complete in EGF-treated cells. Some shortening of fingers is evident after 24 hr (Figure 4B), which may be an indirect consequence of the "HGF-cell scattering" program, which leads to cell-cell dissociation when space is available (Birchmeier et al., 2003). Receptor tyrosine kinases (RTKs) elicit highly overlapping cell signaling networks, which for EGF and HGF have been directly compared in A549 lung adenocarcinoma cells (Hammond et al., 2010). In line with these observations, we see that HGF and EGF elicit similar levels of activation of surrogate markers of the MAPK pathway (pERK) and the class 1 PtdIns3-kinase pathway (pAkt) in MCF10A cells over a 3 hr time point (Figure 4C). Accordingly, this process of dissolution is insensitive to inhibitors of these pathways (LY294002 and AZD6244) (Figure S4B).

Rac1 is rapidly activated following EGF application to MCF10A cells (Figure S5A). This can be strongly suppressed by depletion of the guanine nucleotide exchange factor, Vav2, in accordance with previous findings (Duan et al., 2011) (Figure S5B). However, such depletion does not impede the rapid dissolution of interdigitations provoked by acute EGF (Figure S5C). Thus, while expression of constitutively activated Rac1 can act to suppress interdigitation (Figure S3), the rapid reversal process appears to be largely independent of the major pool of EGF-activated Rac1.

### Resistance to Shear Stresses and Wound Healing

We have tested if the interdigitated state provides a resistance to disruption by shear stresses. Confluent sheets of cells were lifted by treatment with the enzyme dispase and subjected to shear stress by repeated pipetting. Cell sheets cultured with EGF readily fragment, whereas interdigitated/high desmosome sheets cultured without EGF are highly resistant to fragmentation (Figure 5A).

As a corollary of our findings that interdigitations impede the freedom of individual cells to roam within confluent monolayers (Movies S1 and S2), we looked at the ability to close a wound in the confluent monolayer induced by a scratch made with a pipette tip. Cells cultured in the absence of EGF, and hence highly interdigitated, are unable to close such a wound unless EGF is applied to dissolve the interdigitations. Neither HGF nor NRG1 can substitute for this effect, despite being powerful motogenic stimuli in other cell systems (Figure 5B; Movie S5) (Birchmeier et al., 2003; Ritch et al., 2003).

## DISCUSSION

In this study, we provide a detailed characterization of a dramatic reversible change in the architecture of epithelial cell boundaries within a confluent monolayer that can be elicited with a single defined cue. Suppression of interdigitations represents a manifestation of EGFR signaling in nontumorigenic breast epithelial cells. Assembly of interdigitations in the absence of EGF is slow (>12 hr), while dissolution following application of EGF is relatively fast (1–3 hr). Formation is likely to reflect long-term adjustments to the cellular proteome following EGF withdrawal, while dissolution is driven by actin-myosin contractile forces associated with acute EGF application. The rapid dissolution

Please cite this article in press as: Tang et al., Plasticity of Mammary Cell Boundaries Governed by EGF and Actin Remodeling, Cell Reports (2014), http://dx.doi.org/10.1016/j.celrep.2014.08.026



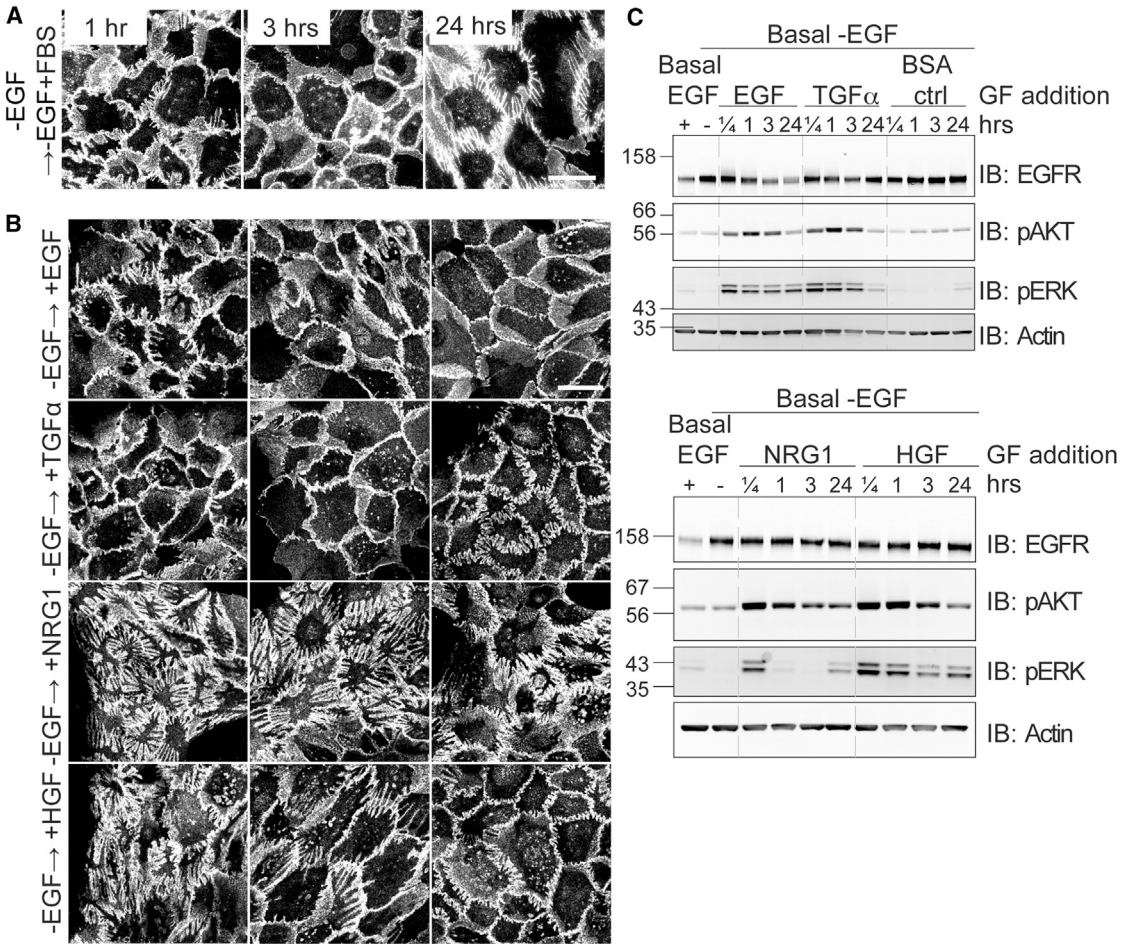


**Figure 4. Differential Abilities of Growth Factors to Reverse Interdigitation**

(A) Transient reversal of interdigitation in MCF10A cells (1–3 hr) when medium is exchanged with fresh medium containing FBS, but no EGF supplement.

(B) Status of interdigitations at 1 hr, 3 hr, and 24 hr after addition of indicated growth factors (GF) EGF (20 ng/ml), HGF (20 ng/ml), NRG1 (6 ng/ml), or TGF-α (20 ng/ml). Images were taken using the Leica confocal DMIRE microscope at 63× magnification, zoom 1.5. Scale bar, 40 μm.

(C) MCF10A cell lysates following addition of growth factors at indicated times, probed with anti-EGFR, anti-pAKT, anti-pERK, and actin. Cells were grown in growth medium lacking EGF for 69.5 hr before addition of growth factors.

process requires actin polymerization and contractility but is independent of PtdIns3-kinase and MAPK pathways. This distinguishes it from the tonic suppression of interdigitation by EGF, for which we provide evidence of the involvement of both these signaling pathways. It is also striking that dissolution is particular to EGF and cannot be recapitulated by ligands for other RTK receptors, MET and ErbB3, despite the strong overlap in downstream signals (Hammond et al., 2010). Our work therefore indicates the involvement of a signaling pathway unique to EGFR.

We have characterized a simple in vitro system to examine a phenomenon, i.e., interdigitation of neighboring cells, which is widespread in stratified animal tissues. Our finding that interdigitation is associated with resistance to shear stress may reflect a key aspect of its physiological function. Mammary ducts are subject to significant mechanical stresses and have to withstand dramatic volume changes during lactation. Other systems in which interdigitation can be observed in vitro include kidney podocytes and keratinocytes (Hoelzle and Svitkina, 2012; Mundel and Kriz, 1995; Vasioukhin et al., 2000). However, in neither case has a molecular cue controlling this process been defined. In the keratinocyte system, so-called adhesion zippers progress to a smooth boundary in a process that requires actin reorganization, recalling the reversal process we have characterized (Vaezi et al., 2002; Vasioukhin et al., 2000). A distinguishing feature of the system described here is that we can invoke interdigitation within a preformed adhesive monolayer. EGFR inhibitors are normally assessed in growth or invasion assays where cells are necessarily subconfluent or dispersed. We propose this system may be useful to assess the efficacy of EGFR inhibitors within a different in vitro context, i.e., cell confluency. The tonic suppression of interdigitation by EGF and the rapid dissolution of established interdigitations by acute administration represent distinct pathways that offer exciting opportunities for further characterization by screening and proteomic strategies.

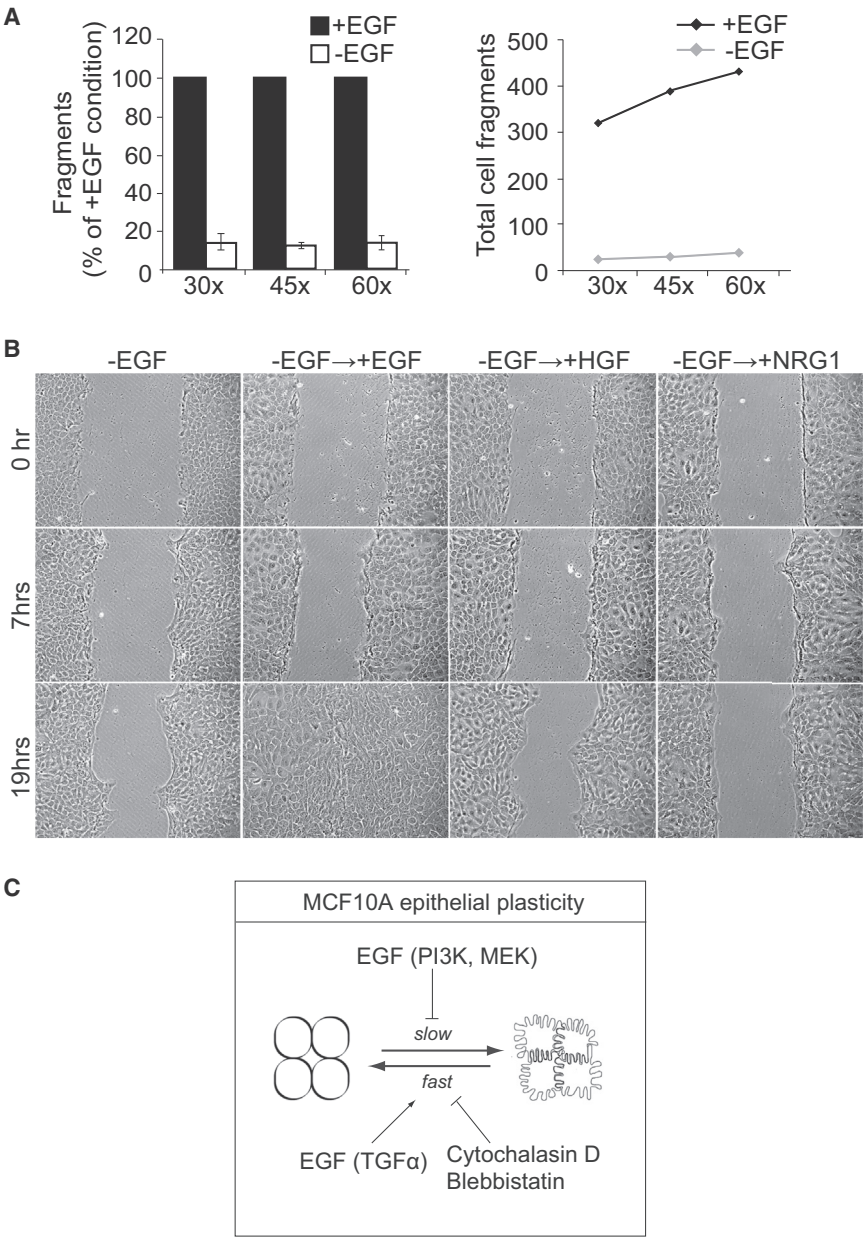


**Figure 5. Interdigitation Dictates MCF10A Cell Monolayer Properties**

(A) Cells cultured in complete growth medium or medium lacking EGF for 93 hr were subjected to a dispase mechanical dissociation assay in triplicate. The number of fragments was assessed sequentially after 30, 45, and 60 pipetting strokes. Left: relative fractions of fragments for cells grown ±EGF (average of two independent experiments, error bars indicate range). Right: cumulative number of fragments of a representative experiment.

(B) Differential cell migration into scratch wounds upon incubation with EGF (20 ng/ml), HGF (20 ng/ml), and NRG1 (6 ng/ml). Cells were cultured in medium lacking EGF for 72 hr. A wound was scratched onto the well 30–40 min prior to live-cell imaging at 10× magnification.

(C) Schematic summary figure.

We suggest that a particular feature of MCF10A cells, which may underlie this phenomenon, is that they are untransformed, nontumorigenic cells. They are distinct from commonly used breast cancer cell lines, which form smooth boundaries in the absence of EGF (e.g., MCF7). Most such cell lines are maintained in simpler media, which are not supplemented with EGF. An exception is the HMT-3522 cell line, which forms similar interdigitations in media lacking EGF (Figure 3C; Holm et al., 1993). Note that these cells are cultured in serum-free media. A specific feature accompanying interdigitation is the shackling of cells to a fixed position within a confluent monolayer. One may envision that this has consequences for normal mammary development and for the development of mammary tumors.

## EXPERIMENTAL PROCEDURES

### Antibodies and Other Reagents

The following primary antibodies or reagents were used for fluorescence microscopy: mouse anti-E-cadherin clone HECD1 (Cancer Research UK Laboratories), AF594-phalloidin (Invitrogen), mouse anti-Desmoplakin and anti-Desmoglein (kindly provided by David Garrod, University of Manchester) (North et al., 1999; Vilela et al., 1995). Antibodies used for western blotting included rabbit anti-EGFR clone D38B1, rabbit anti pEGFR Y1068, rabbit anti-pAKT, rabbit anti-pERK, rabbit anti-Vav2, rabbit anti-CDC42, (Cell Signaling), mouse anti-Rac1 (Cytoskeleton), mouse anti-β actin (Abcam), rabbit anti-ZO1 (Zymed), and rabbit anti-Claudin-1 (Invitrogen). Inhibitors used were Gefitinib, AZD6244 (Stratech), Cytochalasin D, Latrunculin A and blebbistatin (Sigma), and LY294002 (Calbiochem). Growth media and supplements were from the following suppliers: Dulbecco's modified Eagles's medium (DMEM)/F12 Glutamax and fetal bovine serum (FBS) (Invitrogen), horse serum (HS) (First Link), EGF, TGF-α, NRG1 (Preprotech), hydrocortisone, insulin, and cholera toxin (Sigma).

### Cell Culture and EGFR Inhibitor Treatment

MCF10A parental and EGFR ΔE746-A750 cells (Horizon Discovery) were cultured in 5% $CO_2$ in DMEM/F12 Glutamax supplemented with 5% HS, 20 ng/ml EGF, 500 ng/ml hydrocortisone, 0.01 mg/ml insulin, and 100 ng/ml cholera toxin. MCF10A parental cells were seeded in six-well plates at a density of $1.0 \times 10^5$ cells/well (on plastic dish) and $1.5 \times 10^5$ cells/well (on glass coverslips). Medium was exchanged to replace the 5% HS with 10% FBS, with or without 20 ng/ml EGF. Inhibitors were added directly to wells or together with fresh or conditioned medium. In the reversal experiments, the growth factors were added directly to cells cultured in medium without EGF. HMT-3522 S1 cells were cultured in serum-free DMEM/F12 Glutamax supplemented with 250 ng/ml insulin, 10 ng/ml EGF, 10 μg/ml transferrin, 2.6 ng/ml Na-selenite, 27.2 pg/ml 17β-estradiol, 0.5 μg/ml hydrocortisone, and 5 μg/ml human prolactin.

### Immunofluorescence

Cells on coverslips were rinsed twice with PBS (37°C, supplemented with 1 mM $CaCl_2$, 1 mM $MgCl_2$), fixed in 4% paraformaldehyde (PFA) in PBS,

permeabilized with 0.2% Triton X-100, blocked in 10% goat serum, and incubated with primary and secondary antibodies in 5% goat serum (20 min each), all in PBS. Secondary antibodies were conjugated to either Alexa 488 or Alexa Fluor 594. Bright-field and immunofluorescence images were taken using a Nikon Eclipse Ti-E microscope (CFI Super Plan Fluor 20×/ 0.45 NA or CFI Plan Apochromat 40×/ 0.45NA objective lens) and a digital camera (CoolSNAP EZ Turbo 1394; Photometrics). Confocal images were taken using a Leica SP2 microscope (HCX PL Apo 63x/ 1.40NA objective lens at 1.50 or 1.90 zoom). The images were then processed using NIS-Elements Software (Nikon), Leica Confocal Software (Leica Microsystem), Photoshop CS5 Version 12.0 x64, and Illustrator CS5 version 15.0.0 (Adobe).

### Electron Microscopy

Confluent dishes of MCF10A cultured ±EGF were washed with 0.1 M sodium cacodylate buffer (pH 7.4) before fixing with 2.5% (w/v) glutaraldehyde, 1 mg/ml ruthenium red in sodium cacodylate buffer at room temperature for 1 hr. Following rinses with 0.1 M sodium cacodylate buffer, cells were postfixed with 1% osmium tetroxide, 1 mg/ml ruthenium red in 0.1 M cacodylate buffer at room temperature for 2 hr. After rinsing with $dH_2O$, cells were stained with 1% aqueous uranyl acetate (Agar) at room temperature for 1 hr and then dehydrated in a graded series of ethanol on ice. Cells were flat embedded using gelatine capsules in Epon and polymerized at 60°C for 2 days. Ultrathin serial sections (70–85 nm) were cut longitudinally through the whole cell and stained with uranyl acetate and lead citrate before viewing at 100 KV in a FEI Tecnai $G^2$ Spirit. To quantify the number of junctions, a total of 33 micrographs were taken using AnalySIS (SIS, GmbH) with a final magnification of 16,500× for both ±EGF cells incorporating two biological repeats. Seven different grids from six separate resin capsules were used for −EGF and four grids from two different resin capsules for +EGF. Areas imaged were chosen at random where cells were observed to be adjacent and membranes close enough for cell-to-cell adhesion. Touching membranes were measured using AnalySIS and junctions counted and expressed as the number of junctions per μm.

### Wound-Healing Assay and Time-Lapse Microscopy

MCF10A cells were grown to confluency, in media with FBS ± EGF for 71 hr. A scratch wound was made with a pipette tip (multichannel tip 250 μl; Anachem). To remove dead cells, the medium was exchanged for reconditioned media of a parallel plate. Cells were imaged for 3 hr within 30–40 min of scratching before addition of growth factors (EGF and HGF 20 ng/ml, NRG1 6 ng/ml) and followed by time-lapse microscopy using a fully motorized Nikon Ti-E eclipse microscope. Movies were processed using NIS-Elements software (Nikon), FijiIsJust ImageJ 1.48 (NIH), and MPEG Streamclip v1.9.2 (Squared5).

### Dispase Dissociation Assay

MCF10A cells were seeded in 60-mm-diameter dishes (+EGF, $1.75 \times 10^5$ cells/dish; −EGF, $3.3 \times 10^5$ cells/dish), and 93 hr after seeding, dishes were washed three times in PBS and incubated in 2 ml Dispase (2.4 U/ml; Roche) for 30–40 min at 37°C. A total of 5 ml of PBS was added into each dish, and dislodged cell sheets were centrifuged at 4 min at 200 rcf. Supernatant was removed, and cell sheets were disrupted using a p1000 pipette tip by pipetting in 1 ml PBS for the given number of repetitions. Cell fragments (more than one cell) were counted using a hemocytometer.

## SUPPLEMENTAL INFORMATION

Supplemental Information includes Supplemental Experimental Procedures, five figures, and five movies and can be found with this article online at http://dx.doi.org/10.1016/j.celrep.2014.08.026.

## ACKNOWLEDGMENTS

This work was supported by a Cancer Research UK PhD studentship to W.Y.Y.T. We are grateful to Chris Torrance and Horizon Discovery Ltd. for the provision of MCF10A parental and isogenic cell lines.

Received: April 30, 2014
Revised: July 1, 2014
Accepted: August 12, 2014
Published: September 18, 2014

## BIBLIOGRAPHY

Birchmeier, C., Birchmeier, W., Gherardi, E., and Vande Woude, G.F. (2003). Met, metastasis, motility and more. Nat. Rev. Mol. Cell Biol. *4*, 915–925.

Citri, A., and Yarden, Y. (2006). EGF-ERBB signalling: towards the systems level. Nat. Rev. Mol. Cell Biol. *7*, 505–516.

Deneka, M., Pelchen-Matthews, A., Byland, R., Ruiz-Mateos, E., and Marsh, M. (2007). In macrophages, HIV-1 assembles into an intracellular plasma membrane domain containing the tetraspanins CD81, CD9, and CD53. J. Cell Biol. *177*, 329–341.

Duan, L., Raja, S.M., Chen, G., Virmani, S., Williams, S.H., Clubb, R.J., Mukhopadhyay, C., Rainey, M.A., Ying, G., Dimri, M., et al. (2011). Negative regulation of EGFR-Vav2 signaling axis by Cbl ubiquitin ligase controls EGF receptor-mediated epithelial cell adherens junction dynamics and cell migration. J. Biol. Chem. *286*, 620–633.

Dubash, A.D., and Green, K.J. (2011). Desmosomes. Curr. Biol. *21*, R529–R531.

Ewald, A.J., Huebner, R.J., Palsdottir, H., Lee, J.K., Perez, M.J., Jorgens, D.M., Tauscher, A.N., Cheung, K.J., Werb, Z., and Auer, M. (2012). Mammary collective cell migration involves transient loss of epithelial features and individual cell migration within the epithelium. J. Cell Sci. *125*, 2638–2654.

Goldenberg, V.E., Goldenberg, N.S., and Sommers, S.C. (1969). Comparative ultrastructure of atypical ductal hyperplasia, intraductal carcinoma, and infiltrating ductal carcinoma of the breast. Cancer *24*, 1152–1169.

Hammond, D.E., Hyde, R., Kratchmarova, I., Beynon, R.J., Blagoev, B., and Clague, M.J. (2010). Quantitative analysis of HGF and EGF-dependent phosphotyrosine signaling networks. J. Proteome Res. *9*, 2734–2742.

Hatzfeld, M., Haffner, C., Schulze, K., and Vinzens, U. (2000). The function of plakophilin 1 in desmosome assembly and actin filament organization. J. Cell Biol. *149*, 209–222.

Hoelzle, M.K., and Svitkina, T. (2012). The cytoskeletal mechanisms of cell-cell junction formation in endothelial cells. Mol. Biol. Cell *23*, 310–323.

Holm, P.K., Hansen, S.H., Sandvig, K., and van Deurs, B. (1993). Endocytosis of desmosomal plaques depends on intact actin filaments and leads to a non-degradative compartment. Eur. J. Cell Biol. *62*, 362–371.

Huen, A.C., Park, J.K., Godsel, L.M., Chen, X., Bannon, L.J., Amargo, E.V., Hudson, T.Y., Mongiu, A.K., Leigh, I.M., Kelsell, D.P., et al. (2002). Intermediate filament-membrane attachments function synergistically with actin-dependent contacts to regulate intercellular adhesive strength. J. Cell Biol. *159*, 1005–1017.

Kalluri, R., and Weinberg, R.A. (2009). The basics of epithelial-mesenchymal transition. J. Clin. Invest. *119*, 1420–1428.

Katz, M., Amit, I., and Yarden, Y. (2007). Regulation of MAPKs by growth factors and receptor tyrosine kinases. Biochim. Biophys. Acta *1773*, 1161–1176.

Klus, G.T., Rokaeus, N., Bittner, M.L., Chen, Y., Korz, D.M., Sukumar, S., Schick, A., and Szallasi, Z. (2001). Down-regulation of the desmosomal cadherin desmocollin 3 in human breast cancer. Int. J. Oncol. *19*, 169–174.

Lorch, J.H., Klessner, J., Park, J.K., Getsios, S., Wu, Y.L., Stack, M.S., and Green, K.J. (2004). Epidermal growth factor receptor inhibition promotes desmosome assembly and strengthens intercellular adhesion in squamous cell carcinoma cells. J. Biol. Chem. *279*, 37191–37200.

Mundel, P., and Kriz, W. (1995). Structure and function of podocytes: an update. Anat. Embryol. (Berl.) *192*, 385–397.

Nazario, A.C., Simoes, M.J., and de Lima, G.R. (1994). Morphological and ultrastructural aspects of the cyclical changes of human mammary gland during the menstrual cycle. Sao Paulo Med. J. *112*, 543–547.

North, A.J., Bardsley, W.G., Hyam, J., Bornslaeger, E.A., Cordingley, H.C., Trinnaman, B., Hatzfeld, M., Green, K.J., Magee, A.I., and Garrod, D.R. (1999). Molecular map of the desmosomal plaque. J. Cell Sci. *112*, 4325–4336.

Oshiro, M.M., Kim, C.J., Wozniak, R.J., Junk, D.J., Muñoz-Rodríguez, J.L., Burr, J.A., Fitzgerald, M., Pawar, S.C., Cress, A.E., Domann, F.E., and Futscher, B.W. (2005). Epigenetic silencing of DSC3 is a common event in human breast cancer. Breast Cancer Res. *7*, R669–R680.

Ritch, P.A., Carroll, S.L., and Sontheimer, H. (2003). Neuregulin-1 enhances motility and migration of human astrocytic glioma cells. J. Biol. Chem. *278*, 20971–20978.

Russo, J., Furmanski, P., and Rich, M.A. (1975). An ultrastructural study of normal human mammary epithelial cells in culture. Am. J. Anat. *142*, 221–231.

Soule, H.D., Maloney, T.M., Wolman, S.R., Peterson, W.D., Jr., Brenz, R., McGrath, C.M., Russo, J., Pauley, R.J., Jones, R.F., and Brooks, S.C. (1990). Isolation and characterization of a spontaneously immortalized human breast epithelial cell line, MCF-10. Cancer Res. *50*, 6075–6086.

Tarcic, G., Avraham, R., Pines, G., Amit, I., Shay, T., Lu, Y., Zwang, Y., Katz, M., Ben-Chetrit, N., Jacob-Hirsch, J., et al. (2012). EGR1 and the ERK-ERF axis drive mammary cell migration in response to EGF. FASEB J. *26*, 1582–1592.

Tsang, S.M., Brown, L., Gadmor, H., Gammon, L., Fortune, F., Wheeler, A., and Wan, H. (2012). Desmoglein 3 acting as an upstream regulator of Rho GTPases, Rac-1/Cdc42 in the regulation of actin organisation and dynamics. Exp. Cell Res. *318*, 2269–2283.

Vaezi, A., Bauer, C., Vasioukhin, V., and Fuchs, E. (2002). Actin cable dynamics and Rho/Rock orchestrate a polarized cytoskeletal architecture in the early steps of assembling a stratified epithelium. Dev. Cell *3*, 367–381.

Vasioukhin, V., Bauer, C., Yin, M., and Fuchs, E. (2000). Directed actin polymerization is the driving force for epithelial cell-cell adhesion. Cell *100*, 209–219.

Vilela, M.J., Hashimoto, T., Nishikawa, T., North, A.J., and Garrod, D. (1995). A simple epithelial cell line (MDCK) shows heterogeneity of desmoglein isoforms, one resembling pemphigus vulgaris antigen. J. Cell Sci. *108*, 1743–1750.

Yin, T., Getsios, S., Caldelari, R., Godsel, L.M., Kowalczyk, A.P., Müller, E.J., and Green, K.J. (2005). Mechanisms of plakoglobin-dependent adhesion: desmosome-specific functions in assembly and regulation by epidermal growth factor receptor. J. Biol. Chem. *280*, 40355–40363.

**Cell Reports, Volume *8***

**Supplemental Information**

# Plasticity of Mammary Cell Boundaries Governed by EGF and Actin Remodeling

**Wai Ying Yvonne Tang, Alison J. Beckett, Ian A. Prior, Judy M. Coulson, Sylvie Urbé, and Michael J. Clague**

Supplemental data

Figure S1 (related to Fig. 1C,D). Maintenance of interdigitation does not require actin polymerisation or contractility. MCF10A cells were cultured in growth medium lacking EGF for 67 hours before treatment with vehicle (DMSO) (A) Cytochalasin D (5μM) or (B) 25μM Blebbistatin. Coverslips were fixed with 4% PFA at indicated times and stained for E-cadherin, F-actin and with DAPI. Cells were visualised using immunofluorescence microscopy at 40x magnification. Scale; 40μm.

Figure S2 (related to Figure 2). (A) Characterisation of other junctional markers in the MCF10A cell line. MCF10A cell lysates were lysed following culture for 65 hours in growth medium ± EGF, and probed with anti-ZO1, anti-Claudin-1, anti-E-cadherin and Actin. Levels of tight junction and adherens junction proteins are EGF-independent for MCF10A parental cells and ΔE746-A750 cells (B) Desmosomal protein levels remain elevated up to 24 hours after dissolution of fingers. MCF10A cell lysates were prepared from cell cultures incubated for 68 hours in growth medium ± EGF. Other cells were subsequently treated for 1hr, 3hrs and 24 hrs with EGF before lysis. (C) immunofluorescence for cells treated as in (B) showing desmoplakin retention at the plasma membrane during dissolution of interdigitations. Single confocal sections (63x), scale bar; 40μm.

Figure S3 (related to Figure 3). Transient transfection of constitutively active GFP-RacG12V negates the interdigitations invoked by EGF withdrawal. Cells were cultured in the absence of EGF for 48 hours then transfected for 18 hours. Cells on coverslips were fixed with 4% PFA and stained with E-cadherin. Cells were visualised using immunofluorescence microscopy at 40x magnification. Scale; 40μm.

Figure S4. (related to Figure 3) (A) Inhibition of signaling pathways induces interdigitation within confluent monolayers. Combinations of Gefitinib (300nM), AZD6244 (300nM) and LY294002 (20μM), added to confluent MCF10A cells in the presence of EGF, induced highly developed interdigitations. Formation of fingers by EGF withdrawal was not impeded by the presence of the same inhibitors. (B) Dissolution of interdigitations proceeds normally in the presence of MEK (AZD6244) and PI3K (LY294002) inhibitors. Cells were cultured in growth medium without EGF for 67 hrs to induce interdigitation before addition of 20ng/ml EGF with vehicle control DMSO. Coverslips were fixed after 1hr, 3hrs and 24hrs with 4% PFA and stained with E-cadherin. Cells were visualised using immunofluorescence microscopy at 40x magnification. Scale; 40μm.

Figure S5. (related to Figure 3) Vav activated Rac1 is not required for reversal of interdigitations. GST-PAK pulldown from (A) MCF10A cells grown for 62 hrs without EGF then stimulated for 3 minutes with 20ng/ml EGF. Lysates were probed with anti-Rac1, anti-CDC42 and anti-pY1068 EGFR. Lanes were loaded with 4.6% of the input lysate was probed alongside the bound protein fraction isolated with GST-PAK-CRIB beads. (B) Rac1-GTP activation is substantively reduced by Vav2 depletion. MCF10A cells were treated with 40nM siRNA specific for Vav2 and otherwise grown as described in (A). (C) Reversal of interdigitation is unaffected by Vav2 depletion. Cells were cultured in growth medium lacking EGF for 67 hrs to induce interdigitations. Cells treated essentially as described in (B) were incubated for the indicated times with 20ng/ml EGF. Coverslips were fixed after 1hr, 3hrs and 24hrs with 4% PFA and stained with E-cadherin. Cells were visualised using immunofluorescence microscopy at 40x magnification. Scale; 40μm.

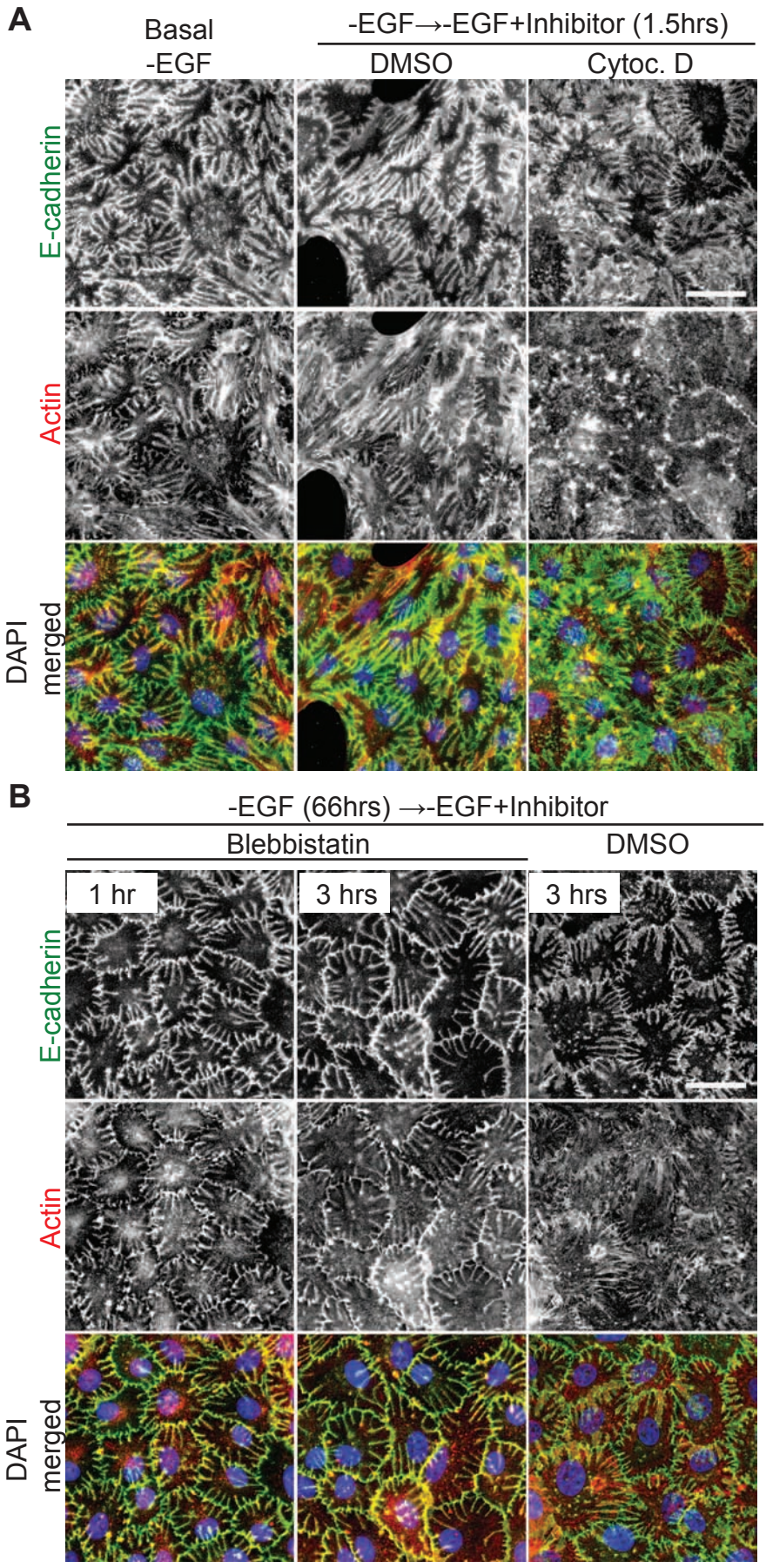


Tang et al Figure S1

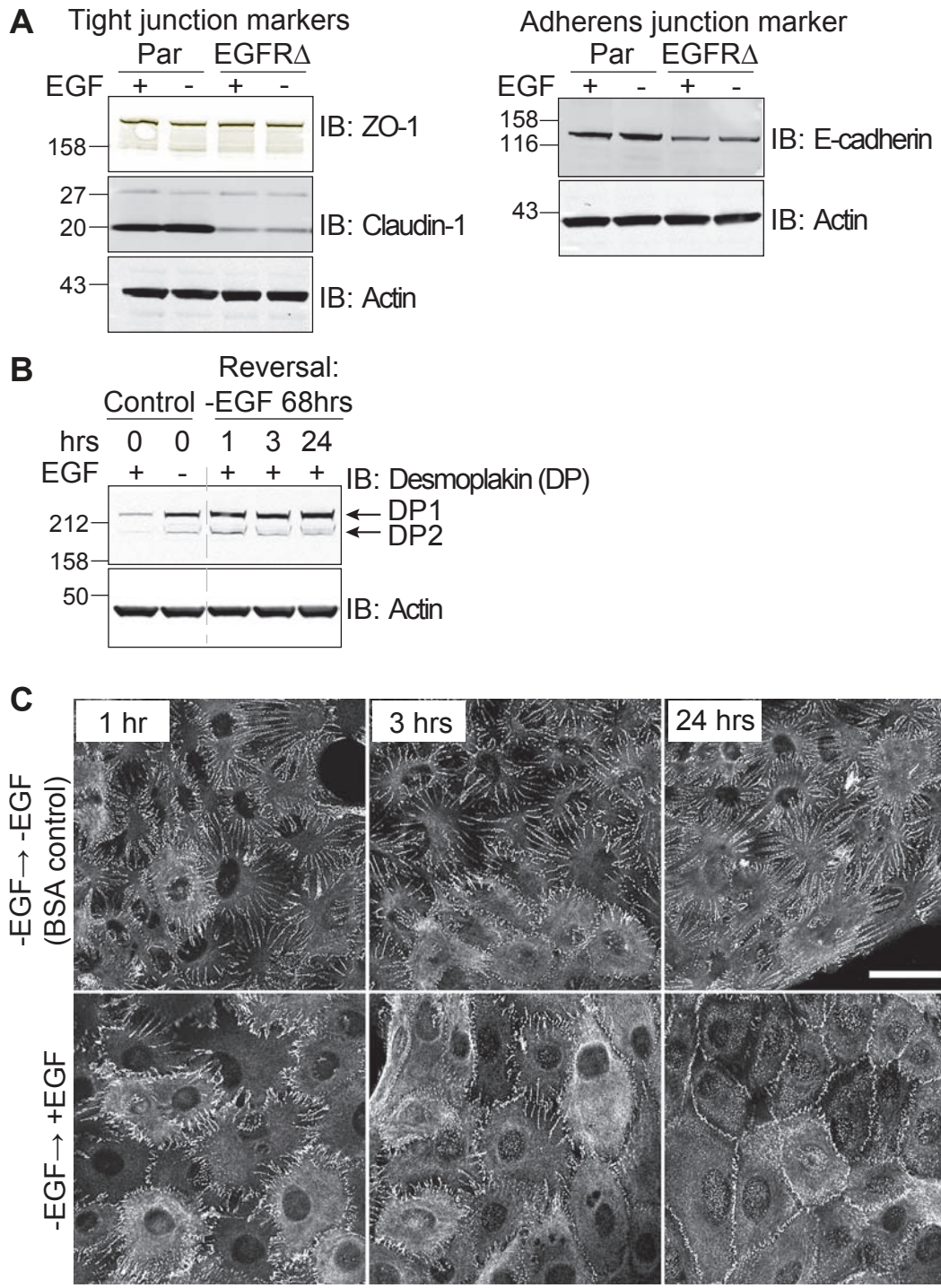


Tang et al Figure S2

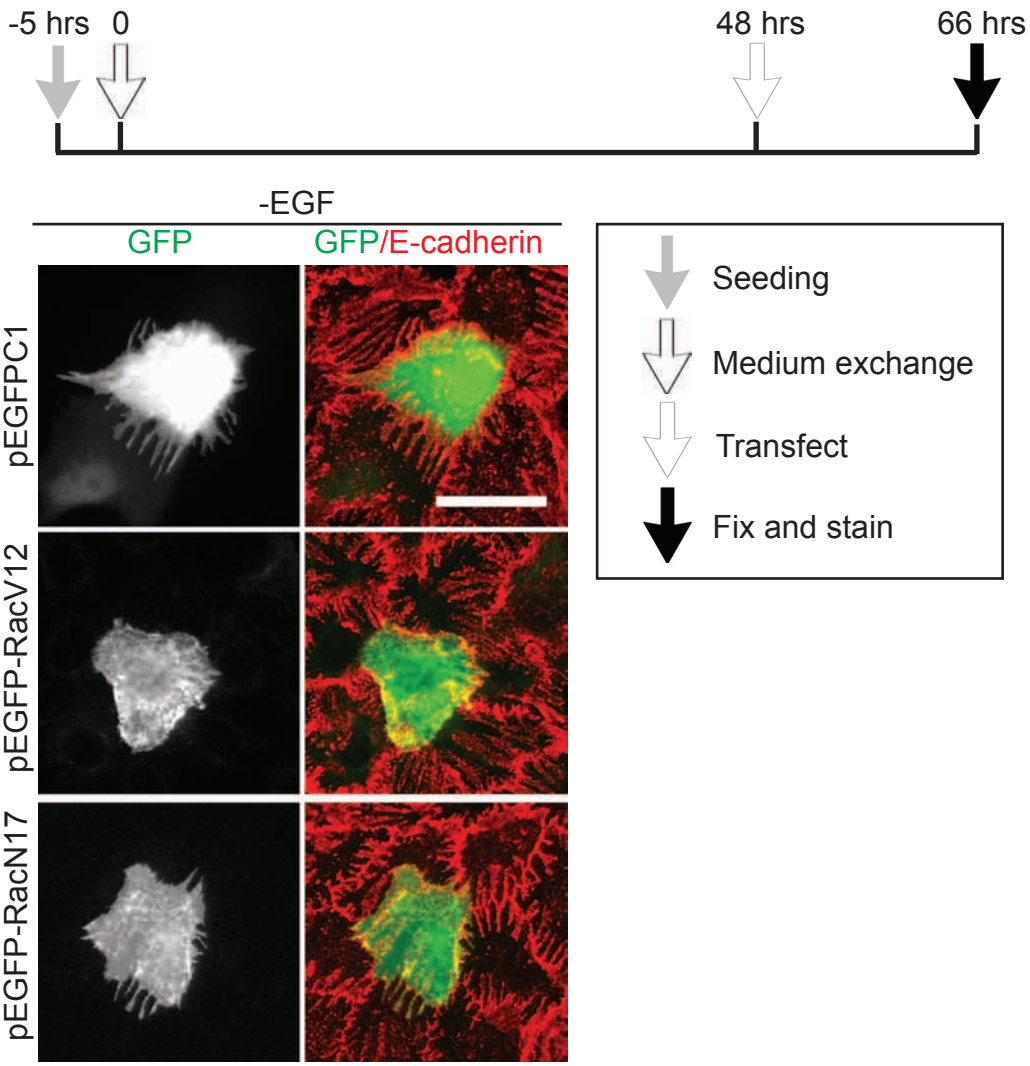


Tang et al Figure S3

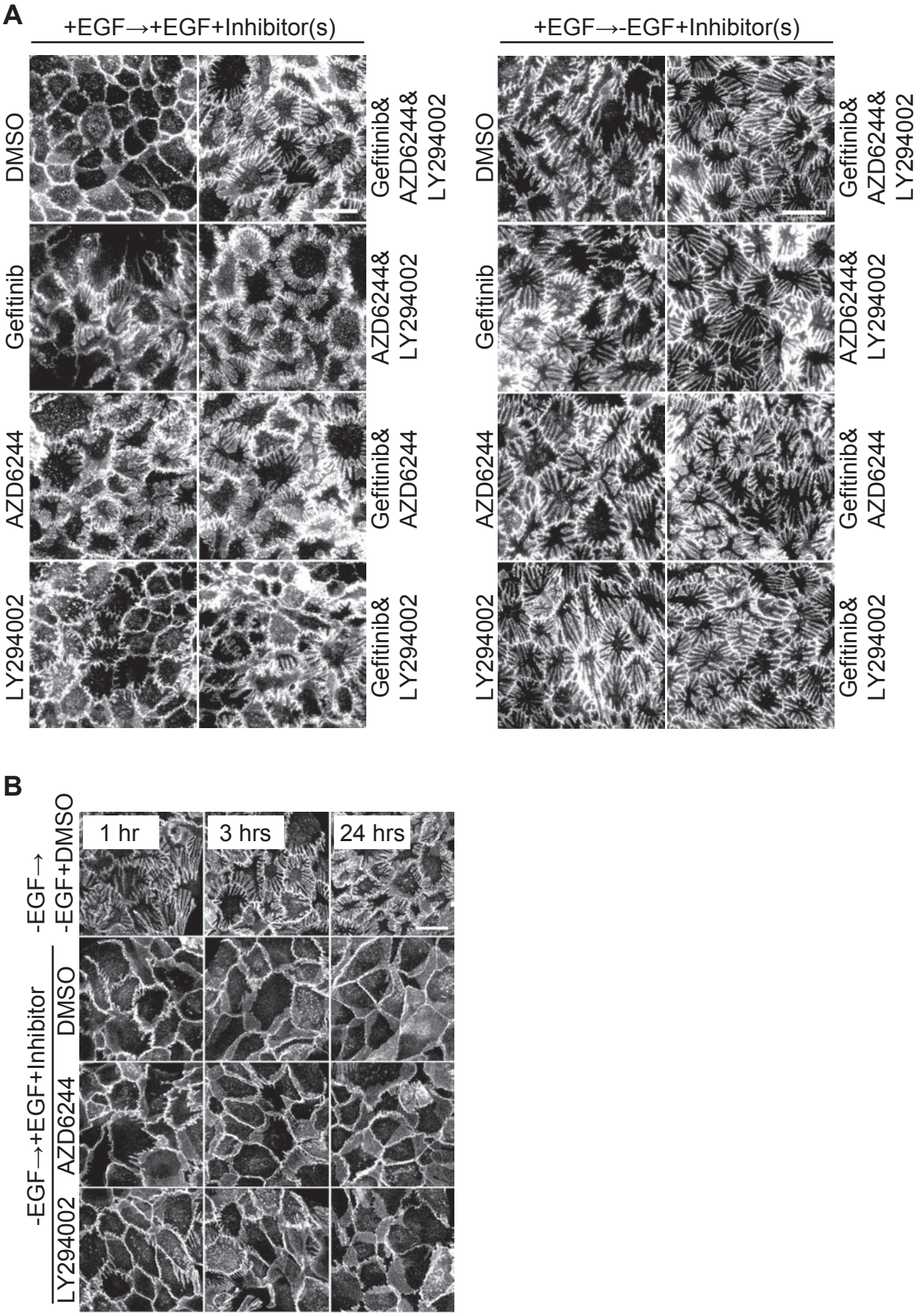


Tang et al Figure S4

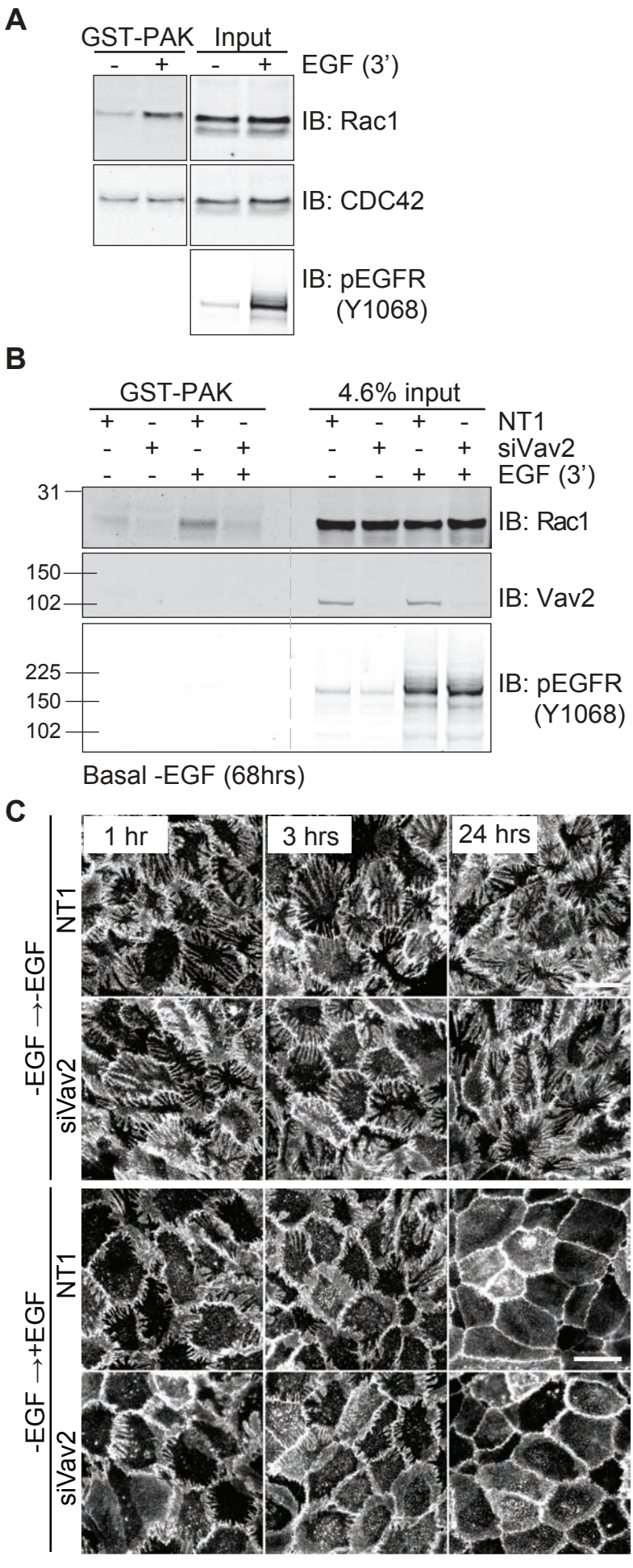


Tang et al Figure S5

Movies S1-S5

Movie S1 (related to Figure 1):

Withdrawal of EGF leads to loss of cellular lateral mobility. MCF10A monolayers grown in complete growth medium, +EGF (left panel) or –EGF (right panel).

Left panel. MCF10A cells were cultured in complete growth medium (+EGF) for 46 hrs before exchange for fresh medium (+EGF), from which point images were collected by time-lapse phase contrast microscopy . Frames were taken every 15 mins for 24 hrs saved for playback at 100ms intervals.

Right panel. MCF10A cells were cultured in growth medium lacking EGF for 67 hrs. Images were captured by time-lapse phase contrast microscopy. Frames were collected every 15 mins for the final 24 hrs saved for playback at 100ms interval.

Movie S2 (related to Figure 3):

Induction of interdigitation in MCF10A cells upon removal of EGF (+EGF→ –EGF).

MCF10A cells were cultured in complete growth medium (+EGF) for 46 hrs before exchange of medium to (-EGF) (20ng/ml). Images were captured by time-lapse phase contrast microscopy using an inverted microscope (Eclipse Ti-E, Nikon). Frames were colected every 15 mins for 24 hrs saved for playback at 100ms interval.

Movie S3 (related to Figure S3)

Transient transfection of constitutively active GFP-RacG12V negates interdigitations.

MCF10A cells were cultured in growth medium lacking EGF for 96 hrs. Cells were transfected with GFP-RacG12V expression plasmid 24hrs before imaging. Images were captured by time-lapse phase contrast and fluorescence microscopy using an inverted microscope (Eclipse Ti-E, Nikon). Frames were collected every 3.24 mins for 2.5 hrs saved for playback at 100ms interval.

Movie S4 (related to Figure 3)

Dissolution of interdigitation in MCF10A cells upon addition of EGF (-EGF → +EGF).

MCF10A cells were cultured in growth medium lacking EGF for 68.8 hrs before addition of EGF (20 ng/ml). Interdigitations started to resolve at time 1:30 hrs (addition of EGF). Images were analysed by time-lapse phase contrast microscopy using an inverted microscope (Eclipse Ti-E, Nikon). Frames were collected every 2 mins for 13 hrs saved for playback 100ms interval. Imaging started 1.5 hrs before addition of EGF and lasted for 13 hrs.

Movie S5 (related to Figure 4,5)
Wound closure of MCF10A cells is specific to addition of EGF.
MCF10A cells were cultured in growth medium lacking EGF for 69 hrs before addition of growth factor; EGF (20ng/ml), HGF (20ng/ml) or NRG1 (6ng/ml). Wound closure is most efficient upon addition of EGF (bottom left). Images were analyzed by time-lapse phase contrast microscopy

using an inverted microscope (Eclipse Ti-E, Nikon). Imaging started 3 hrs before addition of growth factors and frames were collected every 15 mins for 19 hrs, saved for playback at 100ms interval.

Supplemental experimental procedures:

Transfection of MCF10A cells

MCF10A parental cells were transfected with pEGFP-C1 (Clontech), GFP-LifeAct, GFP-RacG12V or GFP-T17N (gifts of Laura Machesky, Beatson Institute, Glasgow), using the Lipofectamine LTX transfection reagent (Invitrogen) according to the manufacturer's instructions. Medium was exchanged 5-8 hours post seeding, and cells were transfected 36-48 hours later once they had reached a minimum of 50% confluence. Transfection medium was replaced by complete medium with or without 20ng/ml EGF 5-6 hours after transfection. Transfected cells were left for another 18-24 hours prior to fixation with 4% paraformaldehyde for immunofluorescence microscopy. For the Vav2 depletion, cells were treated with 40nM of pooled oligos; NT1 or siVav2 (Thermoscientific) on the day of seeding. Medium was exchanged 5-6 hrs later on the same day. Cells were transfected again on day 2 before GST pull-down of activated Rac1 on day 3.

GST pull-down of activated Rac1

GTP-bound forms of Rac1 were pulled down using bacterially expressed, purified GST-PBD (p21-binding domain of PAK; interacts with GTP-boundRac1 and Cdc42; Cytoskeleton) [1]. Cells were washed with ice-cold PBS three times and lysed in the RIPA buffer (50mM Tris. 7.2, 500mM Nacl, 1% Triton X-100, 0.1% SDS w/v, 10mM MgCl2, 1:250 mammalian protease inhibitor (Sigma), 1:10 phosphatase inhibitor cocktail (Roche). The cell lysates were rocked at 4°C for 10 min and clarified of insoluble material by centrifugation at 20,000g at 4°C for 10 min. Equal aliquots of lysates were incubated with Glutathione-Sepharose beads coated with 30µg purified GST-PBD fusion proteins (Cytoskeleton) at 4°C for 1 hour. The beads were washed three times with wash buffer (50 mM Tris. pH 7.5, 1%,Triton X-100, 150 mM NaCl, 5 mM $MgCl_2$ and 1 mM DTT, 1:250 mammalian protease inhibitor (Sigma).

# Appendix 2: Catalogue of figures cross-referenced to experiment index

**Appendix 2. Catalogue of figures cross-referenced to experiment numbers.** This table is compiled to cross-reference figures presented in this thesis to the experiments recorded separately for record-keeping purposes.

| Figure | Figure legends | Expt |
|---|---|---|
| Figure 1.1. | The secondary structure of the EGF motif in human EGF. | |
| Figure 1.2. | A simplified schematic view of EGFR showing key phosphorylation residues and main downstream cascades. | |
| Figure 1.3. | Main effector pathways activated by EGFR. | |
| Figure 1.4. | Simplified schema of mammary duct and terminal end bud. | |
| Figure 1.5. | Structure of AAV targeting construct. | |
| Figure 1.6. | A simplified scheme representing the concept of synthetic lethality. | |
| Figure 1.7 | Schematic representation of junctional complex in epithelial cells. | |
| Figure 1.8. | A simplified model of desmosomal components. | |
| Figure 1.9. | Schematic representation of modulation of Rac activity by GEFs and GAPs. | |
| **Figure 1.10** | **Graphical abstract of the plasticity of mammary epithelial cells governed by EGF and actin remodeling.** | |
| Figure 3.1. | Growth requirements of subconfluent MCF10A cells. | 13, 13.1 |
| Figure 3.2. | EGF withdrawal induces interdigitations in MCF10A cells. | 24 |
| Figure 3.3 | EGFR signaling suppresses interdigitations of MCF10A cells. | 51 |
| Figure 3.4. | Interdigitations observed in different clones of MCF10A parental cells. | 101.1 |
| Figure 3.5. | Variable E-cadherin staining and ability to form interdigitated structures in PIK3CA mutated MCF10A cells. | 103, 101.1 |
| Figure 3.6. | MCF10A PI3K H1047R (clone 1) cells of two distinct phenotypes. | 84 |
| Figure 3.7. | Optimisation of lysis buffers and EGFR antibodies for MCF10A cell lysates. | 59, 76.1 |
| Figure 3.8. | EGFR profile of MCF10A parental, PI3K H1047R and EGFR ΔE746-A750 mutants. | 84.1 |
| Figure 3.9. | EGFR associated profiles of MCF10A parental, PI3K H1047R and E545K mutants of different clones. | 105 |
| Figure 3.10. | MCF10A spheroidal acinar structures. | 41 |
| Figure 3.11. | Similar cross sectional area distributions of MCF10A parental and PI3K H1047R acini. | 41 |
| Figure 3.12. | Cross sectional areas of MCF10A PTEN WT and PTEN null acini show similar distribution. | 41 |

| | | |
|---|---|---|
| Figure 5.7. | EGF addition activates Rac. | 112 |
| Figure 5.8. | Resolution of interdigitations requires actin polymerisation and actomyosin contractility. | 87.2, 123 |
| Figure 5.9. | EGF addition activates Rac but not Cdc 42. | 112.2 |
| Figure 5.10. | Maintenance and reversal of interdigitations independent of Rac1 inhibition. | 123 |
| Figure 5.11. | Rac1 activity reduced by inhibitors and RacGEF knockdown. | 121 |
| Figure 5.12. | Optimisation of Rac1 knockdown in the induction and reversal of interdigitations. | 118.3 |
| Figure 5.13. | Reversal of interdigitations independent of Rac1 knockdown. | 118.3 |
| Figure 5.14. | Vav activated Rac1 is not required for reversal of interdigitations. | 124, 124.3 |
| Figure 5.15. | Interdigitations accompanied by an increase in the number of desmosomes. | 47, 76 |
| Figure 5.16. | Interdigitated cell processes decorated with Desmoplakin. | 62 |
| Figure 5.17. | Co-localisation of Desmoplakin and early endosome marker, EEA1. | 88 |
| Figure 5.18. | Subcellular localisation of caveolin-1 in MCF10A cells. | 47, 136 |
| Figure 5.19. | Subcellular localisation of caveolin-1, Golgi markers and microtubules. | 139 |
| Figure 5.20. | Cycloheximide treatment impedes induction of interdigitations. | 135, 138 |
| Figure 5.21. | Desmoplakin levels remain elevated after resolution of interdigitations. | 81, 83 |
| Figure 5.22. | Demoplakin levels remain basal after interdigitations are induced. | 142 |
| Figure 5.23. | Minimal closure of scratch wounds without ligand stimulation. | 128 |
| Figure 5.24. | Resolution of interdigitations is specific to EGF. | 134 |
| Figure 5.25. | Differential cell migration into scratch wounds. | 134 |
| Figure 5.26. | Interdigitated cells resist mechanical shear stress. | 129, 129.2, 142 |
| Figure 5.27. | Interdigitated cells withstand hypo-osmotic stress. | 141.2 |